Helmholtz Center Munich

Institute of Lung Health and Immunity, Comprehensive Pneumology Center

Director: Dr. Ali Önder Yildirim

Dissertation

zum Erwerb des Doctor of Philosophy (Ph.D.) an der

Medizinischen Fakultät der

Ludwig-Maximilians-Universität zu München

Environmental molecular landscape and tumor microenvironment reprogramming in thoracic malignancies

vorgelegt von:

Georgia Giotopoulou

aus:

Larisa, Greece

Jahr:

2022

Mit Genehmigung der Medizinischen Fakultät der

Ludwig-Maximilians-Universität zu München

First supervisor: *Prof. Dr. med. Jürgen Behr*

Second supervisor: *Dr. Georgios Stathopoulos*

Third supervisor: *Prof. Dr. Markus Rehberg*

Fourth supervisor: *Prof. Dr. med. Thomas Gudermann*

Dean: **Prof. Dr. med. Thomas Gudermann**

Datum der Verteidigung:

21.09.2022

Affidavit

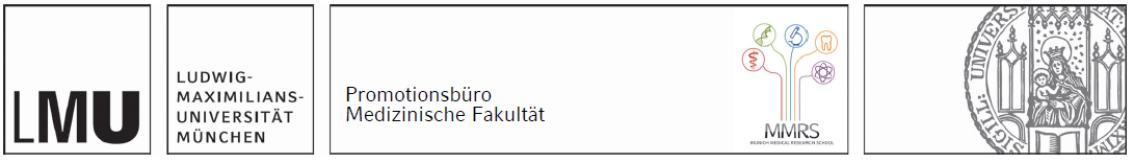

Affidavit

Giotopoulou, Georgia

Surname, first name

Max-Lebsche-Platz 31

Street

81377, Munich, Germany

Zip code, town, country

I hereby declare, that the submitted thesis entitled:

Environmental molecular landscape

and tumor microenvironment reprogramming in thoracic malignancies

……

is my own work. I have only used the sources indicated and have not made unauthorised use of services of a third party. Where the work of others has been quoted or reproduced, the source is always given.

I further declare that the submitted thesis or parts thereof have not been presented as part of an examination degree to any other university.

Munich, 02.03.2022

place, date

Georgia Giotopoulou

Signature doctoral candidate

Confirmation of congruency

LMU LUDWIG-MAXIMILIANS-UNIVERSITÄT MÜNCHEN

Promotionsbüro Medizinische Fakultät

MMRS

Confirmation of congruency between printed and electronic version of the doctoral thesis

Giotopoulou, Georgia

Surname, first name

Max-Lebsche-Platz 31

Street

81377, Munich, Germany

Zip code, town, country

I hereby declare, that the submitted thesis entitled:

Environmental molecular landscape

and tumor microenvironment reprogramming in thoracic malignancies

……

is congruent with the printed version both in content and format.

Munich, 02.03.2022

place, date

Georgia Giotopoulou

Signature doctoral candidate

Table of content

List of abbreviations

Ad	adenovirus
ALK	ALK receptor tyrosine kinase
BAP1	BRCA1 associated protein 1
BRAF	B-Raf proto-oncogene, serine/threonine kinase
CCL2	C-C motif chemokine ligand 2
CDKN2A	cyclin dependent kinase inhibitor 2A
CNA	copy number alterations
ddPCR	droplet digital Polymerase Chain Reaction
DDX3X	DEAD-box helicase 3 X-linked
DNA	Deoxyribonucleic Acid
EC	ethyl carbamate
ECM	extracellular matrix
EGFR	epidermal growth factor receptor
EMT	epithelial-mesenchymal transition
GSEA	Gene set enrichment analysis
HRAS	HRas proto-oncogene, GTPase
IL-1β	interleukin 1 beta
KIT	KIT proto-oncogene, receptor tyrosine kinase
KRAS	KRAS proto-oncogene, GTPase
LLC	Lewis lung carcinoma
LUAD	lung adenocarcinoma
LUSQ	squamous cell carcinoma
MAPK	mitogen-activated protein kinase
MCs	mast cells
MPM	Malignant pleural mesothelioma
MYC	MYC proto-oncogene, bHLH transcription factor
NF2	moesin-ezrin-radixin like (MERLIN) tumor suppressor
NF-κB	nuclear factor-κB
NRAS	NRAS proto-oncogene, GTPase
NSCLC	non-small cell lung cancer
PIK3CA	phosphatidylinositol-4,5-bisphosphate 3-kinase catalytic subunit alpha

PTEN	phosphatase and tensin homolog
RET	ret proto-oncogene
RNA	Ribonucleic acid
RNAseq	RNA sequencing
ROS	reactive oxygen species
ROS1	ROS proto-oncogene 1, receptor tyrosine kinase
SCLC	small cell lung cancer
SETD2	SET domain containing 2, histone lysine methyltransferase
SNV	single nucleotide variants
STK11	serine/threonine kinase 11
TCGA	The Cancer Genome Atlas
TP53	tumor protein p53
TRACERx	TRAcking non-small cell lung Cancer Evolution through therapy [Rx]
TSC1	TSC complex subunit 1

List of publications

I: Marazioti, A.*, Krontira, A. C.*, Behrend, S. J.*, **Giotopoulou, G. A.***, Ntaliarda, G.*, Blanquart, C., Bayram, H., Iliopoulou, M., Vreka, M., Trassl, L., Pepe, M. A. A., Hackl, C. M., Klotz, L. V., Weiss, S. A. I., Koch, I., Lindner, M., Hatz, R. A., Behr, J., Wagner, D. E., Papadaki, H., Antimisiaris, S. G., Jean, D., Deshayes, S., Grégoire, M., Kayalar, Ö., Mortazavi, D., Dilege, Ş., Tanju, S., Erus, S., Yavuz, Ö., Bulutay, P., Fırat, P., Psallidas, I., Spella, M., Giopanou, I., Lilis, I., Lamort, A. S., & Stathopoulos, G. T. (2021). KRAS signaling in malignant pleural mesothelioma. *EMBO Mol Med*, e13631. https://doi.org/10.15252/emmm.202013631

II: Lilis, I., Ntaliarda, G., Papaleonidopoulos, V., **Giotopoulou, G. A.**, Oplopoiou, M., Marazioti, A., Spella, M., Marwitz, S., Goldmann, T., Bravou, V., Giopanou, I., & Stathopoulos, G. T. (2019). Interleukin-1β provided by KIT-competent mast cells is required for KRAS-mutant lung adenocarcinoma. *Oncoimmunology*, 8(7), 1593802. https://doi.org/10.1080/2162402x.2019.1593802

Additional contribution to the dissertation

III: **Giotopoulou, G. A.**, & Stathopoulos, G. T. (2020). Effects of Inhaled Tobacco Smoke on the Pulmonary Tumor Microenvironment. *Adv Exp Med Biol*, 1225, 53-69. https://doi.org/10.1007/978-3-030-35727-6_4

* Equally contributing first authors

Additional publications

Giotopoulou, G. A., Ntaliarda, G., Marazioti, A., Lilis, I., Kalogianni, F., Tourkochristou, E., Spiropoulou, N., Giopanou, I., Spella, M., Iliopoulou, M., Korfiati, A., Mantamadiotis, T., Rosero, C., Goldmann, T., Marwitz, S., & Stathopoulos, G. T. *bioRxiv preprint*. https://doi.org/10.1101/2021.06.19.449094

Arendt, K. A. M., Ntaliarda, G., Armenis, V., Kati, D., Henning, C., **Giotopoulou, G. A.**, Pepe, M. A. A., Klotz, L. V., Lamort, A. S., Hatz, R. A., Kobold, S., Schamberger A. C., & Stathopoulos, G. T. (2022). An in vivo inflammatory loop potentiates KRAS blockade. *bioRxiv preprint*. https://doi.org/10.1101/629139 Accepted in *Biomedicines*.

Lamort, A. S., Kaiser, J. C., Pepe, M. A. A., Lilis, I., Ntaliarda, G., Somogyi, K., Spella, M., Behrend, S. J., **Giotopoulou, G. A.**, Kujawa, W., Lindner, M., Koch, I., Hatz, R. A., Behr, J., Sotillo, R., Schamberger, A. C., & Stathopoulos, G. T. (2021). Prognostic phenotypes of early-stage lung adenocarcinoma. *Eur Respir J*. https://doi.org/10.1183/13993003.01674-2021

Behrend, S. J., **Giotopoulou, G. A.**, Spella, M., & Stathopoulos, G. T. (2021). A role for club cells in smoking-associated lung adenocarcinoma. *Eur Respir Rev*, *30*(162). https://doi.org/10.1183/16000617.0122-2021

Sarode, P., Zheng, X., **Giotopoulou, G. A.**, Weigert, A., Kuenne, C., Günther, S., Friedrich, A., Gattenlöhner, S., Stiewe, T., Brüne, B., Grimminger, F., Stathopoulos, G. T., Pullamsetti, S. S., Seeger, W., & Savai, R. (2020). Reprogramming of tumor-associated macrophages by targeting β-catenin/FOSL2/ARID5A signaling: A potential treatment of lung cancer. *Sci Adv*, *6*(23), eaaz6105. https://doi.org/10.1126/sciadv.aaz6105

Marazioti, A., Lilis, I., Vreka, M., Apostolopoulou, H., Kalogeropoulou, A., Giopanou, I., **Giotopoulou, G. A.**, Krontira, A. C., Iliopoulou, M., Kanellakis, N. I., Agalioti, T., Giannou, A. D., Jones-Paris, C., Iwakura, Y., Kardamakis, D., Blackwell, T. S., Taraviras, S., Spella, M., & Stathopoulos, G. T. (2018). Myeloid-derived interleukin-1β drives oncogenic KRAS-NF-κB addiction in malignant pleural effusion. *Nat Commun*, *9*(1), 672. https://doi.org/10.1038/s41467-018-03051-z

Vreka, M., Lilis, I., Papageorgopoulou, M., **Giotopoulou, G. A.**, Lianou, M., Giopanou, I., Kanellakis, N. I., Spella, M., Agalioti, T., Armenis, V., Goldmann, T., Marwitz, S., Yull, F. E., Blackwell, T. S., Pasparakis, M., Marazioti, A., & Stathopoulos, G. T. (2018). IκB Kinase α Is Required for Development and Progression of KRAS-Mutant Lung Adenocarcinoma. *Cancer Res*, *78*(11), 2939-2951. https://doi.org/10.1158/0008-5472.Can-17-1944

Giannou, A. D., Marazioti, A., Kanellakis, N. I., Giopanou, I., Lilis, I., Zazara, D. E., Ntaliarda, G., Kati, D., Armenis, V., **Giotopoulou, G. A.**, Krontira, A. C., Lianou, M., Agalioti, T., Vreka, M., Papageorgopoulou, M., Fouzas, S., Kardamakis, D., Psallidas, I., Spella, M., & Stathopoulos, G. T. (2017). NRAS destines tumor cells to the lungs. *EMBO Mol Med*, *9*(5), 672-686. https://doi.org/10.15252/emmm.201606978

Contribution to the publications

1.1 Contribution to paper I

The candidate carried out computational biologic analyses, including downloading, filtering and analyzing gene expression data of the cancer genome atlas (TCGA) malignant pleural mesothelioma (MPM) patients. She additionally performed heatmap and clustering visualization of the findings and compiled graphs and figures thereof. Furthermore, she retrieved mutations information for these patients and carried out pathway analyses as well as gene set enrichment (GSEA) analysis. She additionally participated in designing and performing *in vivo* experiments, including intrapleural or intraperitoneal transgene delivery in mice, bioluminescence imaging, pleural lavage isolation, pleural effusion aspiration and lungs harvesting, as well as culturing and performing subcutaneous injections of primary mesothelioma cell lines. She generated portions of the paper draft and provided critical intellectual scientific input on the conceivement and implementation of the main hypothesis. The shared first authorship among Marazioti, A., Krontira, A. C., Behrend, S. J., Ntaliarda, G. and the candidate is based on their cooperation in conducting *in vivo* experiments, as well as on their equal and major contribution on giving intellectual input regarding computational analyses. Furthermore, all first co-authors contributed equivalently in generating portions of the manuscript.

1.2 Contribution to paper II

The candidate performed analyses of publically available gene expression data of human LUAD from smokers and never smokers compared with normal lung tissue (GEO dataset GSE43458; https://www.ncbi.nlm.nih.gov/geo/query/acc.cgi?acc=GSE43458), as well as of human LUAD from *KRAS*- and *EGFR*- mutant patients compared with normal lung tissue (GEO dataset GSE31852; https://www.ncbi.nlm.nih.gov/geo/query/acc.cgi?acc=GSE31852). She analyzed microarrays data from murine mast cells (MCs) populations and performed gene set enrichment analyses (GSEA) to determine the enrichment of MCs signatures to the human phenotypes of lung adenocarcinoma (LUAD) according to the smoking status and mutational profile of the patients.

1.3 Contribution to paper III (Appendix)

The candidate conducted literature research, wrote the first draft of the manuscript, created all figures and corresponded with Adv Exp Med Biol.

2. Introductory summary

Can the pattern of accumulation of mutations in thoracic malignancies unravel molecular clusters of patients? How do the signaling pathways affected by specific mutations in driver genes reshape the immune contexture of tumor microenvironment and determine the progress of thoracic malignancies in distinct molecular subgroups of individuals? With our studies, we address these questions with a broader aim to revise the clinical scenery of thoracic malignancies through the evolution of personalized diagnostic, prognostic and therapeutic modalities and the discovery of new addiction partners as therapeutic targets.

Among all thoracic malignancies, lung cancer is the most dominant, constituting the most common cause of cancer-related mortality worldwide, with lung adenocarcinoma (LUAD) representing the most frequent histologic subtype of the disease. Molecular heterogeneity of LUAD in the interpatient, intratumor and intertumor level represents a crucial challenge in the light of the efficiency of current therapeutic approaches, yet the underlying origins and mechanisms of actions of this diversity remain obscure.

Except for the molecular heterogeneity of malignant cells, there is also heterogeneity of the tumor microenvironment (TME) which consists of several immune cells populations that infiltrate the stroma in response to inflammatory signaling. We studied the role of the mast cells (MC) in the progression of *KRAS*-mutant LUAD, most commonly featured in ever-smoking individuals that also show increased risk for smoking-related chronic inflammation. We employed two murine models of MC deficiency, dependent or independent on the KIT signaling blockade, and three models of *KRAS*-mutant LUAD models. We observed that both populations of MCs infiltrate both human and murine LUAD and we discovered a KIT-dependent mechanism enabling MCs to display pro-tumorigenic functions through the regulation of IL-1β secretion. MC-associated transcriptional imprints are enriched in human LUAD and related with poor survival, while KIT+ MC signature is up-regulated in *KRAS*-mutant human LUAD.

We further broadened our studies of *KRAS*-mutant cluster of patients on malignant pleural mesothelioma (MPM), a highly lethal malignancy, emerging from neoplastic transformation of mesothelial cells lining the pleural cavities of the interior chest wall. We employed the catalog of somatic mutations in cancer (Forbes et al., 2015), ten large molecular studies of human MPM (Bott et al., 2011; Bueno et al., 2016; De Rienzo et al., 2016; Enomoto et al., 2012; Guo et al., 2015; Hmeljak et al., 2018; Kato et al., 2016; Lo Iacono et al., 2015; Mezzapelle et al., 2013; Shukuya et al., 2014), as well as clinical cohorts (Gueugnon et al., 2011; Klotz, Courty, et al., 2019; Klotz, Lindner, et al., 2019; Smeele et al., 2018) to detect a distinct -in terms of histology, survival and molecular features- cluster of patients harboring *KRAS* alterations, alone or in accomplish with *TP53* loss-of function alterations. We established novel high penetrance conditional MPM mouse models of both epithelioid and biphasic subtype, featuring pleural effusion accumulation facilitated by *Trp53* deletion in *KRAS*-mutant cells. We additionally developed three MPM cell lines carrying the driver *KRAS*^{G12D} mutation as well as *Bap1* inactivating alterations, and featuring a molecular profile enriched to the human disease, and we identified KRAS as an actionable target in MPM.

2.1 Molecular landscape of environmentally-induced lung cancer

Lung cancer is a dominant malignancy, constituting the most common cause of global cancer-related mortality and leading to 1,796,144 deaths during the year 2020 (Siegel et al., 2021; Sung et al., 2021). Lung cancer is divided in two histological subtypes: non-small cell lung cancer (NSCLC) and small cell lung cancer (SCLC), with NSCLC including lung adenocarcinoma (LUAD), squamous cell carcinoma (LUSQ) as well as large cell carcinoma and accounting for approximately 85% of all lung cancer incidences. LUAD is the most commonly occurring histological subtype of lung cancer.

Next to genetic susceptibility and replication errors during stem cell divisions, environmental exposures present a fundamental causative factor of LUAD. Tobacco smoking, consisting of chemical carcinogens and emitting radiation, is the predominant environmental cause of LUAD (Thun et al., 2012), however the incidence of the disease is increasing in never- and former-smokers worldwide, accounting for 10-25% of the cases (Couraud et al., 2012; Sun et al., 2007; Wakelee et al., 2007). Other established environmental risk factors are exposure to second-hand tobacco smoke (Whitrow et al., 2003), diet and food supplements, occupational lung carcinogens such as radioactive particulate mass (Boffetta, 2004), indoor and outdoor air pollution including emissions of polycyclic aromatic hydrocarbon compounds or nanoparticles (Vineis & Husgafvel-Pursiainen, 2005), as well as other than tobacco-source high-energy transfer radiation (Alberg et al., 2013; Furukawa et al., 2010; Preston et al., 2007).

Genomic instability presents one of the hallmarks of human cancer (Hanahan & Weinberg, 2011; Negrini et al., 2010). Molecular profiling of LUAD has revealed that it harbors high mutational burden among all studied cancer types, with thousands of genetic alterations per cancer cell genome, including single nucleotide variants (SNV), copy number alterations (CNA), dysregulation of alternative splicing (exon skipping), balanced inversions resulting in gene fusions, with *ALK*, *ROS1* (receptor tyrosine kinase) and *RET*, being the most commonly affected genes, epigenetic alterations leading to overexpression of proto-oncogenes such as *KRAS*, *EGFR* and *PIK3CA* and silencing of tumor suppressor genes, such as *TP53*, *STK11* and *PTEN*, as well as major chromosomal events like kataegis and chromothripsis (Campbell et al., 2016; Chatterjee et al., 2018; "Comprehensive molecular profiling of lung adenocarcinoma," 2014; Devarakonda et al., 2015; Imielinski et al., 2012; Kandoth et al., 2013). LUAD harbors homologous coding mutational burden, represented by transcriptional strand bias for cytosine to adenine transversions (Alexandrov et al., 2013; Kandoth et al., 2013).

Heterogeneity of the molecular profile in the interpatient, intratumor and intertumor level, represents one of the most challenging issues in LUAD, in the light of the effectiveness of current therapeutic approaches (Ramón et al., 2020; Zhang et al., 2014; Zito Marino et al., 2019), yet the mechanisms underlying the development of tumor diversity remain poorly understood. Molecular heterogeneity of LUAD is temporal-dependent, as described by the clonal tumor evolution, with driver mutations arising in the initial clone of tumor cells and passenger mutations acquired later and characterizing the molecular events during the progress of tumor establishment (de Bruin et al., 2014). The involvement of the cancer stem cell hypothesis providing distinct subclonal lineages dynamically maintained in different tumors, as well as of the immune contexture of the microenvironment to the emergence of tumor heterogeneity have been previously described (Kreso & Dick, 2014; Pietras, 2011; Zito Marino et al., 2017). However, the molecular diversity of LUAD is also contingent on the cause of the disease. The implications of exogenous mutagenic

factors, such as tobacco carcinogens and radiation, to which a stem cell niche is exposed years prior to tumor establishment, are sufficient to reveal distinct mutational imprints in LUAD patients (Lawrence et al., 2013).

In particular, the genomic signature of ionizing radiation in thoracic malignancies is composed by redundancy of deletions, as well as enrichment of chromosomal rearrangements, in specific balanced inversions (Behjati et al., 2016). Furthermore, LUAD is molecularly distinct according to the patients' smoking status (Subramanian & Govindan, 2007; Sun et al., 2007), with tumors from smokers displaying higher mutation burden and being predominantly represented by cytosine to adenine transversions (C:G→A:T), whereas cytosine to thymidine (C:G→T:A) transitions are the most enriched type of point mutations in never-smokers (Govindan et al., 2012; Imielinski et al., 2012). Accordingly, different types of base substitutions in the trinucleotide level reflect the causative exogenous exposures of the disease (Alexandrov et al., 2016). More specifically, Alexandrov et al. defined mutational signatures on the trinucleotide context, by determining the bases that flank the 5' and 3' end of the mutated base, and correlated them with clinical exposure data across more than 20 cancer types and 10000 patients, identifying the smoking signature (C>A transversion) (Alexandrov et al., 2016; Alexandrov et al., 2013). *KRAS* mutations appear in higher frequency in smoking individuals, are detected in codons 12, 13 and 61 and are mutually exclusive with *EGFR* mutations ("Comprehensive molecular profiling of lung adenocarcinoma," 2014). Except for the mutational heterogeneity, smokers and non-smokers LUAD patients display distinct tumor microenvironment composition and inflammatory imprints (Giotopoulou & Stathopoulos, 2020; Li et al., 2018), as well as different epigenetic alterations and DNA methylation profiles (Belinsky, 2004; Gao et al., 2016).

Comprehending the pattern of accumulation of mutations inflicted by distinct environmental exposures during oncogenesis, as well as discriminating thoracic malignancies according to the driver oncogene and mutational status of the patients, present an unmet clinical need that benefits from correlation studies, but most importantly necessitates functional studies ("Comprehensive molecular profiling of lung adenocarcinoma," 2014). Our studies focus on a specific molecular cluster of LUAD and malignant pleural mesothelioma (MPM) patients, the ones harboring *KRAS*-mutations, often associated with smoking ("Comprehensive molecular profiling of lung adenocarcinoma," 2014). With our findings we seek to address the molecular diversity of thoracic malignancies, to reshape the clinical landscape by the evolution of personalized diagnostic, prognostic and therapeutic modalities and to enhance the discovery of new addiction partners as therapeutic targets.

2.2 Effects of environmental carcinogens on the respiratory tumor microenvironment

Giotopoulou, G. A., & Stathopoulos, G. T. (2020). Effects of Inhaled Tobacco Smoke on the Pulmonary Tumor Microenvironment. Adv Exp Med Biol, 1225, 53-69. https://doi.org/10.1007/978-3-030-35727-6_4

While tumor initiation is mediated by mutations in oncogenic driver genes, the progression is affected by the interaction between cancer cells and their microenvironment, which is established through the infiltration of various immune cellular populations to the stroma, mainly in response to chemokine secretion by malignant cells (Allavena et al., 2011; Balkwill, 2004; Balkwill, 2012; Balkwill et al., 2012; Bronte et al., 2006; Mantovani et al., 2008). Upon environmental carcinogenic exposures, the microenvironment of the respiratory tract acquires pro-tumorigenic features, enhancing chronic inflammation and favoring the survival, sustained proliferation and migration of mutated malignant respiratory epithelial cells. The tumor microenvironment contexture, as well as the inflammatory signatures harbor high heterogeneity (Balkwill et al., 2012; Chen et al., 2014) and appear to be distinct according to the smoking status of lung cancer patients (Li et al., 2018). Furthermore, ever-smokers LUAD patients show increased risk for smoking-associated chronic inflammation, evident as chronic airflow obstruction (Houghton, 2013; Houghton et al., 2008; Vestbo et al., 2013), in accordance to their higher response to immune checkpoint inhibitors (Rizvi et al., 2015). The mechanisms underlying the environmentally-mediated pro-tumorigenic effects in the tumor microenvironment involve deregulation of the physical and biochemical properties of the extracellular matrix (ECM) (Lu et al., 2012), formation of new vessels (neoangiogenesis) and increase of capillary density (Gazdar, 2003; Heeschen et al., 2001; Heeschen et al., 2003), acquirement of a mesenchymal phenotype by polarized epithelial cells (epithelial-mesenchymal transition- EMT) through reactive oxygen species (ROS) production, increase of the migration capacity and cellular invasion potential (Di Cello et al., 2013; Milara et al., 2013; Sohal et al., 2010; Zhang et al., 2012; Zhang et al., 2001). Furthermore, additional processes enhancing the tumor initiating potential of environmental carcinogenic factors include metabolic alterations resulting in aging acceleration (Pavlides et al., 2009; Salem et al., 2013), immunomodulatory processes with acute (van der Vaart et al., 2004) or chronic pro- inflammatory effects accompanied by diminished responsiveness to infections (Coussens et al., 2013; Crusz & Balkwill, 2015; Herr et al., 2009; Houghton, 2013) as well as epigenetic alterations (Belinsky, 2004; Clark & Molloy, 2017; Liu et al., 2010; Vaz et al., 2017). Unravelling the complexity and the mechanisms of recruitment of the immune cells' populations consisting the tumor microenvironment, as well as their roles in tumorigenesis holds promise for the development of effective immune checkpoint inhibitors therapies for thoracic malignancies.

2.3 Mast cells in *KRAS*-mutant LUAD

Lilis, I., Ntaliarda, G., Papaleonidopoulos, V., **Giotopoulou, G. A.**, Oplopoiou, M., Marazioti, A., Spella, M., Marwitz, S., Goldmann, T., Bravou, V., Giopanou, I., & Stathopoulos, G. T. (2019). Interleukin-1β provided by KIT-competent mast cells is required for KRAS-mutant lung adenocarcinoma. Oncoimmunology, 8(7), 1593802. https://doi.org/10.1080/2162402x.2019.1593802

Mast cells (MCs) are bone marrow-derived tissue-resident immune cells that play key roles in inflammatory responses, acute allergic reactions, tissue homeostasis, as well as angiogenesis (Galli & Tsai, 2012; Marone et al., 2002; Marone et al., 2016; Metcalfe et al., 1997). MCs represent a crucial component of the tumor microenvironment, reshaping its contexture by establishing interactions with other tumor-infiltrating cell populations, promoting invasiveness and metastasis (Aponte-López & Muñoz-Cruz, 2020). Their peritumoral and/or intratumoral density is increased in various cancer types (Aponte-López & Muñoz-Cruz, 2020; Beer et al., 2008; Franco et al., 2014; Giannou et al., 2015; Johansson et al., 2010; Ma et al., 2013; Melillo et al., 2010; Pittoni et al., 2011; Ribatti et al., 1999; Soucek et al., 2007; Theoharides, 2008; Vyzoukaki et al., 2015) and is related to either good or poor prognosis depending on the cancer type and stage, rendering their role in cancer progression ambiguous (Varricchi et al., 2017). Inflammation is a hallmark of cancer (Hanahan & Weinberg, 2011) and in LUAD it has been featured in ever-smoking individuals harboring mutations in *KRAS* proto-oncogene ("Comprehensive molecular profiling of lung adenocarcinoma," 2014), increasing the risk for chronic obstructive pulmonary disease (Houghton, 2013; Houghton et al., 2008; Vestbo et al., 2013). MCs promote an inflammatory chemokine signaling network in malignant cells harboring *KRAS* mutations enabling malignant pleural effusion formation (Giannou et al., 2015), however their role in LUAD remained obscure.

In our study, we employed two models of MC deficiency, based on KIT signaling blockade or genetic ablation, *cKit*^{Wsh} (Giannou et al., 2015; Tono et al., 1992) and *Cpa3.Cre* (Feyerabend et al., 2011; Giannou et al., 2015) respectively, in three *KRAS*-mutant LUAD models; chemically-induced using exposure to the tobacco carcinogen urethane (ethyl carbamate, EC; stand-alone mutagen and tumor promoter) (Stathopoulos et al., 2007), genetically-induced transient Ad-mediated *KRAS*^{G12D} transgene expression in the respiratory epithelium (Vreka et al., 2018) and heterotopic subcutaneous installation of *KRAS*^{G12D} mutation harboring Lewis lung carcinoma LLC cancer cells followed by their spontaneous dissemination to the pulmonary areas. Therefore, our studies enabled us to study two different MC populations, KIT+ and KIT-. We observed that both MCs populations infiltrate murine and human LUAD in response to factors secreted by the malignant cells, where they exert pro-tumorigenic functions. KIT+ MCs are required for tumor initiation, progression and metastasis and reshape the contexture of tumor microenvironment enabling the recruitment of other immune cells populations through the KIT-dependent regulation of IL-1β secretion. We identified MC-relevant transcriptional signatures, significantly over-represented in human LUAD and related with shorter survival, with KIT+ signature being enriched in *KRAS*-mutant LUAD induced by tobacco smoking, in accordance with the findings from our *in vivo KRAS*-mutant-driven LUAD murine models. Therefore, among the controversial role of MCs according to the type of malignancy (Varricchi et al., 2017), our study supports that KIT+ cells are required for *KRAS*-mutant LUAD, through IL-1β secretion which has been previously found to promote tumor progression by mediating nuclear factor-κB (NF-κB) transcriptional activity in other thoracic malignancies (Giannou et al., 2015; Marazioti et al., 2018).

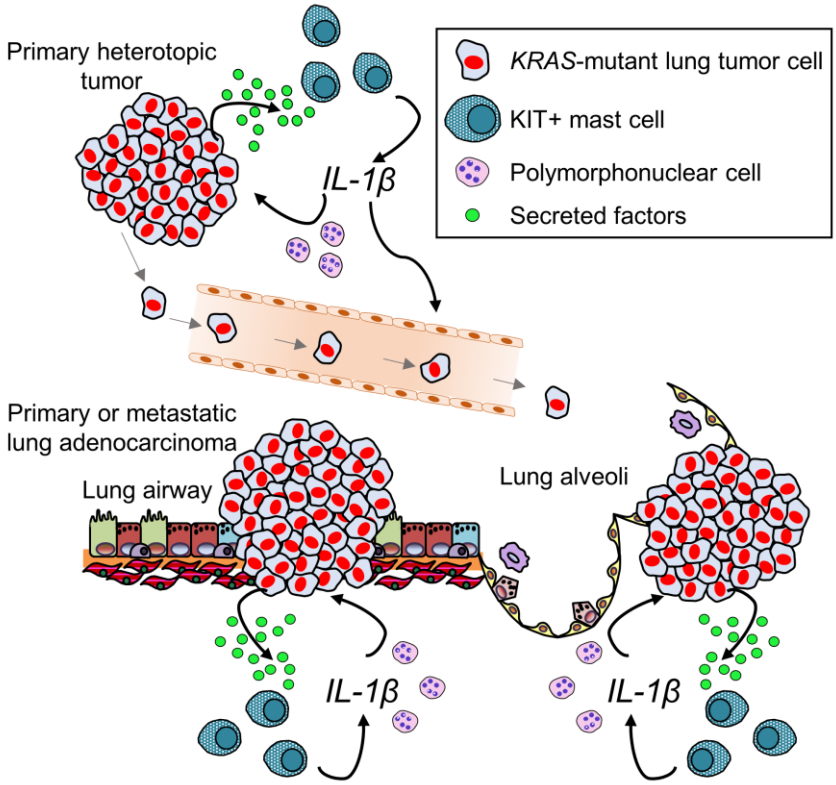

Figure 1: Schematic representation of the role of KIT+ mast cells in *KRAS*-mutant lung adenocarcinoma

KIT+ mast cells infiltrate *KRAS*-mutant LUAD in response to factors secreted by the malignant cells, and are required for tumor growth and metastasis through an *IL-1β*- mediated mechanism.

2.4 KRAS signaling in malignant pleural mesothelioma

Marazioti, A.*, Krontira, A. C.*, Behrend, S. J.*, **Giotopoulou, G. A.***, Ntaliarda, G.*, Blanquart, C., Bayram, H., Iliopoulou, M., Vreka, M., Trassl, L., Pepe, M. A. A., Hackl, C. M., Klotz, L. V., Weiss, S. A. I., Koch, I., Lindner, M., Hatz, R. A., Behr, J., Wagner, D. E., Papadaki, H., Antimisiaris, S. G., Jean, D., Deshayes, S., Grégoire, M., Kayalar, Ö., Mortazavi, D., Dilege, Ş., Tanju, S., Erus, S., Yavuz, Ö., Bulutay, P., Fırat, P., Psallidas, I., Spella, M., Giopanou, I., Lilis, I., Lamort, A. S., & Stathopoulos, G. T. (2021). KRAS signaling in malignant pleural mesothelioma. EMBO Mol Med, e13631. https://doi.org/10.15252/emmm.202013631

Malignant pleural mesothelioma (MPM) is a highly lethal cancer, with a median overall survival of 9 to 17 months (Tsao et al., 2009), arising from neoplastic transformation of the mesothelial cells lining the pleural cavities (visceral pleura), as well as the interior chest wall (parietal pleura) (Bibby et al., 2016; Bueno, 2005; Mutti et al., 2018). MPM is broadly classified into three histological subtypes: epithelioid, sarcomatoid and biphasic (or mixed), with epithelioid presenting the most propitious prognosis and sarcomatoid showing particularly impaired survival outcomes (Galateau-Salle et al., 2016; Scherpereel et al., 2010; Tischoff et al., 2011). The major cause of MPM accounting for >80% of the cases, is asbestos exposure that evokes DNA and chromosomal impairment following phagocytosis of asbestos fibers, ROS production, direct cytotoxicity, mitotic spindle damage consistent with widespread loss of heterozygosity, cytokine and growth factor dysregulation, abnormalities of mitotic process, macrophage recruitment and persistent inflammation, often associated with effusion i.e., exudative fluid accumulation that causes chest pain and dyspnea (Galani et al., 2019; Hmeljak et al., 2018; Huang et al., 2011; Jaurand & Fleury-Feith, 2005; Wagner et al., 1960). Additional risk factors are heredity, prior therapeutic chest radiation exposure, non-asbestos mineral fibers, chronic pleural inflammation, germline genetic mutations as well as spontaneous events (Attanoos et al., 2018; Hofmann et al., 1994; Melaiu et al., 2018; Nagai et al., 2011; Wagner et al., 1960). Although the decrease and strict regulations regarding asbestos use have diminished new incidences in Western countries, its long latency period (10-40 years) between exposure and onset of the disease (Sun et al., 2017) and its continued mining in less developed countries (Frank & Joshi, 2014), combined with the limited advances on the effectiveness of treatment options (Remon et al., 2015), with the first line therapy strategy in the form of combination cisplatin/pemetrexed-based chemotherapy remaining unchanged for decades (Vogelzang et al., 2003), render MPM an ongoing global area of concern (Courtiol et al., 2019; Scherpereel et al., 2018; Yap et al., 2017).

The molecular landscape of MPM reveals high heterogeneity both among patients and within individual tumors, with intratumor diversity emerging as a combination of spatial and longitudinal (Blum et al., 2019; Bueno et al., 2016; Oehl et al., 2018; Wadowski et al., 2020; Yap et al., 2017). Comprehensive characterization of MPM tumors by multiple studies identified the molecular mechanisms underlying MPM tumorigenicity, including gene fusions, splice alterations, aberrant chromosomal alterations, epigenetic modifications, as well as genetic mutations, characterized by loss-of-function mutations in tumor-suppressor genes *TP53* and *CDKN2A* being connected with poor overall survival, as well as *BAP1*, *NF2*, *TSC1*, *DDX3X*, *STK11* and *SETD2*, along with gain-of-function mutations in proto oncogenes *EGFR*, *MYC*, *PIK3CA*, *BRAF*, *NRAS*, *HRAS* and *KRAS* (Bianchi et al., 1995; Bott et al., 2011; Bueno et al., 2016; Cheng et al., 1994; Enomoto et al., 2012; Gao et al., 2013; Guo et al., 2015; Guo et al., 2014; Kato et al., 2016; Lo Iacono et al., 2015; Mezzapelle et al., 2013; Wadowski et al., 2020). Interestingly, the frequency of *KRAS* mutations in all studied human cohorts above is detected with targeted as opposed to next-generation sequencing approaches (Shukuya et al., 2014).

There is an unfulfilled urge for the development of relevant animal models, as preclinical tools that recapitulate the mutation landscape as well as the clinicopathological features of the human MPM. Although several tumor-suppressor genes appear to underlie the pathogenesis of MPM (Bott et al., 2011; Bueno et al., 2016; Gao et al., 2013; Guo et al., 2014), their standalone exclusive conditional deletion does not induce MPM in rodents in the absence of carcinogenic exposure to asbestos (Jongsma et al., 2008; Kukuyan et al., 2019). Two elegant studies developed mouse models for MPM and showed that tumor suppressor genes cooperate to drive the disease, with Jongsma et al targeting *CDKN2A*, *NF2*, and *TP53* and Sementino et al *TP53* and *PTEN* deletions in the pleural mesothelium (Jongsma et al., 2008; Sementino et al., 2018). The mutational diversity of MPM rises the need for the development of such mouse models with high penetrance and rapid evolution, which would genetically and histopathologically represent specific molecular clusters of patients and pave the path for more personalized therapeutic interventions.

KRAS mutations in tumor cells drive malignant pleural effusion (MPE) formation, through a CCL2-dependent signaling cascade and non-canonical NF-κB oncogenic signaling addiction, enabling host to tumor interaction with the recruitment of myeloid cells to the pleural cavity, and are actionable (Agalioti et al., 2017; Marazioti et al., 2018). RAS/MAPK signaling is activated in human MPM cell lines (Patel et al., 2007) and is upregulated in the TCGA cohort of MPM patients (Hmeljak et al., 2018). Furthermore, the GTPase KRAS interacts with TP53 signaling (Yang et al., 2020). Accordingly, we hypothesized that *KRAS* mutations drive MPM formation, possibly in cooperation with *TP53* alterations.

We employed the catalog of somatic mutations in cancer (Forbes et al., 2015), ten large molecular studies of human MPM (Bott et al., 2011; Bueno et al., 2016; De Rienzo et al., 2016; Enomoto et al., 2012; Guo et al., 2015; Hmeljak et al., 2018; Kato et al., 2016; Lo Iacono et al., 2015; Mezzapelle et al., 2013; Shukuya et al., 2014), as well as clinical cohorts (Gueugnon et al., 2011; Klotz, Courty, et al., 2019; Klotz, Lindner, et al., 2019; Smeele et al., 2018) and we identified a subgroup of MPM patients harboring *KRAS* point mutations, copy number alterations and overexpression, alone or in accomplish with *Trp53* loss-of function alterations. *KRAS* alterations were found in low allelic frequency, explained by their heterozygous nature, as well as by the polyclonal disposition of MPM, in accordance to their sporadic occurrence in studies employing massive parallel sequencing approaches that lack sensitivity for low allelic frequency or read depth, compared with ddPCR or maximal depth sequencing (Guo et al., 2015; Jongsma et al., 2008; Kato et al., 2016; Li et al., 2020; Menges et al., 2014; Shukuya et al., 2014). This molecular subset of *KRAS*- driven MPM patients is distinct in terms of gene expression imprints, mutational signatures, histology and survival. We additionally established conditional MPM mouse models by ectopic expression of $KRAS^{G12D}$ in the pleural mesothelium alone, showing histological features of the epithelioid subtype, or in combination with *Trp53* deletion, leading to a more aggressive progression of the disease, with biphasic histological characteristics and pleural effusion accumulation. Although *Trp53* deletions have been ubiquitously observed in human MPM and are connected with poor survival (Bueno et al., 2016; Gao et al., 2013; Guo et al., 2014; Yap et al., 2017), its standalone conditional deletion in mouse models is not sufficient to induce MPM, suggesting that other addiction partners are required (Jongsma et al., 2008; Kukuyan et al., 2019). Our findings, in accordance with our previous studies supporting the inflammatory-promoting effects of *KRAS* in MPE (Agalioti et al., 2017; Marazioti et al., 2018), provide evidence that *KRAS* necessitates *Trp53* to facilitate effusion accumulation, a clinical characteristic of the human disease that had not previously been reproduced in animal models. MPM cell lines derived thereof from these MPM tumors carry the driver $KRAS^{G12D}$ mutation, harbor possibly secondarily-triggered *Bap1* inactivating alterations, with *Bap1* being the most commonly altered gene in

human MPM (Bott et al., 2011; Bueno et al., 2016), show enrichment in the molecular and gene expression profile of the human disease, induce MPM upon pleural transplantation in mice and are actionable by inhibition of *KRAS*.

Therefore, our study proves the presence of a distinct molecular subset of *KRAS*-driven MPM patients, establishes novel conditional mouse models of both epithelioid and biphasic subtype with accompanying effusion for further interrogation of *KRAS* implications in MPM pathogenesis, develops three novel MPM cell lines and identifies *KRAS* as an actionable target that warrants application in clinical trials for the development of more personalized treatment approaches for this previously underestimated molecular group of patients.

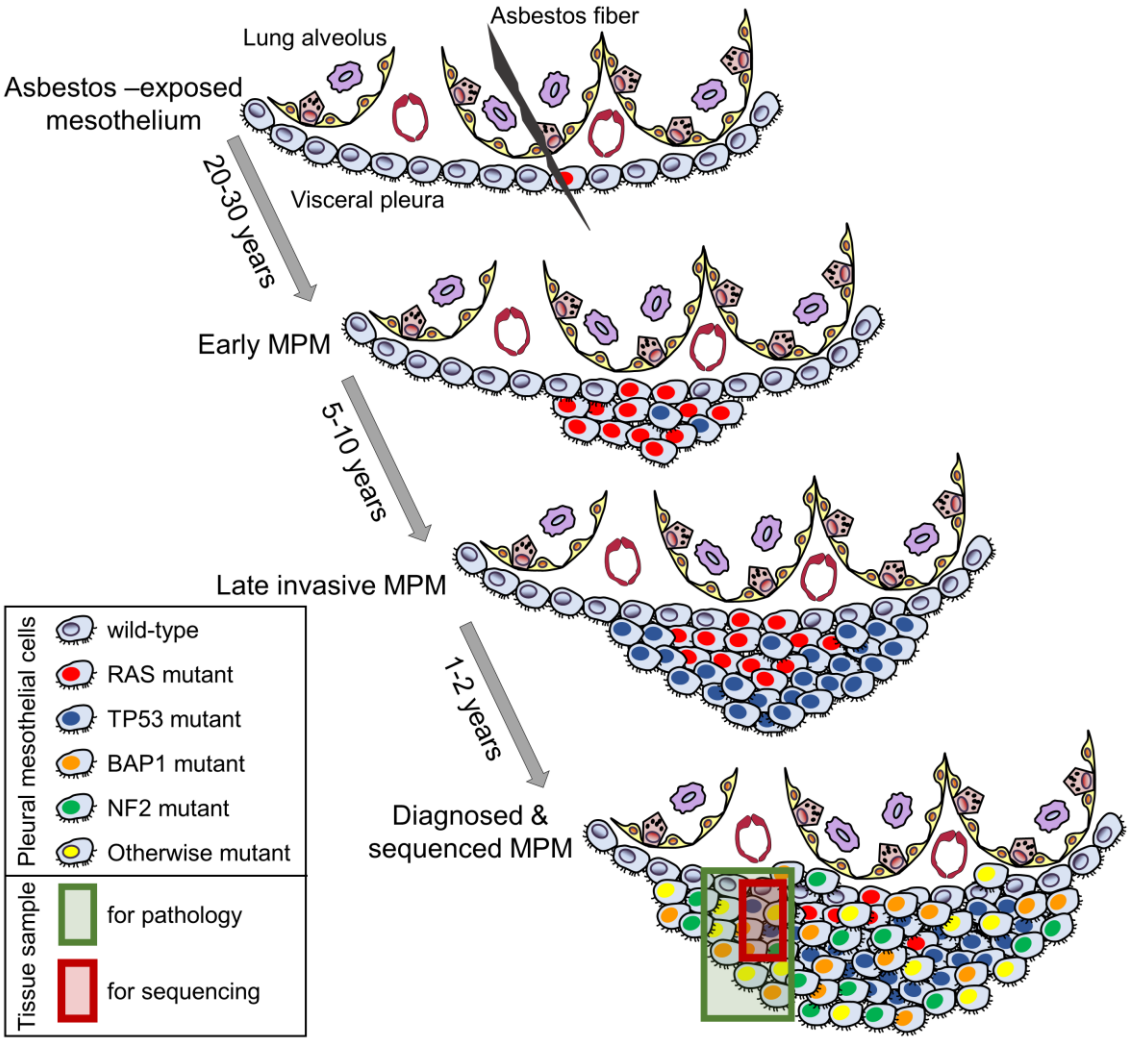

Figure 2: Schematic representation of scenarios for missing of KRAS pathway alterations by next generation sequencing studies via sampling and allelic frequency bias.

KRAS alterations, alone or in accomplice with TP53 alterations, potentially have an essential but underestimated tumor initiating role in MPM. The low allelic frequency of *KRAS* alterations due to their heterozygotic nature, in combination with their persistence at a subclonal level, with the accumulation of various secondary non-driver mutations like *Bap1* or *Nf2*, justifies the sampling bias and the insensitivity of next generation sequencing studies for their detection.

3. Paper I

Article

SOURCE DATA | TRANSPARENT PROCESS | OPEN ACCESS

EMBO Molecular Medicine

KRAS signaling in malignant pleural mesothelioma

Antonia Marazioti[1,2,†], Anthi C Krontira[2,†], Sabine J Behrend[1,3,†], Georgia A Giotopoulou[1,2,3,†], Giannoula Ntaliarda[2,†], Christophe Blanquart[4], Hasan Bayram[5,6], Marianthi Iliopoulou[2], Malamati Vreka[1,2,3], Lilith Trassl[1,3], Mario A A Pepe[1,3], Caroline M Hackl[1,3], Laura V Klotz[1,3], Stefanie A I Weiss[1,3], Ina Koch[3,7], Michael Lindner[3,7], Rudolph A Hatz[3,7], Juergen Behr[3,8], Darcy E Wagner[1,3,9], Helen Papadaki[10], Sophia G Antimisiaris[11,12], Didier Jean[13], Sophie Deshayes[4], Marc Grégoire[4], Özgecan Kayalar[6], Deniz Mortazavi[6], Şükrü Dilege[14], Serhan Tanju[14], Suat Erus[14], Ömer Yavuz[14], Pınar Bulutay[15], Pınar Fırat[15], Ioannis Psallidas[2], Magda Spella[2], Ioanna Giopanou[2], Ioannis Lilis[2], Anne-Sophie Lamort[1,3,‡] & Georgios T Stathopoulos[1,2,3,*,‡]

Abstract

Malignant pleural mesothelioma (MPM) arises from mesothelial cells lining the pleural cavity of asbestos-exposed individuals and rapidly leads to death. MPM harbors loss-of-function mutations in *BAP1*, *NF2*, *CDKN2A*, and *TP53*, but isolated deletion of these genes alone in mice does not cause MPM and mouse models of the disease are sparse. Here, we show that a proportion of human MPM harbor point mutations, copy number alterations, and overexpression of *KRAS* with or without *TP53* changes. These are likely pathogenic, since ectopic expression of mutant $KRAS^{G12D}$ in the pleural mesothelium of conditional mice causes epithelioid MPM and cooperates with *TP53* deletion to drive a more aggressive disease form with biphasic features and pleural effusions. Murine MPM cell lines derived from these tumors carry the initiating $KRAS^{G12D}$ lesions, secondary *Bap1* alterations, and human MPM-like gene expression profiles. Moreover, they are transplantable and actionable by KRAS inhibition. Our results indicate that *KRAS* alterations alone or in accomplice with *TP53* alterations likely play an important and underestimated role in a proportion of patients with MPM, which warrants further exploration.

Keywords asbestos; BAP1; KRAS; NF2; TP53
Subject Categories Cancer; Respiratory System
DOI 10.15252/emmm.202013631 | Received 22 October 2020 | Revised 28 October 2021 | Accepted 15 November 2021
EMBO Mol Med (2021) e13631

Introduction

Malignant mesothelioma annually kills up to forty persons per million population worldwide (Liu *et al*, 2017; Carbone *et al*, 2019). It most commonly arises from the mesothelium of the pleural cavities that line the lungs (visceral pleura) and the interior chest wall (parietal pleura) and only occasionally from the peritoneal mesothelium (Bibby *et al*, 2016; Mutti *et al*, 2018). Human malignant pleural mesothelioma (MPM) is mainly caused by inhaled asbestos, which caused 145,235 deaths in 1990 increasing by 51% to 218,827 deaths in 2016, most of them in high-income countries (GBD 2016 Occupational Carcinogens Collaborators, 2020). However, other bioactive materials such as nanofibers can also cause mesothelioma in rodents and possibly in humans (Ryman-Rasmussen *et al*, 2009;

1 Comprehensive Pneumology Center (CPC) and Institute for Lung Biology and Disease (iLBD), Helmholtz Center Munich-German Research Center for Environmental Health (HMGU) and Ludwig-Maximilian-University (LMU) Munich, Munich, Germany
2 Laboratory for Molecular Respiratory Carcinogenesis, Department of Physiology, Faculty of Medicine, University of Patras, Rio, Greece
3 German Center for Lung Research (DZL), Gießen, Germany
4 Université de Nantes, CNRS, INSERM, CRCINA, Nantes, France
5 Department of Pulmonary Medicine, Koc University School of Medicine, Istanbul, Turkey
6 Koc University Research Center for Translational Medicine (KUTTAM), Koc University School of Medicine, Istanbul, Turkey
7 Center for Thoracic Surgery Munich, Ludwig-Maximilian-University (LMU) Munich and Asklepios Medical Center, Gauting, Germany
8 Department of Medicine V, University Hospital, Ludwig-Maximilian-University (LMU) Munich, Munich, Germany
9 Lung Bioengineering and Regeneration, Department of Experimental Medical Sciences, Lund Stem Cell Center, Wallenberg Molecular Medicine Center, Faculty of Medicine, Lund University, Lund, Sweden
10 Department of Anatomy, Faculty of Medicine, University of Patras, Rio, Greece
11 Laboratory for Pharmaceutical Technology, Department of Pharmacy, School of Health Sciences, University of Patras, Rio, Greece
12 Foundation for Research and Technology Hellas, Institute of Chemical Engineering, FORTH/ICE-HT, Rio, Greece
13 Centre de Recherche des Cordeliers, INSERM, Sorbonne Université, Université de Paris, Functional Genomics of Solid Tumors, Paris, France
14 Department of Thoracic Surgery, Koc University School of Medicine, Istanbul, Turkey
15 Department of Pathology, Koc University School of Medicine, Istanbul, Turkey
*Corresponding author. Tel: +49 (89) 3187 1194; Fax: +49 (89) 3187 4661; E-mail: stathopoulos@helmholtz-muenchen.de
†These authors contributed equally to this work as first authors
‡These authors contributed equally to this work as senior authors

Nagai *et al*, 2011). MPM manifests with or without a malignant pleural effusion (MPE), that is, exudative fluid accumulation that causes chest pain and dyspnea, and is histologically classified into epithelioid, sarcomatoid, or biphasic subtypes (Scherpereel *et al*, 2010; Galateau-Salle *et al*, 2016; Thomas *et al*, 2017; Paajanen *et al*, 2018). The disease progresses relentlessly despite contemporary combination therapies, with a median survival of mere 9–18 months (Zalcman *et al*, 2016; Yap *et al*, 2017; Scherpereel *et al*, 2018; Courtiol *et al*, 2019). The clinicopathologic manifestation of MPM at diagnosis impacts patient survival, with advanced stage, sarcomatoid histologic subtype, poor physical performance status, elevated numbers of peripheral blood leucocytes, male sex, uncontrolled pleural effusion, and other factors portending dismal prognosis (Fennell *et al*, 2005; Tsao *et al*, 2009; Pass *et al*, 2016; Rusch *et al*,

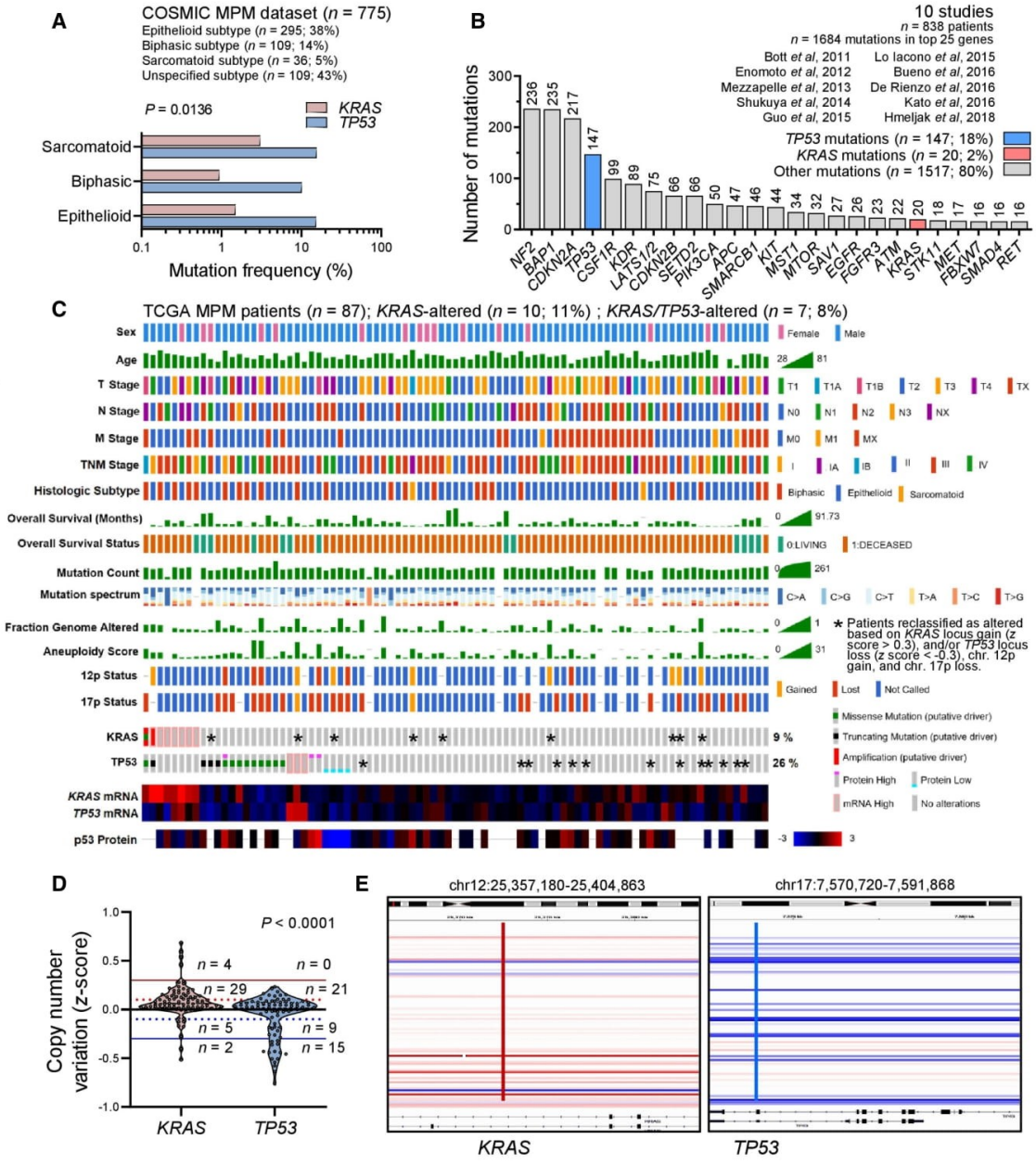

Figure 1.

Figure 1. *KRAS* alterations in human MPM from published datasets and the cancer genome atlas (TCGA) pan-cancer MPM cohort.

A *KRAS* and *TP53* mutation frequencies in MPM from the catalogue of somatic mutations in cancer (COSMIC) stratified by histologic subtype (n = 775 patients).

B Top 25 mutated genes from 10 molecular studies of human MPM (n = 838 patients).

C–E *KRAS* and *TP53* alterations in the cancer genome atlas (TCGA) pan-cancer MPM dataset (n = 86 patients). Shown are clinical and molecular data plot with alteration frequencies (C) and patients reclassified as *KRAS*- or *TP53*-altered (asterisks), copy number variation data summary (D), and segments of the *KRAS* and *TP53* loci (E).

Data information: In (A), data are presented as cumulative percentages of patients tested mutant respective to patients tested for every gene. *P*, overall probability, two-way ANOVA. In (B), data are presented as cumulative numbers (n; numbers above bars) and percentages (%) of patients with *KRAS* (red bar), *TP53* (blue bar), and other (gray bars) mutations. In (C), each column represents one patient and each row one clinical or molecular feature. Asterisks indicate *KRAS* and *TP53* alterations not identified by the TCGA, but reclassified as altered in this study due to 12p gain, 17p loss, *KRAS* locus gain ($z > 0.3$), and/or *TP53* locus loss ($z < -0.3$). In (D), data are presented as raw data points (circles), rotated kernel density distributions (violins), and patient numbers (n) between thresholds of normal (solid black line at $z = 0$), low amplification (dotted red line at $z = 0.1$), low loss (dotted blue line at $z = -0.1$), high amplification (solid red line at $z = 0.3$), and deep loss (solid blue line at $z = -0.3$). *P*, probability, paired Wilcoxon rank sum test. In (E), *KRAS* (red line) and *TP53* (blue line) loci segments of all 87 patients are shown. Each horizontal segment represents one patient. White and shades of red and blue indicate no change and magnitude of gain and loss, respectively.
Source data are available online for this figure.

2016; Cheah *et al*, 2017; Thomas *et al*, 2017; Kindler *et al*, 2018; Hassan *et al*, 2019).

Multiple comprehensive analyses of MPM genomes identified a mosaic mutational landscape characterized by widespread loss-of-function of tumor suppressor genes (*BAP1*, *NF2*, *CDKN2A*, *TP53*, *TSC1*, etc), sporadic gain-of-function of proto-oncogenes (*PIK3CA*, *EGFR*, *KRAS*, *NRAS*, *HRAS*, *BRAF*, etc), and inconclusive addiction/exclusion patterns thereof (Bott *et al*, 2011; Enomoto *et al*, 2012; Mezzapelle *et al*, 2013; Shukuya *et al*; 2014; Guo *et al*, 2015; Lo Iacono *et al*, 2015; Bueno *et al*, 2016; De Rienzo *et al*, 2016; Kato *et al*, 2016; Hmeljak *et al*, 2018). Interestingly, KRAS proto-oncogene GTPase (*KRAS*) alterations were detected more frequently using targeted compared with massive parallel sequencing approaches by the studies above. In addition, *NF2* mutations that cause persistent KRAS signaling (Tikoo *et al*, 1994), as well as *BAP1* and *CDKN2A* mutations that are functionally related with *TP53* loss-of-function (Stott *et al*, 1998; Arizti *et al*, 2000; Bi *et al*, 2016), are very common in MPM. *KRAS* mutations have also been shown to activate the *TP53* cell cycle checkpoint (Matallanas *et al*, 2011). In addition to clinicopathologic presentation, MPM mutations also impact prognosis, with *TP53* and *CDKN2A* loss-of-function occurring more frequently in non-epithelioid MPM and portending poor survival (Bott *et al*, 2011; Yap *et al*, 2017).

There is an unmet clinical need for mouse models that recapitulate the mutation spectrum and clinicopathologic manifestations of human MPM. In this regard, MPM cell lines for transplantable models, asbestos-induced mouse models, and genetic models of the disease are characterized by scarcity, limited availability, and significant difficulty of implementation (Ikediobi *et al*, 2006; Fridlender *et al*, 2009; Forbes *et al*, 2015; Agalioti *et al*, 2017). Interestingly, standalone mesothelial loss-of-function of *BAP1*, *NF2*, *CDKN2A*, *TP53*, and *TSC1* is not sufficient to cause MPM in mice, rendering the drivers of the disease resistant to functional validation (Jongsma *et al*, 2008; Guo *et al*, 2014; Menges *et al*, 2014; Xu *et al*, 2014; Kukuyan *et al*, 2019). Moreover, faithful models of MPM are urgently needed, as most existing studies have focused on the rare

Figure 2. KRAS pathway activation in MPM from the cancer genome atlas (TCGA) pan-cancer MPM dataset.

A–F Molecular and clinical features of the cancer genome atlas (TCGA) pan-cancer MPM patients (n = 87) stratified by the presence of *KRAS* standalone (n = 10) and combined *KRAS*/*TP53* (n = 7) alterations. Shown are unsupervised hierarchical clustering of n = 86 patients (gene expression data were not available for one patient) by 40 genes significantly overexpressed in *KRAS*/*TP53*-altered over *KRAS*-altered over *KRAS*/*TP53*-normal patients (A) and data summaries of mononucleotide change signatures (B), of indices of genomic instability and mutation burden (C), of clinical features and *KRAS*/*TP53*/*NF2* co-mutation frequency (D, E), and of overall survival (F).

G KRAS/TP53 pathway adapted from Matallanas *et al* (2011) and Tikoo *et al* (1994). Color-coded genes were identified by TCGA and PANTHER pathway analyses.

H, I PANTHER and Reactome KRAS and TP53 pathways significantly altered in the cancer genome atlas (TCGA) pan-cancer MPM patients. Shown are volcano plot of fold-enrichment versus $-\log_{10}$(probability) (H), and data summary of fold-enrichment of KRAS and TP53 versus all other pathways with fold-enrichment > 0.5 (I).

Data information: In (A), data are presented as heatmap of 40 differentially expressed genes (rows) in 86 individual patients (columns), color code of unsupervised hierarchical clusters, *KRAS*/*TP53* status, and heatmap (legend), and probabilities (*P*) for enrichment of *KRAS*- and *KRAS*/*TP53*-altered patients in cluster 1. The scale bar represents the color-coded z-scores. In (B), data are presented as heatmap of six different possible mononucleotide changes (rows) in patients grouped by *KRAS*/*TP53* status (columns) and color code of mean mutation number (legend). ****, FDR $q < 2 \times 10^{-7}$ compared with all other mononucleotide changes, 2-way ANOVA with Benjamini, Krieger, and Yekutieli two-stage linear step-up procedure. In (C) and (I), data are presented as raw data points (circles), rotated kernel density distributions (violins), medians (solid lines), and quartiles (dotted lines). *P*, overall probability, Kruskal–Wallis test. (C): * and **: $P < 0.05$ and $P < 0.01$, respectively, compared with *KRAS*/*TP53*-normal patients, Dunn's post-tests. (I): ** and ****: $P < 0.01$ and $P < 0.0001$, respectively, compared with other pathways, Dunn's post-tests. In (D) and (E), data are presented as patient numbers (n) and overall probability (*P*) by χ^2 or Kruskal–Wallis tests (D) or hypergeometric test for enrichment of *KRAS* mutations in *TP53*-altered or biphasic MPM (E). In (F), data are presented as sample size (n), Kaplan–Meier survival estimates (lines), censored observations (line marks), log-rank *P* value, and hazard ratio (HR) with 95% confidence interval (95% CI). In (H), data are presented as color-coded individual pathways (circles), threshold of significance (horizontal dotted line), no enrichment baseline reference (vertical dotted line), and selected pathway names and codes. P and R initials in pathway codes denote PANTHER and Reactome pathways, respectively. n, sample size; FDR q, probability, false discovery rate; ΔGE, differential gene expression.
Source data are available online for this figure.

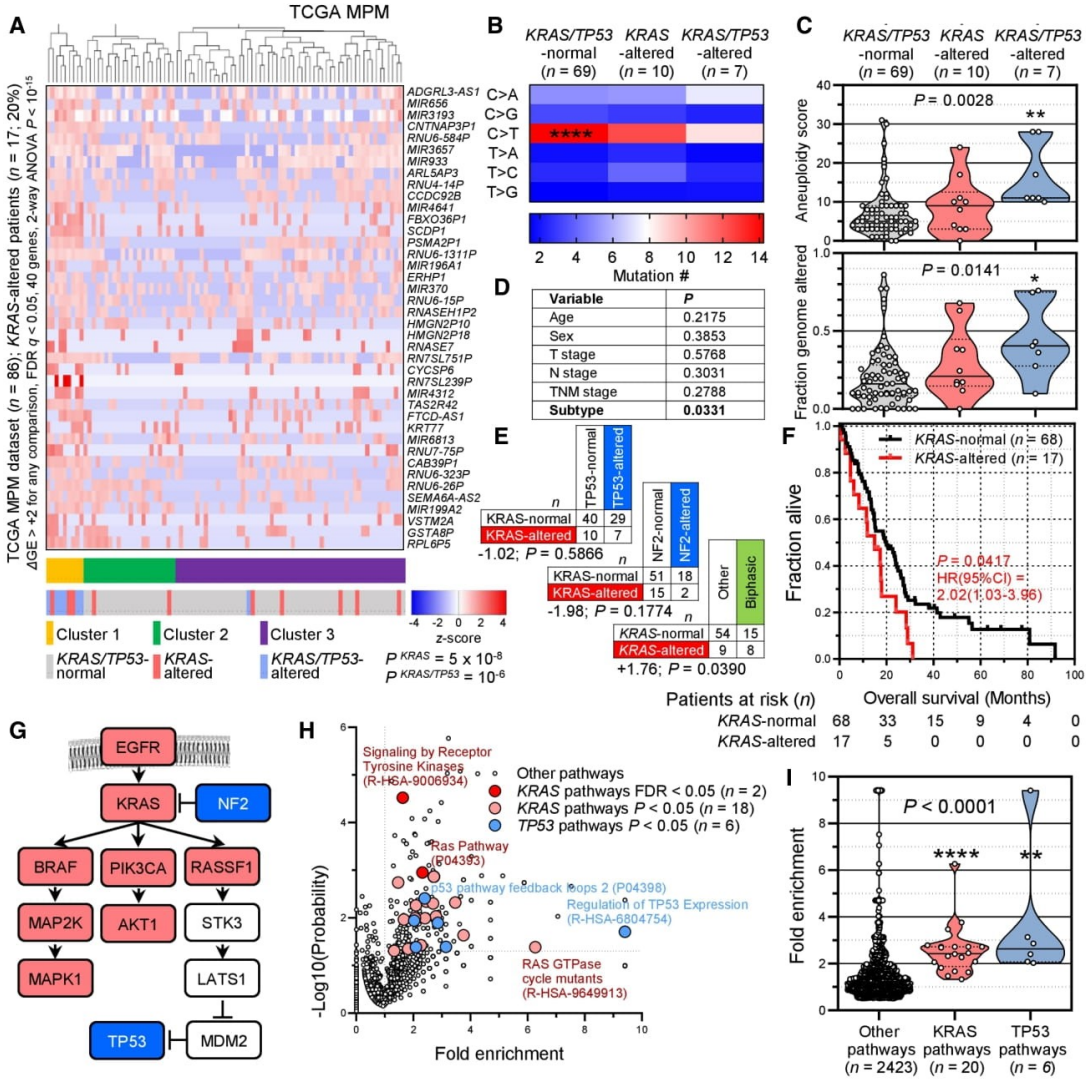

Figure 2.

peritoneal disease and only one elegant study targeted *NF2/CDKN2A/TP53* deletions to the pleural mesothelium (Jongsma *et al*, 2008). Such mouse models would represent different molecular subtypes of MPM, would have high penetrance, and would also be specific for MPM with or without MPE development.

Based on our previous observation of a $Kras^{G12C}$ mutation (*Kras*, *Mus musculus* Kirsten rat sarcoma viral oncogene homolog) in an asbestos-induced murine MPM cell line (Agalioti *et al*, 2017; Marazioti *et al*, 2018), on published work that showed RAS pathway activation in MPM (Patel *et al*, 2007), and on the functional interconnection between mutant *KRAS* and *TP53* signaling (Matallanas *et al*, 2011), we hypothesized that *KRAS* alterations are involved in MPM development, alone or in accomplice with *TP53* alterations. Indeed, here we query the TCGA MPM dataset and employ sensitive methods in our own clinical cohorts to discover *KRAS* and *TP53* alterations in a subset of patients with MPM. We further show that targeting oncogenic $KRAS^{G12D}$ alone to the murine pleural mesothelium causes MPM and, when combined with *Trp53* deletion, triggers aggressive MPM with MPE. Murine MPM is shown to carry the initiating $KRAS^{G12D}$ mutations, to harbor *Bap1* inactivating mutations, to be transmissible to naïve mice, and to resemble the molecular signatures of human MPM. Hence, *KRAS* mutations are implicated in MPM pathobiology, the contributions of *TP53* in shaping the disease's manifestations are described, and new mouse models are provided for the study of the biology and therapy of a molecular subclass of MPM that is driven by *KRAS* signaling.

Results

KRAS and *TP53* alterations in human MPM

In MPM from the catalogue of somatic mutations in cancer (COSMIC; Forbes *et al*, 2015), *KRAS* and *TP53* mutation frequencies of 1–3% and 10–20%, respectively, were evident (Fig 1A; dataset available at https://cancer.sanger.ac.uk/cosmic/browse/tissue?wgs=off&sn=pleura&ss=all&hn=mesothelioma&sh=&in=t&src=tissue&all_data=n). *KRAS* and *TP53* mutations comprised, respectively, 2 and 18% of all mutated genes in a dataset composed of 10 large MPM studies (Bott *et al*, 2011; Enomoto *et al*, 2012; Mezzapelle *et al*, 2013; Shukuya *et al*, 2014; Guo *et al*, 2015; Lo Iacono *et al*, 2015; Bueno *et al*, 2016; De Rienzo *et al*, 2016; Kato *et al*, 2016; Hmeljak *et al*, 2018) (Fig 1B). The aforementioned analysis consisted of manual curation of the main and supplementary data, while the latter study, the cancer genome atlas (TCGA) pan-cancer MPM dataset (n = 86 patients; Hmeljak *et al*, 2018) available at https://www.cbioportal.org/study/summary?id=meso_tcga_pan_can_atlas_2018 (Cerami *et al*, 2012), was analyzed in detail, via a systematic query of mutations, copy number alterations, and mRNA and protein expression of *KRAS* and *TP53*. According to TCGA criteria, eight patients showed alterations in *KRAS* two of which had dual *KRAS/TP53* changes. However, when copy number alterations (CNA) at the *KRAS*12p12.1 (position chr12:25,357,180–25,404,863) and *TP53* 17p13.1 (position chr17:7,570,720–7,591,868) loci were scrutinized using integrative genomics viewer (Robinson *et al*, 2011), additional high *KRAS* gains were discovered in nine and deep *TP53* losses in 13 patients, with five patients harboring changes in both genes (Fig 1C–E). For this, *KRAS* locus gain ($z > 0.3$) and/or *TP53* locus loss ($z < -0.3$), as well as chromosome 12p gains and 17p losses, were taken into account (Smith & Sheltzer, 2018). Hence, a *KRAS* alteration alone was determined in n = 10 patients (12%) and a combined *KRAS/TP53* alteration in n = 7 (8%), for a total *KRAS* alteration rate of 20%.

We subsequently examined the transcriptomes of TCGA MPMs (available at https://xenabrowser.net/datapages/?dataset=TCGA-MESO.htseq_fpkm-uq.tsv&host=https%3A%2F%2Fgdc.xenahubs.net&removeHub=https%3A%2F%2Fxena.treehouse.gi.ucsc.edu%3A443) stratified by the presence of a *KRAS* alteration alone (n = 10), a combined *KRAS/TP53* alteration (n = 7), or none of the above (n = 69). Forty genes were biologically and statistically significantly overrepresented in *KRAS/TP53*-altered over *KRAS*-altered over normal patients, which were able to cluster patients by genetic alteration in an unsupervised hierarchical fashion (Fig 2A). *KRAS/TP53*-altered patients showed loss of a C>T mononucleotide signature that preponderated in *KRAS/TP53*-normal patients and displayed higher aneuploidy and genome alteration indices (Figs 2B and C). *KRAS* and *TP53* alterations were co-occurring at a rate expected by chance, while *KRAS*-altered patients displayed a non-significant repulsion of *NF2* mutations, a statistically significant preponderance of biphasic histology, and significantly worse prognosis (Figs 2D–F). Interestingly, when all mutated genes from this cohort were entered into the Protein Analysis Through Evolutionary Relationships System (PANTHER; http://www.pantherdb.org/), multiple KRAS and TP53 signaling pathways were biologically and statistically significantly enriched in MPM, which, together with the *KRAS-NF2* repulsion described above, aligned along a biological KRAS-TP53 pathway proposed elsewhere (Tikoo *et al*, 1994; Matallanas *et al*, 2011) (Fig 2G–I). Our results were concordant with the TCGA pan-cancer pathway analysis that reported 9 and 21% alteration frequencies of the RTK/RAS and p53 pathways in MPM (Sanchez-Vega *et al*, 2018). Hence, we describe a molecular subclass of MPM patients in the TCGA dataset that involves ~ 20% of patients, which harbor *KRAS* gain-of-function with or without *TP53* loss-of-function. This molecular MPM subset features KRAS pathway activation, different mutation spectra, gene expression profiles, histology, and survival compared to other MPMs.

To further test this, we interrogated *KRAS* and *TP53* in our MPM patients, whose clinical characteristics are given in Appendix Table S1. We employed digital droplet polymerase chain reaction (ddPCR) in order to detect *KRAS* codon 12/13 and 61 mutations, as well as *TP53* CNA in pleural fluid and cell pellets of 45 patients with pleural effusions from our cohorts in Munich, Germany (Klotz *et al*, 2019a, 2019b). The effusions were caused

Figure 3. *KRAS* and *TP53* alterations in human MPM from Germany and human MPM cell lines from France.

A–D Pleural fluid cell pellets and supernatants from 45 patients (called ASK #) with pleural effusion from Munich, Germany (Klotz *et al*, 2019a, 2019b), were subjected to digital droplet polymerase chain reaction (ddPCR) for the detection of mutant (^{MUT}) copies of *KRAS* codon 12/13 ($KRAS^{G12/13}$) and *KRAS* codon 61 ($KRAS^{Q61}$), as well as copies of *TP53* and *TERT*. Diagnoses were benign pleural effusion (n = 5), lung adenocarcinoma (LUAD; n = 16), MPM (n = 12), and other extrathoracic cancers (n = 12). The assays were designed for detection of down to 1:20,000 copies using EKVX ($KRAS^{WT}TP53^{G610T}$), A549 ($KRAS^{G12S}TP53^{WT}$), NCI-H460 ($KRAS^{Q61H}TP53^{WT}$), NCI-H3122 ($KRAS^{WT}TP53^{E285V}$), and NCI-H3255 ($KRAS^{WT}TP53^{G560\text{-}1A}$) human LUAD cells as controls. Shown are individual patient (*KRAS* plot) and individual sample (*TP53* plot) allelic frequencies with color code and limits of normal *TP53* allelic frequency as vertical dashed lines in the *TP53* plot (A), representative gated dotplots of codon 12/13 *KRAS* ddPCR (B) and *TP53*/*TERT* (C), and results summary table (D). Any number of *KRAS*-mutant droplets detected in any sample (*KRAS* plot in A) and any patient that failed to achieve normal *TP53* ploidy by any sample (*TP53* plot in A) was deemed altered.

E–G Results summary (E), representative *KRAS* CNA segments (F), and data summary of individual cell line CNA z-score (G) from Affymetrix CytoScanHD Arrays of 33 primary MPM cell lines (called MESO #) from Nantes, France (GEO dataset GSE134349). Red lines denote the KRAS locus on chromosome 12p12.1.

H Data summary of mutant allelic frequency of *KRAS* compared with *NF2* and *BAP1* in all mutated samples from (A–G).

Data information: In (A), data are presented as data summary of the highest mutant copy percentage detected per individual sample (*KRAS* plot) or of all individual samples assessed (*TP53* plot). In (D), data are presented as number of patients (n). P, probability, hypergeometric test for enrichment of *KRAS* mutations in MPM versus other tumors. In (E), data are presented as individual cell lines (columns), genes (rows), legend, and number of patients (n in table). P, probability, hypergeometric test for enrichment of *KRAS* mutations in *TP53*-mutant MPM. In (G), data are presented as raw data points (circles), rotated kernel density distribution (violins), and cell line numbers (n) outside thresholds of amplification (dotted red line at 2.3) and loss (solid blue line at 1.7). P, probability, paired Wilcoxon rank sum test. In (H), data are presented as raw data points (circles), rotated kernel density distributions (violins), and medians (lines). P, overall probability, one-way ANOVA. * and **: $P < 0.05$ and $P < 0.01$, respectively, compared with *KRAS*, Tukey's post-test.
Source data are available online for this figure.

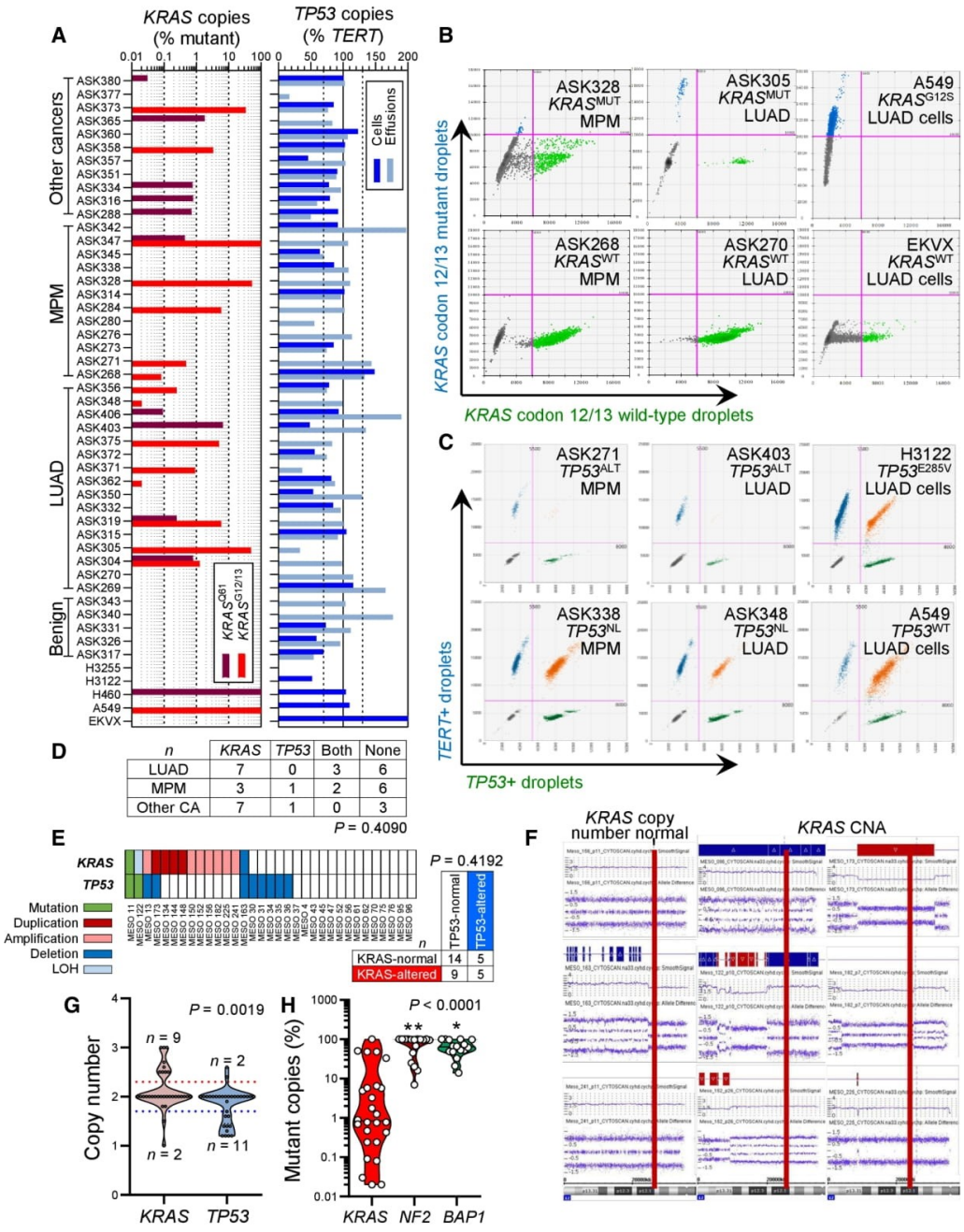

Figure 3.

from benign etiologies (n = 5), MPM (n = 12), metastatic lung adenocarcinoma (LUAD; n = 16), or metastatic other bodily tumors (n = 12). The assays were designed for the detection of down to 1:20,000 mutant (^{MUT}) or wild-type (^{WT}) copies. We detected standalone *KRAS* mutations and combined *KRAS*/*TP53* alterations in three and two of our 12 patients with MPM, respectively (Fig 3A–C). *KRAS* and *TP53* alterations co-occurred at a rate expected by chance (Fig 3D). We next used sensitive Affymetrix CytoScanHD

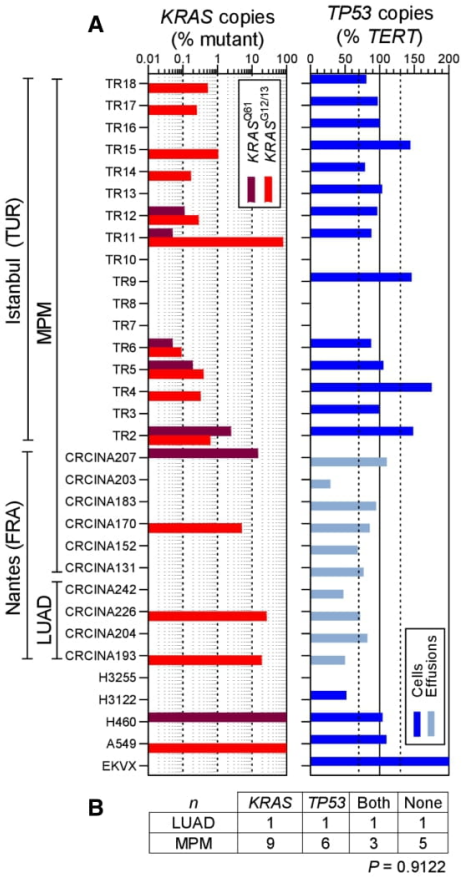

Figure 4. *KRAS* and *TP53* alterations in MPM patients from France and Turkey.

A, B Pleural fluid cell pellets and supernatants from 10 patients (called CRCINA #) with pleural effusion from Nantes, France (Gueugnon *et al*, 2011; Smeele *et al*, 2018), and pleural tumor samples from 17 patients (called TR#) with MPM from Istanbul, Turkey, were subjected to digital droplet polymerase chain reaction (ddPCR) for the detection of mutant (^{MUT}) copies of *KRAS* codon 12/13 ($KRAS^{G12/13}$) and *KRAS* codon 61 ($KRAS^{Q61}$), as well as copies of *TP53* and *TERT*. Diagnoses were lung adenocarcinoma (LUAD; n = 4) and MPM (n = 23). The assays were designed for detection of down to 1:20,000 copies using EKVX ($KRAS^{WT}TP53^{G610T}$), A549 ($KRAS^{G12S}TP53^{WT}$), NCI-H460 ($KRAS^{Q61H}TP53^{WT}$), NCI-H3122 ($KRAS^{WT}TP53^{E285V}$), and NCI-H3255 ($KRAS^{WT}TP53^{G560\text{-}1A}$) human LUAD cells as controls. Shown are individual patient (*KRAS* plot) and individual sample (*TP53* plot) allelic frequencies with color code and limits of normal *TP53* allelic frequency as vertical dashed lines in the *TP53* plot (A) and results summary table (B). Any number of *KRAS*-mutant droplets detected in any sample (*KRAS* plot in A) and any patient that failed to achieve normal *TP53* ploidy by any sample (*TP53* plot in A) was deemed altered.

Data information: In (A), data are presented as data summary of the highest mutant copy percentage detected per individual sample (*KRAS* plot) or of all individual samples assessed (*TP53* plot). In (B), data are presented as number of patients (n). P, probability, χ^2 test.
Source data are available online for this figure.

Arrays utilizing 2.67 million markers and targeted next-generation sequencing to identify *KRAS* and *TP53* alterations in a cohort of 33 primary MPM cell lines from Nantes, France (GEO dataset GSE134349; Gueugnon *et al*, 2011; Data ref: Blanquart *et al*, 2019; Delaunay *et al*, 2020; Quetel *et al*, 2020) The clinical characteristics of the cell line donors are given in Appendix Table S2. We detected standalone *KRAS* and combined *KRAS*/*TP53* alterations in nine and five cell lines, respectively, and *KRAS* and *TP53* alterations again co-occurred at a rate expected by chance (Fig 3E). In addition, the *KRAS* and *TP53* loci were statistically significantly amplified and deleted, respectively, across all cell lines irrespective of genotype (Fig 3F and G). Interestingly, 80% of the samples with $KRAS^{MUT}$ copies from both studies displayed low mutant copy numbers (< 10%) that would be likely missed by other techniques with lower read depths or stringent detection thresholds (Fig 3H). We also tested a patient with MPM from the Malignancy of Pleural Effusions in the Emergency Department (MAPED; ClinicalTrials.gov # NCT03319472) Study (preprint: Marazioti *et al*, 2021) for *KRAS* and *TP53* status by Sanger sequencing, RT–PCR, and qPCR. We found four different KRAS point mutations in this patient, as well as discrepant *TP53* expression levels by RT–PCR and qPCR, strongly indicative of a *TP53* mutation (Fig EV1). To obtain definitive validation, we finally examined by ddPCR for *KRAS* codon 12/13 and 61 mutations, as well as *TP53* CNA, additional six MPM-associated MPE samples from Nantes (Gueugnon *et al*, 2011; Smeele *et al*, 2018) and 17 MPM tumor samples from Istanbul, Turkey (patients' clinical characteristics are given in Appendix Table S3). Indeed, we found that nine patients had standalone KRAS mutations, whereas another three had combined *KRAS*/*TP53* alterations (Fig 4A and B). Taken together, we examined 36 human tumor/effusion samples from four countries to find standalone *KRAS* alterations in 12 (33%) and combined *KRAS*/*TP53* alterations in 6 (17%) patients. These results indicate that a molecular subset of MPM that is driven by *KRAS* with/without *TP53* alterations indeed exists outside the TCGA cohort.

MPM in mice expressing mesothelial-targeted $KRAS^{G12D}$

To functionally validate *KRAS* mutations in MPM, we targeted transgenes to mesothelial surfaces using type 5 adenoviral vectors (Ad). For this, *mT*/*mG* CRE-reporter mice that switch from somatic cell membranous tomato (mT) to green fluorescent protein (mG) expression upon *Cre*-mediated recombination (Muzumdar *et al*, 2007) received 5×10^8 plaque-forming units (PFU) intrapleural Ad encoding *Melanotus* luciferase (Ad-*Luc*) or *Cre* recombinase (Ad-*Cre*) followed by serial bioluminescence imaging. Ad-*Luc*-treated mice developed intense bilateral chest light emission (mice lack mediastinal separations; Stathopoulos *et al*, 2006) that peaked at 4–7 and subsided by 14 days post-injection (Fig EV2A). At this time point, when transient Ad-*Luc* expression ceased and therefore maximal Ad-*Cre*-mediated recombination was achieved, Ad-*Cre*-treated mice displayed widespread recombination of the pleural mesothelium even in contralateral pleural fissures, but not of the lungs, chest wall, or pleural immune cells (Fig EV2B–E). Similar results were obtained from intraperitoneal 5×10^8 PFU Ad-*Cre*-treated *mT*/*mG* mice after 2 weeks (Fig EV2F). Importantly, Ad-*Cre* did not cause inflammation in wild-type (*Wt*) mice, as evident by imaging and cellular analyses of luminescent bone marrow chimeras used as real-time myeloid tracers

(Cao *et al*, 2004; Giannou *et al*, 2015; Agalioti *et al*, 2017; Fig EV3). These results show that intraserosal Ad-*Cre* treatment efficiently and specifically recombines mesothelial surfaces *in vivo*.

To test whether oncogenic *KRAS* can cause MPM, *Wt* mice and mice carrying conditional *KRAS*^{G12D} and/or *Trp53f/f* alleles expressed or deleted, respectively, upon *Cre*-mediated recombination (Marino *et al*, 2000; Jackson *et al*, 2001; Meylan *et al*, 2009) received 5 × 10^8 PFU intrapleural Ad-*Cre* and were longitudinally followed and sampled (Fig 5A–F). *Wt*, *Trp53f/Wt*, and *Trp53f/f* mice survived up to 16 months post-Ad without clinical or pathologic disease manifestations (median survival undefined). In contrast, *KRAS*^{G12D} mice developed cachexia and succumbed by 6–12 months post-injection (median [95% CI] survival = 339 [285–379] days; P = 0.005 compared with controls, log-rank test). At necropsy, no pleural fluid or inflammatory cell accumulation was evident, but diffuse visceral and parietal pleural nodular and peel-like lesions were found in all mice. These lesions expressed proliferating cell nuclear antigen (PCNA) unlike the normal pleura and were diagnosed by a board-certified pathologist as epithelioid MPM (Fig 5G). In addition, chimeric *KRAS*^{G12D} recipients adoptively transplanted with luminescent bone marrow revealed an early pleural inflammatory infiltrate composed of CD11b$^+$Gr1$^+$ myeloid cells at

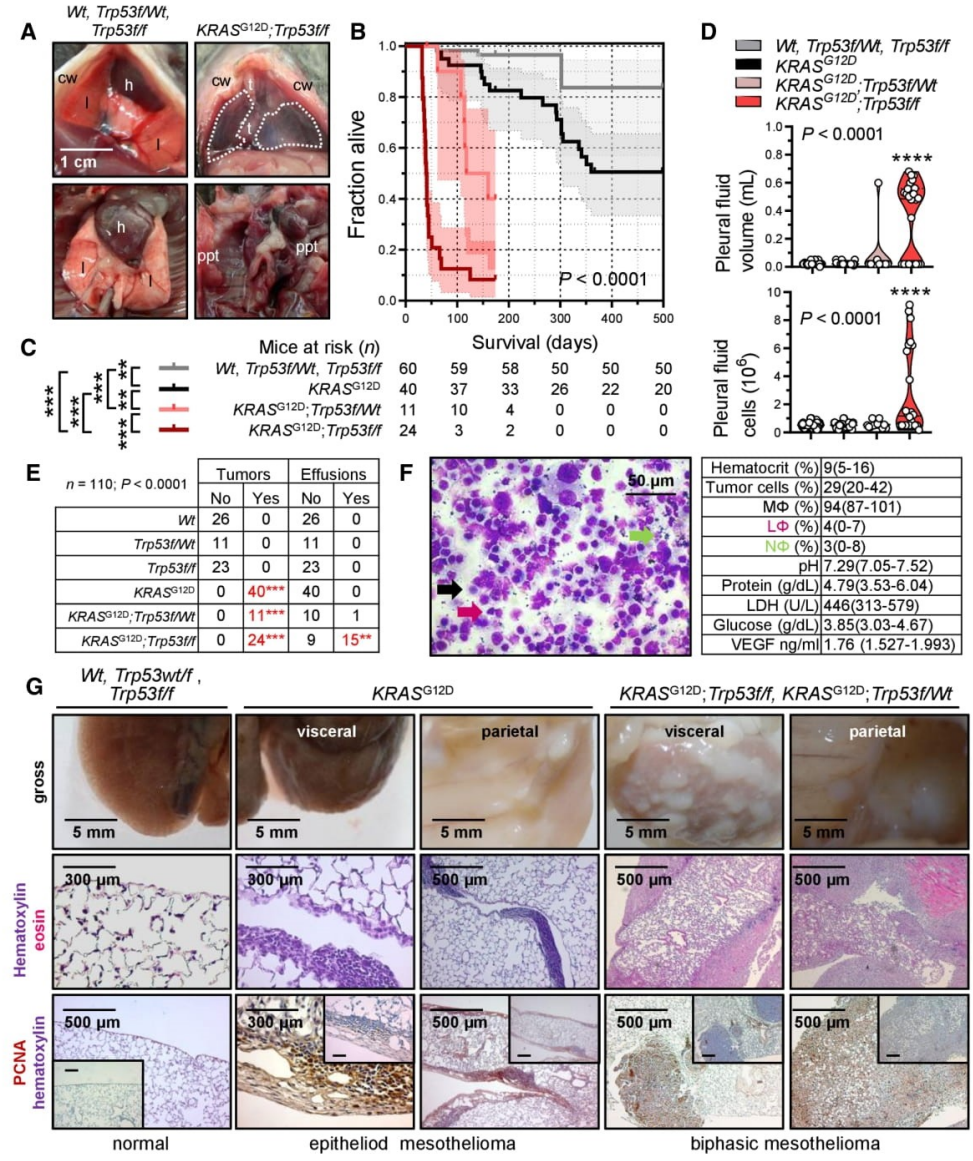

Figure 5.

Figure 5. Human-like malignant pleural mesotheliomas and effusions of mice with pleural mesothelial-targeted oncogenic *KRAS*^{G12D} and/or *Trp53* deletion.

Wild-type (*Wt*), *KRAS*^{G12D}, and *Trp53f/f* mice (all *C57BL/6*) were intercrossed and all possible offspring genotypes received 5 × 10^8 PFU intrapleural Ad-*Cre* (*n* is given in survival table in [C]).

A Representative photographs of the thorax before (top) and after (bottom) chest opening (t, tumors; l, lungs; cw, chest wall; h, heart; dashed lines, effusion; ppt, parietal pleural tumors).
B Kaplan–Meier survival plot.
C Survival table.
D Data summary of pleural effusion volume and nucleated cells (*n* is given in table in [C]).
E Incidence of pleural tumors and effusions.
F Representative May–Gruenwald–Giemsa-stained pleural fluid cytocentrifugal specimen from a *KRAS*^{G12D};*Trp53f/f* mouse showing macrophages (MΦ, black arrow), lymphocytes (LΦ, purple arrow), and neutrophils (NΦ, green arrow) and summary of cellular and biochemical features of effusions of *KRAS*^{G12D};*Trp53f/f* mice (*n* = 10).
G Gross macroscopic and microscopic images of visceral and parietal tumors stained with hematoxylin and eosin or PCNA (*n* is given in table in [E]).

Data information: In (B) and (C), data are presented as Kaplan–Meier survival estimates (lines), censored observations (line marks) 95% confidence interval (shaded areas) and number of mice at risk. *P*, overall probability, log-rank test. ** and ***: $P < 0.01$ and $P < 0.001$, respectively, for the comparisons indicated, log-rank test. In (D), data are presented as raw data points (circles), rotated kernel density distribution (violins), and medians (lines). *P*, overall probability, one-way ANOVA. ****: $P < 0.0001$, for comparison with all other groups, Bonferroni post-tests. In (E), data are presented as number of mice (*n*). *P*, probability for comparison with the top-three groups, Fischer's exact test. In (F), data are presented as mean ± 95% confidence interval. *Wt*, wild-type; *KRAS*^{G12D}, Lox-STOP-Lox.*KRAS*^{G12D}; *Trp53f/f*, conditional *Trp53*-deleted; Ad, adenovirus type 5; PFU, plaque-forming units; *Cre*, CRE recombinase gene; PCNA, proliferating cell nuclear antigen; LDH, lactate dehydrogenase; ANOVA, analysis of variance; VEGF, vascular endothelial growth factor.
Source data are available online for this figure.

7–14 days post-Ad-*Cre* (Fig EV3), emulating the inflammatory response observed after pleural asbestos instillation (Nagai *et al*, 2011) that is thought to drive MPM development (Fridlender *et al*, 2009; Patil *et al*, 2018; Courtiol *et al*, 2019).

The phenotype of intrapleural Ad-*Cre*-injected *KRAS*^{G12D};*Trp53f/f* mice was fulminant, with respiratory and locomotor distress and retracted body posture culminating in death by 3–6 weeks post-Ad-*Cre* (median [95% CI] survival = 41 [38–73] days; $P < 0.001$ compared with any other genotype, log-rank test). Examination of the thorax revealed massive MPE in most and visceral/parietal pleural tumors in all mice, which invaded the lungs, chest wall, and mediastinum and uniformly presented as PCNA$^+$ biphasic MPM with mixed sarcomatoid/epithelioid features. Effusions were bloody but non-coagulating, contained abundant cancer and inflammatory cells, and had low pH and glucose and high protein, VEGF, and lactate dehydrogenase levels, resembling effusions of human advanced MPM (Robinson *et al*, 2005; Patil *et al*, 2018) and of *C57BL/6* mice injected with *KRAS*^{G12C}-mutant AE17 mesothelioma cells (Agalioti *et al*, 2017). *KRAS*^{G12D};*Trp53f/Wt* mice displayed an intermediate phenotype (median [95% CI] survival = 118 [97–160] days; $P < 0.003$ compared with any other genotype, log-rank test), biphasic histology, and a single MPE occurrence. *Wt*, *Trp53f/f*, and *KRAS*^{G12D};*Trp53f/f* mice also received 5 × 10^8 PFU intraperitoneal Ad-*Cre* (Fig EV4). Again, *Wt* and *Trp53f/f* mice displayed unlimited survival without signs of disease (median survival undefined), but K*RAS*^{G12D};*Trp53f/f* mice developed abdominal swelling and succumbed by 2–5 months post-Ad-*Cre* (median [95% CI] survival = 95 [60–123] days; $P < 0.001$ compared with controls, log-rank test). At necropsy, nodular and diffuse tumors throughout the abdominal cavity and loculated ascites with features similar to MPM with MPE were detected.

To corroborate that our mice had mesothelioma and not pleural spread of LUAD (Jackson *et al*, 2001), immunostaining for specific markers of both tumor types was performed based on expert guidelines for distinguishing human MPM from LUAD (Scherpereel *et al*, 2010; Galateau-Salle *et al*, 2016; Courtiol *et al*, 2019) and on previous published experience from mouse models (Jongsma *et al*, 2008). In parallel, LUAD of intratracheal Ad-*Cre*-treated (5 × 10^8 PFU) *KRAS*^{G12D} and of urethane-treated mice were examined (Mason *et al*, 2000; Spella *et al*, 2019). Our murine MPM displayed ubiquitous strong Wilms' tumor 1, patchy moderate vimentin, ubiquitous moderate mesothelin, ubiquitous strong calretinin/podoplanin/osteopontin, and patchy moderate cytokeratin 5/6 expression, but no evidence of surfactant protein C expression, in contrast with LUAD that expressed some of these markers and SFTPC (Fig 6), supporting that our tumors are indeed MPM of the biphasic subtype. These results show that pleural mesothelial-targeted *KRAS*^{G12D} causes epithelioid MPM in mice. Furthermore, that standalone *TP53* loss does not trigger MPM, but cooperates with mutant *KRAS* to accelerate MPM development, to promote biphasic histology, and to precipitate effusion formation.

Figure 6. Molecular phenotyping of murine mesothelioma.

Wild-type (*Wt*), *KRAS*^{G12D}, and *Trp53f/f* mice were intercrossed, and all possible offspring genotypes received 5 × 10^8 PFU intrapleural or intratracheal Ad-*Cre* and were sacrificed when moribund. In parallel, *C57BL/6* mice received 10 consecutive weekly intraperitoneal injections of 1 g/kg urethane and were sacrificed after 6 months. Data summary (heatmap) and representative images of immunoreactivity of tissue sections of pleural and pulmonary tissues and tumors from these mice for different markers of human malignant pleural mesothelioma (MPM) and lung adenocarcinoma (LUAD). *n* = 10 mice/group were analyzed for each marker. Brown color indicates immunoreactivity and blue color nuclear hematoxylin counterstaining. Note the ubiquitous strong expression of Wilms' tumor 1 (WT1), patchy moderate expression of vimentin (VIM), ubiquitous moderate expression of mesothelin (MSLN), ubiquitous strong expression of calretinin (CALB2), podoplanin (PDPN), and osteopontin (SPP1), patchy moderate expression of cytokeratin 5/6 (CK5/6), and the absence of expression of surfactant protein C (SFTPC) in murine *KRAS*-driven mesotheliomas. Note also the ubiquitous strong expression of WT1, the patchy moderate expression of VIM, the ubiquitous low-level expression of MSLN, the ubiquitous strong expression of CALB2 and SPP1, the ubiquitous low-level expression of PDPN, the variable moderate expression of CK5/6, and the ubiquitous moderate expression of SFTPC in murine *KRAS*^{G12D}-driven and urethane-induced LUAD.

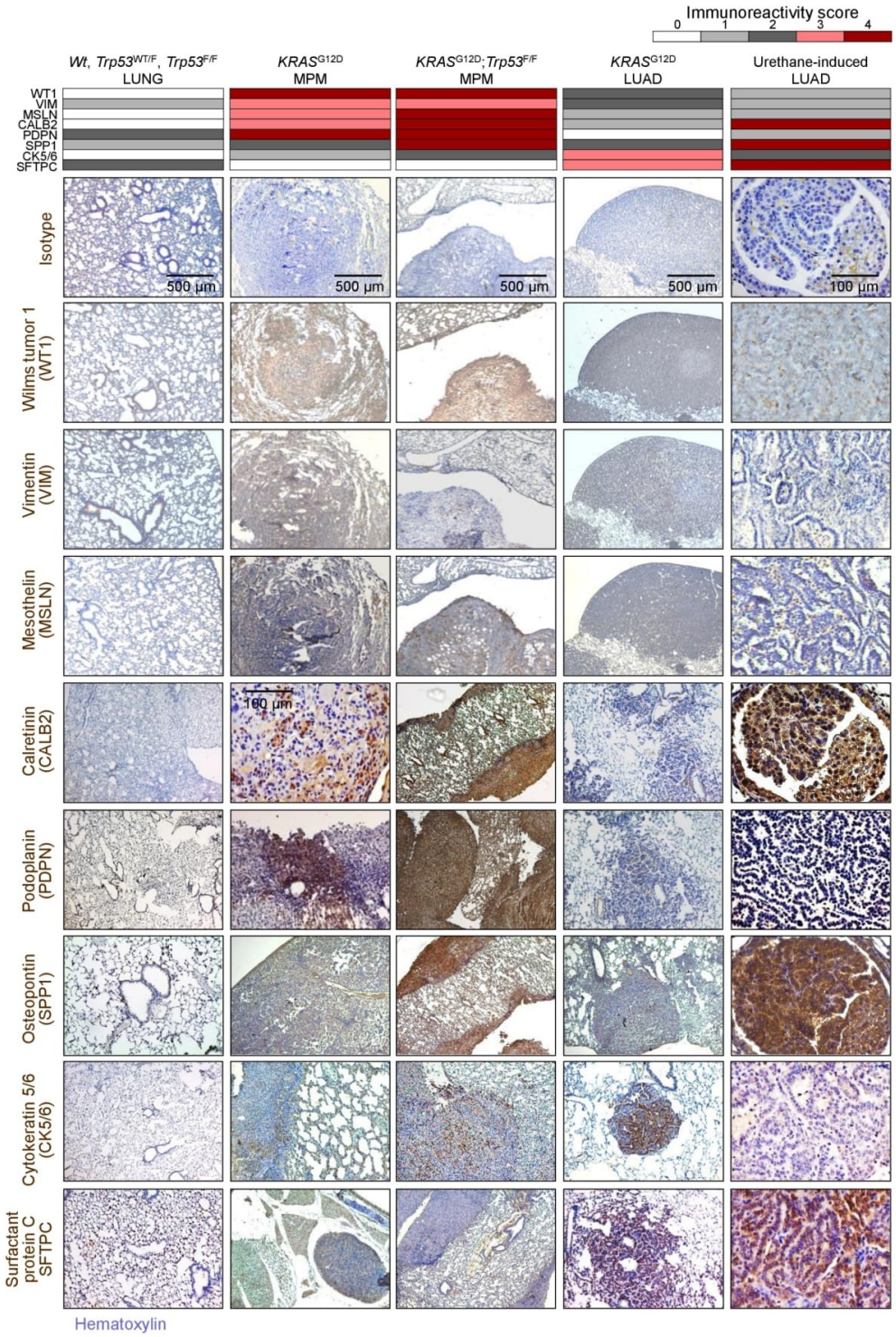

Figure 6.

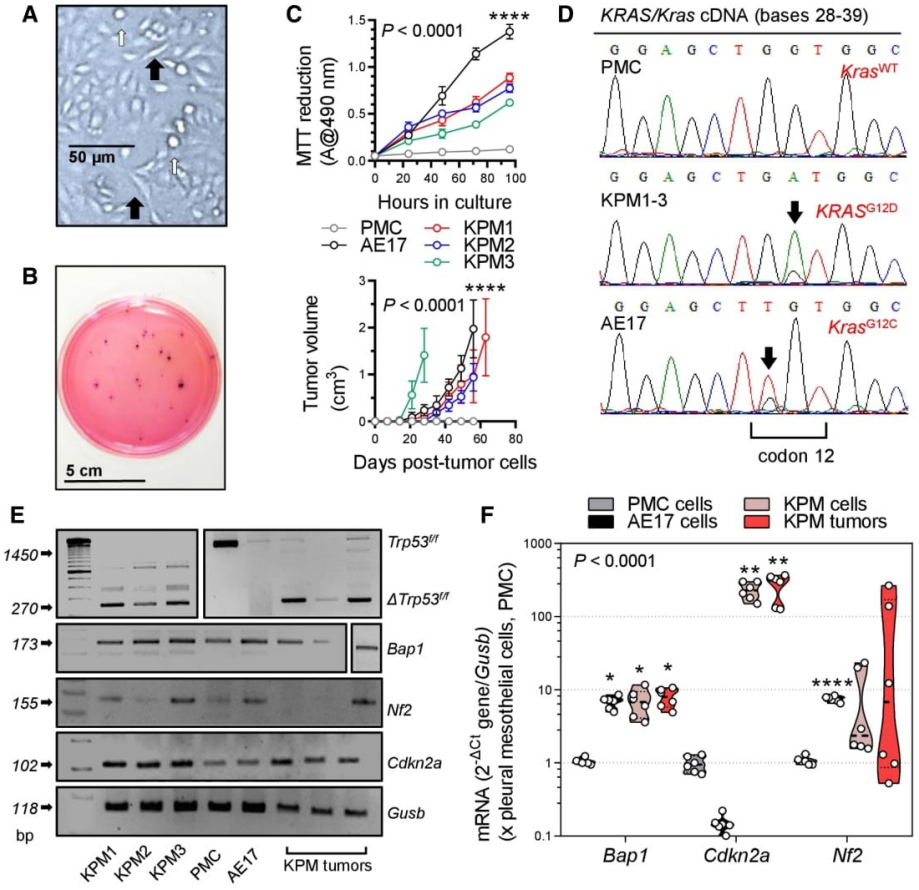

Figure 7. Transplantable *KRAS/TP53*-mutant murine mesothelioma (KPM) cell lines.

KRAS^{G12D};*Trp53f/f* pleural mesothelioma (KPM), pleural mesothelial (PMC), and asbestos-induced AE17 mesothelioma cells (all from *C57BL/6* mice) were analyzed.

A KPM cell culture showing anoikis (white arrows) and spindle-shaped morphology (black arrows).

B Representative colonies of KPM1 cells (7.5×10^3 cells/vessel) seeded on a soft agar-containing 60-mm petri dish and stained with crystal violet after a month (n = 3/group).

C Data summaries from *in vitro* MTT reduction (top; 2×10^4 cells/well; n = 6 independent experiments) and *in vivo* subcutaneous tumor growth after injection of 10^6 cells per *C57BL/6* mouse (bottom; n = 5/group).

D *KRAS/Kras* mRNA Sanger sequencing shows wild-type *Kras* (*Kras*^{WT}) of PMC and mutant murine *Kras*/human *KRAS* alleles (*KRAS*^{G12D} and *Kras*^{G12C}) of KPM and AE17 cells (arrows).

E, F RT–PCR (E) and qPCR (F) of KPM cells and parental tumors show *Trp53f/f* allele deletion (*Δ*) and *Bap1* and *Cdkn2a* overexpression compared with PMC.

Data information: In (C), data are presented as mean (circles) and 95% confidence interval (bars). *P*, overall probability, two-way ANOVA. ****: $P < 0.0001$ for AE17 cells (top) or for KPM cells (bottom) compared with all other groups, Bonferroni post-tests. In (F), data are presented as raw data points (circles), rotated kernel density distribution (violins), and medians (lines). *P*, overall probability, two-way ANOVA. *, **, and ****: $P < 0.05$, $P < 0.01$, and $P < 0.0001$, respectively, for comparison with PMC, Bonferroni post-tests.

Source data are available online for this figure.

Transplantable and actionable murine MPM cell lines with *KRAS*^{G12D}, *Trp53*, and *Bap1* mutations, and a human-like transcriptome

We subsequently isolated three different MPM cell lines from Ad-*Cre*-treated *KRAS*^{G12D};*Trp53f/f* mice (called KPM1–3) using long-term tumor culture (Pauli *et al*, 2017; Kanellakis *et al*, 2019, 2020). KPM cells displayed anchorage-independent growth (anoikis), spindle-shaped morphology, and rapid growth in minimal-supplemented media and in soft agar. In addition, KPM cells were tumorigenic when injected subcutaneously into the flank of *C57BL/6* mice and carried the original *KRAS*^{G12D}/*Trp53* lesions (Fig 7A–E, and Appendix Fig S1). KPM cells and their parental tumors featured enhanced *Bap1* and *Cdkn2a*, but not *Nf2* expression (Fig 7E and F, and Appendix Fig S1), consistent with previous work that identified *TP53*-mediated repression of *BRCA1* and *CDKN2A* expression (Stott

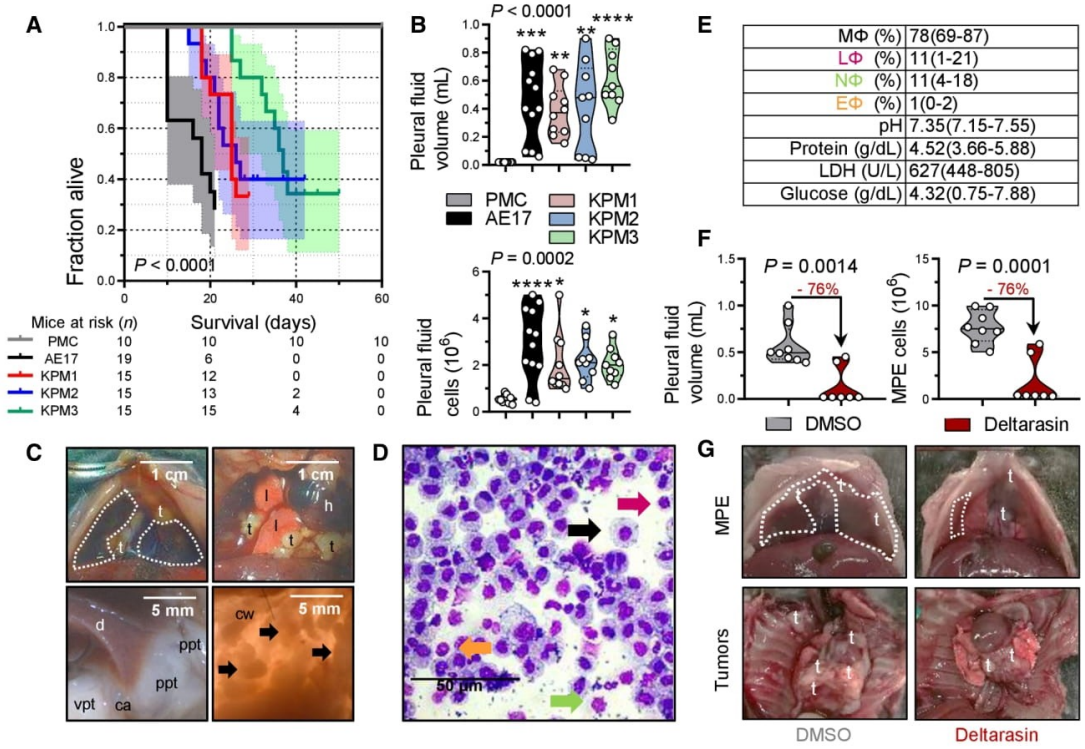

Figure 8. Transplantable and actionable murine mesothelioma models using KPM cells.

C57BL/6 mice received 2×10^5 intrapleural *KRAS*^{G12D};*Trp53f/f* pleural mesothelioma cells (KPM), pleural mesothelial cells (PMC), or asbestos-induced AE17 MPM cells.

A Kaplan–Meier survival plot with survival table.

B Data summary of pleural effusion volume and total cells (n = 10, 12, 10, 9, and 9 mice/group, respectively, from left to right).

C Images of the chest before and after opening, showing effusion (dashed lines), visceral (vpt), and parietal (ppt) pleural tumors on the costophrenic angle (ca), the diaphragm (d), and the chest wall (cw, arrows). t, tumors; l, lungs; h, heart.

D May–Gruenwald–Giemsa-stained pleural cells (macrophages, MΦ: black arrow; lymphocytes, LΦ: purple arrow; neutrophils, NΦ: green arrow; eosinophils, EΦ: orange arrow).

E Effusion cytology and biochemistry data summary (total n = 10 mice; n = 4, 3, and 3 effusions from mice injected with KPM1, KPM2, and KPM3 cells, respectively, were analyzed and shown are pooled data).

F, G *C57BL/6* mice received pleural KPM1 cells followed by a single intrapleural injection of liposomes containing 1% DMSO or 15 mg/kg deltarasin in 1% DMSO at day 9 post-tumor cells. Shown are data summaries of MPE volume (n = 8 and 7 DMSO and deltarasin-treated mice/group, respectively) and pleural fluid nucleated cells at day 19 post-KPM1 cells (F), as well as representative images of pleural effusions (dashed lines) and tumors (t in [G]).

Data information: In (A), data are presented as Kaplan–Meier survival estimates (lines), 95% confidence interval (shaded areas), and number of mice at risk (n). P, probability of overall comparison and of any comparison to PMC, log-rank test. In (B) and (F), data are presented as raw data points (circles), rotated kernel density distribution (violins), and medians (lines). Numbers in red font and arrows in (F) indicate end-point reduction by deltarasin effect. P, probability, one-way ANOVA (B) or Student's t-test (F). *, **, ***, and ****: $P < 0.05$, $P < 0.01$, $P < 0.001$, and $P < 0.0001$, respectively, for comparison with PMC, Bonferroni post-tests. In (E), data are presented as mean ± 95% confidence interval. LDH, lactate dehydrogenase.
Source data are available online for this figure.

et al, 1998; Arizti *et al*, 2000). RNA sequencing of KPM cells (GEO dataset GSE94415; Data ref: Stathopoulos *et al*, 2017) revealed that they carry the pathogenic *KRAS*^{G12D}/*Trp53* lesions, but also multiple stochastic single nucleotide variants in exon 6 and insertions in exon 11 of *Bap1*, all validated by Sanger sequencing, although immunohistochemistry revealed persistent nuclear BAP1 expression rendering these Bap1 mutations of uncertain functional significance (Nasu *et al*, 2015) (Fig EV5). Finally, 2×10^5 pleural-delivered KPM cells could inflict to naïve *C57BL/6* mice secondary disease identical to primary MPM of *KRAS*^{G12D};*Trp53f/f* mice in terms of manifestation, pathology, cytology, and biochemistry (Fig 8A–E), fulfilling modified Koch's postulates (Byrd & Segre, 2016).

To determine the potential efficacy of KRAS inhibition against murine KRAS/TP53-driven MPM, *C57BL/6* mice received pleural KPM1 cells, followed by a single intrapleural injection of liposomal-encapsulated KRAS inhibitor deltarasin (15 mg/kg; Zimmermann *et al*, 2013) or empty liposomes on day nine post-tumor cells, in order to allow initial tumor implantation in the pleural space (Agalioti *et al*, 2017). At day 19 after pleural injection of KPM1 cells, deltarasin-treated *C57BL/6* mice developed fewer and smaller MPE

with decreased cellularity compared with controls (Fig 8F and G). These results collectively show that our murine MPM is indeed malignant, originate from recombined mesothelial cells, and cause transplantable disease that can be used for hypothesis and drug testing.

Finally, RNA sequencing of KPM cells comparative to normal pleural mesothelial cells revealed a distinctive transcriptomic signature that included classic mesothelioma markers (*Msln, Spp1, Efemp1, Pdpn, Wt1*) as well as new candidate mesothelioma genes (Fig 9A–C and Appendix Table S4). A human 150–gene mesothelioma signature derived from a cohort of 113 patients via comparison of MPM against multiple other malignancies (GSE42977; De Rienzo *et al*, 2013; Data ref: De Rienzo *et al*, 2012) was highly enriched in our KPM cell line signature (Fig 9D). These data indicate that murine *KRAS/TP53*-driven MPM present *Bap1* mutations, a gene expression profile that is highly similar to human MPM, and can be used for transplantable and druggable MPM models in syngeneic mice. Collectively, the murine and human findings support the existence of a *KRAS*-driven subset of MPM patients or clones that are likely missed during sequencing and/or sampling (Comertpay *et al*, 2014; Li *et al*, 2020).

Discussion

Our results demonstrate that, alone or in combination with *TP53*, *KRAS* is perturbed in a proportion of human MPM and can potentially drive the murine mesothelium toward MPM development. *KRAS* mutations, amplifications, and overexpression, as well as chromosome 12p gains, are shown to exist in 20% of patients from the TCGA MPM dataset and low allelic frequency *KRAS* mutations are discovered in 50% of MPM samples from our own human cohorts using sensitive techniques. Furthermore, *KRAS* mutations are shown to occasionally co-exist with *TP53* mutations, to repulse *NF2* mutations, and to be associated with biphasic MPM histology. Targeting of oncogenic $KRAS^{G12D}$ alone to the pleural mesothelium caused epithelioid MPM in mice and together with *Trp53* deletion resulted in biphasic MPM with MPE. We further show that murine MPM carry the initiating $KRAS^{G12D}$/*Trp53* mutations and multiple secondary *Bap1* mutations, are transplantable and druggable, and highly similar to human MPM in terms of molecular markers and gene expression. Collectively, the data support a pathogenic role for *KRAS* mutations in a fraction of MPMs and provide new models to study this patient group.

Our striking findings can be reconciled with the sporadic nature of *KRAS* mutations in human MPM sequencing studies (Bott *et al*, 2011; Guo *et al*, 2015; Bueno *et al*, 2016; Hmeljak *et al*, 2018) and the incomplete penetrance of standalone *Bap1, Cdkn2a, Nf2,* or *Trp53* deletions in causing MPM in mice (Jongsma *et al*, 2008; Guo *et al*, 2014; Menges *et al*, 2014; Xu *et al*, 2014; Kukuyan *et al*, 2019). To this end, mesothelial *KRAS* mutations may initiate MPM in some patients, but may be lost during sampling and sequencing, as has been shown for other mutations in LUAD that persist at a subclonal level (Abbosh *et al*, 2017; Jamal-Hanjani *et al*, 2017). The low allelic frequency of *KRAS* mutations is explicable by their heterozygous nature and the robust inflammatory responses *KRAS*-mutant tumors generate (Agalioti *et al*, 2017; Marazioti *et al*, 2018) and is not limiting their driver capabilities in other tumor types (Abbosh *et al*, 2017; Jamal-Hanjani *et al*, 2017; Li *et al*, 2020). The fact that these mutations were not detected by most next-generation sequencing studies of MPM can be explained by the relative low sensitivity of these methods compared with ddPCR, as well as the low allelic frequency of KRAS mutations. To this end, typical read depths of 50–100 are employed in most next-generation sequencing studies yielding a sensitivity of 1–2%, compared with the theoretical 0.005% or actual 0.1% of ddPCR (Demuth *et al*, 2018). In addition, most next-generation sequencing studies set discovery cutoffs of 25% allelic frequency, likely rendering many *KRAS* mutations undiscovered. Our findings are plausible, since MPM is likely polyclonal (Comertpay *et al*, 2014), cell lines display *KRAS* activation and mutations (Patel *et al*, 2007; Agalioti *et al*, 2017), *NF2* is a *KRAS* suppressor (Tikoo *et al*, 1994), and *KRAS* signaling is interconnected with the *TP53* cell cycle checkpoint (Matallanas *et al*, 2011). The postulation that KRAS mutations in MPM might be early events can be tested in the future by genome doubling analyses. Taken together, our data and the literature support that, in a subset of patients, low allelic frequency *KRAS* alterations conditionally accomplice with *TP53* to drive mesothelial cells toward MPM. These tumors may be selectively responsive to *KRAS* blockade and detectable by sensitive methods like ddPCR or maximal depth sequencing (Li *et al*, 2020).

We also corroborate the critical role of *TP53* in MPM progression, since *TP53* mutations are frequent in MPM. Although standalone T*rp53* deletion did not induce MPM in mice, it promoted $KRAS^{G12D}$-driven MPM progression and biphasic histology, as was also observed in combination with *Nf2* and *Tsc1* deletion (Jongsma *et al*, 2008; Guo *et al*, 2014), suggesting that *Trp53* loss may conditionally cooperate with other oncogenes in MPM. In addition, *Trp53*-deleted $KRAS^{G12D}$ MPM was accompanied by effusions, a human MPM phenotype that likely affects survival (Ryu *et al*, 2014) and that was previously not reproducible in mice. Again, *Trp53* loss was not causative, but likely potentiated the effusion-promoting effects of *KRAS*, which we recently identified in metastatic effusions (Agalioti *et al*, 2017). Taken together with published work, our findings functionally validate the role of *TP53* mutations in human MPM in driving biphasic histology, tumor progression and metastasis, and poor survival (Bueno *et al*, 2016; Yap *et al*, 2017). Hence, TP53-targeted therapies may be prioritized for biphasic MPM when available (Brown *et al*, 2009).

Another surprising finding was the multiple and different *Bap1* mutations of our MPM cell lines, since they originated from tumors inflicted by $KRAS^{G12D}$ and *Trp53* loss. Frequent copy number loss and recurrent somatic mutations in *BAP1* have been identified in MPM (Bott *et al*, 2011; Guo *et al*, 2015; Nasu *et al*, 2015). Based on the multiplicity and variety of the *Bap1* mutations we observed, we postulate that they were secondarily triggered by the genomic instability caused from combined *KRAS* mutation and *TP53* loss. Whatever their cause may be, their presence strengthens our findings of an involvement of KRAS signaling in MPM pathobiology, as well as the relevance of the novel mouse models we developed, since *Bap1* is the single most commonly mutated gene in human MPM.

Research on MPM is hampered by the paucity of mouse models (Blanquart *et al*, 2020). We provide multiple new mouse models with defined phenotype, histology, and latency: (i) a genetic mouse model of pleural epithelioid MPM; (ii) genetic and transplantable models of pleural and peritoneal biphasic MPM with accompanying effusion; and (iii) three new MPM cell lines of defined genotype, transcriptome, and phenotype that are syngeneic to *C57BL/6* mice.

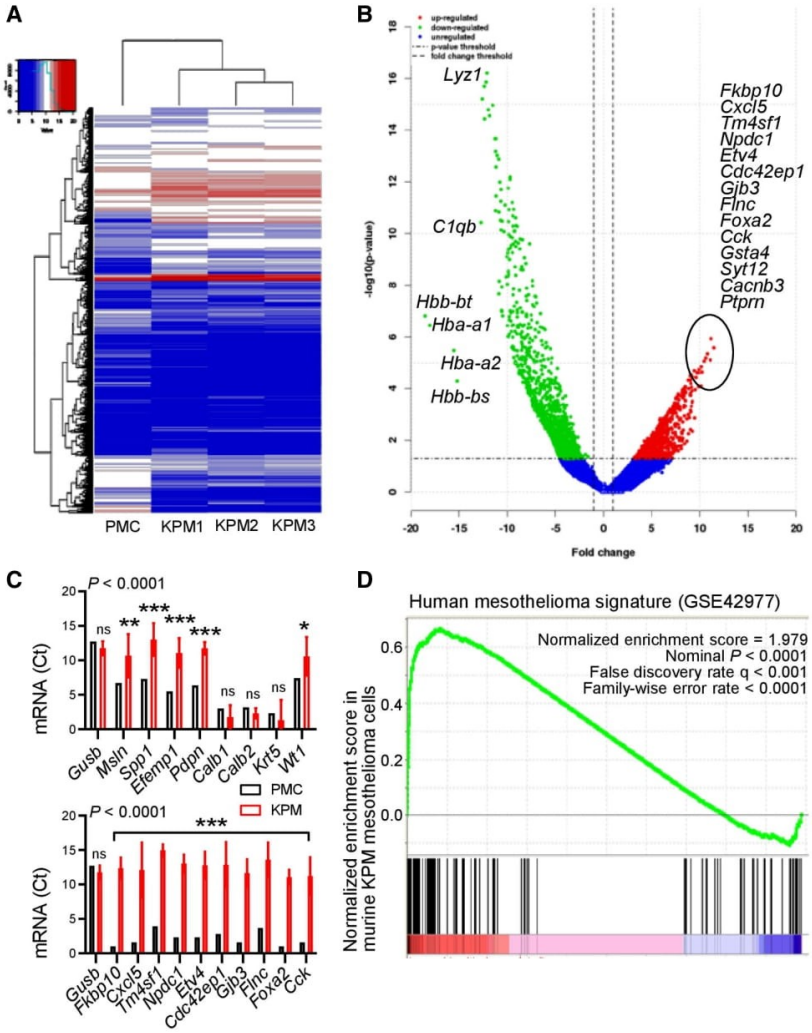

Figure 9. The molecular signature of KPM cells is enriched in human mesothelioma.

RNA sequencing results (GEO dataset GSE94415) of $KRAS^{G12D}$;*Trp53flf* mesothelioma (KPM) cells (n = 3) compared with pleural mesothelial cells (PMC; n = 1 pooled triplicate). n denotes biological replicates, since pooled triplicate technical replicates from each cell line were sequenced.

A Unsupervised hierarchical clustering shows distinctive gene expression of KPM versus PMC.

B Volcano plot showing some top KPM versus PMC differentially expressed genes.

C KPM and PMC expression of classic mesothelioma markers (top) and top KPM versus PMC overexpressed genes (bottom).

D Gene set enrichment analysis, including enrichment score and nominal probability value of the 150 gene-signature specifically over-represented in human mesothelioma compared with other thoracic malignancies derived from 113 patients (GSE42977) within the transcriptome of KPM cells versus PMC shows significant enrichment of the human mesothelioma signature in KPM cells.

Data information: In (C), data are presented as mean (columns) and 95% confidence interval (bars). P: probability, two-way ANOVA. ns, *, **, and ***: $P > 0.05$, $P < 0.05$, $P < 0.01$, and $P < 0.001$, respectively, compared with PMC, Bonferroni post-tests.
Source data are available online for this figure.

These are positioned to enhance MPM research by overcoming the need for immune compromise providing intact immune responses critical for MPM pathogenesis (Burt *et al*, 2012; Westbom *et al*, 2014; Kadariya *et al*, 2016; Patil *et al*, 2018), by widening the repertoire of existing cell lines, by recapitulating MPM with effusion, and by addressing pleural MPM.

In conclusion, our findings support that oncogenic *KRAS* signaling causes MPM in a proportion of humans and in mice. As some

mutations along this signaling pathway are currently druggable or are likely to become such in the near future (Herbst *et al*, 2002; Brown *et al*, 2009; Flaherty *et al*, 2010; Stephen *et al*, 2014), our findings may facilitate therapeutic innovation. Pending validation of our human findings in larger cohorts, we provide novel tools for the study of a molecular subclass of MPM that will hopefully aid in drug discovery and personalized treatment of patients with MPM driven by KRAS signaling.

Materials and Methods

Computational biologic analyses

The dataset for Fig 1A was generated by manual curation of COSMIC data (https://cancer.sanger.ac.uk/cosmic/browse/tissue?wgs=off&sn=pleura&ss=all&hn=mesothelioma&sh=&in=t&src=tissue&all_data=n). The dataset for Fig 1B was generated by manual curation of the main text and supplementary data of publications (Bott *et al*, 2011; Enomoto *et al*, 2012; Mezzapelle *et al*, 2013; Shukuya *et al*; 2014; Guo *et al*, 2015; Lo Iacono *et al*, 2015; Bueno *et al*, 2016; De Rienzo *et al*, 2016; Kato *et al*, 2016; Hmeljak *et al*, 2018). Raw data from 86 human TCGA MPM patients were retrieved from the cBioPortal for Cancer Genomics (www.cbioportal.org/) using inputs "mesothelioma", "Mesothelioma (TCGA, PanCancer Atlas)", "Query by Gene *KRAS* and *TP53*", "Mutations", "Putative copy-number alterations from GISTIC", "mRNA expression *z*-scores", and "Protein expression *z*-scores" were downloaded and analyzed. Gene expression data from these patients, normalized with the $\log_2$(fpkm-uq + 1) method, were downloaded (https://xenabrowser.net/datapages/?dataset=TCGA-MESO.htseq_fpkm-uq.tsv&host=https%3A%2F%2Fgdc.xenahubs.net&removeHub=https%3A%2F%2Fxena.treehouse.gi.ucsc.edu%3A443), ENSEMBL gene IDs were converted to gene symbols using https://www.biotools.fr/mouse/ensembl_symbol_converter, the data were filtered, differential gene expression (ΔGE) was analyzed, and heatmap visualization was performed using R* and packages limma R version 3.42.2 (https://bioconductor.org/packages/release/bioc/html/limma.html) and edgeR (https://bioconductor.org/packages/release/bioc/html/edgeR.html). Both rows and columns were clustered using Pearson correlation and complete linkage. All mutations (n = 2,150) of all patients (n = 86) with MPM from the TCGA pan-cancer dataset were retrieved from www.cbioportal.org/ and were fed into the protein analysis through evolutionary relationships (PANTHER) Classification System (www.pantherdb.org/) using parameters: organism, *Homo Sapiens*; analysis, statistical overrepresentation test > PANTHER pathways or reactome pathways (both analyses were done); whole-genome reference list: *Homo Sapiens*; test type: binomial; and correction: false discovery rate. All raw data from the two independent PANTHER and reactome pathway analyses were retrieved, merged, and analyzed. Gene set enrichment analysis (GSEA) was performed with the Broad Institute pre-ranked GSEA module software (http://software.broadinstitute.org/gsea/index.jsp;Subramanian *et al*, 2005). All aforementioned raw data were downloaded from the sources referenced above in *.csv format, are provided as source data files with this publication, and were reanalyzed using R*, Prism v8.0 (GraphPad, La Jolla, CA), and Excel (Microsoft, Redmont, WA).

Reagents

Adenoviruses type 5 (Ad) encoding *Melanotus* luciferase (*Luc*) or CRE-recombinase (*Cre*) were from the Vector Development Laboratory, Baylor College of Medicine (Houston, TX); 3-(4,5-dimethylthiazol-2-yl)-2,5-diphenyltetrazolium bromide (MTT) assay from Sigma-Aldrich (St. Louis, MO), and D-luciferin from Gold Biotechnology (St. Louis, MO). Primers and antibodies are listed in Appendix Tables S5 and S6. All cell culture reagents were from Thermo Fisher Scientific.

Human studies

All human experiments conformed to the principles set out in the WMA Declaration of Helsinki and the Department of Health and Human Services Belmont Report. The Munich clinical study was prospectively approved by the Ludwig-Maximilians-University Munich Ethics Committee (approvals #623–15 and #711–16). All patients gave written informed consent *a priori*. Diagnoses were made according to current standards by a board-certified pathologist at the Asklepios Fachkliniken Gauting, Munich, Germany. Pleural fluid was centrifuged at 300 *g* for 10 min at 4°C, genomic DNA was extracted from cell pellets, supernatants, and pleural tumor tissues using TRIzol (Thermo Fisher) and purified using GenElute Mammalian Genomic DNA Miniprep (Sigma Aldrich), and 200 ng DNA were used to analyze *KRAS* codons 12/13 and 61, and *TP53* copies with ddPCR *KRAS* G12/G13, *KRAS* G61, *TP53* CNV, and TERT CNV Kits and QuantaSoft Analysis Pro software (BioRad, Hercules, CA) as described elsewhere (Poole *et al*, 2019). Thresholds for $KRAS^{WT}$, $KRAS^{MUT}$, *TP53*, and *TERT* droplet amplitude gates were, respectively, 6,000, 10,000, 5,500, and 7,000. Data were normalized by accepted droplet numbers to yield absolute mutant (^{MUT}) and wild-type (^{WT}) droplet percentages, which were determined using thresholds derived from cell line controls and from LUAD patient samples clinically confirmed to have *KRAS* mutations and *TP53* copy number changes, according to the formula:

$$KRAS\,\text{mutant copies}\,\% = \frac{n_{\text{positive mutant droplets}}}{\left(n_{\text{positive mutant droplets}} + n_{\text{positive wild type droplets}}\right)} * 100$$

$$TP53\ \text{copies}\ \% = \frac{n_{\text{TP53 positive droplets}}}{n_{\text{TERT positive droplets}}} * 100.$$

In the Nantes Study, MPM cell lines, as well as pleural fluid cells and supernatants, were derived from pleural fluid aspirates obtained for diagnostic and therapeutic purposes. The study was approved by the French Ministry of Research (DC-2011-1399), and all patients gave written informed consent *a priori* for their excess pleural fluid to be used for the establishment of cell lines. MPE samples from over 120 patients with MPM were used to generate the 33 cell lines, since the success rate is < 30%, as described elsewhere (Gueugnon *et al*, 2011; Delaunay *et al*, 2020). Diagnoses were established by both fluid cytology and immunohistochemical staining of pleural biopsies performed by the pathology department at Laënnec Hospital (St-Herblain, France) and then externally confirmed by MESOPATH, the French panel of pathology experts for the diagnosis of mesothelioma. All recruited patients had received no prior

anticancer therapy. All cell lines were maintained in RPMI-1640 medium supplemented with 2 mM L-glutamine, 100 IU/ml penicillin, 0.1 mg/ml streptomycin, and 10% heat-inactivated fetal calf serum and cultured at 37°C in 5% CO_2-95% air. Genomic DNA from 33 MPM cell lines was extracted with Nucleospin Blood kit (Macherey-Nagel, Düren, Germany) and 500 ng were hybridized to Affymetrix CytoScanHD Arrays (Thermo Fisher). Detection, quantification, and visualization of single nucleotide variations (SNV) and copy number alterations (CNA) were performed using Affymetrix Chromosome Analysis Suite v3.1.1.27 (Thermo Fisher) and data are available at GEO datasets (GSE134349; Data ref: Blanquart *et al*, 2019). The cell lines were also sequenced in a targeted fashion focusing on 21 genes and the TERT promoter on a MiSeq system (Illumina, San Diego, CA) (Quetel *et al*, 2020). The MAPED (Clinical identification of malignant pleural effusions in the emergency department) study entailed a few samples from patients enrolled in a prospective clinical trial (preprint: Marazioti *et al*, 2021). MAPED was registered with ClinicalTrials.gov (#NCT03319472), and written informed consent was obtained from all patients *a priori*. MAPED was approved by the University of Patras Ethics Committee (approval #22699/21.11.2013). Pleural fluid was centrifuged at 300 *g* for 10 min at 4°C, RNA and DNA were extracted from cell pellets using TRIzol (Thermo Fisher) and purified using GenElute Mammalian Genomic DNA Miniprep (Sigma-Aldrich), and 200 ng RNA/DNA were used for RT–PCR, qPCR, and Sanger sequencing. The Istanbul study was approved by the Koç University Ethics Committee on Human Research (approval #2021.223.IRB2.042/06.05.2021). Both Nantes pleural fluid and Istanbul pleural tumor specimens were processed and analyzed identical to the Munich study.

Mice

C57BL/6 (#000664), *B6.129(Cg)-Gt(ROSA)26Sor*$^{tm4(ACTB-tdTomato,-EGFP)Luo}$*/J* (*mT/mG*; #007676; Muzumdar *et al*, 2007), *FVB-Tg(CAG-luc,-GFP)L2G85Chco/J* (*CAG.Luc.eGFP*; #008450; Cao *et al*, 2004)[64], B6.129S4-*Kras*^{tm4Tyj}*/J* (*KRAS*^{G12D}; #008179; Jackson *et al*, 2001), and B6.129P2-*Trp53*^{tm1Brn}*/J* (*Trp53f/f*; #008462; Meylan *et al*, 2009) mice were obtained from Jackson Laboratories (Bar Harbor, ME) and bred on the *C57BL/6* background at the University of Patras Center for Animal Models of Disease. Experiments were approved by the Prefecture of Western Greece's Veterinary Administration (approval 118018/578-30.04.2014) and were conducted according to Directive 2010/63/EU (http://eur-lex.europa.eu/legal-content/EN/TXT/?uri=CELEX%3A32010L0063). Sex-, weight (20–25 g)-, and age (6–12 week)-matched experimental mice were used, and their numbers (total $n = 432$) are detailed in Appendix Table S7.

Mesothelial transgene delivery

Isoflurane-anesthetized *C57BL/6* and *mT/mG* mice received 5×10^8 PFU intrapleural or intraperitoneal Ad-*Cre* or Ad-*Luc* in 100 μl PBS and were serially imaged for bioluminescence on a Xenogen Lumina II (Perkin-Elmer, Waltham, MA) after receiving 1 mg retro-orbital D-luciferin under isoflurane anesthesia, and data were analyzed using Living Image v.4.2 (Perkin-Elmer; Stathopoulos *et al*, 2006; Spella *et al*, 2019), or were euthanized and pleural lavage was performed, lungs were explanted, and parietal pleura was stripped. For pleural lavage, 1 ml PBS was injected, was withdrawn after 30 s, and was cytocentrifuged onto glass slides (5×10^4 cells, 300 *g*, 10 min) using CellSpin (Tharmac, Marburg, Germany). Lungs were embedded in optimal cutting temperature (OCT; Sakura, Tokyo, Japan) and sectioned into 10-μm cryosections. The parietal pleura was placed apical side up onto glass slides. Samples were stained with Hoechst 55238 and were examined on AxioObserver D1 (Zeiss, Jena, Germany) or TCS SP5 (Leica, Heidelberg, Germany) microscopes.

Primary MPM models

Wild-type (*Wt*), *KRAS*^{G12D}, and *Trp53f/f* mice were intercrossed and all possible offspring genotypes received isoflurane anesthesia and 5×10^8 PFU intrapleural or intraperitoneal Ad-*Cre*. Mice were monitored daily and sacrificed when moribund or prematurely for pathology. Mice with pleural fluid volume ≥ 100 μl were judged to have effusions that were aspirated. Animals with pleural fluid volume < 100 μl were judged not to have effusions and underwent pleural lavage. For isolation of primary murine pleural mesothelial cells (PMC), pleural myeloid and lymphoid cells were removed by pleural lavage followed by pleural instillation of 1 ml DMEM, 2% trypsin EDTA, aspiration after 1 min, and culture.

Bone marrow transfer

For adoptive BMT, *C57BL/6* mice received 10^7 bone marrow cells obtained from *CAG.Luc.eGFP* donors i.v. 12 h after total-body irradiation (1,100 Rad). Full bone marrow reconstitution was completed after one month, as described elsewhere (Agalioti *et al*, 2017).

Transplantable mesothelioma cell lines

Murine *KRAS*^{G12D}*;Trp53f/f* pleural mesotheliomas were minced and cultured in DMEM 10% FBS for > 30 passages, yielding three *KRAS*^{G12D}*;Trp53f/f* mesothelioma (KPM1–3) cell lines, which were compared to AE17 cells (*Kras*^{G12C}-mutant asbestos-induced murine mesothelioma) and PMC (Agalioti *et al*, 2017). PMC were generated in our laboratory as primary cultures of murine pleural lavage with DMEM 2% trypsin, whereas AE17 cells were donated by Dr. YC Gary Lee (University of Western Australia, Perth, Australia) and have been both extensively described elsewhere (Giannou *et al*, 2015, 2017; Agalioti *et al*, 2017; Marazioti *et al*, 2018). For this, 2×10^5 cells in 100 μl PBS were delivered intrapleurally to isoflurane-anesthetized *C57BL/6* mice that were followed as above. For solid tumor formation, *C57BL/6* mice received 10^6 subcutaneous PMC, KPM, or AE17 cells in the rear flank, three vertical tumor dimensions (δ^1, δ^2, δ^3) were monitored serially, and the formula $\pi\delta^1\delta^2\delta^3/6$ was used to calculate tumor volume. RNA sequencing was done on an IonTorrent sequencer (Thermo Fisher); data were deposited at GEO datasets (GSE94415) and were analyzed using Bioconductor (Data ref: Stathopoulos *et al*, 2017). Gene set enrichment was done with the Broad Institute pre-ranked GSEA module (Subramanian *et al*, 2005).

PCR and Sanger sequencing

Cellular RNA was isolated using TRIzol (Thermo Fisher Scientific, Waltham, MA) followed by RNAeasy purification and genomic DNA removal (Qiagen, Hilden, Germany). For tumor RNA, tissues were

passed through 70-μm strainers (BD Biosciences, San Jose, CA) and 10^7 cells were subjected to RNA extraction. One μg RNA was reverse-transcribed using Oligo$(dT)_{18}$ and Superscript III (Thermo Fisher). cDNAs were amplified using specific primers (Appendix Table S5) and Phusion Hot Start Flex polymerase (New England Biolabs, Ipswich, MA). DNA fragments were run on 2% agarose gels or were purified with NucleoSpin gel and PCR clean-up columns (Macherey-Nagel, Düren, Germany) and were sequenced using their primers by VBC Biotech (Vienna, Austria). qPCR was performed using specific primers (Appendix Table S5) and SYBR FAST qPCR Kit (Kapa Biosystems, Wilmington, MA) in a StepOne cycler (Applied Biosystems, Carlsbad, CA). Ct values from triplicate reactions were analyzed with the $2^{-\Delta CT}$ method (Pfaffl, 2001). mRNA abundance was determined relative to glycuronidase beta (*Gusb*) and is given as $2^{-\Delta CT} = 2^{-(\text{Ct of transcript})-(\text{Ct of Gusb})}$. The Sanger sequencing trace files were further analyzed for double peak parser using Bioconductor (https://www.bioconductor.org/) with a threshold of 25 Phred quality core (Ewing *et al*, 1998). The mismatch base-calls in respect to the wild-type samples were grouped by sample and used as template to generate the lollipop plot per each KPM cell line for a visual representation of all the mutations detected (Jay & Brouwer, 2016). Lollipop plots were generated using MutationMapper (https://www.cbioportal.org/mutation_mapper; Cerami *et al*, 2012).

RNA sequencing

RNA sequencing was done on an IonTorrent sequencer (Thermo Fisher), and data were analyzed using Bioconductor (https://www.bioconductor.org/). File alignments were performed with Tmap (https://github.com/iontorrent/TMAP). Coverage and alignments plot from sequencing were generated using Integrative genome viewer (Robinson *et al*, 2011). Alignments are represented as gray polygons with reads mismatching the reference indicated by color. Loci with a large percentage of mismatches relative to the reference are flagged in the coverage plot as color-coded bars. Alignments with inferred small insertion or small deletion are represented with vertical or horizontal bars, respectively. Gene set enrichment analysis (GSEA) was performed with the Broad Institute pre-ranked GSEA module software (http://software.broadinstitute.org/gsea/index.jsp; Subramanian *et al*, 2005). The raw *.bam files, one for each RNA-Seq sample, were summarized to a gene read counts table, using the Bioconductor package GenomicRanges. In the final read counts table, each row represented one gene, each column one RNAseq sample, and each cell the corresponding read counts associated with each row and column. The gene counts table was normalized for inherent systematic or experimental biases (e.g., sequencing depth, gene length, and GC content bias) using the Bioconductor package DESeq after removing genes that had zero counts over all RNASeq samples (20,007 genes). The output of the normalization algorithm was a table with normalized counts, which can be used for differential expression analysis with statistical algorithms developed specifically for count data. Prior to the statistical testing procedure, the gene read counts were filtered for possible artifacts that could affect the subsequent statistical testing procedures. Genes presenting any of the following were excluded from further analysis: (i) genes with length less than 500 bp (2,051 genes), (ii) genes whose average reads per 100 bp was less than the 25^{th} percentile of the total normalized distribution of average reads per 100 bp (0 genes with cutoff value 0.02248 average reads per 100 bp), (iii) genes with read counts below the median read counts of the total normalized count distribution (11,358 genes with cutoff value 16 normalized read counts). The total number of genes excluded due to the application of gene filters was 5,298. The total (unified) number of genes excluded due to the application of all filters was 32,595. The resulting gene counts table was subjected to differential expression analysis for the contrast KPM versus PMC using the Bioconductor package DESeq. The final numbers of statistically significant differentially expressed genes were 2,344 genes and of these, 650 were up-regulated and 1,694 were down-regulated according to an absolute fold-change cutoff value of 2.

Cell culture

All KPM cell lines are available upon request. Cells were cultured at 37°C in 5% CO_2-95% air using DMEM 10% FBS, 2 mM L-glutamine, 1 mM pyruvate, 100 U/ml penicillin, and 100 mg/ml streptomycin and were tested biannually for identity (by short tandem repeats) and *Mycoplasma Spp*. (by PCR). *In vitro* cell proliferation was determined using 3-(4,5-dimethylthiazol-2-yl)-2,5-diphenyltetrazolium bromide (MTT) assay. For *in vivo* injections, cells were harvested with trypsin, incubated with Trypan blue, counted on a hemocytometer, and > 95% viable cells were injected into the pleural space (2×10^5) or into the skin (10^6) as described elsewhere (Agalioti *et al*, 2017). Mouse numbers used are detailed in Appendix Table S7.

Cell and tissue analyses

MPE fluid was diluted in 10-fold excess red blood cells lysis buffer (155 mM NH_4Cl, 12 mM $NaHCO_3$, 0.1 mM EDTA). Total pleural cell counts were determined microscopically in a hemocytometer and cytocentrifugal specimens (5×10^4 cells each) of pleural fluid cells were fixed with methanol for 2 min. Cells were stained with May–Grünwald stain in 1 mM Na_2HPO_4, 2.5 mM KH_2PO_4, pH = 6.4 for 6 min and Giemsa stain in 2 mM Na_2HPO_4, 5 mM KH_2PO_4, pH = 6.4 for 40 min, washed with H_2O, and dried. Slides were mounted with Entellan (Merck Millipore, Darmstadt, Germany), coverslipped, and analyzed. For flow cytometry, 10^6 nucleated pleural fluid cells suspended in 50 μl PBS supplemented with 2% FBS and 0.1% NaN_3 were stained with the indicated antibodies according to manufacturer's instructions (Appendix Table S6) for 20 min in the dark, washed, and resuspended in buffer for further analysis. Lungs, visceral pleural tumors, parietal pleural tumors, and chest walls were fixed in 4% paraformaldehyde overnight, embedded in paraffin or optimal cutting temperature (OCT) and were stored at room temperature or −80°C, respectively. Five-μm paraffin or 10-μm cryosections were mounted on glass slides. Sections were labeled using the indicated antibodies (Appendix Table S6), counterstained with Envision (Dako, Carpinteria, CA) or Hoechst 33258 (Sigma-Aldrich, St. Louis, MO), and mounted with Entellan new (Merck Millipore) or Mowiol 4-88 (Calbiochem, Gibbstown, NJ). For isotype control, primary antibody was omitted. Bright-field and fluorescent microscopy were done on AxioLab.A1 (Zeiss), AxioObserver.D1 (Zeiss), or TCS SP5 (Leica) microscopes and digital images were processed with Fiji (Schindelin *et al*, 2012).

The paper explained

Problem
In a proportion of patients with human malignant pleural mesothelioma (MPM), a dreadful disease most commonly inflicted by occupational asbestos inhalation but also possibly by smoking, sporadic mutations of KRAS is observed. However, their functional impact and significance have not been addressed and experimental model systems suitable for the study of this molecular subclass of MPM are not available.

Results
We systematically interrogate *KRAS* alterations in the TCGA pan-cancer dataset of human MPM and in MPM patients from our centers employing sensitive techniques. 20% of TCGA and 50% of our patients show activating mutations or amplification of *KRAS*, in 30% of the cases accompanied by *TP53* mutations or loss. These changes are associated with enhanced signaling downstream of *KRAS*. *KRAS* and *TP53* are shown to cooperate for MPM development in conditional mouse models. Three new MPM cell lines are developed that are highly similar to the human disease, and these experimental MPM models are shown to be actionable by a novel KRAS inhibitor.

Impact
Multiple new tools for investigations on MPM biology are provided together with proof-of-concept data that support involvement of *KRAS* signaling in MPM pathogenesis. The findings can be rapidly translated to clinical trials of KRAS pathway inhibition in a molecular subset of MPM patients.

Liposomal deltarasin preparation and treatment

Deltarasin-encapsulating liposomes were prepared as described elsewhere (Markoutsa *et al*, 2014; Marazioti *et al*, 2019), by freeze-drying 30 mg of empty DSPC/PG/Chol (9:1:5 mol/mol/mol) unilamelar sonicated vesicles with 1 ml of deltarasin solution (5 mg/ml) in PBS, or plain PBS (for empty liposomes), followed by controlled rehydration. Liposome size was decreased by extrusion though Lipo-so-fast extruder polycarbonate membranes (Avestin Europe, Mannheim, Germany) with 400-nm pore diameter. Liposome lipid concentration, size distribution, surface charge (zeta-sizer, Malvern Panalytical Ltd, Malvern, United Kingdom), and drug encapsulation efficiency were estimated by measuring non-liposomal drug absorption at 284 nm as reported elsewhere (Markoutsa *et al*, 2014; Marazioti *et al*, 2019). Deltarasin-encapsulating liposomes were delivered intrapleurally into *C57BL/6* mice 9 days post-intrapleural KPM1 cells, when the first pleural tumors were already established (Agalioti *et al*, 2017).

Statistics

Sample size was estimated using G*power (Faul *et al*, 2007) assuming $\alpha = 0.05$, $\beta = 0.05$, and effect size d or $\varphi = 1.5$. Animals were allocated to treatments by alternation and transgenic animals case-control-wise. Data acquisition was blinded and no data were excluded from analyses. Data were tested for normality of distribution by Kolmogorov–Smirnov test and are given as mean $\pm$ 95% confidence interval (CI). Sample size (n) refers to biological replicates. Differences in means or medians were examined by *t*-test, Mann–Whitney test, Wilcoxon matched-pairs signed rank test, one-way analysis of variance (ANOVA) with Tukey's or Bonferroni's post-tests, or Kruskal–Wallis test with Dunn's post-tests, as indicated and appropriate. Differences in frequencies were tested by Fischer's exact or χ^2 tests. Molecular and longitudinal (bioluminescence, MTT, tumor growth) data were analyzed by two-way ANOVA with Bonferroni's, Sidak's, Dunnett's, or Tukey's post-tests, or with two-stage linear step-up procedure of Benjamini, Krieger, and Yekutieli. Survival was analyzed using Kaplan–Meier estimates, log-rank (Mantel–Cox) test for probability, and Mantel–Haenszel estimates of hazard ratio. Probability (P) values are two-tailed and $P < 0.05$ was considered significant. Analyses and plots were done on Prism v8.0 (GraphPad, La Jolla, CA) and Excel (Microsoft, Redmont, WA).

Data availability

Affymetrix CytoScanHD Microarray data: GEO dataset GSE134349 (https://www.ncbi.nlm.nih.gov/geo/query/acc.cgi?acc=GSE134349).
IonTorrent RNA sequencing data: GEO dataset GSE94415 (https://www.ncbi.nlm.nih.gov/geo/query/acc.cgi?&acc=GSE94415).

Expanded View for this article is available online.

Acknowledgements
The authors thank Dr. YC Gary Lee (University of Western Australia, Perth, Australia) for donating AE17 cells and the cluster LUNG innovation (LUNG O2) for logistic support. This work was supported by European Research Council 2010 Starting Independent Investigator (#260524) and 2015 Proof of Concept (#679345) grants, the Graduate College (Graduiertenkolleg, GRK) #2338 of the German Research Society (Deutsche Forschungsgemeinschaft, DFG), the target validation project for pharmaceutical development ALTERNATIVE of the German Ministry for Education and Research (Bundesministerium für Bildung und Forschung, BMBF), and a Translational Research Grant by the German Center for Lung Research (Deutsches Zentrum für Lungenforschung, DZL) (all to GTS); the Greek State Scholarship Foundation Program "Reinforcement of Postdoctoral Researchers-1st and 2nd cycles" co-financed by the European Union Social Fund and Greek national funds (NSRF 2014–2020 and MIS-5033021) (to IG, MS, and IL); General Secretariat for Research and Innovation and Hellenic Foundation for Research and Innovation grant #1853a (to MS); REPSIRE European Respiratory Society Fellowship (LTRF 2015-1824) (to IP); INSERM, CNRS, the "Institut de Recherche en Santé Respiratoire des Pays de la Loire", ARSMESO44, the National Research Agency under the Programme d' Investissements d' Avenir (ANR-16-IDEX-0007), and the Pays de la Loire Region research program (all to CB, MG, and SD); as well as INSERM, the Ligue Contre le Cancer (Ile de France committee), and the Chancellerie des Universités de Paris (Legs POIX) (all to DJ). Open Access funding enabled and organized by Projekt DEAL.

Author contributions
AM, ACK, GAG, SJB, and GN designed and carried out experiments, analyzed data, provided critical intellectual input, and generated portions of the paper draft; CB, DJ, SD, and MG designed and carried out microarray analyses, provided the French MPM cell line cohort, and provided and characterized the Nantes patient cohort; HB, ÖK, DM, ŞD, ST, SE, ÖY, PB, and PF provided and characterized the Istanbul patient cohort; SAIW, LT, MAAP, and CMH designed and carried out sequencing experiments and analysis, immunohistochemistry,

RNA sequencing analysis, and digital droplet PCR; LVK, IK, ML, RAH, and JB provided the German MPM and LUAD tumor cohort; MI and MV performed *in vivo* CRE reporter assays and experiments using $KRAS^{G12D}$ mice; ACK and IL performed molecular phenotyping of murine tumors; DEW performed GSEA; HP evaluated and diagnosed mouse pathology; SGA prepared liposomes; IP, MS, and IG designed and performed experiments and provided critical intellectual input and partial funding; A-SL carried out and analyzed immunohistochemistry and digital droplet PCR, and organized the experiments for the revision of the manuscript; and GTS conceived the idea, obtained funding, supervised the study, designed experiments, analyzed the data, performed statistics, analyzed public datasets, generated graphs and figures, wrote the original paper and its revised form, and is the guarantor of the study's integrity. All authors reviewed and concur with the submitted manuscript.

Conflict of interest

IP works as a Senior Director in AstraZeneca Pharmaceutical in a non-related field with the publication. The remaining authors declare no competing financial interests.

For more information

Institute of Lung Biology and Disease (ILBD) & Comprehensive Pneumology Center (CPC): https://www.helmholtz-muenchen.de/ilbd/index.html
Helmholtz Center Munich-German Research Center for Environmental Health (HMGU): https://www.helmholtz-muenchen.de/en/helmholtz-zentrum-muenchen/index.html
Ludwig-Maximilian-University (LMU) Munich: https://www.en.uni-muenchen.de/index.html
The Regional Center for Research in Cancerology and Immunology Nantes / Angers: https://www.crcina.org/?lang=en
The Koc University School of Medicine: https://medicine.ku.edu.tr/en/
The cancer genome atlas (TCGA) pan-cancer human malignant pleural mesothelioma (MPM) dataset available at cBioportal: https://www.cbioportal.org/study/summary?id=meso_tcga_pan_can_atlas_2018
The cancer genome atlas (TCGA) pan-cancer human malignant pleural mesothelioma (MPM) gene expression dataset available at: https://xenabrowser.net/datapages/?dataset=TCGA-MESO.htseq_fpkm-uq.tsv&host=https%3A%2F%2Fgdc.xenahubs.net&removeHub=https%3A%2F%2Fxena.treehouse.gi.ucsc.edu%3A443
The catalogue of somatic mutations in cancer (COSMIC) human MPM dataset: https://cancer.sanger.ac.uk/cosmic/browse/tissue?wgs=off&sn=pleura&ss=all&hn=mesothelioma&sh=&in=t&src=tissue&all_data=n
Human MPM datasets at Gene Expression Omnibus: https://www.ncbi.nlm.nih.gov/geo/query/acc.cgi?acc=GSE51024, https://www.ncbi.nlm.nih.gov/geo/query/acc.cgi?acc=GSE134349, https://www.ncbi.nlm.nih.gov/geo/query/acc.cgi?acc=GSE42977
Novel mouse MPM cell line and normal mesothelial cell RNA sequencing dataset at Gene Expression Omnibus: https://www.ncbi.nlm.nih.gov/geo/query/acc.cgi?&acc=GSE94415
Using Pleural Effusions to Diagnose Cancer (MAPED) study page at ClinicalTrials.gov: https://www.clinicaltrials.gov/ct2/show/NCT03319472?term=maped&draw=2&rank=1
Links to patient support, advocate, and charity organizations: https://www.mesotheliomagroup.com/, https://www.mesothelioma.com/, https://www.mesotheliomahelp.org/, https://www.asbestos.com/support/, https://mesothelioma.net/mesothelioma-support/, https://www.curemeso.org/, https://www.mesotheliomahope.com/resources/cancer-foundations/, https://www.mesothelioma.uk.com/.

References

Abbosh C, Birkbak NJ, Wilson GA, Jamal-Hanjani M, Constantin T, Salari R, Le Quesne J, Moore DA, Veeriah S, Rosenthal R *et al* (2017) Phylogenetic ctDNA analysis depicts early-stage lung cancer evolution. *Nature* 545: 446–451

Agalioti T, Giannou AD, Krontira AC, Kanellakis NI, Kati D, Vreka M, Pepe M, Spella M, Lilis I, Zazara DE *et al* (2017) Mutant KRAS mediates malignant pleural effusion formation. *Nat Commun* 8: 15205

Arizti P, Fang L, Park I, Yin Y, Solomon E, Ouchi T, Aaronson SA, Lee SW (2000) Tumor suppressor p53 is required to modulate BRCA1 expression. *Mol Cell Biol* 20: 7450–7459

Bi M, Zhao S, Said JW, Merino MJ, Adeniran AJ, Xie Z, Nawaf CB, Choi J, Belldegrun AS, Pantuck AJ *et al* (2016) Genomic characterization of sarcomatoid transformation in clear cell renal cell carcinoma. *Proc Natl Acad Sci USA* 113: 2170–2175

Bibby AC, Tsim S, Kanellakis N, Ball H, Talbot DC, Blyth KG, Maskell NA, Psallidas I (2016) Malignant pleural mesothelioma: an update on investigation, diagnosis and treatment. *Eur Respir Rev* 25: 472–486

Blanquart C, Fonteneau J, Minvielle S (2019) Gene Expression Omnibus GSE134349 (https://www.ncbi.nlm.nih.gov/geo/query/acc.cgi?acc=GSE134349). [DATASET]

Blanquart C, Jaurand MC, Jean D (2020) The biology of malignant mesothelioma and the relevance of preclinical models. *Front Oncol* 10: 388

Bott M, Brevet M, Taylor BS, Shimizu S, Ito T, Wang LU, Creaney J, Lake RA, Zakowski MF, Reva B *et al* (2011) The nuclear deubiquitinase BAP1 is commonly inactivated by somatic mutations and 3p21.1 losses in malignant pleural mesothelioma. *Nat Genet* 43: 668–672

Brown CJ, Lain S, Verma CS, Fersht AR, Lane DP (2009) Awakening guardian angels: drugging the p53 pathway. *Nat Rev Cancer* 9: 862–873

Bueno R, Stawiski EW, Goldstein LD, Durinck S, De Rienzo A, Modrusan Z, Gnad F, Nguyen TT, Jaiswal BS, Chirieac LR *et al* (2016) Comprehensive genomic analysis of malignant pleural mesothelioma identifies recurrent mutations, gene fusions and splicing alterations. *Nat Genet* 48: 407–416

Burt BM, Bader A, Winter D, Rodig SJ, Bueno R, Sugarbaker DJ (2012) Expression of interleukin-4 receptor alpha in human pleural mesothelioma is associated with poor survival and promotion of tumor inflammation. *Clin Cancer Res* 18: 1568–1577

Byrd AL, Segre JA (2016) Infectious disease. Adapting Koch's postulates. *Science* 351: 224–226

Cao YA, Wagers AJ, Beilhack A, Dusich J, Bachmann MH, Negrin RS, Weissman IL, Contag CH (2004) Shifting foci of hematopoiesis during reconstitution from single stem cells. *Proc Natl Acad Sci USA* 101: 221–226

Carbone M, Adusumilli PS, Alexander HR, Baas P, Bardelli F, Bononi A, Bueno R, Felley-Bosco E, Galateau-Salle F, Jablons D *et al* (2019) Mesothelioma: scientific clues for prevention, diagnosis, and therapy. *CA Cancer J Clin* 69: 402–429

Cerami E, Gao J, Dogrusoz U, Gross BE, Sumer SO, Aksoy BA, Jacobsen A, Byrne CJ, Heuer ML, Larsson E *et al* (2012) The cBio cancer genomics portal: an open platform for exploring multidimensional cancer genomics data. *Cancer Discov* 2: 401–404

Cheah HM, Lansley SM, Varano Della Vergiliana JF, Tan AL, Thomas R, Leong SL, Creaney J, Lee YC (2017) Malignant pleural fluid from mesothelioma has potent biological activities. *Respirology* 22: 192–199

Comertpay S, Pastorino S, Tanji M, Mezzapelle R, Strianese O, Napolitano A, Baumann F, Weigel T, Friedberg J, Sugarbaker P *et al* (2014) Evaluation of clonal origin of malignant mesothelioma. *J Transl Med* 12: 301

Courtiol P, Maussion C, Moarii M, Pronier E, Pilcer S, Sefta M, Manceron P, Toldo S, Zaslavskiy M, Le Stang N *et al* (2019) Deep learning-based

classification of mesothelioma improves prediction of patient outcome. *Nat Med* 25: 1519–1525

De Rienzo A, Richards WG, Yeap BY, Coleman MH, Sugarbaker PE, Chirieac LR, Wang YE, Quackenbush J, Jensen RV, Bueno R (2012) Gene Expression Omnibus GSE42977 (https://www.ncbi.nlm.nih.gov/geo/query/acc.cgi?acc=GSE42977). [DATASET]

De Rienzo A, Richards WG, Yeap BY, Coleman MH, Sugarbaker PE, Chirieac LR, Wang YE, Quackenbush J, Jensen RV, Bueno R (2013) Sequential binary gene ratio tests define a novel molecular diagnostic strategy for malignant pleural mesothelioma. *Clin Cancer Res* 19: 2493–2502

De Rienzo A, Archer MA, Yeap BY, Dao N, Sciaranghella D, Sideris AC, Zheng Y, Holman AG, Wang YE, Dal Cin PS *et al* (2016) Gender-specific molecular and clinical features underlie malignant pleural mesothelioma. *Cancer Res* 76: 319–328

Delaunay T, Achard C, Boisgerault N, Grard M, Petithomme T, Chatelain C, Dutoit S, Blanquart C, Royer P-J, Minvielle S *et al* (2020) Frequent homozygous deletions of type I interferon genes in pleural mesothelioma confer sensitivity to oncolytic measles virus. *J Thorac Oncol* 15: 827–842

Demuth C, Spindler KG, Johansen JS, Pallisgaard N, Nielsen D, Hogdall E, Vittrup B, Sorensen BS (2018) Measuring KRAS mutations in circulating tumor DNA by droplet digital PCR and next-generation sequencing. *Transl Oncol* 11: 1220–1224

Enomoto Y, Kasai T, Takeda M, Takano M, Morita K, Kadota E, Iizuka N, Maruyama H, Haratake J, Kojima YU *et al* (2012) Epidermal growth factor receptor mutations in malignant pleural and peritoneal mesothelioma. *J Clin Pathol* 65: 522–527

Ewing B, Hillier L, Wendl MC, Green P (1998) Base-calling of automated sequencer traces using phred I accuracy assessment. *Genome Res* 8: 175–185

Faul F, Erdfelder E, Lang AG, Buchner A (2007) G*Power 3: a flexible statistical power analysis program for the social, behavioral, and biomedical sciences. *Behav Res Methods* 39: 175–191

Fennell DA, Parmar A, Shamash J, Evans MT, Sheaff MT, Sylvester R, Dhaliwal K, Gower N, Steele J, Rudd R (2005) Statistical validation of the EORTC prognostic model for malignant pleural mesothelioma based on three consecutive phase II trials. *J Clin Oncol* 23: 184–189

Flaherty KT, Puzanov I, Kim KB, Ribas A, McArthur GA, Sosman JA, O'Dwyer PJ, Lee RJ, Grippo JF, Nolop K *et al* (2010) Inhibition of mutated, activated BRAF in metastatic melanoma. *N Engl J Med* 363: 809–819

Forbes SA, Beare D, Gunasekaran P, Leung K, Bindal N, Boutselakis H, Ding M, Bamford S, Cole C, Ward S *et al* (2015) COSMIC: exploring the world's knowledge of somatic mutations in human cancer. *Nucleic Acids Res* 43: D805–D811

Fridlender ZG, Sun J, Kim S, Kapoor V, Cheng G, Ling L, Worthen GS, Albelda SM (2009) Polarization of tumor-associated neutrophil phenotype by TGF-beta: "N1" versus "N2" TAN. *Cancer Cell* 16: 183–194

Galateau-Salle F, Churg A, Roggli V, Travis WD; World Health Organization Committee for Tumors of the Pleura (2016) The 2015 World Health Organization classification of tumors of the pleura: advances since the 2004 classification. *J Thorac Oncol* 11: 142–154

Giannou AD, Marazioti A, Kanellakis NI, Giopanou I, Lilis I, Zazara DE, Ntaliarda G, Kati D, Armenis V, Giotopoulou GA *et al* (2017) *NRAS* destines tumor cells to the lungs. *EMBO Mol Med* 9: 672–686

Giannou AD, Marazioti A, Spella M, Kanellakis NI, Apostolopoulou H, Psallidas I, Prijovich ZM, Vreka M, Zazara DE, Lilis I *et al* (2015) Mast cells mediate malignant pleural effusion formation. *J Clin Invest* 125: 2317–2334

Global Burden of Disease (GBD) 2016 Occupational Carcinogens Collaborators (2020) Global and regional burden of cancer in 2016 arising from occupational exposure to selected carcinogens: a systematic analysis for the Global Burden of Disease Study 2016. *Occup Environ Med* 77: 151–159

Gueugnon F, Leclercq S, Blanquart C, Sagan C, Cellerin L, Padieu M, Perigaud C, Scherpereel A, Gregoire M (2011) Identification of novel markers for the diagnosis of malignant pleural mesothelioma. *Am J Pathol* 178: 1033–1042

Guo Y, Chirieac LR, Bueno R, Pass H, Wu W, Malinowska IA, Kwiatkowski DJ (2014) Tsc1-Tp53 loss induces mesothelioma in mice, and evidence for this mechanism in human mesothelioma. *Oncogene* 33: 3151–3160

Guo G, Chmielecki J, Goparaju C, Heguy A, Dolgalev I, Carbone M, Seepo S, Meyerson M, Pass HI (2015) Whole-exome sequencing reveals frequent genetic alterations in BAP1, NF2, CDKN2A, and CUL1 in malignant pleural mesothelioma. *Cancer Res* 75: 264–269

Hassan M, Mercer RM, Maskell NA, Asciak R, McCracken DJ, Bedawi EO, Shaarawy H, El-Ganady A, Psallidas I, Miller RF *et al* (2019) Survival in patients with malignant pleural effusion undergoing talc pleurodesis. *Lung Cancer* 137: 14–18

Herbst RS, Maddox A-M, Rothenberg ML, Small EJ, Rubin EH, Baselga J, Rojo F, Hong WK, Swaisland H, Averbuch SD *et al* (2002) Selective oral epidermal growth factor receptor tyrosine kinase inhibitor ZD1839 is generally well-tolerated and has activity in non-small-cell lung cancer and other solid tumors: results of a phase I trial. *J Clin Oncol* 20: 3815–3825

Hmeljak J, Sanchez-Vega F, Hoadley KA, Shih J, Stewart C, Heiman D, Tarpey P, Danilova L, Drill E, Gibb EA *et al* (2018) Integrative molecular characterization of malignant pleural mesothelioma. *Cancer Discov* 8: 1548–1565

Ikediobi ON, Davies H, Bignell G, Edkins S, Stevens C, O'Meara S, Santarius T, Avis T, Barthorpe S, Brackenbury L *et al* (2006) Mutation analysis of 24 known cancer genes in the NCI-60 cell line set. *Mol Cancer Ther* 5: 2606–2612

Jackson EL, Willis N, Mercer K, Bronson RT, Crowley D, Montoya R, Jacks T, Tuveson DA (2001) Analysis of lung tumor initiation and progression using conditional expression of oncogenic K-ras. *Genes Dev* 15: 3243–3248

Jamal-Hanjani M, Wilson GA, McGranahan N, Birkbak NJ, Watkins TBK, Veeriah S, Shafi S, Johnson DH, Mitter R, Rosenthal R *et al* (2017) Tracking the evolution of non-small-cell lung cancer. *N Engl J Med* 376: 2109–2121

Jay JJ, Brouwer C (2016) Lollipops in the clinic: information dense mutation plots for precision medicine. *PLoS One* 11: e0160519

Jongsma J, van Montfort E, Vooijs M, Zevenhoven J, Krimpenfort P, van der Valk M, van de Vijver M, Berns A (2008) A conditional mouse model for malignant mesothelioma. *Cancer Cell* 13: 261–271

Kadariya Y, Menges CW, Talarchek J, Cai KQ, Klein-Szanto AJ, Pietrofesa RA, Christofidou-Solomidou M, Cheung M, Mossman BT, Shukla A *et al* (2016) Inflammation-related IL1β/IL1R signaling promotes the development of asbestos-induced malignant mesothelioma. *Cancer Prev Res (Phila)* 9: 406–414

Kanellakis NI, Giannou AD, Pepe MAA, Agalioti T, Zazara DE, Giopanou I, Psallidas I, Spella M, Marazioti A, Arendt KAM *et al* (2019) Tobacco chemical-induced mouse lung adenocarcinoma cell lines pin the prolactin orthologue proliferin as a lung tumour promoter. *Carcinogenesis* 40: 1352–1362

Kanellakis NI, Asciak R, Hamid MA, Yao X, McCole M, McGowan S, Seraia E, Hatch S, Hallifax RJ, Mercer RM *et al* (2020) Patient-derived malignant pleural mesothelioma cell cultures: a tool to advance biomarker-driven treatments. *Thorax* 75: 1004–1008

Kato S, Tomson BN, Buys TP, Elkin SK, Carter JL, Kurzrock R (2016) Genomic landscape of malignant mesotheliomas. *Mol Cancer Ther* 15: 2498–2507

Kindler HL, Ismaila N, Armato SG, Bueno R, Hesdorffer M, Jahan T, Jones CM, Miettinen M, Pass H, Rimner A *et al* (2018) Treatment of malignant pleural mesothelioma: American Society of Clinical Oncology Clinical Practice Guideline. *J Clin Oncol* 36: 1343–1373

Klotz LV, Courty Y, Lindner M, Petit-Courty A, Stowasser A, Koch I, Eichhorn ME, Lilis I, Morresi-Hauf A, Arendt KAM *et al* (2019) Comprehensive clinical profiling of the Gauting locoregional lung adenocarcinoma donors. *Cancer Med* 8: 1486–1499

Klotz LV, Lindner M, Eichhorn ME, Grützner U, Koch I, Winter H, Kauke T, Duell T, Hatz RA (2019) Pleurectomy/decortication and hyperthermic intrathoracic chemoperfusion using cisplatin and doxorubicin for malignant pleural mesothelioma. *J Thorac Dis* 11: 1963–1972

Kukuyan AM, Sementino E, Kadariya Y, Menges CW, Cheung M, Tan Y, Cai KQ, Slifker MJ, Peri S, Klein-Szanto AJ *et al* (2019) Inactivation of Bap1 cooperates with losses of Nf2 and Cdkn2a to drive the development of pleural malignant mesothelioma in conditional mouse models. *Cancer Res* 79: 4113–4123

Liu B, van Gerwen M, Bonassi S, Taioli E; International Association for the Study of Lung Cancer Mesothelioma Task Force (2017) Epidemiology of Environmental Exposure and Malignant Mesothelioma. *J Thorac Oncol* 12: 1031–1045

Li S, MacAlpine DM, Counter CM (2020) Capturing the primordial Kras mutation initiating urethane carcinogenesis. *Nat Commun* 11: 1800

Lo Iacono M, Monica V, Righi L, Grosso F, Libener R, Vatrano S, Bironzo P, Novello S, Musmeci L, Volante M *et al* (2015) Targeted next-generation sequencing of cancer genes in advanced stage malignant pleural mesothelioma: a retrospective study. *J Thorac Oncol* 10: 492–499

Marazioti A, Lilis I, Vreka M, Apostolopoulou H, Kalogeropoulou A, Giopanou I, Giotopoulou GA, Krontira AC, Iliopoulou M, Kanellakis NI *et al* (2018) Myeloid-derived interleukin-1β drives oncogenic KRAS-NF-κB addiction in malignant pleural effusion. *Nat Commun* 9: 672

Marazioti A, Papadia K, Giannou A, Stathopoulos GT, Antimisiaris SG (2019) Prolonged retention of liposomes in the pleural cavity of normal mice and high tumor distribution in mice with malignant pleural effusion, after intrapleural injection. *Int J Nanomed* 14: 3773–3784

Marazioti A, Voulgaridis A, Psallidas I, Lamort AS, Iliopoulou M, Krontira AC, Lilis I, Asciak R, Kanellakis NI, Rahman NM *et al* (2021) Clinical identification of malignant pleural effusions. *medRxiv* https://doi.org/10.1101/2020.05.31.20118307 [PREPRINT]

Marino S, Vooijs M, van Der Gulden H, Jonkers J, Berns A (2000) Induction of medulloblastomas in p53-null mutant mice by somatic inactivation of Rb in the external granular layer cells of the cerebellum. *Genes Dev* 14: 994–1004

Markoutsa E, Papadia K, Giannou AD, Spella M, Cagnotto A, Salmona M, Stathopoulos GT, Antimisiaris SG (2014) Mono and dually decorated nanoliposomes for brain targeting, *in vitro* and *in vivo* studies. *Pharm Res* 31: 1275–1289

Mason RJ, Kalina M, Nielsen LD, Malkinson AM, Shannon JM (2000) Surfactant protein C expression in urethane-induced murine pulmonary tumors. *Am J Pathol* 156: 175–182

Matallanas D, Romano D, Al-Mulla F, O'Neill E, Al-Ali W, Crespo P, Doyle B, Nixon C, Sansom O, Drosten M *et al* (2011) Mutant K-Ras activation of the proapoptotic MST2 pathway is antagonized by wild-type K-Ras. *Mol Cell* 44: 893–906

Menges CW, Kadariya Y, Altomare D, Talarchek J, Neumann-Domer E, Wu Y, Xiao G-H, Shapiro IM, Kolev VN, Pachter JA *et al* (2014) Tumor suppressor alterations cooperate to drive aggressive mesotheliomas with enriched cancer stem cells via a p53-miR-34a-c-Met axis. *Cancer Res* 74: 1261–1271

Meylan E, Dooley AL, Feldser DM, Shen L, Turk E, Ouyang C, Jacks T (2009) Requirement for NF-kappaB signalling in a mouse model of lung adenocarcinoma. *Nature* 462: 104–107

Mezzapelle R, Miglio U, Rena O, Paganotti A, Allegrini S, Antona J, Molinari F, Frattini M, Monga G, Alabiso O *et al* (2013) Mutation analysis of the EGFR gene and downstream signalling pathway in histologic samples of malignant pleural mesothelioma. *Br J Cancer* 108: 1743–1749

Mutti L, Peikert T, Robinson BWS, Scherpereel A, Tsao AS, de Perrot M, Woodard GA, Jablons DM, Wiens J, Hirsch FR *et al* (2018) Scientific advances and new frontiers in mesothelioma therapeutics. *J Thorac Oncol* 13: 1269–1283

Muzumdar MD, Tasic B, Miyamichi K, Li L, Luo L (2007) A global double-fluorescent Cre reporter mouse. *Genesis* 45: 593–605

Nagai H, Okazaki Y, Chew SH, Misawa N, Yamashita Y, Akatsuka S, Ishihara T, Yamashita K, Yoshikawa Y, Yasui H *et al* (2011) Diameter and rigidity of multiwalled carbon nanotubes are critical factors in mesothelial injury and carcinogenesis. *Proc Natl Acad Sci USA* 108: E1330–E1338

Nasu M, Emi M, Pastorino S, Tanji M, Powers A, Luk H, Baumann F, Zhang Y-A, Gazdar A, Kanodia S *et al* (2015) High incidence of somatic BAP1 alterations in sporadic malignant mesothelioma. *J Thorac Oncol* 10: 565–576

Paajanen J, Laaksonen S, Ilonen I, Wolff H, Husgafvel-Pursiainen K, Kuosma E, Ollila H, Myllärniemi M, Vehmas T (2018) Computed tomography in the evaluation of malignant pleural mesothelioma-Association of tumor size to a sarcomatoid histology, a more advanced TNM stage and poor survival. *Lung Cancer* 116: 73–79

Pass H, Giroux D, Kennedy C, Ruffini E, Cangir AK, Rice D, Asamura H, Waller D, Edwards J, Weder W *et al* (2016) The IASLC mesothelioma staging project: improving staging of a rare disease through international participation. *J Thorac Oncol* 11: 2082–2088

Patel MR, Jacobson BA, De A, Frizelle SP, Janne P, Thumma SC, Whitson BA, Farassati F, Kratzke RA (2007) Ras pathway activation in malignant mesothelioma. *J Thorac Oncol* 2: 789–795

Patil NS, Righi L, Koeppen H, Zou W, Izzo S, Grosso F, Libener R, Loiacono M, Monica V, Buttigliero C *et al* (2018) Molecular and histopathological characterization of the tumor immune microenvironment in advanced stage of malignant pleural mesothelioma. *J Thorac Oncol* 13: 124–133

Pauli C, Hopkins BD, Prandi D, Shaw R, Fedrizzi T, Sboner A, Sailer V, Augello M, Puca L, Rosati R *et al* (2017) Personalized *in vitro* and *in vivo* cancer models to guide precision medicine. *Cancer Discov* 7: 462–477

Pfaffl MW (2001) A new mathematical model for relative quantification in real-time RT-PCR. *Nucleic Acids Res* 29: e45

Poole JC, Wu S-F, Lu TT, Vibat CRT, Pham A, Samuelsz E, Patel M, Chen J, Daher T, Singh VM *et al* (2019) Analytical validation of the target selector ctDNA platform featuring single copy detection sensitivity for clinically actionable EGFR, BRAF, and KRAS mutations. *PLoS One* 14: e0223112

Quetel L, Meiller C, Assié J-B, Blum Y, Imbeaud S, Montagne F, Tranchant R, Wolf J, Caruso S, Copin M-C *et al* (2020) Genetic alterations of malignant pleural mesothelioma: association with tumor heterogeneity and overall survival. *Mol Oncol* 14: 1207–1223

Robinson BW, Musk AW, Lake RA (2005) Malignant mesothelioma. *Lancet* 366: 397–408

Robinson JT, Thorvaldsdóttir H, Winckler W, Guttman M, Lander ES, Getz G, Mesirov JP (2011) Integrative genomics viewer. *Nat Biotechnol* 29: 24

Rusch VW, Chansky K, Kindler HL, Nowak AK, Pass HI, Rice DC, Shemanski L, Galateau-Sallé F, McCaughan BC, Nakano T *et al* (2016) The IASLC mesothelioma staging project: proposals for the M descriptors and for revision of the TNM stage groupings in the forthcoming (Eighth) edition of the TNM classification for mesothelioma. *J Thorac Oncol* 11: 2112–2119

Ryman-Rasmussen JP, Cesta MF, Brody AR, Shipley-Phillips JK, Everitt JI, Tewksbury EW, Moss OR, Wong BA, Dodd DE, Andersen ME *et al* (2009) Inhaled carbon nanotubes reach the subpleural tissue in mice. *Nat Nanotechnol* 4: 747–751

Ryu JS, Ryu HJ, Lee SN, Memon A, Lee SK, Nam HS, Kim HJ, Lee KH, Cho JH, Hwang SS (2014) Prognostic impact of minimal pleural effusion in non-small-cell lung cancer. *J Clin Oncol* 32: 960–967

Sanchez-Vega F, Mina M, Armenia J, Chatila WK, Luna A, La KC, Dimitriadoy S, Liu DL, Kantheti HS, Saghafinia S *et al* (2018) Oncogenic signaling pathways in the cancer genome atlas. *Cell* 173: 321–337

Scherpereel A, Astoul P, Baas P, Berghmans T, Clayson H, de Vuyst P, Dienemann H, Galateau-Salle F, Hennequin C, Hillerdal G *et al* (2010) Guidelines of the European Respiratory Society and the European Society of Thoracic Surgeons for the management of malignant pleural mesothelioma. *Eur Respir J* 35: 479–495

Scherpereel A, Wallyn F, Albelda SM, Munck C (2018) Novel therapies for malignant pleural mesothelioma. *Lancet Oncol* 19: e161–e172

Schindelin J, Arganda-Carreras I, Frise E, Kaynig V, Longair M, Pietzsch T, Preibisch S, Rueden C, Saalfeld S, Schmid B *et al* (2012) Fiji: an open-source platform for biological-image analysis. *Nat Methods* 9: 676–682

Shukuya T, Serizawa M, Watanabe M, Akamatsu H, Abe M, Imai H, Tokito T, Ono A, Taira T, Kenmotsu H *et al* (2014) Identification of actionable mutations in malignant pleural mesothelioma. *Lung Cancer* 86: 35–40

Smeele P, d'Almeida SM, Meiller C, Chéné A-L, Liddell C, Cellerin L, Montagne F, Deshayes S, Benziane S, Copin M-C *et al* (2018) Brain-derived neurotrophic factor, a new soluble biomarker for malignant pleural mesothelioma involved in angiogenesis. *Mol Cancer* 17: 148

Smith JC, Sheltzer JM (2018) Systematic identification of mutations and copy number alterations associated with cancer patient prognosis. *Elife* 7: e39217

Spella M, Lilis I, Pepe MAA, Chen Y, Armaka M, Lamort A-S, Zazara DE, Roumelioti F, Vreka M, Kanellakis NI *et al* (2019) Club cells form lung adenocarcinomas and maintain the alveoli of adult mice. *Elife* 8: e45571

Stathopoulos GT, Zhu Z, Everhart MB, Kalomenidis I, Lawson WE, Bilaceroglu S, Peterson TE, Mitchell D, Yull FE, Light RW *et al* (2006) Nuclear factor-kappaB affects tumor progression in a mouse model of malignant pleural effusion. *Am J Respir Cell Mol Biol* 34: 142–150

Stathopoulos GT, Kanellakis NI, Pepe M (2017) Gene Expression Omnibus GSE94415: Transcriptomic profiling of KPM cell lines through RNA-Seq (https://www.ncbi.nlm.nih.gov/geo/query/acc.cgi?acc=GSE94415). [DATASET]

Stephen AG, Esposito D, Bagni RK, McCormick F (2014) Dragging ras back in the ring. *Cancer Cell* 25: 272–281

Stott FJ, Bates S, James MC, McConnell BB, Starborg M, Brookes S, Palmero I, Ryan K, Hara E, Vousden KHJ *et al* (1998) The alternative product from the human CDKN2A locus, p14(ARF), participates in a regulatory feedback loop with p53 and MDM2. *EMBO J* 17: 5001–5014

Subramanian A, Tamayo P, Mootha VK, Mukherjee S, Ebert BL, Gillette MA, Paulovich A, Pomeroy SL, Golub TR, Lander ES *et al* (2005) Gene set enrichment analysis: a knowledge-based approach for interpreting genome-wide expression profiles. *Proc Natl Acad Sci USA* 102: 15545–15550

Thomas R, Fysh ETH, Smith NA, Lee P, Kwan BCH, Yap E, Horwood FC, Piccolo F, Lam DCL, Garske LA *et al* (2017) Effect of an indwelling pleural catheter vs talc pleurodesis on hospitalization days in patients with malignant pleural effusion: the AMPLE randomized clinical trial. *JAMA* 318: 1903–1912

Tikoo A, Varga M, Ramesh V, Gusella J, Maruta H (1994) An anti-Ras function of neurofibromatosis type 2 gene product (NF2/Merlin). *J Biol Chem* 269: 23387–23390

Tsao AS, Wistuba I, Roth JA, Kindler HL (2009) Malignant pleural mesothelioma. *J Clin Oncol* 27: 2081–2090

Westbom CM, Shukla A, MacPherson MB, Yasewicz EC, Miller JM, Beuschel SL, Steele C, Pass HI, Vacek PM, Shukla A (2014) CREB-induced inflammation is important for malignant mesothelioma growth. *Am J Pathol* 184: 2816–2827

Xu J, Kadariya Y, Cheung M, Pei J, Talarchek J, Sementino E, Tan Y, Menges CW, Cai KQ, Litwin S *et al* (2014) Germline mutation of Bap1 accelerates development of asbestos-induced malignant mesothelioma. *Cancer Res* 74: 4388–4397

Yap TA, Aerts JG, Popat S, Fennell DA (2017) Novel insights into mesothelioma biology and implications for therapy. *Nat Rev Cancer* 17: 475–488

Zalcman G, Mazieres J, Margery J, Greillier L, Audigier-Valette C, Moro-Sibilot D, Molinier O, Corre R, Monnet I, Gounant V *et al* (2016) French Cooperative Thoracic Intergroup (IFCT). Bevacizumab for newly diagnosed pleural mesothelioma in the Mesothelioma Avastin Cisplatin Pemetrexed Study (MAPS): a randomised, controlled, open-label, phase 3 trial. *Lancet* 387: 1405–1414

Zimmermann G, Papke B, Ismail S, Vartak N, Chandra A, Hoffmann M, Hahn SA, Triola G, Wittinghofer A, Bastiaens PIH *et al* (2013) Small molecule inhibition of the KRAS-PDEδ interaction impairs oncogenic KRAS signalling. *Nature* 497: 638–642

4. Paper II

ONCOIMMUNOLOGY
2019, VOL. 8, NO. 7, e1593802 (18 pages)
https://doi.org/10.1080/2162402X.2019.1593802

Taylor & Francis
Taylor & Francis Group

ORIGINAL RESEARCH

OPEN ACCESS Check for updates

Interleukin-1β provided by KIT-competent mast cells is required for *KRAS*-mutant lung adenocarcinoma

Ioannis Lilis[a], Giannoula Ntaliarda[a], Vassilios Papaleonidopoulos [a], Georgia A Giotopoulou[a], Maria Oplopoiou[a], Antonia Marazioti[a], Magda Spella[a], Sebastian Marwitz[b], Torsten Goldmann[b], Vasiliki Bravou[c], Ioanna Giopanou [a], and Georgios T. Stathopoulos [a,d]

[a]Laboratory for Molecular Respiratory Carcinogenesis, Department of Physiology, Faculty of Medicine, University of Patras, Rio, Achaia, Greece; [b]Clinical and Experimental Pathology, Research Center Borstel, Airway Research Center North (ARCN), Member of the German Center for Lung Research (DZL), Borstel, Germany; [c]Department of Anatomy-Histology-Embryology, Faculty of Medicine, University of Patras, Rio, Achaia, Greece; [d]Comprehensive Pneumology Center (CPC) and Institute for Lung Biology and Disease (iLBD), University Hospital, Ludwig-Maximilians University and Helmholtz Zentrum München, Member of the German Center for Lung Research (DZL), Munich, Bavaria, Germany

ABSTRACT

Mast cells (MC) have been identified in human lung adenocarcinoma (LADC) tissues, but their functional role has not been investigated *in vivo*. For this, we applied three mouse models of *KRAS*-mutant LADC to two different MC-deficient mouse strains (*cKit*^{Wsh} and *Cpa3.Cre*). Moreover, we derived MC gene signatures from murine bone marrow-derived MC and used them to interrogate five human cohorts of LADC patients. Tumor-free *cKit*^{Wsh} and *Cpa3.Cre* mice were deficient in alveolar and skin KIT-dependent (KIT+) MC, but *cKit*^{Wsh} mice retained normal KIT-independent (KIT-) MC in the airways. Both KIT+ and KIT- MC infiltrated murine LADC to varying degrees, but KIT+ MC were more abundant and promoted LADC initiation and progression through interleukin-1β secretion. KIT+ MC and their transcriptional signature were significantly enriched in human LADC compared to adjacent normal tissue, especially in the subset of patients with *KRAS* mutations. Importantly, MC density increased with tumor stage and high overall expression of the KIT+ MC signature portended poor survival. Collectively, our results indicate that KIT+ MC foster LADC development and represent marked therapeutic targets.

ARTICLE HISTORY
Received 1 August 2018
Revised 23 February 2019
Accepted 28 February 2019

KEYWORDS
Carboxypeptidase 3/mutation/IL; 1β/lung cancer/urethane

Introduction

Lung adenocarcinoma (LADC) is the number one cancer killer worldwide, constituting the majority of newly diagnosed lung cancer cases and continuously rising in incidence.[1,2] Epidemiologic and molecular evidence indicates an increased risk of LADC harboring mutations in the KRAS proto-oncogene GTPase (*KRAS*) in ever-smoking individuals.[1,3] These patients also feature smoking-associated chronic inflammation that is clinically evident as chronic airflow obstruction.[4–7] It is generally believed that this inflammation alters the microenvironment of tobacco carcinogen-mutated respiratory epithelial cells, fostering their survival and sustained growth instead of their eradication.[4,8] This pulmonary inflamed microenvironment of smokers encompasses complex interactions between tumor-initiated respiratory epithelial cells and host immune cells and has been only poorly charted.[9–11]

Mast cells (MC) are bone marrow-derived inflammatory leukocytes which can secrete upon activation a battery of biologically active products.[12–15] MC are distributed in all vascularized tissues and are particularly abundant at the bodily interfaces to the environment, including the lungs, skin, and gut.[14,16–19] Although MC are well-recognized initiators of acute allergic reactions, it is now apparent that these multifarious cells infiltrate a wide spectrum of malignancies and execute various important functions in tumor initiation and progression.[20–24] To this end, MC play pro-tumorigenic roles in some malignancies (i.e., gastric, prostate, and pancreatic cancers), gate-keeper roles in others (i.e., breast and ovarian cancers), and function as innocent bystanders in yet others.[25] While the reasons for divergent MC functions in cancer remain elusive, new models of MC ablation lend promise to solve this riddle but have not been widely employed in cancer models.[26,27]

MC have been identified in human and murine LADC, and have been found to promote lung adenocarcinoma cell growth *in vitro* and to be associated with poor patient survival.[28–31] We recently showed that *KRAS* mutations in tumor cells and host co-opted MC cooperate to promote the development of an inflammatory chemokine signaling network that culminates in metastatic malignant pleural effusions.[32–34] However, the functional role of MC in *KRAS*-mutant LADC development remained elusive. Here we generated various types of *KRAS*-mutant LADC in two different mouse models of MC ablation (*cKit*^{Wsh} and *Cpa3.Cre* mice) that feature, respectively, selective

CONTACT Georgios T. Stathopoulos gstathop@upatras.gr; Ioannis Lilis ioannislilis@upatras.gr Biomedical Sciences Research Building, 2nd floor, Room B40; 1 Asklepiou Str., University Campus, Rio 26504, Greece
Ioannis Lilis and Giannoula Ntaliarda are equally contributing first authors
Georgios T. Stathopoulos and Ioanna Giopanou are equally contributing senior authors

elimination of KIT-dependent MC and complete ablation of all MC. Interestingly, KIT-dependent MC were more abundant and were found to promote experimental *KRAS*-mutant LADC initiated by the tobacco carcinogen urethane, by oncogenic $KRAS^{G12D}$ expression in the lungs, and by transplanted LADC cells. KIT-dependent MC and their transcriptome signatures were evident in different human LADC cohorts and correlated with poor survival, indicating a potential actionable role for these cells in human disease progression.

Results

Mast cells infiltrate murine lung adenocarcinomas

To identify whether MC infiltrate experimental LADC, we used three different mouse models of the disease arising in distinct anatomical compartments. In a first line of experiments, *C57BL/6* mice received 10 consecutive weekly intraperitoneal injections of the tobacco-contained carcinogen urethane (1g/Kg) and were sacrificed after six months, a model that results in stochastic chemical mutagenesis of the airway epithelium (Figure 1A, D).[35–38] Alternatively, *C57BL/6* mice carrying a conditional loxP-STOP-loxP. $KRAS^{G12D}$ allele ($KRAS^{G12D}$ mice) received 5×10^8 intratracheal plaque-forming units (pfu) Ad-*Cre* and were killed after four months. In this model, progressive lesions carrying the inciting $KRAS^{G12D}$ mutation are inflicted in alveolar epithelial cells infected by Ad-*Cre* via excision of the STOP codon that hinders expression of the mutant transgene (Figures 1B, E).[39,40] In a third line of experiments, *C57BL/6* mice received 10^6 LLC cells into the rear flank dermis, a model of established LADC heterotopic growth and spontaneous pulmonary metastasis (Figures 1C, F).[41–43] We labeled with the metachromatic stain toluidine blue (TB) that distinctively stains MC violet on a blue background and systematically evaluated MC abundance on randomly sampled sections of lungs from the former two models, and primary tumors and lungs with metastases from the latter model, as well as tumor-free lungs of *C57BL/6* mice (n = 10/group). MC were identified in LADC of all three models examined, preferentially located in early lesions, at the tumor front, at subbronchial and subpleural sites, or within alveolar inflammatory infiltrates frequently observed in juxtatumoral areas (Figures 1G–N). Importantly, alveoli were less MC-dense, and MC infiltrates of urethane-induced tumors were less prominent compared with the $KRAS^{G12D}$ and LLC models (Figure 1O). Overall, MC infiltrates accounted for approximately 1 in 50 tumor cells. These findings are in accord with a previous report from the urethane model,[29] and indicate that MC are present in experimental LADC developing in the airways, alveoli, and skin.

Compartmentalized mast cell deficiency of $cKit^{wsh}$ and *Cpa3.cre* mice

We next assessed lung and skin MC density in two different strains of genetically MC-deficient mice that either lack functional KIT receptors required for mastopoiesis ($cKit^{Wsh}$ mice),[33,44] or express CRE recombinase exclusively in MC leading to tumor-related protein 53 (TRP53)-mediated spontaneous apoptosis of these cells (*Cpa3.Cre* mice).[27,33] For this, the airways, alveoli, and skin of mice on a pure *C57BL/6* background carrying one or two $cKit^{Wsh}$ alleles (designated $cKit^{Wsh/Wt}$ and $cKit^{Wsh/Wsh}$, respectively) or one *Cpa3.Cre* allele, as well as littermate controls of both strains (collectively designated *C57BL/6*; n = 10/group; total n = 40) were sectioned and stained with toluidine blue. In more detail, the control *C57BL/6* group consisted of $cKit^{Wt/Wt}$ littermates of $cKit^{Wsh/Wt}$ and $cKit^{Wsh/Wt}$ mice, wild-type (*Wt*) littermates of *Cpa3.Cre* mice, as well as *Lyz2.Cre* mice that express CRE recombinase under the control of the endogenous *Lyz2* promoter as additional controls for *Cpa3.Cre* mice.[45] Surprisingly, MC were identified throughout the airways of *C57BL/6*, but also of $cKit^{Wsh/Wt}$ and $cKit^{Wsh/Wsh}$ mice and were absent from the airways of *Cpa3.Cre* mice. In contrast, MC were present in the alveolar regions, pulmonary vasculature, mediastinal organs, and the skin of *C57BL/6* mice, but were significantly decreased in these compartments of $cKit^{Wsh/Wt}$, $cKit^{Wsh/Wsh}$, and *Cpa3.Cre* mice (Figures 2A–G). These results are consistent with the initial descriptions of these mice,[27,44] as well as with our previous study of pleural MC,[33] and indicate that $cKit^{Wsh/Wsh}$ and *Cpa3.Cre* mice can serve as compartmentalized mouse models of MC deficiency of the alveoli/skin and of the airways/alveoli/skin, respectively (Figure 2H).

Mast cells are required for lung adenocarcinoma formation and progression

To determine whether MC are functionally involved in LADC development, we reproduced all three mouse models of airway, alveolar, and cutaneous LADC described above in *C57BL/6* (*Wt* littermates and *Lyz2.Cre* heterozygotes), $cKit^{Wsh/Wt}$, $cKit^{Wsh/Wsh}$, and *Cpa3.Cre* mice. In a first line of experiments, *C57BL/6*, $cKit^{Wsh/Wt}$, $cKit^{Wsh/Wsh}$, and *Cpa3.Cre* mice received 10 consecutive weekly intraperitoneal urethane (1g/Kg) injections (total n = 143; Figure 3A). Thirty-eight mice succumbed to repeat carcinogen treatment (14 of 58 *C57BL/6*, 2 of 21 $cKit^{Wsh/Wt}$, 21 of 55 $cKit^{Wsh/Wsh}$, and 1 of 9 *Cpa3.Cre* mice; χ^2 P = 0.0419, Fisher's exact P = 0.0236 for comparison of $cKit^{Wsh/Wt}$ with $cKit^{Wsh/Wsh}$ mice), while the remaining 105 mice were sacrificed after six months for lung tumor evaluation (Figure 3B). *Cpa3.Cre* mice were markedly protected from urethane-induced bronchial carcinomas in terms of tumor multiplicity, size, and cellular proliferation rate, suggesting an important role for MC in tumor initiation and progression, whereas $cKit^{Wsh/Wt}$ and $cKit^{Wsh/Wsh}$ mice were susceptible to the carcinogen to a degree similar to *C57BL/6* mice, a result consistent with their sufficiency in MC of the airways, the site of tumor initiation induced by urethane (Figure 3C–E). In a second line of experiments, $KRAS;^{G12D}$ $KRAS;^{G12D}cKit^{Wsh/Wt}$, and $KRAS;^{G12D}cKit^{Wsh/Wsh}$ mice (*C57BL/6* background) received 5×10^8 intratracheal pfu Ad-*Cre* and were killed after four months. $KRAS^{G12D}$ x *Cpa3.Cre* intercrosses failed to generate double heterozygote offspring suggesting fetal lethality (n = three intercrosses; 11 litters; 53 off-springs; P = 0.0001 for 0/53 genotype frequencies obtained compared to 13/40 expected by Fischer's exact test). $KRAS;^{G12D}cKit^{Wsh/Wsh}$ mice were significantly protected from *KRAS*-driven alveolar carcinomas compared with $KRAS^{G12D}$ mice, with $KRAS;^{G12D}cKit^{Wsh/Wt}$ mice

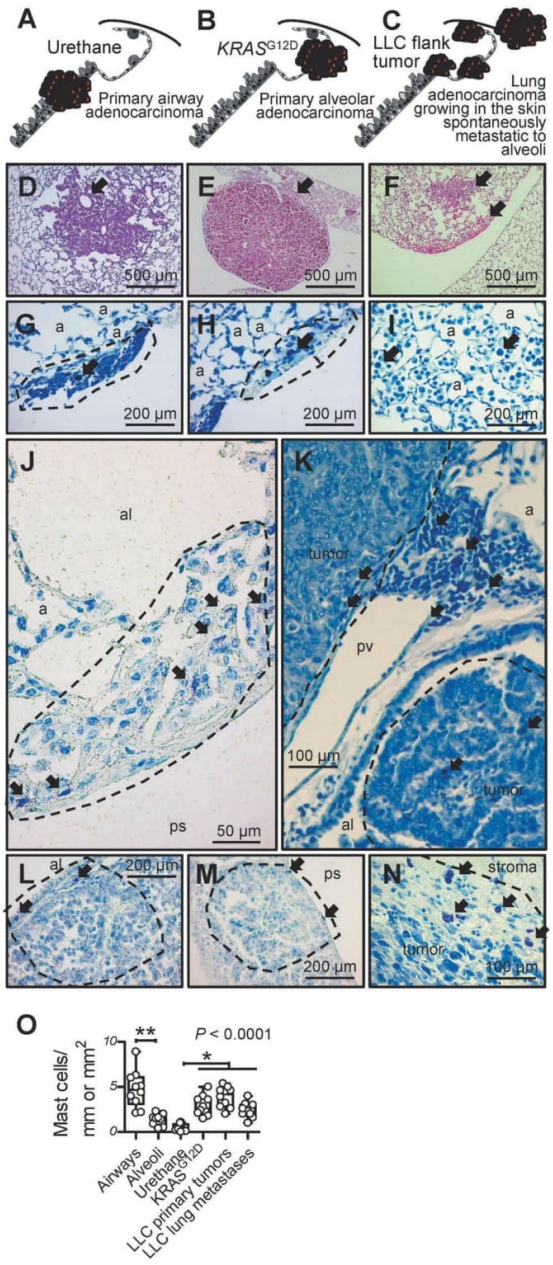

Figure 1. Mast cells in murine lung adenocarcinomas.

A-F Schematics depicting tumors (red) of the airways, alveoli, and skin (A-C) and representative microscopic images of hematoxylin/eosin-stained sections (D-F) of airway-originated lung adenocarcinomas (LADC) induced in *C57BL/6* mice by 10 weekly consecutive intraperitoneal injections of 1 g/Kg urethane (six months latency; A and D; arrow in D denotes originating bronchus), of alveolar-derived LADC induced in *KRAS*^{G12D}-transgenic mice by intratracheal injection of 5×10^8 pfu Ad-*Cre* (four months latency; B and E; arrow in E denotes originating alveolar region), and of skin heterotopic LADC spontaneously metastasizing to the alveolar regions induced by subcutaneous delivery of 10^6 LLC cells (one month latency; C and F; arrows in F denote alveolar regions involved by metastases). G-N Toluidine blue-stained lung and tumor sections from the above-described three mouse models of LADC showing metachromatic (purple) mast cells (arrows) in early urethane-induced atypical alveolar hyperplasias (dashed lines in G and H), in tumor-adjacent alveolar inflammatory infiltrates (I), in and adjacent to urethane-induced LADC (dashed lines in J and K), entering alveolar *KRAS*^{G12D}-transgenic tumors from the airway lumen and the pleural space (dashed lines, L and M), and in subcutaneous LLC tumor (dashed line in N). a, alveoli; al, airway lumen; ps, pleural space; pv, pulmonary vein. O Mast cell abundance of urethane- and *KRAS*^{G12D}-primary tumors and LLC primary tumors and metastases compared with airways and alveoli of naïve *C57BL/6* mice (n = 10/group). Data are presented as median with Tukey's whiskers (boxes: interquartile range; bars: 50% extreme quartiles), raw data points (dots),and Kruskal–Wallis analysis of variance (ANOVA) probability (P) value.* and **: $P < 0.05$ and $P < 0.01$, respectively, for the indicated comparisons by Dunn's post-tests. Only statistically significant differences are indicated.

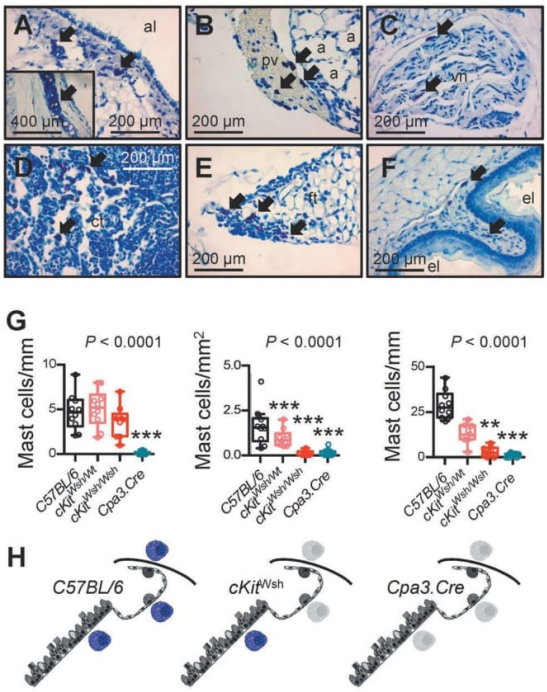

Figure 2. Thoracic and skin mast cells in two different mouse models of mast cell deficiency.

The airways, alveoli, and skin of mice carrying one or two *cKit*^{Wsh} alleles (designated *cKit*$^{Wsh/Wt}$ and *cKit*$^{Wsh/Wsh}$, respectively) or one *Cpa3.Cre* allele on a pure *C57BL/6* background, and *C57BL/6* littermate or *Lyz2.Cre* heterozygous control mice (n = 10/group) were sectioned and stained with toluidine blue. Representative microscopic images of toluidine blue-stained tissue sections (A-F), summary of data from n = 10 mice/group (G), and schematics of mast cell competence (colored mast cells) and deficiency (grey mast cell shadows) (H). A-F Arrows indicate mast cells in the submucosa of a large airway (A; inlay shows tracheal cartilage as positive control of metachromatic purple staining), in a large pulmonary vein (B), in the vagus nerve (C), in the thymus of a 6-week-old (D) and a 20-week-old (E) mouse, and in the esophageal submucosa (F) of *C57BL/6* controls. a, alveoli; pv, pulmonary vein; al, airway lumen; vn, vagus nerve; ct, cellular thymus; ft, fatty thymus; el, esophagus lumen. G Airway, alveolar, and skin mast cell density of *C57BL/6* control, *cKit*$^{Wsh/Wt}$, *cKit*$^{Wsh/Wsh}$, and *Cpa3.Cre* mice (summary of data from n = 10 mice/group). Shown are median with Tukey's whiskers (boxes: interquartile range; bars: 50% extreme quartiles), raw data points (dots), and Kruskal–Wallis analysis of variance (ANOVA) probability (P) value. **, and ***: P< 0.01 and P< 0.001, respectively, for comparisons with *C57BL/6* controls by Dunn's post-tests. Only statistically significant differences are indicated. Note the airway mast cell competence of *cKit*$^{Wsh/Wt}$ and *cKit*$^{Wsh/Wsh}$ mice, and the complete mast cell deficiency of *Cpa3.Cre* mice. H Schematics depicting mast cells (purple) of the airways, alveoli, and skin of *C57BL/6*, *cKit*$^{Wsh/Wt}$, *cKit*$^{Wsh/Wsh}$, and *Cpa3.Cre* mice. Grey mast cell fade-outs indicate mast cell deficiency of the given anatomic compartment.

displaying an intermediate phenotype, indicating a significant tumor-promoting role of MC in the disease (Figure 4). Finally, separate cohorts of *C57BL/6*, *cKit*$^{Wsh/Wt}$, *cKit*$^{Wsh/Wsh}$, and *Cpa3.Cre* mice, all on the *C57BL/6* background, received 10^6 subcutaneous LLC cells and were followed for one month. *cKit*$^{Wsh/Wsh}$ and *Cpa3.Cre* mice displayed significantly delayed primary tumor growth, as well as decreased spontaneous metastasis to the lungs compared with controls; interestingly, *cKit*$^{Wsh/Wt}$ mice displayed sustained primary tumor growth, but significantly decreased metastasis (Figure 5A–C). Co-labeling of MC and proliferating cells in primary tumors from these mice using toluidine blue and anti-proliferating cell nuclear antigen (PCNA) antibody revealed that MC directly contacted PCNA+ tumor cells (Figures 5D–J), that LLC tumors of *Cpa3.Cre* mice had decreased numbers of proliferating tumor cells and were devoid of MC, while *cKit*$^{Wsh/Wt}$ and *cKit*$^{Wsh/Wsh}$ mice displayed intermediate phenotypes, and that PCNA+ tumor cells were significantly increased in MC hotspots of LLC tumors of control mice (Figures 5K–N). Collectively, these data indicate that MC are important for LADC development, growth, and metastasis.

Mast cells respond to lung adenocarcinoma-secreted factors

To identify MC-derived mediators that drive LADC, we isolated MC from *C57BL/6* mouse bone marrow (bone marrow-derived MC, BMMC) using one month's incubation with 100 ng/mL interleukin (IL)-3 alone or 100 ng/mL IL-3 plus 100 ng/mL KIT ligand (KITL), a method that yields > 95% pure BMMC, as described elsewhere.[33] KIT-dependent (KIT+) and KIT-independent (KIT-) BMMC were then exposed to cell-free LLC-conditioned media (CM) for 24 h and their RNA was examined for changes in gene expression compared with non-CM-exposed counterparts by microarray [Gene Expression Omnibus (GEO) identifier GSE58189; https://www.ncbi.nlm.nih.gov/geo/query/acc.cgi?acc=GSE58189]. This experiment revealed distinct gene sets that are differentially regulated in KIT+ and KIT- BMMC or both upon LADC cell encounter (Figure 6A, B). The human orthologues of the top transcripts of these three sets were used to compile KIT+, KIT-, and common MC signatures and included *Il1b* (Figure 6C), which we previously identified to promote LADC-induced malignant pleural effusion.[33] *Ex-vivo* generated KIT+ BMMC displayed marked increases in IL-1β production and caspase-1 (CASP1) expression upon LADC cell encounter (Figure 6D–F), consistent with the role of CASP1 in IL-1β processing.[46] IL-1β also promoted subcutaneous LADC growth, since *Il1b*-deficient mice displayed significantly delayed tumor growth after subcutaneous LLC injection (Figure 6H). These results indicate that both KIT+ and KIT- MC respond transcriptionally to LADC-secreted factors and identify candidate gene sets of MC-derived LADC promoters for future research. In addition, the data support that MC can develop and respond to tumor cells in the absence of functional KIT (i.e., in *cKit*$^{Wsh/Wt}$ and *cKit*$^{Wsh/Wsh}$ mice).

Mast cells impact the microenvironment of lung adenocarcinoma

We next evaluated the abundance of other immune cells in our experimental LADC models on backgrounds of MC-competence and -deficiency. While mononuclear and lymphoid cells were equally abundant in LADC from MC-competent and – deficient mice, we observed a statistically significant increase in polymorphonuclear cells in *cKit*$^{Wsh/Wsh}$ mice (Figure 7A–F), in accord with a previous report.[47] Interleukin-1β immunoreactivity was statistically significantly decreased in LADC from MC-deficient mice, indicating that MC are a cardinal source of the cytokine in LADC (Figure 7G). We next co-labeled MC with anti-KIT antibody and toluidine blue in LADC of MC-competent mice, to observe that KIT+ MC were more abundant compared with

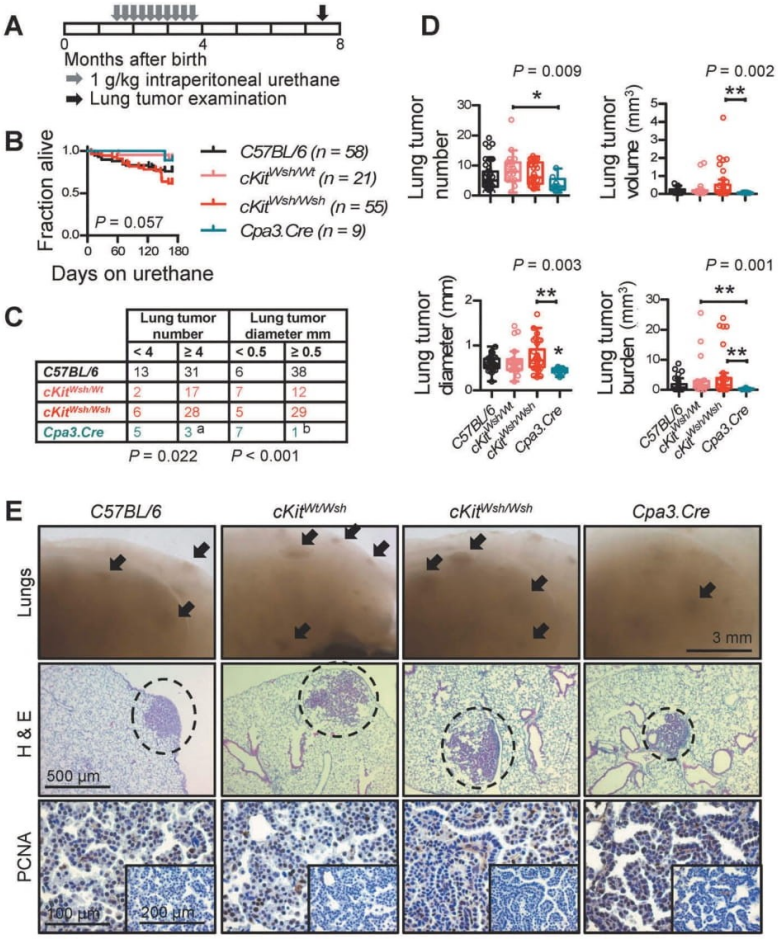

Figure 3. Mast cell deficiency protects mice from urethane-induced lung adenocarcinoma of the airways.
C57BL/6 controls ($cKit^{Wt/Wt}$ and $Cpa3.Cre^{-/-}$ littermate controls, as well as *Lyz2.Cre* mice), $cKit^{Wsh/Wt}$, $cKit^{Wsh/Wsh}$, and *Cpa3.Cre* mice received ten consecutive weekly intraperitoneal urethane (1g/Kg) injections (n = 58, 21, 55, and 9, respectively) and were followed for survival and lung tumor analyses at six months post-urethane start. A Schematic time-course of the experiment with boxes representing one month. B Kaplan–Meier survival curves and log-rank P value. C Frequency distribution of tumor number and size with n and χ^2 P values. a: $P < 0.05$ for *Cpa3.Cre* mice compared with $cKit^{Wsh/Wt}$ and $cKit^{Wsh/Wsh}$ mice by Fischer's exact test. b: $P < 0.05$ for *Cpa3.Cre* mice compared with $cKit^{Wsh/Wt}$ mice and $P < 0.001$ for *Cpa3.Cre* mice compared with *C57BL/6* control and $cKit^{Wsh/Wsh}$ mice by Fischer's exact test. D Data summary of tumor number, size, mean volume, and burden per lung shown as median with Tukey's whiskers (boxes: interquartile range; bars: 50% extreme quartiles), raw data points (dots), and Kruskal–Wallis analysis of variance (ANOVA) probability (P) value. *, and **: $P < 0.05$, and $P < 0.01$, respectively, for the indicated comparisons by Dunn's post-tests. Only statistically significant differences are indicated. E Representative images of gross lungs and hematoxylin/eosin (H&E)- and proliferating cell nuclear antigen (PCNA)-stained lung sections. Arrows and dashed lines denote lung adenocarcinomas.

KIT- MC (Figure 7H, I). Collectively, these findings indicate that KIT+ MC are the predominant MC population in LADC that regulate the recruitment of other immune cells and that contribute to IL-1β secretion.

Interleukin-1β provided by KIT+ mast cells is required for KRAS-mutant LADC

Based on the *in vivo* results obtained from the different mouse models of LADC, we hypothesized that KIT+ and KIT- MC may possess different LADC-promoting properties. To test this, as well as to determine the impact of IL-1β on LADC growth, BMMC were cultured from *WT* and *Il1b-/-* mice,[48] as described above and elsewhere.[33] After 30 days in culture on 100 ng/mL IL-3 alone or 100 ng/mL IL-3 plus 100 ng/mL KITL, more than 95% of BMMC from both *WT* and *Il1b-/-* mice differentiated into MC of various maturation stages displaying metachromasia, i.e. purple staining with toluidine blue (Figure 8A), as well as MC-specific molecular markers. We next co-cultured LLC cells with DMEM control or with KIT+ or KIT- BMMC from *WT* or *Il1b-/-* mice at a physiologically relevant 50:1 ratio identified from *in vivo* LADC (Figures 1O, 8A). Co-cultures were assessed for *in vitro* cellular proliferation by 3-(4,5-dimethylthiazol-2-yl)-2,5-diphenyltetrazolium bromide (MTT) reduction, for *in vitro* cell migration by scratch assay, and for *in vivo* tumor growth after subcutaneous injection of a million cells into syngeneic *Ccr2* gene-deficient mice (n = 5–6/group), selected to prevent confounding chemorecruitment of endogenous host mouse

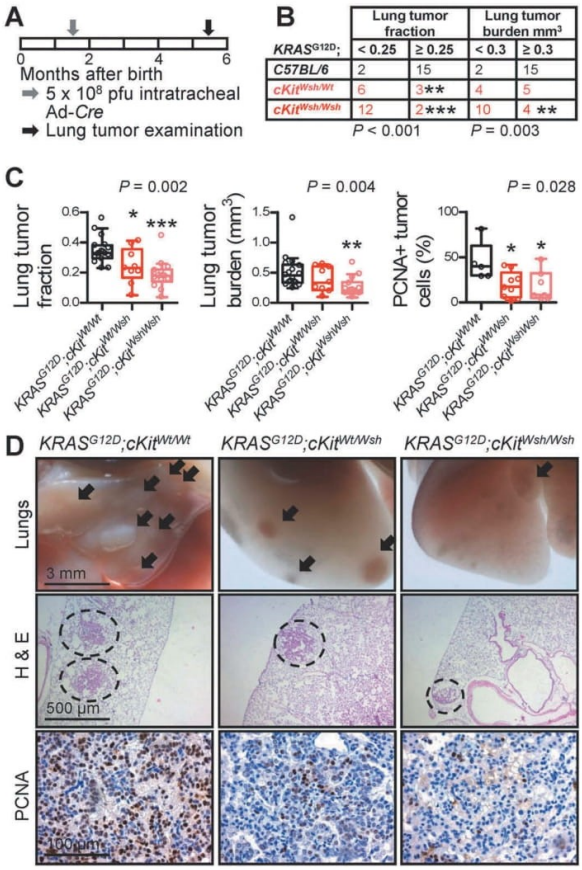

Figure 4. Mast cell deficiency protects mice from *KRAS*^{G12D}-induced lung adenocarcinoma of the alveoli.
KRAS,^{G12D} *KRAS*;^{G12D}*cKit*$^{Wsh/Wt}$, and *KRAS*;^{G12D}*cKit*$^{Wsh/Wsh}$ mice (*C57BL/6* background) received 5 × 10^8 intratracheal plaque-forming units (pfu) Ad-*Cre* and were killed after four months (n = 17, 9, and 14, respectively). A Schematic time-course of the experiment with boxes representing one month. B Frequency distribution of relative lung tumor fraction and absolute lung tumor volume (burden) with n and χ^2 P values. ** and ***: P< 0.01 and P< 0.001, respectively, for comparisons with *KRAS*^{G12D} controls by Fischer's exact test. C Data summary of relative lung tumor fraction and absolute lung tumor volume (burden) per lung, as well as percentage of proliferating cell nuclear antigen (PCNA)+ tumor cells with Tukey's whiskers (boxes: interquartile range; bars: 50% extreme quartiles), raw data points (dots), and Kruskal–Wallis ANOVA P values. *, **, and ***: P< 0.05, P< 0.01, and P< 0.001, respectively, for comparison with *KRAS*^{G12D} controls by Dunn's post-tests. Only statistically significant differences are indicated. D Representative images of gross lungs and hematoxylin/eosin (H & E)- and PCNA-stained lung sections. Arrows and dashed lines denote lung adenocarcinomas.

MC.[33,49] These experiments clearly showed that exclusively KIT+ MC competent in IL-1β can promote LADC cell proliferation and migration *in vitro* and *in vivo* (Figure 8B–D).

Mast cells in human lung adenocarcinoma

To determine whether our findings are relevant to human LADC, we analyzed MC infiltrates in 37 patients with histologically documented LADC from one of our previous studies from Greece.[50] MC preferentially accumulated in tumor tissue compared with adjacent normal-appearing lung tissue (Figure 9A; Table 1). In addition, the human orthologue of the murine KIT+ MC signature above, generated at http://lighthouse.ucsf.edu/orthoretriever/,[51] was significantly over-represented in tumor tissue compared with adjacent lung tissues of 10 patients with histologically documented LADC from one of our previous studies from Germany (Figure 9B; Table 2).[52] Individual transcripts from all three MC signatures, including *TNFRSF9* and *CD72* from the common, *NLRP6* from the KIT-, as well as *SLC43A3, TRAF1*, and *HSPA1B* from the KIT+ MC signature were significantly over-represented in tumor tissue compared with adjacent lung tissue (Figure 9C). In addition, MC density significantly increased with T, N, and TNM stage in the former series of patients (Figure 9D–I). These results are in line with the increased tumor cell proliferation indices of LADC from MC-competent mice compared with MC-deficient counterparts and suggest that MC infiltrate human LADC, where they exert pro-tumor functions. Moreover, the data suggest that primarily KIT+ MC infiltrate human LADC. We further interrogated the presence of MC transcriptional signatures in human LADC, employing published transcriptomes of normal lung tissues from never smokers and LADC tissues from never- and current smokers from the Biomarker-integrated Approaches of Targeted Therapy for Lung Cancer Elimination (BATTLE) study (GEO dataset GSE43458; https://www.ncbi.nlm.nih.gov/geo/query/acc.cgi?acc=GSE43458).[53] Unsupervised clustering of this patient cohort by our humanized transcriptional signatures of KIT+ and KIT- MC accurately discriminated normal from LADC tissues and several genes of these MC signatures were overrepresented in tumor versus normal tissues, but also in smokers' versus never-smokers' LADC, validating the results from our small cohort from Germany (Figure 10A, B).[52] Although all MC signatures could discern LADC tissues from normal lungs, the KIT+ signature emerges to be functionally important in LADC, since LADC patients with high expression of exclusively this footprint displayed significantly shorter survival (http://kmplot.com/analysis/index.php?p=service&cancer=lung; Figure 10C).[54] Finally, gene set enrichment analyses (GSEA) of humanized KIT+ and KIT- MC signatures were done in LADC from smokers and never smokers compared with normal lung tissue (GEO dataset GSE43458; https://www.ncbi.nlm.nih.gov/geo/query/acc.cgi?acc=GSE43458) and in *KRAS*- and *EGFR*-mutant LADC compared with normal lung tissue (GEO dataset GSE31852; https://www.ncbi.nlm.nih.gov/geo/query/acc.cgi?acc=GSE31852).[53,55,56] Using stringent cut-offs of false discovery rate (FDR) q values <0.05 and family-wise error rate (FWER) probability (P) values <0.05, we found that exclusively the KIT+ MC signature was focally enriched in *KRAS*-mutant LADC, while missing significance levels by a margin in smokers' LADC (Figure 11). These results connect KIT+ MC with *KRAS*-mutant LADC caused by tobacco smoking, in line with the results from the animal models of *KRAS*-mutant LADC employed (Figures 1–5). Collectively, these results from five human cohorts of LADC indicated that both KIT+ and KIT- MC and their transcriptional signatures are present in human LADC, and suggested that KIT+ MC are specifically important for disease progression of *KRAS*-mutant LADC.

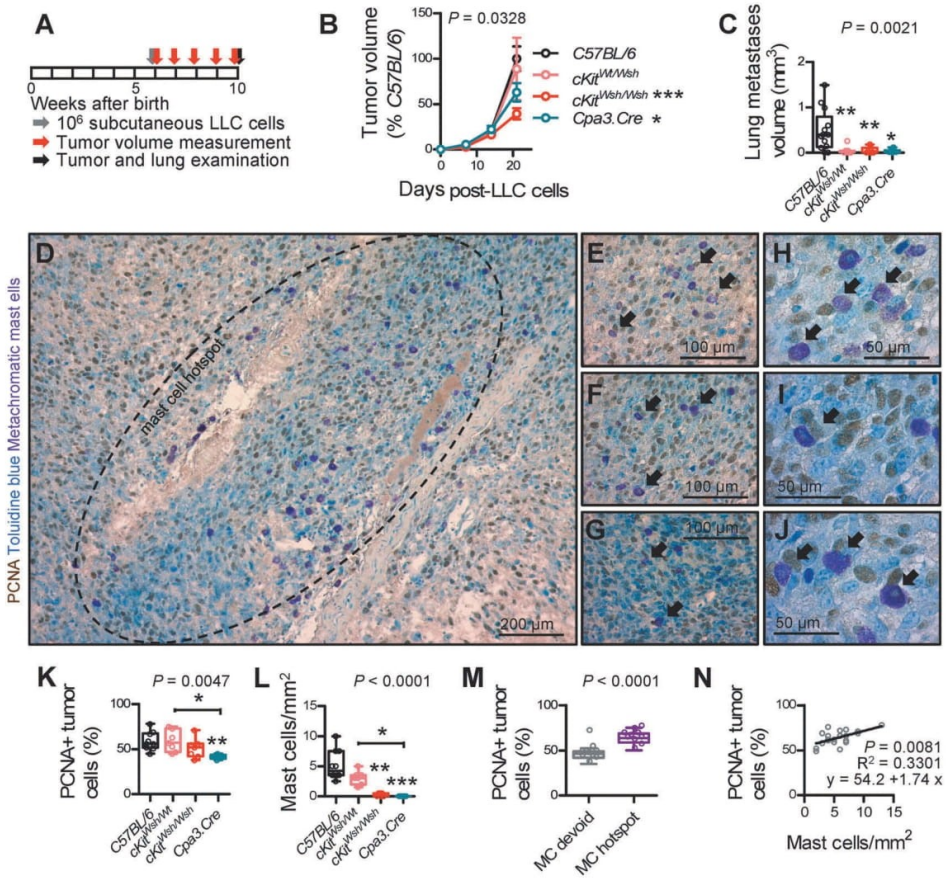

Figure 5. Mast cell deficiency protects mice from Lewis lung adenocarcinoma growth in the skin and its metastasis to the alveolar regions.
C57BL/6 controls ($cKit^{Wt/Wt}$ and $Cpa3.Cre^{-/-}$ littermate controls, as well as *Lyz2.Cre* mice), $cKit^{Wsh/Wt}$, $cKit^{Wsh/Wsh}$, and *Cpa3.Cre* mice, all on the *C57BL/6* background (n = 13, 7, 7, and 6, respectively), received 10^6 subcutaneous Lewis lung carcinoma cells (LLC), were followed for one month by weekly measurement of three vertical primary tumor diameters (δ) and calculation of primary flank tumor volume ($V = \pi\delta^3/6$) and were sacrificed for primary tumor and spontaneous lung metastasis analyses at one month post-LLC cells. A Schematic time-course of the experiment with boxes representing one week. B Data summary of primary subcutaneous tumor volume expressed as percentage of *C57BL/6* controls (mean±SEM) with two-way ANOVA P value. * and ***: $P< 0.05$ and $P< 0.001$, respectively, for comparison with *C57BL/6* controls by Bonferroni post-tests. C Data summary of absolute lung metastasis volume (burden) per lung. D-J Toluidine blue-counterstained primary LLC tumor sections of *C57BL/6* control mice (n = 10) labeled for proliferating cell nuclear antigen (PCNA), a technique that allows simultaneous visualization and quantification of proliferating cells (brown), mast cells (purple), and nuclei (blue). Shown are representative mast cell hotspot (D; dashed line) and areas of such hotspots featuring mast cells in close association/contact with proliferating tumor cells (E-J; arrows). K-N Data summary of percentage of PCNA+ primary tumor cells (K), primary tumor mast cell density (L), percentage of PCNA+ cells in mast cell hotspots versus mast cell-devoid areas of primary tumors of *C57BL/6* mice (M), and correlation of these two parameters in mast cell hotspots of primary tumors of *C57BL/6* mice (N). (K, L) n = 10, 7, 7, and 6, respectively. (M) n = 10 *C57BL/6* mice. (N) n = 2 hotspots from each of 10 *C57BL/6* mice. Data information: (C, K, L, M) Data are shown as Tukey's whiskers (boxes: interquartile range; bars: 50% extreme quartiles), raw data points (dots), and Kruskal–Wallis ANOVA (C, K, L) and Mann–Whitney u-test (M) P values. *, **, and ***: $P< 0.05$, $P< 0.01$, and $P< 0.001$, respectively, for comparison with *C57BL/6* controls or as indicated by Dunn's post-tests. Only statistically significant differences are indicated. (N) Shown are data points, Pearson correlation P value and coefficient, and linear regression line and formula.

Discussion

This is the first *in vivo* study on the role of mast cells in lung adenocarcinoma. We show that KIT+ MC possess potent biological activity fostering disease progression in three different mouse models of *KRAS*-mutant LADC either endogenously arising from the airways or the alveoli, or heterotopically implanted in the skin and spontaneously disseminating to the alveolar areas. For this, we used two divergent genetic models of MC deficiency, one resting on defective KIT signaling ($cKit^{Wsh}$ mice) and another relying on genetic MC ablation (*Cpa3.Cre* mice). The results indicate that KIT+ MC are required for LADC, since each MC-deficient strain was markedly protected from tumorigenesis in at least two models of LADC: $cKit^{Wsh}$ mice from $KRAS^{G12D}$- and LLC-induced tumors, and *Cpa3.Cre* mice from urethane and LLC-induced tumors. Albeit both MC populations infiltrate experimental and human LADC, we show how KIT+ MC foster LADC progression conditional on their competence for IL-1β secretion, while KIT- MC appear to have a neutral role. Moreover, we identify MC gene sets that are differentially regulated upon LADC cell encounter, facilitating the future discovery of MC-derived effectors that foster LADC. Human results from five different patient cohorts lend support to our experimental findings of an LADC promoting role for

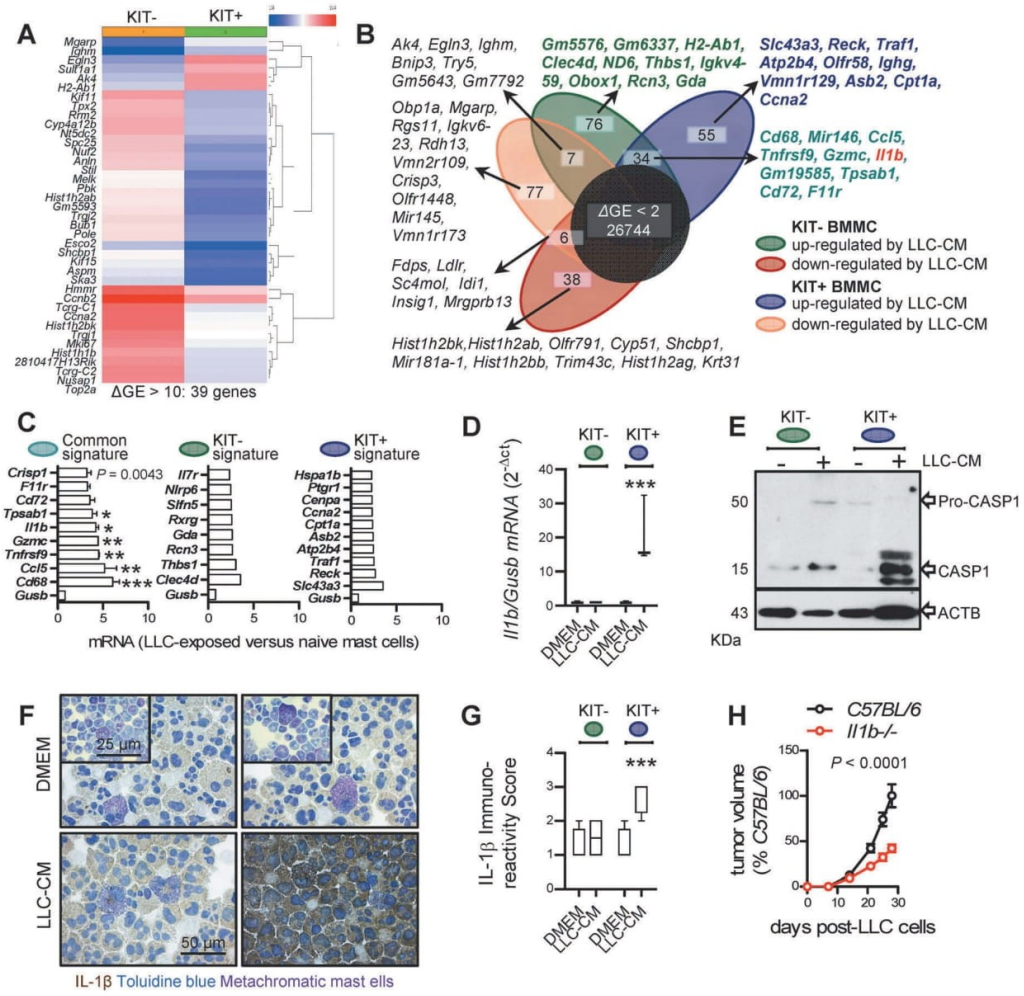

Figure 6. Response of bone marrow-derived mast cells to lung adenocarcinoma cells and lung adenocarcinoma growth in interleukin-1β-deficient mice.

A Genes differentially expressed (39 genes, ΔGE ≥ 2) between KIT-dependent (KIT+) and KIT-independent (KIT-) bone marrow-derived mast cells (BMMC). B Venn diagram of differentially expressed genes (ΔGE ≥ 2) of BMMC pre-cultured for one month with interleukin (IL-3) plus cKIT ligand (KITL) (KIT+ BMMC) or with IL-3 only (KIT- BMMC) upon 24-h incubation with cell-free Lewis lung carcinoma-conditioned media (LLC-CM) by Affymetrix Mouse Gene ST2.0 microarrays. Top 10 transcripts from each gene set are listed. Note the 55 genes selectively up-regulated in KIT+ BMMC (blue signature), the 76 genes selectively up-regulated in KIT- BMMC (green signature), and the 34 genes up-regulated in both BMMC (turquoise signature) featuring *Il1b* (red font). C Normalized microarray expression values of top genes with human orthologues from each signature compared with *Gusb* control (n = 2/data point). D qPCR data summary of *Il1b* normalized to *Gusb* expression of KIT+ and KIT- BMMC upon 24-h incubation with cell-free LLC-CM (n = 3). Data are shown as Tukey's whiskers (boxes: interquartile range; bars: 50% extreme quartiles). ***: P < 0.001 for LLC-CM-treated KIT+ BMMC compared with all other groups by two-way ANOVA with Bonferroni post-tests. Only statistically significant differences are indicated. E KIT+ and KIT- BMMC were assessed for caspase-1 (CASP1) and β-actin (ACTB) immunoreactivity by Western immunoblot upon 24-h incubation with DMEM (-) or cell-free LLC-CM (+). F Representative cytocentrifugal specimens of IL-1β immunostained and toluidine blue counter-stained KIT+ and KIT- BMMC upon 24-h incubation with DMEM or cell-free LLC-CM. G Data summary from n = 5 samples from (F). Data are shown as Tukey's whiskers (boxes: interquartile range; bars: 50% extreme quartiles). ***: P < 0.001 for LLC-CM-treated KIT+ BMMC compared with all other groups by two-way ANOVA with Bonferroni post-tests. Only statistically significant differences are indicated. H *C57BL/6* and *Il1b* gene-deficient (*Il1b-/-*) mice on the *C57BL/6* background (n = 5/group), received 10^6 subcutaneous Lewis lung carcinoma cells (LLC) and were followed for one month by weekly measurement of three vertical primary tumor diameters (δ) and calculation of primary flank tumor volume ($V = \pi\delta^3/6$). Data summary of primary subcutaneous tumor volume expressed as percentage of *C57BL/6* controls (mean±SEM) with two-way ANOVA P value.

KIT+ MC. Hence, this report presents the first direct evidence for a requirement for KIT+, IL-1β-competent mast cells in *KRAS*-mutant LADC, identifying new targets for therapy.

The results favor an important role for MC during the whole spectrum of LADC formation, progression, and metastasis.[35] To this end, MC-deficient mice were protected from direct tumor initiation of the airway and alveolar epithelium using the tobacco carcinogen urethane and oncogenic *KRAS*,^{G12D} respectively, and were also resistant to the heterotopic growth of established LADC in the skin, as well as to its spontaneous metastasis back to the lungs. MC are known to heavily colonize the airways of mice and men,[12–19,29] where tumor initiation by environmental carcinogens occurs,[1,37] and were shown here to progressively infiltrate LADC of increasing stage, positioning

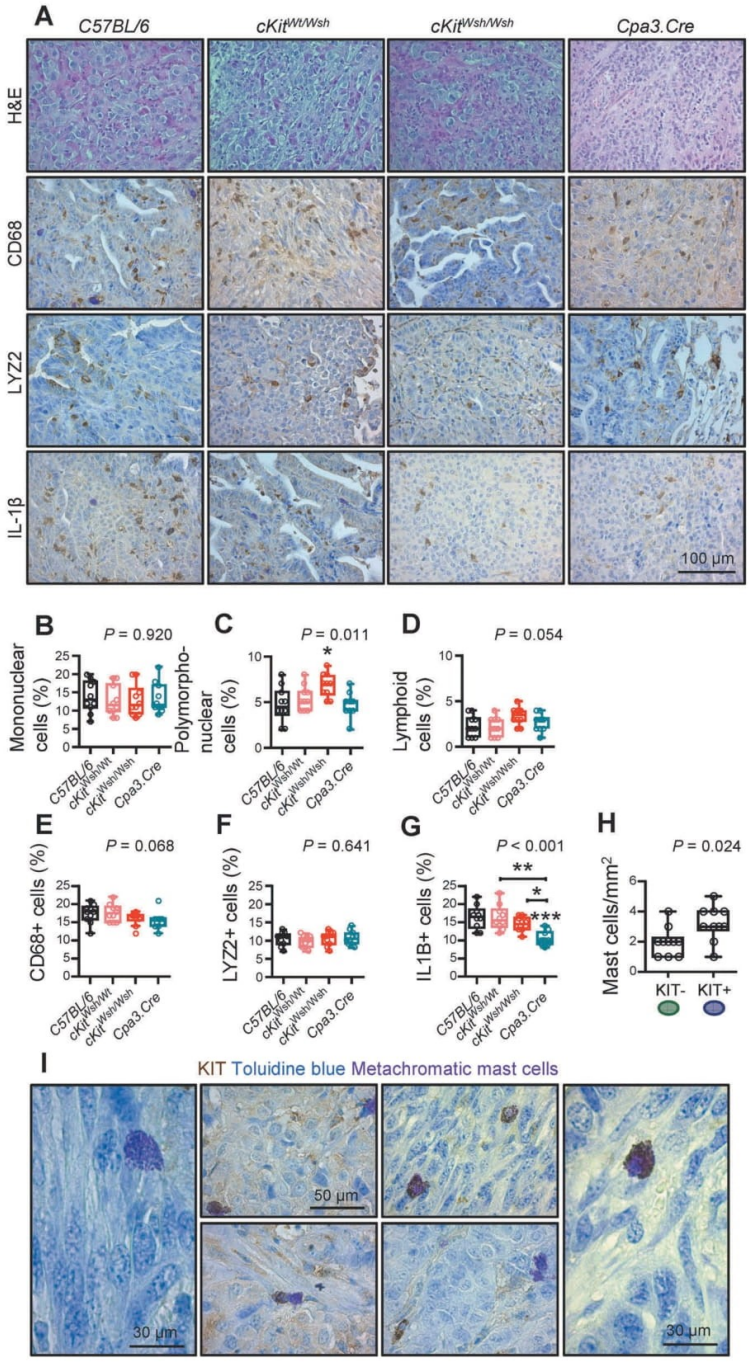

Figure 7. Lung adenocarcinoma microenvironment of mast cell-competent and incompetent mice.

A Representative images of lung adenocarcinomas from Figures 3–5 (n = 10 mice/group randomly chosen from the urethane, *KRAS*,^{G12D} and heterotopic models) stained with hematoxylin and eosin (H & E) or immunostained with anti-CD68, anti-LYZ2, and anti-IL-1β antibodies and counterstained with toluidine blue. B-G Data summary from (A). Data are shown as Tukey's whiskers (boxes: interquartile range; bars: 50% extreme quartiles), raw data points (dots), and Kruskal–Wallis ANOVA P values. Comparisons shown are. *: $P < 0.05$ for comparisons with *C57BL/6* controls or as indicated by Dunn's post-tests. Only statistically significant differences are indicated. H Representative lung adenocarcinomas from Figures 3–5 (n = 10 mice/group randomly chosen from the urethane, *KRAS*, ^{G12D} and heterotopic models) were immunostained with anti-KIT antibody and counterstained with toluidine blue. Data summary shown as Tukey's whiskers (boxes: interquartile range; bars: 50% extreme quartiles), raw data points (dots), and Mann–Whitney u-test P value. I Representative images of LADC-infiltrating KIT+ (left) and KIT- (right) MC and their co-localization in tumors (middle).

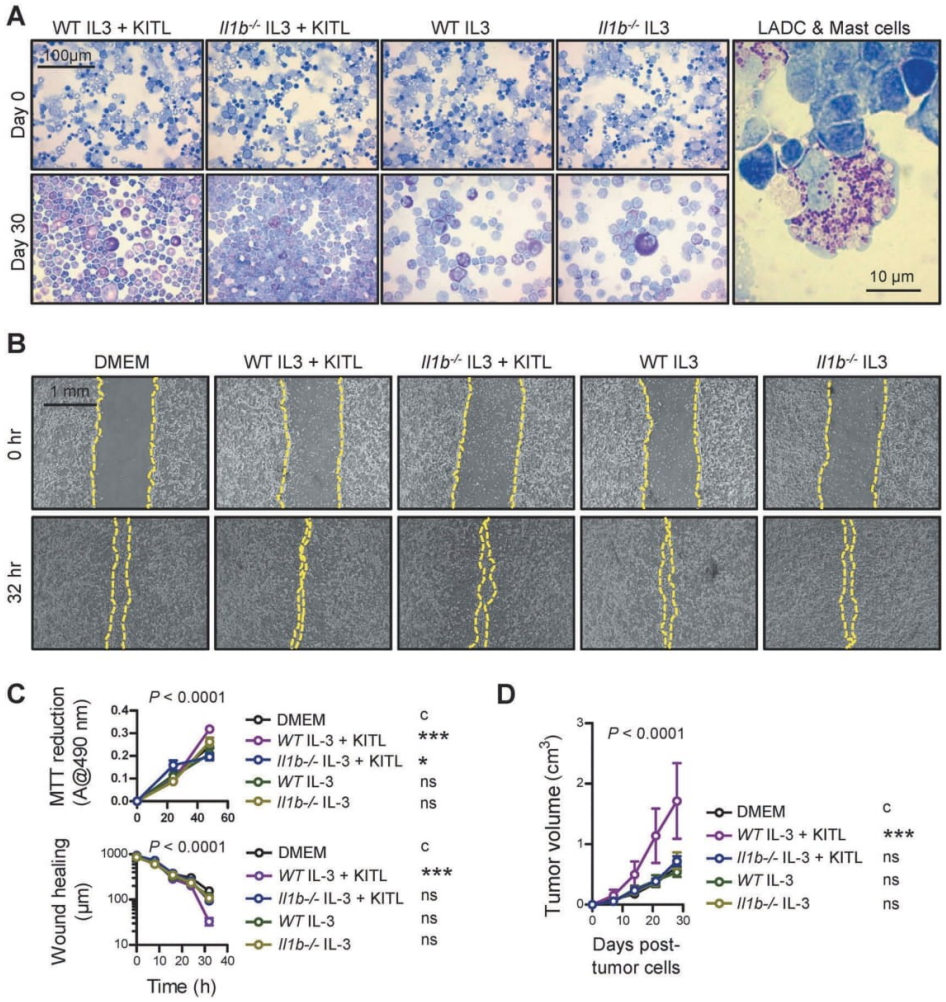

Figure 8. KIT-dependent mast cells competent in interleukin-1β are required for lung adenocarcinoma.

A *Left*: Representative cytocentrifugal specimens of toluidine blue-stained bone marrow-derived cells from *WT* and *Il1b-/-* mice before (top) and after one-month incubation with 100 µg/mL interleukin (IL)-3 and 100 µg/mL KIT ligand (KITL) or with 100 µg/mL IL-3 alone (bottom). Note the >95% metachromasia of bone marrow-derived mast cells (BMMC) of different maturation stages after treatment. *Right*: Representative cytocentrifugal specimen of toluidine blue-stained BMMC mixed with LLC cells at 1:50 ratio before experiments. B, C LLC cells alone or co-cultured with BMMC from (A) were assessed for *in vitro* cellular proliferation by MTT reduction and for *in vitro* cell migration by scratch assay. (B) Representative scratch assay images at experiment start and conclusion. (C) Summary of data from n = 5–6 independent experiments expressed as mean±SEM with two-way ANOVA P values. ns, *, and ***: P> 0.05, P< 0.05, and P< 0.001, respectively, for comparison with DMEM control (c) by Bonferroni post-tests. D *Ccr2* gene-deficient mice (n = 6/group) received 10^6 subcutaneous LLC cells alone or mixed with BMMC at 50:1 ratio and were followed for a month by weekly measurements of three vertical primary tumor diameters and calculation of flank tumor volume. Summary of data from n = 6 mice/group expressed as mean±SEM with two-way ANOVA P value. ns and ***: P> 0.05 and P< 0.001, respectively, for comparison with DMEM control (c) by Bonferroni post-tests.

MC as plausible effectors of LADC development and progression. The results also favor a ubiquitous LADC-promoting role for MC across anatomical compartments of the lungs, since MC-deficient mice were protected from both airway- and alveolar-inflicted LADC.[36,38] This is important given the diversity of the cellular origin of LADC in mice and humans if MC-based therapy is ever contemplated.[35–39]

But how can the divergent results from urethane-treated *cKit*^{Wsh} and *Cpa3.Cre* mice be explained? We believe that the results do not contradict the proposed tumor-promoting role for MC in LADC and can be explained on several counts. First, *cKit*^{Wsh} mice were not completely devoid of airway MC, and we recently showed urethane-induced tumors to stem from the airways.[36] Second, urethane-caused LADC were less infiltrated by MC compared with *KRAS*^{G12D} and LLC tumors, likely reflecting their more early nature compared with the other models,[37,40,43] and probably dictating their lesser dependence from MC. This assumption is in line with the increasing MC infiltrates of advanced human LADC, as well as the more profound impact of MC deficiency in mouse models of more advanced disease like the *KRAS*^{G12D} and LLC model shown here and the malignant pleural effusion models shown elsewhere.[33]

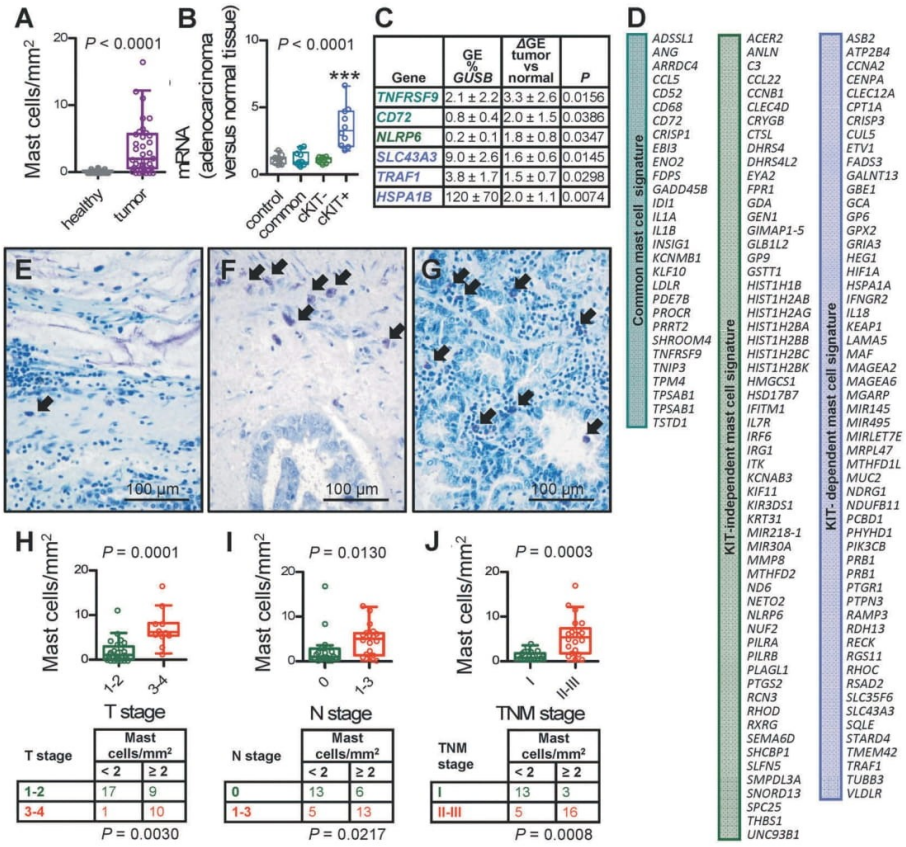

Figure 9. Mast cells and mast cell signatures in human lung adenocarcinoma.

A Data summary of mast cell (MC) density of 37 patients with lung adenocarcinoma.[50] Data are shown as Tukey's whiskers (boxes: interquartile range; bars: 50% extreme quartiles), raw data points (dots), and paired Student's t-test *P* value. Full patient data are provided in Table 1. B Data summary of gene expression (GE) levels of the human orthologues of the murine MC signatures identified in Figure 6 relative to *GUSB* and *HPRT* (control) of tumor and adjacent normal-appearing lung tissues of 10 patients with lung adenocarcinoma.[52] Blue: KIT-dependent MC signature; green: KIT-independent MC signature; turquoise: common MC signature. Data are shown as Tukey's whiskers (boxes: interquartile range; bars: 50% extreme quartiles), raw data points (dots), and repeated measures ANOVA *P* value. ***: $P < 0.001$ for comparison with all other groups by repeated measures ANOVA with Bonferroni post-tests. Full patient data are provided in Table 2. C Select transcripts from the three signatures from (B) significantly over-represented in tumor versus adjacent normal-appearing lung tissues with GE versus *GUSB*, differential GE (ΔGE) of tumor tissue versus normal lung, and *P* values by paired Student's t-test. D The human orthologues of the three murine MC signatures identified in Figure 6. E-G Representative toluidine blue-stained tissue sections showing purple mast cells (arrows) in primary lung adenocarcinomas of a 68-year-old female with stage $T_2N_0M_0$ disease featuring 3.6 mast cells/mm^2, a 51-year-old male with $T_2N_1M_0$ disease displaying 11.2 mast cells/mm^2, and a 64-year-old male with $T_4N_0M_0$ disease exhibiting 16.6 mast cells/mm^2. H-J Data summary (graphs) and frequency distribution (tables) of mast cell density of 37 patients with lung adenocarcinoma,[50] classified by T, N, and TNM6 stage according to the sixth edition of the TNM staging system.[63] Data are shown as Tukey's whiskers (boxes: interquartile range; bars: 50% extreme quartiles), raw data points (dots), *n* (tables), and Mann–Whitney u-test (graphs) and Fischer's exact (tables) *P* values. Full patient data are provided in Table 1.

Third, rebound immune responses are at play in *cKit*^{Wsh} mice, such as myeloid suppressor and regulatory T cell expansion,[47,57] cell types we have previously shown to promote early urethane-induced and advanced LADC.[43,58] Finally, as the founders of *Cpa3.Cre* mice and our group previously showed,[27,33] these mice represent truly and exclusively MC-deficient models that behave differently compared with *cKit*^{Wsh} mice in response to various challenges,[27] rendering the results from this strain more closely related to MC function and not to KIT signaling. To this end, *Cpa3.Cre* mice were ubiquitously protected from urethane, as well as from LLC tumors and their metastases, corroborating the requirement for MC in LADC.

The data presented here are novel and unprecedented and explain previous clinical and preclinical observations and *in vitro* functional findings.[28–31] Our *in vivo* results are important additions to the field, since MC play divergent tumor-promoting or gate-keeping roles in different cancers.[20–23,33] The reasons for this may be multiple, including the different tumor models employed and the multifaceted phenotypes of MC in the various bodily anatomic compartments.[15,17,27,33,44] Whatever the impact of these cells in other tumor types, the results shown here establish for the first time KIT+ MC as culprits of *KRAS*-mutant LADC promotion and as candidate therapeutic targets against a disease that presents a current pandemic.[1,2] In addition to identifying their role and to provide mechanistic insights, we describe gene sets that may mediate LADC promotion by MC for future research. These signatures include *IL1B, TNFRSF9, CD72, NLRP6, SLC43A3, TRAF1,*

Table 1. Clinical data and mast cell density of 37 patients with lung adenocarcinoma from Patras, Greece.[50] No patient had metastasis (M_0 for all).

#	Gender	Age (years)	Histologic subtype(s)	Grade (1–3)	T	N	TNM	Mast cells/ mm^2
1	M	60	Solid	1	4	1	IIIb	5,4
2	M	73	Acinar	2	2	0	Ib	2,8
3	M	56	Solid/papillary	3	3	1	IIIa	5,6
4	M	68	Micropapillary	3	1	0	Ia	2
5	M	63	Acinar	2	2	0	Ib	0,4
6	M	63	Acinar/papillary	2	2	0	Ib	0
7	M	63	Solid	3	2	1	IIb	2,2
8	M	67	Acinar (cribriform)	3	1	0	Ia	0
9	M	62	Acinar	2	2	1	IIb	4,6
10	M	72	Acinar/solid	3	2	1	IIb	0
11	M	66	Acinar/solid	3	4	1	IIIb	1,4
12	F	55	Acinar	1	2	1	IIb	4,4
13	M	64	Acinar	3	2	1	IIb	4
14	M	53	Acinar	1	1	0	Ia	0,2
15	M	64	Lepidic/acinar/ micropapillary	3	4	0	IIIb	16,6
16	M	70	Acinar	2	1	1	IIa	1,2
17	M	50	Solid	3	2	1	IIb	0
18	M	51	Acinar/ micropapillary	3	2	1	IIb	11,2
19	M	68	Solid	3	3	1	IIIa	5,8
20	M	69	Micropapillary/ acinar	2	3	1	IIIa	6,6
21	M	53	Acinar	2	1	0	Ia	0,4
22	M	49	Acinar	2	1	0	Ia	1,8
23	M	72	Solid	2	1	0	Ia	0,8
24	M	60	Solid	2	2	0	Ib	0
25	M	58	Acinar	3	2	0	Ib	1,8
26	M	71	Acinar	3	2	0	Ib	1
27	F	53	Solid	2	3	0	IIb	3
28	M	59	Colloid	1	3	1	IIIa	8,2
29	M	72	Acinar	2	2	1	IIb	6
30	M	54	Acinar	3	3	0	IIb	8,2
31	M	62	Solid	2	1	0	Ia	0
32	F	67	Solid	3	2	1	IIb	0,8
33	M	58	Solid	3	3	1	IIIa	6,2
34	M	54	Acinar/solid	2	1	0	Ia	0,8
35	M	69	Solid	3	3	1	IIIa	12,2
36	F	68	Colloid	2	2	0	Ib	3,6
37	M	65	Papillary/acinar	2	1	0	Ia	1,4

HSPA1B, and other genes of the KIT+ MC signature, genes likely important for MC expansion in tumor tissues, MC signal transduction upon tumor cell encounter, inflammasome activation, transmembrane transport, and telomere maintenance, and may promote further research on tumor-associated MC functions in the future. To this end, MC-derived IL-1β can fuel transcriptional activity of nuclear factor-κB in tumor cells.[33,34] Our results may explain the findings of the Canakinumab Anti-inflammatory Thrombosis Outcomes Study (CANTOS) aiming at prevention of cardiovascular events using the IL-1β-neutralizing antibody canakinumab.[59,60] After three years of intervention, CANTOS investigators detected biologically and statistically significant reductions in overall and lung cancer incidence, findings consistent with the protumorigenic role of IL-1β reported here and elsewhere.[33,34]

In conclusion, KIT-dependent mast cells were found here to fuel *KRAS*-mutant lung adenocarcinoma formation, growth, and metastasis in mice by secreting IL-1β and to be associated with lung adenocarcinoma progression in humans, setting a rational framework for further study of mast cell functions in lung tumors.

Materials and methods

Cells

Lewis lung carcinoma (LLC; NCI Tumor Repository, Frederick, MD) cells were cultured at 37°C in 5% CO_2-95% air using DMEM supplemented with 10% FBS, 2 mM L-glutamine, 1 mM pyruvate, 100 U/ml penicillin, and 100 mg/ml streptomycin. Cells were tested biannually for identity (by the short tandem repeat method) and for *Mycoplasma*spp. (by PCR). For *in vivo* injections, cells were harvested using trypsin, incubated with Trypan blue, and counted.[33] Only 95% viable cells were used *in vivo*. BMMC were derived from bone marrow cells flushed from mouse femurs and tibias using full DMEM after one month of culture in full culture media, supplemented with 100 ng/mL IL-3 alone or 100 ng/mL IL-3 plus 100 ng/mL KITL.[33] LLC cells alone or co-cultured with BMMC at a ratio of 50:1 were assessed for cellular proliferation by MTT reduction and cell migration *in vitro* with scratch assay for 48 and 32 h respectively. This LLC:BMMC ratio was selected as physiologically relevant based on *in vivo* MC densities observed in all three tumor models employed herein.

Mouse models

C57BL/6 (#000664), B6.129P2-*Lyz2*$^{tm(Cre)Ifo}$/J(#004781),[45] B6.129S4-*Ccr2*^{tm1Ifc}/J(#004999),[47] B6.129S4-Kras^{tm4Tyj}/J (*KRAS*;^{G12D} #008179),[40] and B6.Cg-*Kit*$^{W\text{-}sh}$/HNihrJaeBs mGlliJ (*cKit*^{Wsh}; #012861)[44] mice were from Jackson Laboratory (Bar Harbor, MN), *Cpa3.Cre* mice were a gift from Dr. HR Rodewald, University of Heidelberg, Germany,[27] and *Il1b*-deficient mice from Dr. Y Iwakura, Tokyo University of Science, Tokyo, Japan.[48] All mice were bred at the Center for Animal Models of Disease of the Department of Physiology at the Faculty of

Table 2. Clinical data and mast cell signature gene expression data of 10 patients with lung adenocarcinoma from Borstel, Germany.[52]

								Normalized expression of mast cell signature genes in lung adenocarcinoma compared with adjacent normal-appearing lung tissue (fold control genes *GUSB/HPRT*)			
#	Gender	Age (years)	Grade (1–3)	T	N	M	TNM	control	common	cKIT-	cKIT+
1	F	61	3	3	1	0	IIIa	1,44	0,89	0,99	2,12
2	M	69	3	3	3	0	IIIb	1,11	0,79	1,22	1,77
3	F	66	3	3	0	0	IIb	0,82	0,55	1,28	6,59
4	F	58	3	2	2	1	IV	1,77	0,90	0,92	2,02
5	F	71	3	4	2	0	IIIb	1,23	0,92	1,10	3,05
6	M	74	3	3	2	0	IIIa	0,72	0,71	1,21	4,67
7	F	54	3	4	3	0	IIIb	1,19	1,53	0,72	4,81
8	F	53	3	3	0	0	IIb	0,69	2,06	0,80	3,48
9	F	74	2	2	2	0	IIIa	1,20	1,43	1,31	2,68
10	F	57	2–3	1	0	0	Ia	1,13	1,97	1,25	4,12

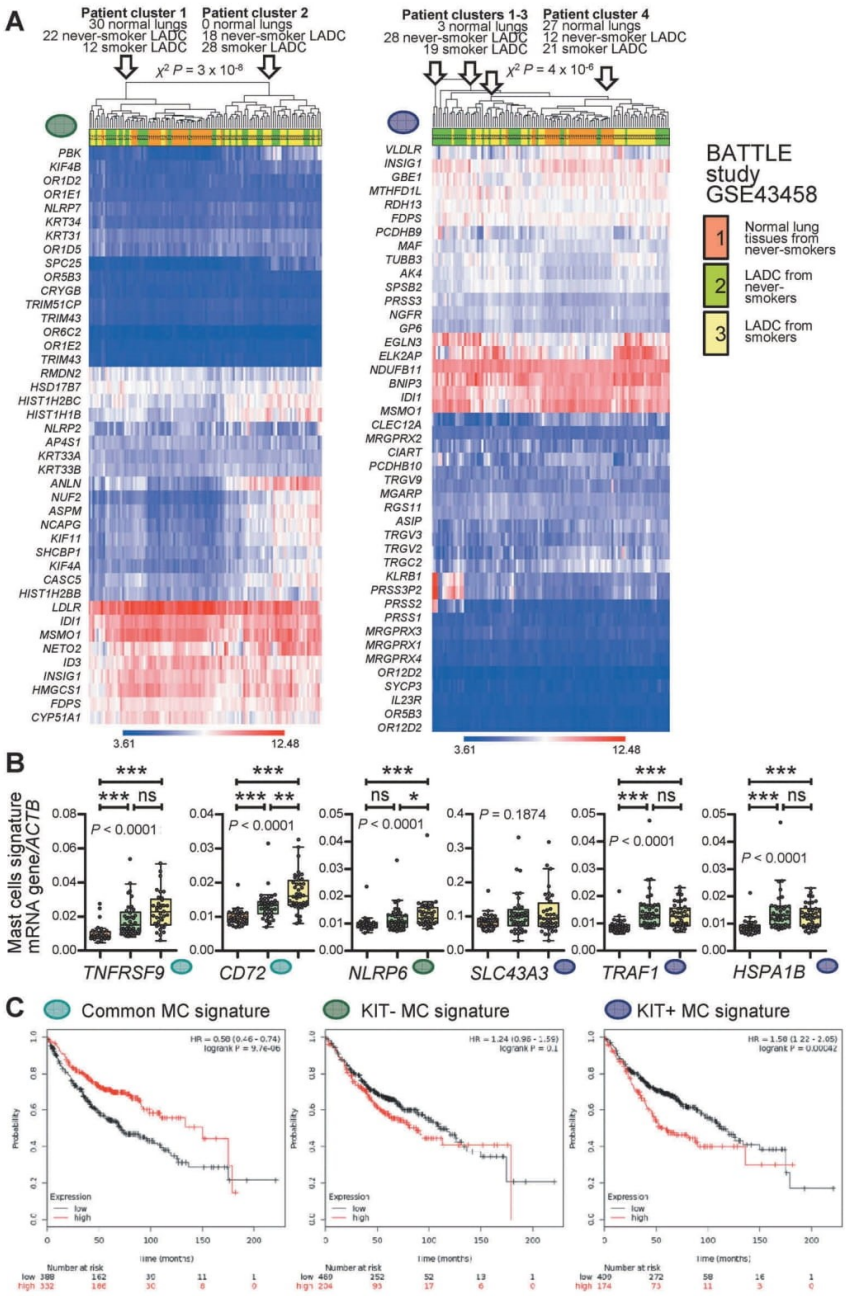

Figure 10. Mast cell signatures in human lung adenocarcinoma.

A Unsupervised clustering of 30 normal lung tissues from never-smokers (orange), 40 lung adenocarcinoma (LADC) tissues from never-smokers (green), and 40 LADC tissues from smokers (yellow) from the Biomarker-integrated Approaches of Targeted Therapy for Lung Cancer Elimination (BATTLE) study [Gene Expression Omnibus (GEO) dataset GSE43458; freely available at https://www.ncbi.nlm.nih.gov/geo/query/acc.cgi?acc=GSE43458][51] by the humanized KIT-independent (left) and KIT-dependent (right) mast cell (MC) signatures from Figure 9D. Both signatures could accurately discriminate normal lung from LADC tissues. *P*, exact χ^2 probability values calculated at http://courses.atlas.illinois.edu/spring2016/STAT/STAT200/pchisq.html. B Data summary of gene expression of the transcripts from Figure 9C normalized to *ACTB* expression in the BATTLE study validates five of the six genes. Color code is as in Figure 10A. Data are shown as Tukey's whiskers (boxes: interquartile range; bars: 50% extreme quartiles), raw data points (dots), and Kruskal–Wallis ANOVA *P* values. ns, *, **, and ***: $P > 0.05$, $P < 0.05$, $P < 0.01$, and $P < 0.001$, respectively, for the indicated comparisons by Dunn's post-tests. C Overall survival of patients with LADC stratified by low (black lines) or high (red lines) average expression of MC signatures from Figure 9D. Data from http://kmplot.com/analysis/index.php?p=service&cancer=lung.[54] Note that exclusively high expression of the KIT-dependent MC signature correlates with poor survival (A). Shown are Kaplan–Meier survival estimates with hazard ratios (HR) for high compared with low signature expression with their 95% confidence intervals, as well as log-rank test *P* values.

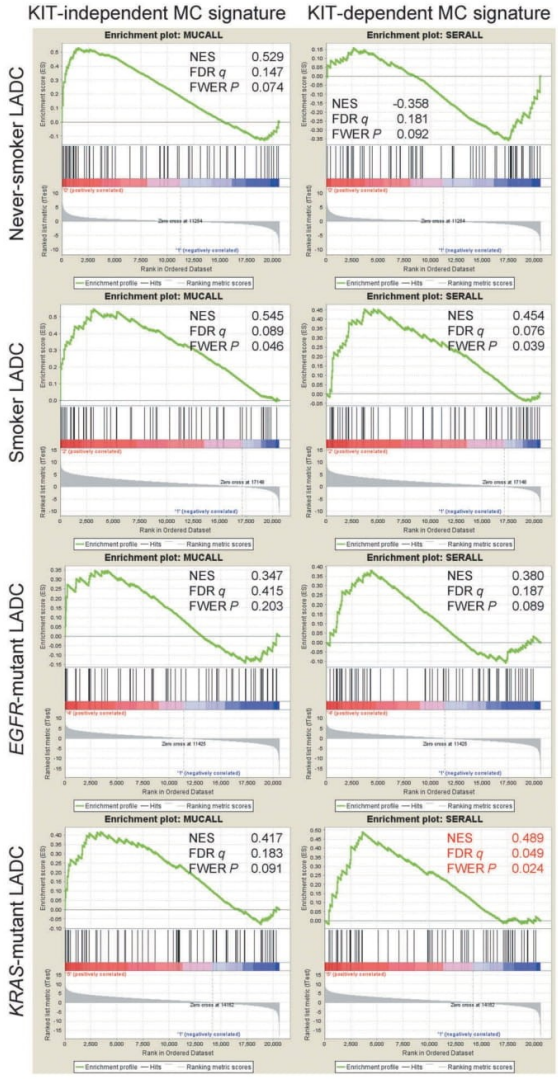

Figure 11. The KIT-dependent mast cell signature is focally enriched in KRAS-mutant lung adenocarcinoma.

Pre-ranked gene set enrichment analysis of the humanized KIT-independent (left) and KIT-dependent (right) mast cell (MC) signatures from Figure 9D against 40 lung adenocarcinoma (LADC) tissues from never-smokers, 40 LADC tissues from smokers, 15 *EGFR*-mutant LADC, and 22 *KRAS*-mutant LADC from the Biomarker-integrated Approaches of Targeted Therapy for Lung Cancer Elimination (BATTLE) study [Gene Expression Omnibus (GEO) datasets GSE43458 and GSE31852; freely available at https://www.ncbi.nlm.nih.gov/geo/query/acc.cgi?acc=GSE43458 and https://www.ncbi.nlm.nih.gov/geo/query/acc.cgi?acc=GSE31852].[53,55,56] GSEA was performed with the Broad Institute pre-ranked GSEA module software (http://software.broadinstitute.org/gsea/index.jsp).[65] Normal lung tissue from 40 never smokers were used as controls (GSE31852). Note that using stringent cut-offs of both false discovery rate (FDR) *q* values <0.05 and family-wise error rate (FWER) probability (*P*) values <0.05 the KIT-dependent MC signature is focally enriched in the molecular signature of *KRAS*-mutant LADC (red fonts). Shown are enrichment plots, normalized enrichment scores (NES), FDR, and FWER values.

Medicine of University of Patras, Greece. Experiments were approved by the Veterinary Administration of the Prefecture of Western Greece (#118018/578/30.04.2014) and were conducted according to Directive 2010/63/EU (http://eurlex.europa.eu/legal-content/EN/TXT/?uri=CELEX%3A32010L0063). Male and female mice were sex-, weight (20–25 g)-, and age (6–12 week)-matched. For LADC induction using the pulmonary carcinogen urethane (ethyl carbamate, EC; CAS #51–79-6; Sigma, St. Louis, MO), mice on the *C57BL/6* background received 10 weekly intraperitoneal injections (1g/Kg per 100μl saline prepared on the same day) and were sacrificed 6 months after the first injection.[37] For mutant $KRAS^{G12D}$-driven LADC, *C57BL/6* mice heterozygous for the loxP-STOP-loxP.$KRAS^{G12D}$ transgene ($KRAS^{G12D}$ mice), which express mutant $KRAS^{G12D}$ in all somatic cells upon CRE-mediated recombination, received 5×10^8 intratracheal plaque-forming units (pfu) adenovirus encoding CRE recombinase (Ad-*Cre*; Baylor College of Medicine, Houston, TX) and were killed after four months.[40] Control mice (designated *C57BL/6*) were a mixture of littermates negative for the transgenes of interest, including $cKit^{Wt/Wt}$ mice as appropriate controls for $cKit^{Wsh}$ mice and *Lyz2.Cre* mice as appropriate controls for *Cpa3.Cre* mice.[45] *C57BL/6* mice were anesthetized by isoflurane and received 10^6 LLC cells alone or combined with 2×10^4 BMMC subcutaneously into the rear flank. The 50:1 ratio of co-injected LLC and BMMC cells was chosen in order to replicate the number of MC in LADC MC hotspots. Three vertical tumor diameters (δ) were measured weekly, tumor volume (V) was calculated as $V = \pi \times (\delta 1 \times \delta 2 \times \delta 3)/6$, and mice were killed after one month.[43] Lungs were exsanguinated, inflated at 20 cm H_2O with 10% neutral-buffered formalin, and fixed overnight. Lung tumor number and δ were measured under a Stemi DV4 stereoscope (Zeiss; Jena, Germany) and V was calculated as $\pi\delta^3/6$ and averaged/summed. Lung volume was measured by saline immersion, lungs were embedded in paraffin, randomly sampled by 5 μm-thick sections (n = 10/lung), mounted on glass slides, and stained with hematoxylin and eosin (H&E). A 100-point-grid was superimposed on ≥5 random non-overlapping fields of ≥10 sections/lung using Fiji (https://fiji.sc/) and lung tumor burden was determined by extrapolating tumor-to-lung point counts to lung volume.[61,62]

Quantification of lung tumors

Specimens were examined by two blinded participants of this study and the results obtained by each investigator were compared and re-evaluated if deviant by >20%. In the urethane and lung metastasis models, tumors are approximately spherical with well-defined borders. Lungs and lung tumors were thus inspected macroscopically under a Stemi DV4 stereoscope equipped with a micrometric scale incorporated into one eyepiece and an Axiocam ERc5s camera (Zeiss, Jena, Germany) in trans-illumination mode, allowing for visualization of both superficial and deeply located lung tumors.[37] Tumor location was charted and δ was measured. Tumor number (multiplicity) per mouse was counted and mean tumor δ per mouse was calculated as the average of individual δ of all tumors found in a given mouse lung.

Individual tumor volume was calculated as $\pi\delta^3/6$. Mean tumor volume per mouse was calculated as the average of individual volumes of all tumors found in a given mouse lung, and total lung tumor burden per mouse as their sum. In the *KRAS*^{G12D} model, lung tumors are irregularly shaped with ill-defined borders. Hence, lung volume was measured by saline immersion, and lungs were embedded in paraffin, randomly sampled by cutting 5 µm-thick lung sections, mounted on glass slides, and stained with hematoxylin and eosin for morphometry. For this, a digital grid of 100 intersections of vertical lines (points) was superimposed on multiple digital images of all lung sections from lung tissue of a given mouse using Fiji.[61] Total lung tumor burden was determined by point counting of the ratio of the area occupied by neoplastic lesions versus total lung area and by extrapolating the average ratio per mouse to total lung volume.[62] The results of this stereologic approach were compared with the macroscopic method detailed above and were scrutinized if deviant by >20%. All quantifications were done by counting at least five random non-overlapping fields of view of at least 10 sections per lung.

Human samples

Matched tumor and normal lung tissue of 37 previously reported patients with LADC treated at the Faculty of Medicine of the University of Patras, Greece were used for MC counts,[50] and of 10 previously reported patients with LADC treated at the Research Center Borstel of the Airway Research Center North, Germany for microarray.[52] Patients were staged according to the sixth edition of the tumor-node-metastasis system for lung cancer.[63]

Histology

Five µm-thick tissue sections were stained with H&E or with toluidine blue (pH = 2.0; 10 min; RT; Sigma, St. Louis, MO) or were incubated with primary antibodies (Table 3) overnight at 4 °C followed by Envision/diaminobenzidine detection (Dako, Glostrup, Denmark) and hematoxylin or toluidine blue counterstaining/mounting (Entellan; Merck, Darmstadt, Germany). Nuclear PCNA immunoreactivity was defined as the percentage of positive cells in tumor areas. Sections were counted at high power (x 400) and 5–8 fields were assessed randomly for tumor cells. One thousand cell nuclei were counted and the number of cells showing positive nuclear staining was recorded. KIT, CD68, and LYZ2 immunoreactivity were defined as the percentage of positive cells. IL-1β immunostaining intensity was defined semiquantitatively (0: negative; 1: weak; 2: moderate; 3: strong). To assess the number of MC, slides were scanned at low power (x 20) to identify the 10 fields with the greatest number of MC (hotspots) separately in control lung tissue and in LADC. MC number was counted at high power (x 200) in every hotspot and the average was determined. Perivascular areas, where mast cells naturally accumulate, were excluded. Mononuclear, polymorphonuclear, and lymphocytic infiltrates were identified morphologically from H&E staining in 10 fields at a magnification of x 400 and the average was determined. Images were captured with an AxioLab.A1 upright microscope (Zeiss, Jena, Germany). Staining was evaluated by two blinded readers (IG, IL) and was verified by a certified pathologist (VB).

Table 3. Antibodies used for immunohistochemistry.

Product name/Target	Host species	Provider	Catalog#	Dilution
Anti-proliferating cell nuclear antigen antibody (PCNA)	Rabbit	Abcam, London, UK	ab2426	1:2000
Anti-CD68 antibody (CD68)	Mouse	Abcam, London, UK	ab955	1:200
Anti-Lysozyme antibody (LYZ2)	Rabbit	Abcam, London, UK	ab10850	1:250
Anti-Interleukin-1β antibody (IL-1β)	Rabbit	Abcam, London, UK	ab9722	1:200
Anti c-KIT (c-Kit)	Mouse	Santa Cruz Biotechnology, INC	sc-365504	1:100

qPCR

RNA was isolated using Trizol (Invitrogen, Carlsbad, CA) followed by RNAeasy (Qiagen, Hilden, Germany), was reverse transcribed using Superscript III (Invitrogen), and qPCR was performed using SYBR Green Master Mix and specific primers for *Il1b* (Il1bF: TTTGACAGTGATGAGAATGACC; Il1bR: AATGAGTGATACTGCCTGCC; GusbF: TTACTTTAAGAC GCTGATCACC; GusbR: ACCTCCAAATGCCCATAGTC) in a StepOne Plus thermocycler (Applied Biosystems, Carlsbad, CA). Ct values from triplicate qPCR reactions were analyzed by the $2^{-\Delta\Delta CT}$ method relative to *Gusb* mRNA levels.[64]

Immunoblotting

Total protein extracts from BMMC were extracted using Radioimmunoprecipitation assay buffer (Thermo Fisher Scientific, Waltham, MA), were separated by 12% SDS polyacrylamide gel electrophoresis, and were electroblotted to polyvinylidene difluoride membranes (Merck Millipore, Darmstadt, Germany). Membranes were probed with anti-CASP1 and anti-β-Actin (ACTB) antibodies (Table 3) and were visualized by film exposure after incubation with enhanced chemiluminescence substrate (Merck Millipore, Darmstadt, Germany).

Transcriptome analyses

Microarray data were analyzed with Gene Expression and Transcriptome Analysis Consoles using as cut-off differential gene expression > 2 (Affymetrix, Santa Clara, CA). Murine BMMC microarrays were reported elsewhere (GEO series GSE58189; https://www.ncbi.nlm.nih.gov/geo/query/acc.cgi?acc=GSE58189).[33] Humanized MC signatures were derived from mouse BMMC signatures using Orthoretriever (http://lighthouse.ucsf.edu/orthoretriever/).[51] Hierarchical clustering of BATTLE study patients by MC signatures was performed using GEO series GSE43458.[53] Human LADC patient survival analyses were done using Kaplan–Meier Plotter (http://kmplot.com/analysis/index.php?p=service&cancer=lung) and parameters auto-select best cutoff, compute median survival, censor at threshold, and histologic subtype lung adenocarcinoma.[54] GSEA was performed with the Broad Institute pre-ranked GSEA module (http://software.broadinstitute.org/gsea/index.

jsp) using BATTLE study transcriptomes from GEO series GSE43458 and GSE31852.[65]

Statistics

Sample size (n; always biological) was determined using G*power,[66] assuming $\alpha = 0.05$, $\beta = 0.05$, and Cohen's $d = 1.5$. Data were acquired by two blinded readers, reevaluated if >20% deviant (no data were excluded), examined for normality by Kolmogorov–Smirnov test, and presented as median (interquartile range) or mean±SEM. Differences in frequencies were examined by Fischer's exact or χ^2 tests, in means of normally distributed variables by t-test or one-way ANOVA/Bonferroni post-tests, and in medians of non-normally distributed variables by Mann–Whitney test or Kruskal–Wallis/Dunn's posttests. Survival and flank tumor volume were examined by Kaplan–Meier estimates/log-rank tests and two-way ANOVA/Bonferroni post-tests. Probability (P) is two-tailed and $P< 0.05$ was considered significant. Statistics and plots were done on Prism v5.0 (GraphPad, La Jolla, CA).

Study approval

All animal experiments were approved *a priori* by the Veterinary Administration of the Prefecture of Western Greece according to a full and detailed protocol (approval number 118018/578/30.04.2014) and were conducted according to Directive 2010/63/EU (http://eurlex.europa.eu/legal-content/EN/TXT/?uri=CELEX%3A32010L0063). Human studies were approved *a priori* by the Ethics Committee of the University of Lübeck, Germany (approval # AZ 12–220),[52] and by the ethics committee of the University Hospital of Patras, Greece.[50] The study's protocols were conducted according to the Declaration of Helsinki and all patients gave written informed consent.

Acknowledgments

The authors thank the University of Patras Center for Animal Models of Disease for experimental support, Dr. Hans-Reimer Rodewald for kindly providing *Cpa3.Cre* mice, and Dr. Yoichiro Iwakura for kindly providing *Il1b*-deficient mice. This work was supported by European Research Council 2010 Starting Independent Investigator and 2015 Proof of Concept Grants (260524 and 679345, respectively, to GTS), a Hellenic State Scholarships Foundation ('Ιδρυμα Κρατικών Υποτροφιών, IKY) Research Fellowship 2015–16 (to IL) and by Greek National Funds through the action National Science and Research Foundation (NSRF) 2014–2020 "Reinforcement of Postdoctoral Researchers" (to IG).

Authors' contributions

IL performed most *in vivo* experiments, histology and microscopy, analyzed the data, designed the study and wrote the draft of the manuscript; GN performed pilot *in* vivo experiments, histology and microscopy; VP performed pilot *in vivo* experiments; GAG performed GSEA; MO, AM, and MS performed *in vivo* experiments, genotyping, cell culture, RNA isolation, tumor cell and carcinogen injections, and tissue processing; SM and TG performed and analyzed human microarrays; VB analyzed human lung adenocarcinomas for mast cell content and provided expert pathologic advice; GTS and IG designed and guided the study, analyzed the data and wrote the final version of the manuscript. GTS also funded the study, is the guarantor of the study's integrity, and wrote/designed the final paper/figure set submitted. All authors critically reviewed and edited the paper for important intellectual content and approved the final submitted version.

Disclosure of Potential Conflicts of Interest

No potential conflicts of interest were disclosed.

Funding

This work was supported by the European Research Council [260524, 679345], Hellenic State Scholarships Foundation.

ORCID

Vassilios Papaleonidopoulos http://orcid.org/0000-0001-7324-9796
Ioanna Giopanou http://orcid.org/0000-0003-4393-7517
Georgios T. Stathopoulos http://orcid.org/0000-0002-9215-6461

References

1. Alberg AJ, Ford JG, Samet JM, American College of Chest Physicians. Epidemiology of lung cancer: ACCP evidence-based clinical practice guidelines (2nd edition). Chest. 2007;132(3 Suppl):29S–55S. doi:10.1378/chest.07-1347.
2. Torre LA, Bray F, Siegel RL, Ferlay J, Lortet-Tieulent J, Jemal A. Global cancer statistics, 2012. CA Cancer J Clin. 2015;65(2):87–108. doi:10.3322/caac.21262.
3. Cancer Genome Atlas Research Network. Comprehensive molecular profiling of lung adenocarcinoma. Nature. 2014;511(7511):543–550. doi:10.1038/nature13385.
4. Houghton AM. Mechanistic links between COPD and lung cancer. Nat Rev Cancer. 2013;13(4):233–245. doi:10.1038/nrc3477.
5. Houghton AM, Mouded M, Shapiro SD. Common origins of lung cancer and COPD. Nat Med. 2008;14(10):1023–1024. doi:10.1038/nm1008-1023.
6. Vestbo J, Hurd SS, Agusti AG, Jones PW, Vogelmeier C, Anzueto A, Barnes PJ, Fabbri LM, Martinez FJ, Nishimura M, et al. Global strategy for the diagnosis, management, and prevention of chronic obstructive pulmonary disease: GOLD executive summary. Am J Respir Crit Care Med. 2013;187(4):347–365. doi:10.1164/rccm.201204-0596PP.
7. Young RP, Hopkins RJ, Christmas T, Black PN, Metcalf P, Gamble GD. COPD prevalence is increased in lung cancer, independent of age, sex and smoking history. Eur Respir J. 2009;34(2):380–386. doi:10.1183/09031936.00144208.
8. Hanahan D, Weinberg RA. Hallmarks of cancer: the next generation. Cell. 2011;144(5):646–674. doi:10.1016/j.cell.2011.02.013.
9. Coussens LM, Pollard JW. Leukocytes in mammary development and cancer. Cold Spring Harb Perspect Biol. 2011;3(3). doi:10.1101/cshperspect.a003285.
10. Floor SL, Dumont JE, Maenhaut C, Raspe E. Hallmarks of cancer: of all cancer cells, all the time? Trends Mol Med. 2012;18(9):509–515. doi:10.1016/j.molmed.2012.06.005.
11. Swamy M, Jamora C, Havran W, Hayday A. Epithelial decision makers: in search of the 'epimmunome'. Nat Immunol. 2010;11(8):656–665. doi:10.1038/ni.1905.
12. Blair RJ, Meng H, Marchese MJ, Ren S, Schwartz LB, Tonnesen MG, Gruber BL. Human mast cells stimulate vascular tube formation. Tryptase is a novel, potent angiogenic factor. J Clin Invest. 1997;99(11):2691–2700. doi:10.1172/JCI119458.
13. Chen R, Ning G, Zhao ML, Fleming MG, Diaz LA, Werb Z, Liu Z. Mast cells play a key role in neutrophil recruitment in experimental bullous pemphigoid. J Clin Invest. 2001;108(8):1151–1158. doi:10.1172/JCI11494.
14. Galli SJ, Kalesnikoff J, Grimbaldeston MA, Piliponsky AM, Williams CM, Tsai M. Mast cells as "tunable" effector and

immunoregulatory cells: recent advances. Annu Rev Immunol. 2005:23749–23786. doi:10.1146/annurev.immunol.21.120601.141025.
15. Theoharides TC, Kempuraj D, Tagen M, Conti P, Kalogeromitros D. Differential release of mast cell mediators and the pathogenesis of inflammation. Immunol Rev. 2007:21765–21778. doi:10.1111/j.1600-065X.2007.00519.x.
16. Galli SJ, Nakae S, Tsai M. Mast cells in the development of adaptive immune responses. Nat Immunol. 2005;6(2):135–142. doi:10.1038/ni1158.
17. Kitamura Y. Heterogeneity of mast cells and phenotypic change between subpopulations. Annu Rev Immunol. 1989:759–776. doi:10.1146/annurev.iy.07.040189.000423.
18. Marone G, Triggiani M, Genovese A, De Paulis A. Role of human mast cells and basophils in bronchial asthma. Adv Immunol. 2005:88 97–160. doi:10.1016/S0065-2776(05)88004-6.
19. Metcalfe DD, Baram D, Mekori YA. Mast cells. Physiol Rev. 1997;77(4):1033–1079. doi:10.1152/physrev.1997.77.4.1033.
20. Dalton DK, Noelle RJ. The roles of mast cells in anticancer immunity. Cancer Immunol Immunother. 2012;61(9):1511–1520. doi:10.1007/s00262-012-1246-0.
21. Pittoni P, Colombo MP. The dark side of mast cell-targeted therapy in prostate cancer. Cancer Res. 2012;72(4):831–835. doi:10.1158/0008-5472.CAN-11-3110.
22. Sinnamon MJ, Carter KJ, Sims LP, Lafleur B, Fingleton B, Matrisian LM. A protective role of mast cells in intestinal tumorigenesis. Carcinogenesis. 2008;29(4):880–886. doi:10.1093/carcin/bgn040.
23. Soucek L, Lawlor ER, Soto D, Shchors K, Swigart LB, Evan GI. Mast cells are required for angiogenesis and macroscopic expansion of Myc-induced pancreatic islet tumors. Nat Med. 2007;13(10):1211–1218. doi:10.1038/nm1649.
24. Theoharides TC. Mast cells and pancreatic cancer. New Eng J Med. 2008;358(17):1860–1861. doi:10.1056/NEJMcibr0801519.
25. Varricchi G, Galdiero MR, Loffredo S, Marone G, Iannone R, Marone G, Granata F. Are mast cells MASTers in cancer? Front Immunol. 2017:8424. doi:10.3389/fimmu.2017.00424.
26. Dudeck A, Dudeck J, Scholten J, Petzold A, Surianarayanan S, Kohler A, Peschke K, Vohringer D, Waskow C, Krieg T, et al. Mast cells are key promoters of contact allergy that mediate the adjuvant effects of haptens. Immunity. 2011;34(6):973–984. doi:10.1016/j.immuni.2011.03.028.
27. Feyerabend TB, Weiser A, Tietz A, Stassen M, Harris N, Kopf M, Radermacher P, Moller P, Benoist C, Mathis D, et al. Cre-mediated cell ablation contests mast cell contribution in models of antibody- and T cell-mediated autoimmunity. Immunity. 2011;35(5):832–844. doi:10.1016/j.immuni.2011.09.015.
28. Imada A, Shijubo N, Kojima H, Abe S. Mast cells correlate with angiogenesis and poor outcome in stage I lung adenocarcinoma. Eur Respir J. 2000;15(6):1087–1093. PMID:10885428.
29. Redente EF, Orlicky DJ, Bouchard RJ, Malkinson AM. Tumor signaling to the bone marrow changes the phenotype of monocytes and pulmonary macrophages during urethane-induced primary lung tumorigenesis in A/J mice. Am J Pathol. 2007;170(2):693–708. doi:10.2353/ajpath.2007.060566.
30. Stoyanov E, Uddin M, Mankuta D, Dubinett SM, Levi-Schaffer F. Mast cells and histamine enhance the proliferation of non-small cell lung cancer cells. Lung Cancer. 2012;75(1):38–44. doi:10.1016/j.lungcan.2011.05.029.
31. Xiao H, Lasser C, Shelke GV, Wang J, Radinger M, Lunavat TR, Malmhall C, Lin LH, Li J, Li L, et al. Mast cell exosomes promote lung adenocarcinoma cell proliferation - role of KIT-stem cell factor signaling. Cell Commun Signal. 2014;1264. doi:10.1186/s12964-014-0064-8.
32. Agalioti T, Giannou AD, Krontira AC, Kanellakis NI, Kati D, Vreka M, Pepe M, Spella M, Lilis I, Zazara DE, et al. Mutant KRAS promotes malignant pleural effusion formation. Nat Commun. 2017;815205. doi:10.1038/ncomms15205.
33. Giannou AD, Marazioti A, Spella M, Kanellakis NI, Apostolopoulou H, Psallidas I, Prijovich ZM, Vreka M, Zazara DE, Lilis I, et al. Mast cells mediate malignant pleural effusion formation. J Clin Invest. 2015;125(6):2317–2334. doi:10.1172/JCI79840.
34. Marazioti A, Lilis I, Vreka M, Apostolopoulou H, Kalogeropoulou A, Giopanou I, Giotopoulou GA, Krontira AC, Iliopoulou M, Kanellakis NI, et al. Myeloid-derived interleukin-1beta drives oncogenic KRAS-NF-kappaBeta addiction in malignant pleural effusion. Nat Commun. 2018;9(1):672. doi:10.1038/s41467-018-03051-z.
35. Nikitin AY, Alcaraz A, Anver MR, Bronson RT, Cardiff RD, Dixon D, Fraire AE, Gabrielson EW, Gunning WT, Haines DC, et al. Classification of proliferative pulmonary lesions of the mouse: recommendations of the mouse models of human cancers consortium. Cancer Res. 2004;64(7):2307–2316. doi:10.1158/0008-5472.CAN-03-3376.
36. Spella MLI, Vreka M, Marazioti A, Giopanou I, Aidinis V, Stathopoulos GT. An airway epithelial origin for tobacco carcinogen-induced lung adenocarcinoma. Eur Respir J. 2015:46OA4980. doi:10.1183/13993003.congress-2015.OA4980.
37. Stathopoulos GT, Sherrill TP, Cheng DS, Scoggins RM, Han W, Polosukhin VV, Connelly L, Yull FE, Fingleton B, Blackwell TS. Epithelial NF-kappaB activation promotes urethane-induced lung carcinogenesis. Proc Natl Acad Sci U S A. 2007;104(47):18514–18519. doi:10.1073/pnas.0705316104.
38. Westcott PM, Halliwill KD, To MD, Rashid M, Rust AG, Keane TM, Delrosario R, Jen KY, Gurley KE, Kemp CJ, et al. The mutational landscapes of genetic and chemical models of Kras-driven lung cancer. Nature. 2015;517(7535):489–492. doi:10.1038/nature13898.
39. Desai TJ, Brownfield DG, Krasnow MA. Alveolar progenitor and stem cells in lung development, renewal and cancer. Nature. 2014;507(7491):190–194. doi:10.1038/nature12930.
40. Jackson EL, Willis N, Mercer K, Bronson RT, Crowley D, Montoya R, Jacks T, Tuveson DA. Analysis of lung tumor initiation and progression using conditional expression of oncogenic K-ras. Genes Dev. 2001;15(24):3243–3248. doi:10.1101/gad.943001.
41. Giannou AD, Marazioti A, Kanellakis NI, Giopanou I, Lilis I, Zazara DE, Ntaliarda G, Kati D, Armenis V, Giotopoulou GA, et al. NRAS destines tumor cells to the lungs. EMBO Mol Med. 2017;9(5):672–686. doi:10.15252/emmm.201606978.
42. Giopanou I, Lilis I, Papaleonidopoulos V, Agalioti T, Kanellakis NI, Spiropoulou N, Spella M, Stathopoulos GT. Tumor-derived osteopontin isoforms cooperate with TRP53 and CCL2 to promote lung metastasis. Oncoimmunology. 2017;6(1):e1256528. doi:10.1080/2162402X.2016.1256528.
43. Stathopoulos GT, Sherrill TP, Karabela SP, Goleniewska K, Kalomenidis I, Roussos C, Fingleton B, Yull FE, Peebles RS Jr., Blackwell TS. Host-derived interleukin-5 promotes adenocarcinoma-induced malignant pleural effusion. Am J Respir Crit Care Med. 2010;182(10):1273–1281. doi:10.1164/rccm.201001-0001OC.
44. Tono T, Tsujimura T, Koshimizu U, Kasugai T, Adachi S, Isozaki K, Nishikawa S, Morimoto M, Nishimune Y, Nomura S, et al. c-kit Gene was not transcribed in cultured mast cells of mast cell-deficient Wsh/Wsh mice that have a normal number of erythrocytes and a normal c-kit coding region. Blood. 1992;80(6):1448–1453. PMID:1381627.
45. Clausen BE, Burkhardt C, Reith W, Renkawitz R, Forster I. Conditional gene targeting in macrophages and granulocytes using LysMcre mice. Transgenic Res. 1999;8(4):265–277. doi:10.1023/A:1008942828960.
46. Thornberry NA, Bull HG, Calaycay JR, Chapman KT, Howard AD, Kostura MJ, Miller DK, Molineaux SM, Weidner JR, Aunins J, et al. A novel heterodimeric cysteine protease is required for interleukin-1 beta processing in monocytes. Nature. 1992;356(6372):768–774. doi:10.1038/356768a0.
47. Michel A, Schuler A, Friedrich P, Doner F, Bopp T, Radsak M, Hoffmann M, Relle M, Distler U, Kuharev J, et al. Mast cell-deficient Kit(W-sh) “Sash” mutant mice display aberrant myelopoiesis leading to the accumulation of splenocytes that act as

myeloid-derived suppressor cells. J Immunol. 2013;190 (11):5534–5544. doi:10.4049/jimmunol.1203355.
48. Horai R, Asano M, Sudo K, Kanuka H, Suzuki M, Nishihara M, Takahashi M, Iwakura Y. Production of mice deficient in genes for interleukin (IL)-1alpha, IL-1beta, IL-1alpha/beta, and IL-1 receptor antagonist shows that IL-1beta is crucial in turpentine-induced fever development and glucocorticoid secretion. J Exp Med. 1998;187 (9):1463–1475. doi:10.1084/jem.187.9.1463.
49. Boring L, Gosling J, Chensue SW, Kunkel SL, Farese RV Jr., Broxmeyer HE, Charo IF. Impaired monocyte migration and reduced type 1 (Th1) cytokine responses in C-C chemokine receptor 2 knockout mice. J Clin Invest. 1997;100(10):2552–2561. doi:10.1172/JCI119798.
50. Giopanou I, Lilis I, Papaleonidopoulos V, Marazioti A, Spella M, Vreka M, Papadaki H, Stathopoulos GT. Comprehensive evaluation of nuclear factor-kappaBeta expression patterns in non-small cell lung cancer. PLoS One. 2015;10(7):e0132527. doi:10.1371/journal.pone.0132527.
51. Kasprzyk A. BioMart: driving a paradigm change in biological data management. Database (Oxford). 2011:2011bar049. doi:10.1093/database/bar049.
52. Marwitz S, Depner S, Dvornikov D, Merkle R, Szczygiel M, Muller-Decker K, Lucarelli P, Wasch M, Mairbaurl H, Rabe KF, et al. Downregulation of the TGFbeta pseudoreceptor BAMBI in non-small cell lung cancer enhances TGFbeta signaling and invasion. Cancer Res. 2016;76(13):3785–3801. doi:10.1158/0008-5472.CAN-15-1326.
53. Kabbout M, Garcia MM, Fujimoto J, Liu DD, Woods D, Chow CW, Mendoza G, Momin AA, James BP, Solis L, et al. ETS2 mediated tumor suppressive function and MET oncogene inhibition in human non-small cell lung cancer. Clin Cancer Res. 2013;19(13):3383–3395. doi:10.1158/1078-0432.CCR-13-0341.
54. Gyorffy B, Surowiak P, Budczies J, Lanczky A. Online survival analysis software to assess the prognostic value of biomarkers using transcriptomic data in non-small-cell lung cancer. PLoS One. 2013;8(12):e82241. doi:10.1371/journal.pone.0082241.
55. Blumenschein GR Jr., Saintigny P, Liu S, Kim ES, Tsao AS, Herbst RS, Alden C, Lee JJ, Tang X, Stewart DJ, et al. Comprehensive biomarker analysis and final efficacy results of sorafenib in the BATTLE trial. Clin Cancer Res. 2013;19 (24):6967–6975. doi:10.1158/1078-0432.CCR-12-1818.
56. Byers LA, Diao L, Wang J, Saintigny P, Girard L, Peyton M, Shen L, Fan Y, Giri U, Tumula PK, et al. An epithelial-mesenchymal transition gene signature predicts resistance to EGFR and PI3K inhibitors and identifies Axl as a therapeutic target for overcoming EGFR inhibitor resistance. Clin Cancer Res. 2013;19(1):279–290. doi:10.1158/1078-0432.CCR-12-1558.
57. Morita H, Arae K, Unno H, Miyauchi K, Toyama S, Nambu A, Oboki K, Ohno T, Motomura K, Matsuda A, et al. An interleukin-33-mast cell-interleukin-2 axis suppresses papain-induced allergic inflammation by promoting regulatory T cell numbers. Immunity. 2015;43 (1):175–186. doi:10.1016/j.immuni.2015.06.021.
58. Zaynagetdinov R, Stathopoulos GT, Sherrill TP, Cheng DS, McLoed AG, Ausborn JA, Polosukhin VV, Connelly L, Zhou W, Fingleton B, et al. Epithelial nuclear factor-kappaB signaling promotes lung carcinogenesis via recruitment of regulatory T lymphocytes. Oncogene. 2012;31(26):3164–3176. doi:10.1038/onc.2011.480.
59. Ridker PM, MacFadyen JG, Thuren T, Everett BM, Libby P, Glynn RJ, Group CT. Effect of interleukin-1beta inhibition with canakinumab on incident lung cancer in patients with atherosclerosis: exploratory results from a randomised, double-blind, placebo-controlled trial. Lancet. 2017;390(10105):1833–1842. doi:10.1016/S0140-6736(17)32247-X.
60. Ridker PM, MacFadyen JG, Everett BM, Libby P, Thuren T, Glynn RJ, Group CT. Relationship of C-reactive protein reduction to cardiovascular event reduction following treatment with canakinumab: a secondary analysis from the CANTOS randomised controlled trial. Lancet. 2018;391(10118):319–328. doi:10.1016/S0140-6736(17)32814-3.
61. Schindelin J, Arganda-Carreras I, Frise E, Kaynig V, Longair M, Pietzsch T, Preibisch S, Rueden C, Saalfeld S, Schmid B, et al. Fiji: an open-source platform for biological-image analysis. Nat Methods. 2012;9(7):676–682. doi:10.1038/nmeth.2019.
62. Hsia CC, Hyde DM, Ochs M, Weibel ER, Structure AEJTFoQAoL. An official research policy statement of the American Thoracic Society/European Respiratory Society: standards for quantitative assessment of lung structure. Am J Respir Crit Care Med. 2010;181(4):394–418. doi:10.1164/rccm.200809-1522ST.
63. Travis WD, Brambilla E, Noguchi M, Nicholson AG, Geisinger KR, Yatabe Y, Beer DG, Powell CA, Riely GJ, Van Schil PE, et al. International association for the study of lung cancer/american thoracic society/european respiratory society international multidisciplinary classification of lung adenocarcinoma. J Thorac Oncol. 2011;6(2):244–285. doi:10.1097/JTO.0b013e318206a221.
64. Pfaffl MW. A new mathematical model for relative quantification in real-time RT-PCR. Nucleic Acids Res. 2001;29(9):e45. PMID:11328886. doi:10.1093/nar/29.9.e45.
65. Subramanian A, Tamayo P, Mootha VK, Mukherjee S, Ebert BL, Gillette MA, Paulovich A, Pomeroy SL, Golub TR, Lander ES, et al. Gene set enrichment analysis: a knowledge-based approach for interpreting genome-wide expression profiles. Proc Natl Acad Sci U S A. 2005;102(43):15545–15550. doi:10.1073/pnas.0506580102.
66. Faul F, Erdfelder E, Lang AG, Buchner A. G*Power 3: a flexible statistical power analysis program for the social, behavioral, and biomedical sciences. Behav Res Methods. 2007;39(2):175–191. PMID:17695343.

References

Agalioti, T., Giannou, A. D., Krontira, A. C., Kanellakis, N. I., Kati, D., Vreka, M., Pepe, M., Spella, M., Lilis, I., Zazara, D. E., Nikolouli, E., Spiropoulou, N., Papadakis, A., Papadia, K., Voulgaridis, A., Harokopos, V., Stamou, P., Meiners, S., Eickelberg, O., Snyder, L. A., Antimisiaris, S. G., Kardamakis, D., Psallidas, I., Marazioti, A., & Stathopoulos, G. T. (2017). Mutant KRAS promotes malignant pleural effusion formation. *Nat Commun*, *8*, 15205. https://doi.org/10.1038/ncomms15205

Alberg, A. J., Brock, M. V., Ford, J. G., Samet, J. M., & Spivack, S. D. (2013). Epidemiology of lung cancer: Diagnosis and management of lung cancer, 3rd ed: American College of Chest Physicians evidence-based clinical practice guidelines. *Chest*, *143*(5 Suppl), e1S-e29S. https://doi.org/10.1378/chest.12-2345

Alexandrov, L. B., Ju, Y. S., Haase, K., Van Loo, P., Martincorena, I., Nik-Zainal, S., Totoki, Y., Fujimoto, A., Nakagawa, H., Shibata, T., Campbell, P. J., Vineis, P., Phillips, D. H., & Stratton, M. R. (2016). Mutational signatures associated with tobacco smoking in human cancer. *Science*, *354*(6312), 618-622. https://doi.org/10.1126/science.aag0299

Alexandrov, L. B., Nik-Zainal, S., Wedge, D. C., Aparicio, S. A., Behjati, S., Biankin, A. V., Bignell, G. R., Bolli, N., Borg, A., Børresen-Dale, A. L., Boyault, S., Burkhardt, B., Butler, A. P., Caldas, C., Davies, H. R., Desmedt, C., Eils, R., Eyfjörd, J. E., Foekens, J. A., Greaves, M., Hosoda, F., Hutter, B., Ilicic, T., Imbeaud, S., Imielinski, M., Jäger, N., Jones, D. T., Jones, D., Knappskog, S., Kool, M., Lakhani, S. R., López-Otín, C., Martin, S., Munshi, N. C., Nakamura, H., Northcott, P. A., Pajic, M., Papaemmanuil, E., Paradiso, A., Pearson, J. V., Puente, X. S., Raine, K., Ramakrishna, M., Richardson, A. L., Richter, J., Rosenstiel, P., Schlesner, M., Schumacher, T. N., Span, P. N., Teague, J. W., Totoki, Y., Tutt, A. N., Valdés-Mas, R., van Buuren, M. M., van 't Veer, L., Vincent-Salomon, A., Waddell, N., Yates, L. R., Zucman-Rossi, J., Futreal, P. A., McDermott, U., Lichter, P., Meyerson, M., Grimmond, S. M., Siebert, R., Campo, E., Shibata, T., Pfister, S. M., Campbell, P. J., & Stratton, M. R. (2013). Signatures of mutational processes in human cancer. *Nature*, *500*(7463), 415-421. https://doi.org/10.1038/nature12477

Allavena, P., Germano, G., Marchesi, F., & Mantovani, A. (2011). Chemokines in cancer related inflammation. *Exp Cell Res*, *317*(5), 664-673. https://doi.org/10.1016/j.yexcr.2010.11.013

Aponte-López, A., & Muñoz-Cruz, S. (2020). Mast Cells in the Tumor Microenvironment. *Adv Exp Med Biol*, *1273*, 159-173. https://doi.org/10.1007/978-3-030-49270-0_9

Attanoos, R. L., Churg, A., Galateau-Salle, F., Gibbs, A. R., & Roggli, V. L. (2018). Malignant Mesothelioma and Its Non-Asbestos Causes. *Arch Pathol Lab Med*, *142*(6), 753-760. https://doi.org/10.5858/arpa.2017-0365-RA

Balkwill, F. (2004). Cancer and the chemokine network. *Nat Rev Cancer*, *4*(7), 540-550. https://doi.org/10.1038/nrc1388

Balkwill, F. R. (2012). The chemokine system and cancer. *J Pathol*, *226*(2), 148-157. https://doi.org/10.1002/path.3029

Balkwill, F. R., Capasso, M., & Hagemann, T. (2012). The tumor microenvironment at a glance. *J Cell Sci*, *125*(Pt 23), 5591-5596. https://doi.org/10.1242/jcs.116392

Beer, T. W., Ng, L. B., & Murray, K. (2008). Mast cells have prognostic value in Merkel cell carcinoma. *Am J Dermatopathol*, *30*(1), 27-30. https://doi.org/10.1097/DAD.0b013e31815c932a

Behjati, S., Gundem, G., Wedge, D. C., Roberts, N. D., Tarpey, P. S., Cooke, S. L., Van Loo, P., Alexandrov, L. B., Ramakrishna, M., Davies, H., Nik-Zainal, S., Hardy, C., Latimer, C., Raine, K. M., Stebbings, L., Menzies, A., Jones, D., Shepherd, R., Butler, A. P., Teague, J. W., Jorgensen, M., Khatri, B., Pillay, N., Shlien, A., Futreal, P. A., Badie, C., McDermott, U., Bova, G. S., Richardson, A. L., Flanagan, A. M., Stratton, M. R., & Campbell, P. J. (2016). Mutational signatures of ionizing radiation in second malignancies. *Nat Commun*, *7*, 12605. https://doi.org/10.1038/ncomms12605

Belinsky, S. A. (2004). Gene-promoter hypermethylation as a biomarker in lung cancer. *Nat Rev Cancer*, *4*(9), 707-717. https://doi.org/10.1038/nrc1432

Bianchi, A. B., Mitsunaga, S. I., Cheng, J. Q., Klein, W. M., Jhanwar, S. C., Seizinger, B., Kley, N., Klein-Szanto, A. J., & Testa, J. R. (1995). High frequency of inactivating mutations in the neurofibromatosis type 2 gene (NF2) in primary malignant mesotheliomas. *Proc Natl Acad Sci U S A*, *92*(24), 10854-10858. https://doi.org/10.1073/pnas.92.24.10854

Bibby, A. C., Tsim, S., Kanellakis, N., Ball, H., Talbot, D. C., Blyth, K. G., Maskell, N. A., & Psallidas, I. (2016). Malignant pleural mesothelioma: an update on investigation, diagnosis and treatment. *Eur Respir Rev*, *25*(142), 472-486. https://doi.org/10.1183/16000617.0063-2016

Blum, Y., Meiller, C., Quetel, L., Elarouci, N., Ayadi, M., Tashtanbaeva, D., Armenoult, L., Montagne, F., Tranchant, R., Renier, A., de Koning, L., Copin, M. C., Hofman, P., Hofman, V., Porte, H., Le Pimpec-Barthes, F., Zucman-Rossi, J., Jaurand, M. C., de Reyniès, A., & Jean, D. (2019). Dissecting heterogeneity in malignant pleural mesothelioma through histo-molecular gradients for clinical applications. *Nat Commun*, *10*(1), 1333. https://doi.org/10.1038/s41467-019-09307-6

Boffetta, P. (2004). Epidemiology of environmental and occupational cancer. *Oncogene*, *23*(38), 6392-6403. https://doi.org/10.1038/sj.onc.1207715

Bott, M., Brevet, M., Taylor, B. S., Shimizu, S., Ito, T., Wang, L., Creaney, J., Lake, R. A., Zakowski, M. F., Reva, B., Sander, C., Delsite, R., Powell, S., Zhou, Q., Shen, R., Olshen, A., Rusch, V., & Ladanyi, M. (2011). The nuclear deubiquitinase BAP1 is commonly inactivated by somatic mutations and 3p21.1 losses in malignant pleural mesothelioma. *Nat Genet*, *43*(7), 668-672. https://doi.org/10.1038/ng.855

Bronte, V., Cingarlini, S., Marigo, I., De Santo, C., Gallina, G., Dolcetti, L., Ugel, S., Peranzoni, E., Mandruzzato, S., & Zanovello, P. (2006). Leukocyte infiltration in cancer creates an unfavorable environment for antitumor immune responses: a novel target for therapeutic intervention. *Immunol Invest*, *35*(3-4), 327-357. https://doi.org/10.1080/08820130600754994

Bueno, R. (2005). Multimodality treatments in the management of malignant pleural mesothelioma: an update. *Hematol Oncol Clin North Am*, *19*(6), 1089-1097, vii. https://doi.org/10.1016/j.hoc.2005.09.011

Bueno, R., Stawiski, E. W., Goldstein, L. D., Durinck, S., De Rienzo, A., Modrusan, Z., Gnad, F., Nguyen, T. T., Jaiswal, B. S., Chirieac, L. R., Sciaranghella, D., Dao, N., Gustafson, C. E., Munir, K. J., Hackney, J. A., Chaudhuri, A., Gupta, R., Guillory, J., Toy, K., Ha, C., Chen, Y. J., Stinson, J., Chaudhuri, S., Zhang, N., Wu, T. D., Sugarbaker, D. J., de Sauvage, F. J., Richards, W. G., & Seshagiri, S. (2016). Comprehensive genomic analysis of malignant pleural mesothelioma identifies recurrent mutations, gene fusions and splicing alterations. *Nat Genet*, *48*(4), 407-416. https://doi.org/10.1038/ng.3520

Campbell, J. D., Alexandrov, A., Kim, J., Wala, J., Berger, A. H., Pedamallu, C. S., Shukla, S. A., Guo, G., Brooks, A. N., Murray, B. A., Imielinski, M., Hu, X., Ling, S., Akbani, R., Rosenberg, M., Cibulskis, C., Ramachandran, A., Collisson, E. A., Kwiatkowski, D. J., Lawrence, M. S., Weinstein, J. N., Verhaak, R. G., Wu, C. J., Hammerman, P. S., Cherniack, A. D., Getz, G., Artyomov, M. N., Schreiber, R., Govindan, R., & Meyerson, M. (2016). Distinct patterns of somatic genome alterations in lung adenocarcinomas and squamous cell carcinomas. *Nat Genet*, *48*(6), 607-616. https://doi.org/10.1038/ng.3564

Chatterjee, A., Rodger, E. J., & Eccles, M. R. (2018). Epigenetic drivers of tumourigenesis and cancer metastasis. *Semin Cancer Biol*, *51*, 149-159. https://doi.org/10.1016/j.semcancer.2017.08.004

Chen, Z., Fillmore, C. M., Hammerman, P. S., Kim, C. F., & Wong, K. K. (2014). Non-small-cell lung cancers: a heterogeneous set of diseases. *Nat Rev Cancer*, *14*(8), 535-546. https://doi.org/10.1038/nrc3775

Cheng, J. Q., Jhanwar, S. C., Klein, W. M., Bell, D. W., Lee, W. C., Altomare, D. A., Nobori, T., Olopade, O. I., Buckler, A. J., & Testa, J. R. (1994). p16 alterations and deletion mapping of 9p21-p22 in malignant mesothelioma. *Cancer Res*, *54*(21), 5547-5551.

Clark, S. J., & Molloy, P. L. (2017). Smoke-Induced Changes to the Epigenome Provide Fertile Ground for Oncogenic Mutation. *Cancer Cell*, *32*(3), 278-280. https://doi.org/10.1016/j.ccell.2017.08.016

Comprehensive molecular profiling of lung adenocarcinoma. (2014). *Nature*, *511*(7511), 543-550. https://doi.org/10.1038/nature13385

Couraud, S., Zalcman, G., Milleron, B., Morin, F., & Souquet, P. J. (2012). Lung cancer in never smokers--a review. *Eur J Cancer*, *48*(9), 1299-1311. https://doi.org/10.1016/j.ejca.2012.03.007

Courtiol, P., Maussion, C., Moarii, M., Pronier, E., Pilcer, S., Sefta, M., Manceron, P., Toldo, S., Zaslavskiy, M., Le Stang, N., Girard, N., Elemento, O., Nicholson, A. G., Blay, J. Y., Galateau-Sallé, F., Wainrib, G., & Clozel, T. (2019). Deep learning-based classification of mesothelioma improves prediction of patient outcome. *Nat Med*, *25*(10), 1519-1525. https://doi.org/10.1038/s41591-019-0583-3

Coussens, L. M., Zitvogel, L., & Palucka, A. K. (2013). Neutralizing tumor-promoting chronic inflammation: a magic bullet? *Science*, *339*(6117), 286-291. https://doi.org/10.1126/science.1232227

Crusz, S. M., & Balkwill, F. R. (2015). Inflammation and cancer: advances and new agents. *Nat Rev Clin Oncol*, *12*(10), 584-596. https://doi.org/10.1038/nrclinonc.2015.105

de Bruin, E. C., McGranahan, N., Mitter, R., Salm, M., Wedge, D. C., Yates, L., Jamal-Hanjani, M., Shafi, S., Murugaesu, N., Rowan, A. J., Grönroos, E., Muhammad, M. A., Horswell, S., Gerlinger, M., Varela, I., Jones, D., Marshall, J., Voet, T., Van Loo, P., Rassl, D. M., Rintoul, R. C., Janes, S. M., Lee, S. M., Forster, M., Ahmad, T., Lawrence, D., Falzon, M., Capitanio, A., Harkins, T. T., Lee, C. C., Tom, W., Teefe, E., Chen, S. C., Begum, S., Rabinowitz, A., Phillimore, B., Spencer-Dene, B., Stamp, G., Szallasi, Z., Matthews, N., Stewart, A., Campbell, P., & Swanton, C. (2014). Spatial and temporal diversity in genomic instability processes defines lung cancer evolution. *Science*, *346*(6206), 251-256. https://doi.org/10.1126/science.1253462

De Rienzo, A., Archer, M. A., Yeap, B. Y., Dao, N., Sciaranghella, D., Sideris, A. C., Zheng, Y., Holman, A. G., Wang, Y. E., Dal Cin, P. S., Fletcher, J. A., Rubio, R., Croft, L., Quackenbush, J., Sugarbaker, P. E., Munir, K. J., Battilana, J. R., Gustafson, C. E., Chirieac, L. R., Ching, S. M., Wong, J., Tay, L. C., Rudd, S., Hercus, R., Sugarbaker, D. J., Richards, W. G., & Bueno, R. (2016). Gender-Specific Molecular and Clinical Features Underlie Malignant Pleural Mesothelioma. *Cancer Res*, *76*(2), 319-328. https://doi.org/10.1158/0008-5472.Can-15-0751

Devarakonda, S., Morgensztern, D., & Govindan, R. (2015). Genomic alterations in lung adenocarcinoma. *Lancet Oncol*, *16*(7), e342-351. https://doi.org/10.1016/s1470-2045(15)00077-7

Di Cello, F., Flowers, V. L., Li, H., Vecchio-Pagán, B., Gordon, B., Harbom, K., Shin, J., Beaty, R., Wang, W., Brayton, C., Baylin, S. B., & Zahnow, C. A. (2013). Cigarette smoke induces epithelial to mesenchymal transition and increases the metastatic ability of breast cancer cells. *Mol Cancer*, *12*, 90. https://doi.org/10.1186/1476-4598-12-90

Enomoto, Y., Kasai, T., Takeda, M., Takano, M., Morita, K., Kadota, E., Iizuka, N., Maruyama, H., Haratake, J., Kojima, Y., Ikeda, N., Inatsugi, N., & Nonomura, A. (2012). Epidermal growth factor receptor mutations in malignant pleural and peritoneal mesothelioma. *J Clin Pathol*, *65*(6), 522-527. https://doi.org/10.1136/jclinpath-2011-200631

Feyerabend, T. B., Weiser, A., Tietz, A., Stassen, M., Harris, N., Kopf, M., Radermacher, P., Möller, P., Benoist, C., Mathis, D., Fehling, H. J., & Rodewald, H. R. (2011). Cre-mediated cell ablation contests mast cell contribution in models of antibody- and T cell-mediated autoimmunity. *Immunity*, *35*(5), 832-844. https://doi.org/10.1016/j.immuni.2011.09.015

Forbes, S. A., Beare, D., Gunasekaran, P., Leung, K., Bindal, N., Boutselakis, H., Ding, M., Bamford, S., Cole, C., Ward, S., Kok, C. Y., Jia, M., De, T., Teague, J. W., Stratton, M. R., McDermott, U., & Campbell, P. J. (2015). COSMIC: exploring the world's knowledge of somatic mutations in human cancer. *Nucleic Acids Res*, *43*(Database issue), D805-811. https://doi.org/10.1093/nar/gku1075

Franco, G., Guarnotta, C., Frossi, B., Piccaluga, P. P., Boveri, E., Gulino, A., Fuligni, F., Rigoni, A., Porcasi, R., Buffa, S., Betto, E., Florena, A. M., Franco, V., Iannitto, E., Arcaini, L., Pileri, S. A., Pucillo, C., Colombo, M. P., Sangaletti, S., & Tripodo, C. (2014). Bone

marrow stroma CD40 expression correlates with inflammatory mast cell infiltration and disease progression in splenic marginal zone lymphoma. *Blood*, *123*(12), 1836-1849. https://doi.org/10.1182/blood-2013-04-497271

Frank, A. L., & Joshi, T. K. (2014). The global spread of asbestos. *Ann Glob Health*, *80*(4), 257-262. https://doi.org/10.1016/j.aogh.2014.09.016

Furukawa, K., Preston, D. L., Lönn, S., Funamoto, S., Yonehara, S., Matsuo, T., Egawa, H., Tokuoka, S., Ozasa, K., Kasagi, F., Kodama, K., & Mabuchi, K. (2010). Radiation and smoking effects on lung cancer incidence among atomic bomb survivors. *Radiat Res*, *174*(1), 72-82. https://doi.org/10.1667/rr2083.1

Galani, V., Varouktsi, A., Papadatos, S. S., Mitselou, A., Sainis, I., Constantopoulos, S., & Dalavanga, Y. (2019). The role of apoptosis defects in malignant mesothelioma pathogenesis with an impact on prognosis and treatment. *Cancer Chemother Pharmacol*, *84*(2), 241-253. https://doi.org/10.1007/s00280-019-03878-3

Galateau-Salle, F., Churg, A., Roggli, V., & Travis, W. D. (2016). The 2015 World Health Organization Classification of Tumors of the Pleura: Advances since the 2004 Classification. *J Thorac Oncol*, *11*(2), 142-154. https://doi.org/10.1016/j.jtho.2015.11.005

Galli, S. J., & Tsai, M. (2012). IgE and mast cells in allergic disease. *Nat Med*, *18*(5), 693-704. https://doi.org/10.1038/nm.2755

Gao, J., Aksoy, B. A., Dogrusoz, U., Dresdner, G., Gross, B., Sumer, S. O., Sun, Y., Jacobsen, A., Sinha, R., Larsson, E., Cerami, E., Sander, C., & Schultz, N. (2013). Integrative analysis of complex cancer genomics and clinical profiles using the cBioPortal. *Sci Signal*, *6*(269), pl1. https://doi.org/10.1126/scisignal.2004088

Gao, X., Zhang, Y., Breitling, L. P., & Brenner, H. (2016). Tobacco smoking and methylation of genes related to lung cancer development. *Oncotarget*, *7*(37), 59017-59028. https://doi.org/10.18632/oncotarget.10007

Gazdar, A. F. (2003). Environmental tobacco smoke, carcinogenesis, and angiogenesis: a double whammy? *Cancer Cell*, *4*(3), 159-160. https://doi.org/10.1016/s1535-6108(03)00222-8

Giannou, A. D., Marazioti, A., Spella, M., Kanellakis, N. I., Apostolopoulou, H., Psallidas, I., Prijovich, Z. M., Vreka, M., Zazara, D. E., Lilis, I., Papaleonidopoulos, V., Kairi, C. A., Patmanidi, A. L., Giopanou, I., Spiropoulou, N., Harokopos, V., Aidinis, V., Spyratos, D., Teliousi, S., Papadaki, H., Taraviras, S., Snyder, L. A., Eickelberg, O., Kardamakis, D., Iwakura, Y., Feyerabend, T. B., Rodewald, H. R., Kalomenidis, I., Blackwell, T. S., Agalioti, T., & Stathopoulos, G. T. (2015). Mast cells mediate malignant pleural effusion formation. *J Clin Invest*, *125*(6), 2317-2334. https://doi.org/10.1172/jci79840

Giotopoulou, G. A., & Stathopoulos, G. T. (2020). Effects of Inhaled Tobacco Smoke on the Pulmonary Tumor Microenvironment. *Adv Exp Med Biol*, *1225*, 53-69. https://doi.org/10.1007/978-3-030-35727-6_4

Govindan, R., Ding, L., Griffith, M., Subramanian, J., Dees, N. D., Kanchi, K. L., Maher, C. A., Fulton, R., Fulton, L., Wallis, J., Chen, K., Walker, J., McDonald, S., Bose, R., Ornitz, D., Xiong, D., You, M., Dooling, D. J., Watson, M., Mardis, E. R., & Wilson, R. K. (2012). Genomic landscape of non-small cell lung cancer in smokers and never-smokers. *Cell*, *150*(6), 1121-1134. https://doi.org/10.1016/j.cell.2012.08.024

Gueugnon, F., Leclercq, S., Blanquart, C., Sagan, C., Cellerin, L., Padieu, M., Perigaud, C., Scherpereel, A., & Gregoire, M. (2011). Identification of novel markers for the diagnosis of malignant pleural mesothelioma. *Am J Pathol*, *178*(3), 1033-1042. https://doi.org/10.1016/j.ajpath.2010.12.014

Guo, G., Chmielecki, J., Goparaju, C., Heguy, A., Dolgalev, I., Carbone, M., Seepo, S., Meyerson, M., & Pass, H. I. (2015). Whole-exome sequencing reveals frequent genetic alterations in BAP1, NF2, CDKN2A, and CUL1 in malignant pleural mesothelioma. *Cancer Res*, *75*(2), 264-269. https://doi.org/10.1158/0008-5472.Can-14-1008

Guo, Y., Chirieac, L. R., Bueno, R., Pass, H., Wu, W., Malinowska, I. A., & Kwiatkowski, D. J. (2014). Tsc1-Tp53 loss induces mesothelioma in mice, and evidence for this mechanism

in human mesothelioma. *Oncogene*, *33*(24), 3151-3160. https://doi.org/10.1038/onc.2013.280

Hanahan, D., & Weinberg, R. A. (2011). Hallmarks of cancer: the next generation. *Cell*, *144*(5), 646-674. https://doi.org/10.1016/j.cell.2011.02.013

Heeschen, C., Jang, J. J., Weis, M., Pathak, A., Kaji, S., Hu, R. S., Tsao, P. S., Johnson, F. L., & Cooke, J. P. (2001). Nicotine stimulates angiogenesis and promotes tumor growth and atherosclerosis. *Nat Med*, *7*(7), 833-839. https://doi.org/10.1038/89961

Heeschen, C., Weis, M., & Cooke, J. P. (2003). Nicotine promotes arteriogenesis. *J Am Coll Cardiol*, *41*(3), 489-496. https://doi.org/10.1016/s0735-1097(02)02818-8

Herr, C., Beisswenger, C., Hess, C., Kandler, K., Suttorp, N., Welte, T., Schroeder, J. M., & Vogelmeier, C. (2009). Suppression of pulmonary innate host defence in smokers. *Thorax*, *64*(2), 144-149. https://doi.org/10.1136/thx.2008.102681

Hmeljak, J., Sanchez-Vega, F., Hoadley, K. A., Shih, J., Stewart, C., Heiman, D., Tarpey, P., Danilova, L., Drill, E., Gibb, E. A., Bowlby, R., Kanchi, R., Osmanbeyoglu, H. U., Sekido, Y., Takeshita, J., Newton, Y., Graim, K., Gupta, M., Gay, C. M., Diao, L., Gibbs, D. L., Thorsson, V., Iype, L., Kantheti, H., Severson, D. T., Ravegnini, G., Desmeules, P., Jungbluth, A. A., Travis, W. D., Dacic, S., Chirieac, L. R., Galateau-Sallé, F., Fujimoto, J., Husain, A. N., Silveira, H. C., Rusch, V. W., Rintoul, R. C., Pass, H., Kindler, H., Zauderer, M. G., Kwiatkowski, D. J., Bueno, R., Tsao, A. S., Creaney, J., Lichtenberg, T., Leraas, K., Bowen, J., Felau, I., Zenklusen, J. C., Akbani, R., Cherniack, A. D., Byers, L. A., Noble, M. S., Fletcher, J. A., Robertson, A. G., Shen, R., Aburatani, H., Robinson, B. W., Campbell, P., & Ladanyi, M. (2018). Integrative Molecular Characterization of Malignant Pleural Mesothelioma. *Cancer Discov*, *8*(12), 1548-1565. https://doi.org/10.1158/2159-8290.Cd-18-0804

Hofmann, J., Mintzer, D., & Warhol, M. J. (1994). Malignant mesothelioma following radiation therapy. *Am J Med*, *97*(4), 379-382. https://doi.org/10.1016/0002-9343(94)90307-7

Houghton, A. M. (2013). Mechanistic links between COPD and lung cancer. *Nat Rev Cancer*, *13*(4), 233-245. https://doi.org/10.1038/nrc3477

Houghton, A. M., Mouded, M., & Shapiro, S. D. (2008). Common origins of lung cancer and COPD. *Nat Med*, *14*(10), 1023-1024. https://doi.org/10.1038/nm1008-1023

Huang, S. X., Jaurand, M. C., Kamp, D. W., Whysner, J., & Hei, T. K. (2011). Role of mutagenicity in asbestos fiber-induced carcinogenicity and other diseases. *J Toxicol Environ Health B Crit Rev*, *14*(1-4), 179-245. https://doi.org/10.1080/10937404.2011.556051

Imielinski, M., Berger, A. H., Hammerman, P. S., Hernandez, B., Pugh, T. J., Hodis, E., Cho, J., Suh, J., Capelletti, M., Sivachenko, A., Sougnez, C., Auclair, D., Lawrence, M. S., Stojanov, P., Cibulskis, K., Choi, K., de Waal, L., Sharifnia, T., Brooks, A., Greulich, H., Banerji, S., Zander, T., Seidel, D., Leenders, F., Ansén, S., Ludwig, C., Engel-Riedel, W., Stoelben, E., Wolf, J., Goparju, C., Thompson, K., Winckler, W., Kwiatkowski, D., Johnson, B. E., Jänne, P. A., Miller, V. A., Pao, W., Travis, W. D., Pass, H. I., Gabriel, S. B., Lander, E. S., Thomas, R. K., Garraway, L. A., Getz, G., & Meyerson, M. (2012). Mapping the hallmarks of lung adenocarcinoma with massively parallel sequencing. *Cell*, *150*(6), 1107-1120. https://doi.org/10.1016/j.cell.2012.08.029

Jaurand, M. C., & Fleury-Feith, J. (2005). Pathogenesis of malignant pleural mesothelioma. *Respirology*, *10*(1), 2-8. https://doi.org/10.1111/j.1440-1843.2005.00694.x

Johansson, A., Rudolfsson, S., Hammarsten, P., Halin, S., Pietras, K., Jones, J., Stattin, P., Egevad, L., Granfors, T., Wikström, P., & Bergh, A. (2010). Mast cells are novel independent prognostic markers in prostate cancer and represent a target for therapy. *Am J Pathol*, *177*(2), 1031-1041. https://doi.org/10.2353/ajpath.2010.100070

Jongsma, J., van Montfort, E., Vooijs, M., Zevenhoven, J., Krimpenfort, P., van der Valk, M., van de Vijver, M., & Berns, A. (2008). A conditional mouse model for malignant mesothelioma. *Cancer Cell*, *13*(3), 261-271. https://doi.org/10.1016/j.ccr.2008.01.030

Kandoth, C., McLellan, M. D., Vandin, F., Ye, K., Niu, B., Lu, C., Xie, M., Zhang, Q., McMichael, J. F., Wyczalkowski, M. A., Leiserson, M. D. M., Miller, C. A., Welch, J. S., Walter, M. J.,

Wendl, M. C., Ley, T. J., Wilson, R. K., Raphael, B. J., & Ding, L. (2013). Mutational landscape and significance across 12 major cancer types. *Nature*, *502*(7471), 333-339. https://doi.org/10.1038/nature12634

Kato, S., Tomson, B. N., Buys, T. P., Elkin, S. K., Carter, J. L., & Kurzrock, R. (2016). Genomic Landscape of Malignant Mesotheliomas. *Mol Cancer Ther*, *15*(10), 2498-2507. https://doi.org/10.1158/1535-7163.Mct-16-0229

Klotz, L. V., Courty, Y., Lindner, M., Petit-Courty, A., Stowasser, A., Koch, I., Eichhorn, M. E., Lilis, I., Morresi-Hauf, A., Arendt, K. A. M., Pepe, M., Giopanou, I., Ntaliarda, G., Behrend, S. J., Oplopoiou, M., Gissot, V., Guyetant, S., Marchand-Adam, S., Behr, J., Kaiser, J. C., Hatz, R. A., Lamort, A. S., & Stathopoulos, G. T. (2019). Comprehensive clinical profiling of the Gauting locoregional lung adenocarcinoma donors. *Cancer Med*, *8*(4), 1486-1499. https://doi.org/10.1002/cam4.2031

Klotz, L. V., Lindner, M., Eichhorn, M. E., Grützner, U., Koch, I., Winter, H., Kauke, T., Duell, T., & Hatz, R. A. (2019). Pleurectomy/decortication and hyperthermic intrathoracic chemoperfusion using cisplatin and doxorubicin for malignant pleural mesothelioma. *J Thorac Dis*, *11*(5), 1963-1972. https://doi.org/10.21037/jtd.2019.04.93

Kreso, A., & Dick, J. E. (2014). Evolution of the cancer stem cell model. *Cell Stem Cell*, *14*(3), 275-291. https://doi.org/10.1016/j.stem.2014.02.006

Kukuyan, A. M., Sementino, E., Kadariya, Y., Menges, C. W., Cheung, M., Tan, Y., Cai, K. Q., Slifker, M. J., Peri, S., Klein-Szanto, A. J., Rauscher, F. J., 3rd, & Testa, J. R. (2019). Inactivation of Bap1 Cooperates with Losses of Nf2 and Cdkn2a to Drive the Development of Pleural Malignant Mesothelioma in Conditional Mouse Models. *Cancer Res*, *79*(16), 4113-4123. https://doi.org/10.1158/0008-5472.Can-18-4093

Lawrence, M. S., Stojanov, P., Polak, P., Kryukov, G. V., Cibulskis, K., Sivachenko, A., Carter, S. L., Stewart, C., Mermel, C. H., Roberts, S. A., Kiezun, A., Hammerman, P. S., McKenna, A., Drier, Y., Zou, L., Ramos, A. H., Pugh, T. J., Stransky, N., Helman, E., Kim, J., Sougnez, C., Ambrogio, L., Nickerson, E., Shefler, E., Cortés, M. L., Auclair, D., Saksena, G., Voet, D., Noble, M., DiCara, D., Lin, P., Lichtenstein, L., Heiman, D. I., Fennell, T., Imielinski, M., Hernandez, B., Hodis, E., Baca, S., Dulak, A. M., Lohr, J., Landau, D. A., Wu, C. J., Melendez-Zajgla, J., Hidalgo-Miranda, A., Koren, A., McCarroll, S. A., Mora, J., Crompton, B., Onofrio, R., Parkin, M., Winckler, W., Ardlie, K., Gabriel, S. B., Roberts, C. W. M., Biegel, J. A., Stegmaier, K., Bass, A. J., Garraway, L. A., Meyerson, M., Golub, T. R., Gordenin, D. A., Sunyaev, S., Lander, E. S., & Getz, G. (2013). Mutational heterogeneity in cancer and the search for new cancer-associated genes. *Nature*, *499*(7457), 214-218. https://doi.org/10.1038/nature12213

Li, S., MacAlpine, D. M., & Counter, C. M. (2020). Capturing the primordial Kras mutation initiating urethane carcinogenesis. *Nat Commun*, *11*(1), 1800. https://doi.org/10.1038/s41467-020-15660-8

Li, X., Li, J., Wu, P., Zhou, L., Lu, B., Ying, K., Chen, E., Lu, Y., & Liu, P. (2018). Smoker and non-smoker lung adenocarcinoma is characterized by distinct tumor immune microenvironments. *Oncoimmunology*, *7*(10), e1494677. https://doi.org/10.1080/2162402x.2018.1494677

Liu, F., Killian, J. K., Yang, M., Walker, R. L., Hong, J. A., Zhang, M., Davis, S., Zhang, Y., Hussain, M., Xi, S., Rao, M., Meltzer, P. A., & Schrump, D. S. (2010). Epigenomic alterations and gene expression profiles in respiratory epithelia exposed to cigarette smoke condensate. *Oncogene*, *29*(25), 3650-3664. https://doi.org/10.1038/onc.2010.129

Lo Iacono, M., Monica, V., Righi, L., Grosso, F., Libener, R., Vatrano, S., Bironzo, P., Novello, S., Musmeci, L., Volante, M., Papotti, M., & Scagliotti, G. V. (2015). Targeted next-generation sequencing of cancer genes in advanced stage malignant pleural mesothelioma: a retrospective study. *J Thorac Oncol*, *10*(3), 492-499. https://doi.org/10.1097/jto.0000000000000436

Lu, P., Weaver, V. M., & Werb, Z. (2012). The extracellular matrix: a dynamic niche in cancer progression. *J Cell Biol*, *196*(4), 395-406. https://doi.org/10.1083/jcb.201102147

Ma, Y., Hwang, R. F., Logsdon, C. D., & Ullrich, S. E. (2013). Dynamic mast cell-stromal cell interactions promote growth of pancreatic cancer. *Cancer Res*, *73*(13), 3927-3937. https://doi.org/10.1158/0008-5472.Can-12-4479

Mantovani, A., Allavena, P., Sica, A., & Balkwill, F. (2008). Cancer-related inflammation. *Nature*, *454*(7203), 436-444. https://doi.org/10.1038/nature07205

Marazioti, A., Lilis, I., Vreka, M., Apostolopoulou, H., Kalogeropoulou, A., Giopanou, I., Giotopoulou, G. A., Krontira, A. C., Iliopoulou, M., Kanellakis, N. I., Agalioti, T., Giannou, A. D., Jones-Paris, C., Iwakura, Y., Kardamakis, D., Blackwell, T. S., Taraviras, S., Spella, M., & Stathopoulos, G. T. (2018). Myeloid-derived interleukin-1β drives oncogenic KRAS-NF-κB addiction in malignant pleural effusion. *Nat Commun*, *9*(1), 672. https://doi.org/10.1038/s41467-018-03051-z

Marone, G., Galli, S. J., & Kitamura, Y. (2002). Probing the roles of mast cells and basophils in natural and acquired immunity, physiology and disease. *Trends Immunol*, *23*(9), 425-427. https://doi.org/10.1016/s1471-4906(02)02274-3

Marone, G., Varricchi, G., Loffredo, S., & Granata, F. (2016). Mast cells and basophils in inflammatory and tumor angiogenesis and lymphangiogenesis. *Eur J Pharmacol*, *778*, 146-151. https://doi.org/10.1016/j.ejphar.2015.03.088

Melaiu, O., Gemignani, F., & Landi, S. (2018). The genetic susceptibility in the development of malignant pleural mesothelioma. *J Thorac Dis*, *10*(Suppl 2), S246-s252. https://doi.org/10.21037/jtd.2017.10.41

Melillo, R. M., Guarino, V., Avilla, E., Galdiero, M. R., Liotti, F., Prevete, N., Rossi, F. W., Basolo, F., Ugolini, C., de Paulis, A., Santoro, M., & Marone, G. (2010). Mast cells have a protumorigenic role in human thyroid cancer. *Oncogene*, *29*(47), 6203-6215. https://doi.org/10.1038/onc.2010.348

Menges, C. W., Kadariya, Y., Altomare, D., Talarchek, J., Neumann-Domer, E., Wu, Y., Xiao, G. H., Shapiro, I. M., Kolev, V. N., Pachter, J. A., Klein-Szanto, A. J., & Testa, J. R. (2014). Tumor suppressor alterations cooperate to drive aggressive mesotheliomas with enriched cancer stem cells via a p53-miR-34a-c-Met axis. *Cancer Res*, *74*(4), 1261-1271. https://doi.org/10.1158/0008-5472.Can-13-2062

Metcalfe, D. D., Baram, D., & Mekori, Y. A. (1997). Mast cells. *Physiol Rev*, *77*(4), 1033-1079. https://doi.org/10.1152/physrev.1997.77.4.1033

Mezzapelle, R., Miglio, U., Rena, O., Paganotti, A., Allegrini, S., Antona, J., Molinari, F., Frattini, M., Monga, G., Alabiso, O., & Boldorini, R. (2013). Mutation analysis of the EGFR gene and downstream signalling pathway in histologic samples of malignant pleural mesothelioma. *Br J Cancer*, *108*(8), 1743-1749. https://doi.org/10.1038/bjc.2013.130

Milara, J., Peiró, T., Serrano, A., & Cortijo, J. (2013). Epithelial to mesenchymal transition is increased in patients with COPD and induced by cigarette smoke. *Thorax*, *68*(5), 410-420. https://doi.org/10.1136/thoraxjnl-2012-201761

Mutti, L., Peikert, T., Robinson, B. W. S., Scherpereel, A., Tsao, A. S., de Perrot, M., Woodard, G. A., Jablons, D. M., Wiens, J., Hirsch, F. R., Yang, H., Carbone, M., Thomas, A., & Hassan, R. (2018). Scientific Advances and New Frontiers in Mesothelioma Therapeutics. *J Thorac Oncol*, *13*(9), 1269-1283. https://doi.org/10.1016/j.jtho.2018.06.011

Nagai, H., Okazaki, Y., Chew, S. H., Misawa, N., Yamashita, Y., Akatsuka, S., Ishihara, T., Yamashita, K., Yoshikawa, Y., Yasui, H., Jiang, L., Ohara, H., Takahashi, T., Ichihara, G., Kostarelos, K., Miyata, Y., Shinohara, H., & Toyokuni, S. (2011). Diameter and rigidity of multiwalled carbon nanotubes are critical factors in mesothelial injury and carcinogenesis. *Proc Natl Acad Sci U S A*, *108*(49), E1330-1338. https://doi.org/10.1073/pnas.1110013108

Negrini, S., Gorgoulis, V. G., & Halazonetis, T. D. (2010). Genomic instability--an evolving hallmark of cancer. *Nat Rev Mol Cell Biol*, *11*(3), 220-228. https://doi.org/10.1038/nrm2858

Oehl, K., Vrugt, B., Opitz, I., & Meerang, M. (2018). Heterogeneity in Malignant Pleural Mesothelioma. *Int J Mol Sci*, *19*(6). https://doi.org/10.3390/ijms19061603

Patel, M. R., Jacobson, B. A., De, A., Frizelle, S. P., Janne, P., Thumma, S. C., Whitson, B. A., Farassati, F., & Kratzke, R. A. (2007). Ras pathway activation in malignant mesothelioma. *J Thorac Oncol*, *2*(9), 789-795. https://doi.org/10.1097/JTO.0b013e31811f3aab

Pavlides, S., Whitaker-Menezes, D., Castello-Cros, R., Flomenberg, N., Witkiewicz, A. K., Frank, P. G., Casimiro, M. C., Wang, C., Fortina, P., Addya, S., Pestell, R. G., Martinez-Outschoorn, U. E., Sotgia, F., & Lisanti, M. P. (2009). The reverse Warburg effect: aerobic glycolysis in cancer associated fibroblasts and the tumor stroma. *Cell Cycle*, *8*(23), 3984-4001. https://doi.org/10.4161/cc.8.23.10238

Pietras, A. (2011). Cancer stem cells in tumor heterogeneity. *Adv Cancer Res*, *112*, 255-281. https://doi.org/10.1016/b978-0-12-387688-1.00009-0

Pittoni, P., Tripodo, C., Piconese, S., Mauri, G., Parenza, M., Rigoni, A., Sangaletti, S., & Colombo, M. P. (2011). Mast cell targeting hampers prostate adenocarcinoma development but promotes the occurrence of highly malignant neuroendocrine cancers. *Cancer Res*, *71*(18), 5987-5997. https://doi.org/10.1158/0008-5472.Can-11-1637

Preston, D. L., Ron, E., Tokuoka, S., Funamoto, S., Nishi, N., Soda, M., Mabuchi, K., & Kodama, K. (2007). Solid cancer incidence in atomic bomb survivors: 1958-1998. *Radiat Res*, *168*(1), 1-64. https://doi.org/10.1667/rr0763.1

Ramón, Y. C. S., Sesé, M., Capdevila, C., Aasen, T., De Mattos-Arruda, L., Diaz-Cano, S. J., Hernández-Losa, J., & Castellví, J. (2020). Clinical implications of intratumor heterogeneity: challenges and opportunities. *J Mol Med (Berl)*, *98*(2), 161-177. https://doi.org/10.1007/s00109-020-01874-2

Remon, J., Reguart, N., Corral, J., & Lianes, P. (2015). Malignant pleural mesothelioma: new hope in the horizon with novel therapeutic strategies. *Cancer Treat Rev*, *41*(1), 27-34. https://doi.org/10.1016/j.ctrv.2014.10.007

Ribatti, D., Vacca, A., Nico, B., Quondamatteo, F., Ria, R., Minischetti, M., Marzullo, A., Herken, R., Roncali, L., & Dammacco, F. (1999). Bone marrow angiogenesis and mast cell density increase simultaneously with progression of human multiple myeloma. *Br J Cancer*, *79*(3-4), 451-455. https://doi.org/10.1038/sj.bjc.6690070

Rizvi, N. A., Hellmann, M. D., Snyder, A., Kvistborg, P., Makarov, V., Havel, J. J., Lee, W., Yuan, J., Wong, P., Ho, T. S., Miller, M. L., Rekhtman, N., Moreira, A. L., Ibrahim, F., Bruggeman, C., Gasmi, B., Zappasodi, R., Maeda, Y., Sander, C., Garon, E. B., Merghoub, T., Wolchok, J. D., Schumacher, T. N., & Chan, T. A. (2015). Cancer immunology. Mutational landscape determines sensitivity to PD-1 blockade in non-small cell lung cancer. *Science*, *348*(6230), 124-128. https://doi.org/10.1126/science.aaa1348

Salem, A. F., Al-Zoubi, M. S., Whitaker-Menezes, D., Martinez-Outschoorn, U. E., Lamb, R., Hulit, J., Howell, A., Gandara, R., Sartini, M., Galbiati, F., Bevilacqua, G., Sotgia, F., & Lisanti, M. P. (2013). Cigarette smoke metabolically promotes cancer, via autophagy and premature aging in the host stromal microenvironment. *Cell Cycle*, *12*(5), 818-825. https://doi.org/10.4161/cc.23722

Scherpereel, A., Astoul, P., Baas, P., Berghmans, T., Clayson, H., de Vuyst, P., Dienemann, H., Galateau-Salle, F., Hennequin, C., Hillerdal, G., Le Péchoux, C., Mutti, L., Pairon, J. C., Stahel, R., van Houtte, P., van Meerbeeck, J., Waller, D., & Weder, W. (2010). Guidelines of the European Respiratory Society and the European Society of Thoracic Surgeons for the management of malignant pleural mesothelioma. *Eur Respir J*, *35*(3), 479-495. https://doi.org/10.1183/09031936.00063109

Scherpereel, A., Wallyn, F., Albelda, S. M., & Munck, C. (2018). Novel therapies for malignant pleural mesothelioma. *Lancet Oncol*, *19*(3), e161-e172. https://doi.org/10.1016/s1470-2045(18)30100-1

Sementino, E., Menges, C. W., Kadariya, Y., Peri, S., Xu, J., Liu, Z., Wilkes, R. G., Cai, K. Q., Rauscher, F. J., 3rd, Klein-Szanto, A. J., & Testa, J. R. (2018). Inactivation of Tp53 and Pten drives rapid development of pleural and peritoneal malignant mesotheliomas. *J Cell Physiol*, *233*(11), 8952-8961. https://doi.org/10.1002/jcp.26830

Shukuya, T., Serizawa, M., Watanabe, M., Akamatsu, H., Abe, M., Imai, H., Tokito, T., Ono, A., Taira, T., Kenmotsu, H., Naito, T., Murakami, H., Takahashi, T., Endo, M., Ohde, Y., Nakajima, T., Yamamoto, N., & Koh, Y. (2014). Identification of actionable mutations in

malignant pleural mesothelioma. *Lung Cancer*, *86*(1), 35-40. https://doi.org/10.1016/j.lungcan.2014.08.004

Siegel, R. L., Miller, K. D., Fuchs, H. E., & Jemal, A. (2021). Cancer Statistics, 2021. *CA Cancer J Clin*, *71*(1), 7-33. https://doi.org/10.3322/caac.21654

Smeele, P., d'Almeida, S. M., Meiller, C., Chéné, A. L., Liddell, C., Cellerin, L., Montagne, F., Deshayes, S., Benziane, S., Copin, M. C., Hofman, P., Le Pimpec-Barthes, F., Porte, H., Scherpereel, A., Grégoire, M., Jean, D., & Blanquart, C. (2018). Brain-derived neurotrophic factor, a new soluble biomarker for malignant pleural mesothelioma involved in angiogenesis. *Mol Cancer*, *17*(1), 148. https://doi.org/10.1186/s12943-018-0891-0

Sohal, S. S., Reid, D., Soltani, A., Ward, C., Weston, S., Muller, H. K., Wood-Baker, R., & Walters, E. H. (2010). Reticular basement membrane fragmentation and potential epithelial mesenchymal transition is exaggerated in the airways of smokers with chronic obstructive pulmonary disease. *Respirology*, *15*(6), 930-938. https://doi.org/10.1111/j.1440-1843.2010.01808.x

Soucek, L., Lawlor, E. R., Soto, D., Shchors, K., Swigart, L. B., & Evan, G. I. (2007). Mast cells are required for angiogenesis and macroscopic expansion of Myc-induced pancreatic islet tumors. *Nat Med*, *13*(10), 1211-1218. https://doi.org/10.1038/nm1649

Stathopoulos, G. T., Sherrill, T. P., Cheng, D. S., Scoggins, R. M., Han, W., Polosukhin, V. V., Connelly, L., Yull, F. E., Fingleton, B., & Blackwell, T. S. (2007). Epithelial NF-kappaB activation promotes urethane-induced lung carcinogenesis. *Proc Natl Acad Sci U S A*, *104*(47), 18514-18519. https://doi.org/10.1073/pnas.0705316104

Subramanian, J., & Govindan, R. (2007). Lung cancer in never smokers: a review. *J Clin Oncol*, *25*(5), 561-570. https://doi.org/10.1200/jco.2006.06.8015

Sun, H. H., Vaynblat, A., & Pass, H. I. (2017). Diagnosis and prognosis-review of biomarkers for mesothelioma. *Ann Transl Med*, *5*(11), 244. https://doi.org/10.21037/atm.2017.06.60

Sun, S., Schiller, J. H., & Gazdar, A. F. (2007). Lung cancer in never smokers--a different disease. *Nat Rev Cancer*, *7*(10), 778-790. https://doi.org/10.1038/nrc2190

Sung, H., Ferlay, J., Siegel, R. L., Laversanne, M., Soerjomataram, I., Jemal, A., & Bray, F. (2021). Global Cancer Statistics 2020: GLOBOCAN Estimates of Incidence and Mortality Worldwide for 36 Cancers in 185 Countries. *CA Cancer J Clin*, *71*(3), 209-249. https://doi.org/10.3322/caac.21660

Theoharides, T. C. (2008). Mast cells and pancreatic cancer. *N Engl J Med*, *358*(17), 1860-1861. https://doi.org/10.1056/NEJMcibr0801519

Thun, M., Peto, R., Boreham, J., & Lopez, A. D. (2012). Stages of the cigarette epidemic on entering its second century. *Tob Control*, *21*(2), 96-101. https://doi.org/10.1136/tobaccocontrol-2011-050294

Tischoff, I., Neid, M., Neumann, V., & Tannapfel, A. (2011). Pathohistological diagnosis and differential diagnosis. *Recent Results Cancer Res*, *189*, 57-78. https://doi.org/10.1007/978-3-642-10862-4_5

Tono, T., Tsujimura, T., Koshimizu, U., Kasugai, T., Adachi, S., Isozaki, K., Nishikawa, S., Morimoto, M., Nishimune, Y., Nomura, S., & et al. (1992). c-kit Gene was not transcribed in cultured mast cells of mast cell-deficient Wsh/Wsh mice that have a normal number of erythrocytes and a normal c-kit coding region. *Blood*, *80*(6), 1448-1453.

Tsao, A. S., Wistuba, I., Roth, J. A., & Kindler, H. L. (2009). Malignant pleural mesothelioma. *J Clin Oncol*, *27*(12), 2081-2090. https://doi.org/10.1200/jco.2008.19.8523

van der Vaart, H., Postma, D. S., Timens, W., & ten Hacken, N. H. (2004). Acute effects of cigarette smoke on inflammation and oxidative stress: a review. *Thorax*, *59*(8), 713-721. https://doi.org/10.1136/thx.2003.012468

Varricchi, G., Galdiero, M. R., Loffredo, S., Marone, G., Iannone, R., Marone, G., & Granata, F. (2017). Are Mast Cells MASTers in Cancer? *Front Immunol*, *8*, 424. https://doi.org/10.3389/fimmu.2017.00424

Vaz, M., Hwang, S. Y., Kagiampakis, I., Phallen, J., Patil, A., O'Hagan, H. M., Murphy, L., Zahnow, C. A., Gabrielson, E., Velculescu, V. E., Easwaran, H. P., & Baylin, S. B. (2017).

Chronic Cigarette Smoke-Induced Epigenomic Changes Precede Sensitization of Bronchial Epithelial Cells to Single-Step Transformation by KRAS Mutations. *Cancer Cell*, *32*(3), 360-376.e366. https://doi.org/10.1016/j.ccell.2017.08.006

Vestbo, J., Hurd, S. S., Agustí, A. G., Jones, P. W., Vogelmeier, C., Anzueto, A., Barnes, P. J., Fabbri, L. M., Martinez, F. J., Nishimura, M., Stockley, R. A., Sin, D. D., & Rodriguez-Roisin, R. (2013). Global strategy for the diagnosis, management, and prevention of chronic obstructive pulmonary disease: GOLD executive summary. *Am J Respir Crit Care Med*, *187*(4), 347-365. https://doi.org/10.1164/rccm.201204-0596PP

Vineis, P., & Husgafvel-Pursiainen, K. (2005). Air pollution and cancer: biomarker studies in human populations. *Carcinogenesis*, *26*(11), 1846-1855. https://doi.org/10.1093/carcin/bgi216

Vogelzang, N. J., Rusthoven, J. J., Symanowski, J., Denham, C., Kaukel, E., Ruffie, P., Gatzemeier, U., Boyer, M., Emri, S., Manegold, C., Niyikiza, C., & Paoletti, P. (2003). Phase III study of pemetrexed in combination with cisplatin versus cisplatin alone in patients with malignant pleural mesothelioma. *J Clin Oncol*, *21*(14), 2636-2644. https://doi.org/10.1200/jco.2003.11.136

Vreka, M., Lilis, I., Papageorgopoulou, M., Giotopoulou, G. A., Lianou, M., Giopanou, I., Kanellakis, N. I., Spella, M., Agalioti, T., Armenis, V., Goldmann, T., Marwitz, S., Yull, F. E., Blackwell, T. S., Pasparakis, M., Marazioti, A., & Stathopoulos, G. T. (2018). IκB Kinase α Is Required for Development and Progression of KRAS-Mutant Lung Adenocarcinoma. *Cancer Res*, *78*(11), 2939-2951. https://doi.org/10.1158/0008-5472.Can-17-1944

Vyzoukaki, R., Tsirakis, G., Pappa, C. A., Devetzoglou, M., Tzardi, M., & Alexandrakis, M. G. (2015). The Impact of Mast Cell Density on the Progression of Bone Disease in Multiple Myeloma Patients. *Int Arch Allergy Immunol*, *168*(4), 263-268. https://doi.org/10.1159/000443275

Wadowski, B., De Rienzo, A., & Bueno, R. (2020). The Molecular Basis of Malignant Pleural Mesothelioma. *Thorac Surg Clin*, *30*(4), 383-393. https://doi.org/10.1016/j.thorsurg.2020.08.005

Wagner, J. C., Sleggs, C. A., & Marchand, P. (1960). Diffuse pleural mesothelioma and asbestos exposure in the North Western Cape Province. *Br J Ind Med*, *17*(4), 260-271. https://doi.org/10.1136/oem.17.4.260

Wakelee, H. A., Chang, E. T., Gomez, S. L., Keegan, T. H., Feskanich, D., Clarke, C. A., Holmberg, L., Yong, L. C., Kolonel, L. N., Gould, M. K., & West, D. W. (2007). Lung cancer incidence in never smokers. *J Clin Oncol*, *25*(5), 472-478. https://doi.org/10.1200/jco.2006.07.2983

Whitrow, M. J., Smith, B. J., Pilotto, L. S., Pisaniello, D., & Nitschke, M. (2003). Environmental exposure to carcinogens causing lung cancer: epidemiological evidence from the medical literature. *Respirology*, *8*(4), 513-521. https://doi.org/10.1046/j.1440-1843.2003.00497.x

Yang, H., Xiang, S., Kazi, A., & Sebti, S. M. (2020). The GTPase KRAS suppresses the p53 tumor suppressor by activating the NRF2-regulated antioxidant defense system in cancer cells. *J Biol Chem*, *295*(10), 3055-3063. https://doi.org/10.1074/jbc.RA119.011930

Yap, T. A., Aerts, J. G., Popat, S., & Fennell, D. A. (2017). Novel insights into mesothelioma biology and implications for therapy. *Nat Rev Cancer*, *17*(8), 475-488. https://doi.org/10.1038/nrc.2017.42

Zhang, H., Liu, H., Borok, Z., Davies, K. J., Ursini, F., & Forman, H. J. (2012). Cigarette smoke extract stimulates epithelial-mesenchymal transition through Src activation. *Free Radic Biol Med*, *52*(8), 1437-1442. https://doi.org/10.1016/j.freeradbiomed.2012.01.024

Zhang, J., Fujimoto, J., Zhang, J., Wedge, D. C., Song, X., Zhang, J., Seth, S., Chow, C. W., Cao, Y., Gumbs, C., Gold, K. A., Kalhor, N., Little, L., Mahadeshwar, H., Moran, C., Protopopov, A., Sun, H., Tang, J., Wu, X., Ye, Y., William, W. N., Lee, J. J., Heymach, J. V., Hong, W. K., Swisher, S., Wistuba, II, & Futreal, P. A. (2014). Intratumor heterogeneity in localized lung adenocarcinomas delineated by multiregion sequencing. *Science*, *346*(6206), 256-259. https://doi.org/10.1126/science.1256930

Zhang, Z., Oliver, P., Lancaster, J. R., Jr., Schwarzenberger, P. O., Joshi, M. S., Cork, J., & Kolls, J. K. (2001). Reactive oxygen species mediate tumor necrosis factor alpha-converting, enzyme-dependent ectodomain shedding induced by phorbol myristate acetate. *Faseb j*, *15*(2), 303-305. https://doi.org/10.1096/fj.00-0371fje

Zito Marino, F., Ascierto, P. A., Rossi, G., Staibano, S., Montella, M., Russo, D., Alfano, R., Morabito, A., Botti, G., & Franco, R. (2017). Are tumor-infiltrating lymphocytes protagonists or background actors in patient selection for cancer immunotherapy? *Expert Opin Biol Ther*, *17*(6), 735-746. https://doi.org/10.1080/14712598.2017.1309387

Zito Marino, F., Bianco, R., Accardo, M., Ronchi, A., Cozzolino, I., Morgillo, F., Rossi, G., & Franco, R. (2019). Molecular heterogeneity in lung cancer: from mechanisms of origin to clinical implications. *Int J Med Sci*, *16*(7), 981-989. https://doi.org/10.7150/ijms.34739

Apendix A: Paper III (Book chapter)

Effects of Inhaled Tobacco Smoke on the Pulmonary Tumor Microenvironment

4

Georgia A. Giotopoulou
and Georgios T. Stathopoulos

Abstract

Tobacco smoke is a multicomponent mixture of chemical, organic, and inorganic compounds, as well as additive substances and radioactive materials. Many studies have proved the carcinogenicity of various of these compounds through the induction of DNA adducts, mutational potential, epigenetic changes, gene fusions, and chromosomal events. The tumor microenvironment plays an important role in malignant tumor formation and progression through the regulation of expression of key molecules which mediate the recruitment of immune cells to the tumor site and subsequently regulate tumor growth and metastasis. In this chapter, we discuss the effects of inhaled tobacco smoke in the tumor microenvironment of the respiratory tract. The mechanisms underlying these effects as well as their link with tumor progression are analyzed.

G. A. Giotopoulou (✉) · G. T. Stathopoulos
Comprehensive Pneumology Center (CPC) and Institute for Lung Biology and Disease (iLBD), University Hospital, Ludwig-Maximilians University and Helmholtz Center Munich, Member of the German Center for Lung Research (DZL), Munich, Bavaria, Germany

Laboratory for Molecular Respiratory Carcinogenesis, Faculty of Medicine, University of Patras, Rio, Greece
e-mail: georgia.giotopoulou@helmholtz-muenchen.de; stathopoulos@helmholtz-muenchen.de; gstathop@upatras.gr

Keywords

Tobacco smoke · Carcinogenicity · Lung cancer · Tumor microenvironment · Tumor-associated macrophages · Cancer-associated fibroblasts · Extracellular matrix · Epithelial-mesenchymal transition · Angiogenesis · Metabolism · Acute inflammation · Chronic inflammation · Epigenetics · Tumor growth · Metastasis

4.1 Tobacco Smoke

4.1.1 Composition of Tobacco Smoke

4.1.1.1 Nicotine

Nicotine, composing 0.2–0.6% of the particulate phase of tobacco smoke, is the main addictive compound of tobacco smoke and, while it is a weak carcinogen, is responsible for tobacco addiction and continued smoking. Nicotine exerts its addictive functions by its interaction with neuronal nicotinergic acetylcholine receptors in the brain [1]. As soon as it is inhaled, smoke reaches the airways and alveoli, and nicotine is absorbed by the lungs. Pulmonary absorption of nicotine is mediated by the alkaline pH of cigarettes, which converts nicotine to its nonionized form. Following absorption, nicotine enters the bloodstream and is distributed to the various bodily organs. Nicotine is metabolized in the liver by the

A. Birbrair (ed.), *Tumor Microenvironment*, Advances in Experimental Medicine and Biology 1225, https://doi.org/10.1007/978-3-030-35727-6_4

enzymes cytochrome P450 2A6 (CYP2A6), uridine diphosphate glucuronosyltransferase (UGT), and flavin-containing monooxygenase (FMO) to a number of metabolites, the most important of which is cotinine. Cotinine is the most well-known biomarker for detecting nicotine levels, measured in blood, saliva, urine, hair, and nails [2].

4.1.1.2 Chemical Carcinogens

Polycyclic Aromatic Hydrocarbons (PAH)

PAH have been linked with the induction of tumors in the skin and lungs [3, 4]. The members of this compound family that are proven to be carcinogenic are benzo[*b*]fluoranthene, benzo[*j*]fluoranthene, benzo[*k*]fluoranthene, dibenzo[*a,i*]pyrene, indeno[1,2,3-*cd*]pyrene, dibenz[*a,h*]anthracene, and 5-methylchrysene [5]. Smokers present higher metabolic activation of dibenzo[*a,i*]pyrene (BαP), mediated by aryl hydrocarbon hydroxylase (AHH) activity [6, 7], which is connected with higher cancer risk [8]. Furthermore, PAH are responsible for the induction of DNA adduct formation in the *TP53* gene [9].

Nitrosamines

N-Nitrosodimethylamine was found in 1956 to induce liver tumors in rats [10]. Since then, increasing interest on the carcinogenic potential of nitrosamines aroused. Metabolism of nicotine produces nitrosamines, with *N′*-nitrosonornicotine(NNN),4-(methylnitrosamino) -1-(3-pyridyl)-1-butanone (NNK), and 4-(methylnitrosamino)-1-(3-pyridyl)butanal (NNAL) being the most carcinogenic [11, 12], mainly causing adenomas and adenocarcinomas [13].

Butadiene

Exposure of mice to inhalation of 1,3-butadiene induced alveolar and bronchiolar carcinomas, as well as lymphoma and forestomach papilloma [14]. Butadiene is metabolized to carcinogenic epoxybutene, diepoxides, and diol epoxide.

Ethyl Carbamate (Urethane)

Urethane, also known as ethyl carbamate, or carbamic acid ethyl ester, is an ester of carbamic acid. Many studies in experimental animals support the carcinogenic role of urethane in various tissues and through different routes of administration. Urethane-induced tumors of the lung (adenocarcinomas and squamous cell carcinomas), as well as of the liver (hepatocellular carcinomas), and blood vessels (hemangiomas or hemangiosarcomas of the liver, spleen, uterus, or unspecified site) have been observed in many studies [15–18]. Since then, urethane has been used for induction of tumors in mice models [19–21].

4.1.1.3 Radioactive Materials

Except for chemicals, tobacco smoke also contains radioactive elements, including uranium and thorium isotopes (^{234}U, ^{238}U, ^{228}Th, ^{230}Th, ^{232}Th), as well as products of their decay (e.g. ^{226}Ra, ^{210}Pb, ^{210}Po) [22, 23]. Radioactive materials enter the tobacco plant through the soil and phosphate fertilizers, or through direct deposition of airborne ^{222}Rn products. Smoking results in their absorption by the respiratory system and the subsequent increased risk for lung cancer [24, 25].

4.1.1.4 Reactive Oxygen Species (ROS)

ROS are a family of oxygen-derived small molecules that contain oxygen radicals such as superoxide (O_2), hydroxyl (OH), peroxyl (RO_2), and alkoxyl (RO), as well as non-radicals such as hypochlorous acid (HOCl), ozone (O_3), and hydrogen peroxide (H_2O_2). ROS play key roles in homeostasis and intracellular signaling. However, the disruption of the balance between antioxidant defense mechanisms and ROS production leads to DNA damage, mediates oxidative stress, and is implicated in cancer progression. ROS are directly synthesized by the enzymes nicotinamide adenine dinucleotide phosphate (NADPH) oxidase and myeloperoxidase (MPO). ROS are produced endogenously as a product of cellular respiration, although there are also exogenous factors driving their production, such as ionizing radiation and tobacco smoking [26]. ROS dam-

age airway epithelial cells through lipid peroxidation of the cell membrane, activation of oxidative-sensitive cellular pathways, and DNA damage [27].

4.1.1.5 Tobacco Additives

The word additive is used for compounds "...the intended use of which results or may reasonably be expected to result, directly or indirectly, in its becoming a component or otherwise affecting the characteristic of any tobacco product …" [28]. Tobacco additives are used in order to reduce its alkaloid bitterness resulting in easier nicotine delivery to the user. Levulinic acid decreases the sensitivity of the upper respiratory tract, resulting in deeper inhalation in the respiratory system, while at the same time it mediates the binding of nicotine to neurons [29]. Pyrazines enhance product appeal, mediate easier initiation of smoking, and promote relapse [30]. Menthol increases the smoothness of the smoke and subsequently enhances deeper inhaling due to its cooling effect. Therefore, tobacco additives increase the attractiveness and addictiveness of tobacco increasing smokers' exposure to toxic compounds contained in smoke and resulting to health risks. However, there are no sufficient studies regarding the toxicity of the additives alone, since tobacco smoke is a multicomponent mixture, with the different compounds interacting with each other [31].

4.1.1.6 Other

Tobacco smoke contains inorganic compounds—metals, such as arsenic, cadmium, chromium, and nickel, all of them related to high risk of different types of cancer [32]. Other agents contained in tobacco smoke and also related to increased risk for lung cancer are isoprene, benzene, acetaldehyde, and formaldehyde [5].

4.1.2 Carcinogenicity of Tobacco Smoke

4.1.2.1 Epidemiologic Evidence

Tobacco smoke constitutes the largest exposure of humans to chemical carcinogens. It causes one out of five cancer-related deaths in the world and 1.4 million deaths per year. The largest effect of tobacco smoke is on lung cancer, constituting the cause for 80% and 50% of global lung cancer deaths for men and women, respectively [33]. However, tobacco smoke has also been linked with a variety of cancers other than lung cancer types, such as cancers of the oral cavity, pharynx, larynx, esophagus, pancreas, bladder, stomach, liver, kidney, ureter, cervix, and nasal cavity, as well as myeloid leukemia [32, 34].

4.1.2.2 Molecular Evidence

The Cancer Genome Atlas (TCGA) project aims to collect and analyze human tissues in order to generate comprehensive multidimensional maps of the key genomic changes in 33 types of cancer [35]. Lung cancer is a dominant malignancy, resulting in the largest number of cancer-related deaths worldwide [36] and lung adenocarcinoma (LADC) is its most frequent histologic subtype [37, 38]. LADC is mainly caused by environmental exposures such as tobacco smoke (TS) and high-energy transfer irradiation (IR) [39–42]. TS is the predominant cause of lung cancer [43]; however, there is a worldwide increase in the number of lung cancers in nonsmokers [44, 45]. Molecular profiling of lung cancers has revealed a heterogeneous disease that harbors thousands of mutations per cancer genome, including single nucleotide variants (SNV), copy number alterations (CNA), dysregulation of alternative splicing (exon skipping, EXS), balanced inversions resulting in gene fusions, and major chromosomal events like kataegis and chromothripsis [35, 46, 47]. LADC mutations lead to activation of proto-oncogenes such as *KRAS*, *EGFR*, and *PIK3CA* and inactivation of tumor suppressors such as *TP53*, *STK11*, and *PTEN* [48]. Interestingly, the genomic profiles of LADC differs between smokers and nonsmokers, with smokers displaying higher mutation burdens [35].

4.1.2.3 Experimental Evidence

The carcinogenicity of some compounds of tobacco smoke has been proven in vivo. Using single-hit models, LADC development was achieved in carcinogen-sensitive *FVB* mice

6–9 months posttreatment with intraperitoneal injection of urethane and diethylnitrosamine [21, 49]. Moreover, metabolically activated 4-(methylnitrosamino)-1-(3-pyridyl)-1-butanone (NNK) and *N*′-nitrosonornicotine (NNN) are implicated in carcinogenesis by inducing mutations which result in the formation of DNA adducts, promoting tumor growth, cancer cell survival, and migration [50]. In vivo studies have shown that NNN causes esophageal and nasal tumors in rats and respiratory tract tumors in mice and hamsters [51–53]. Furthermore, Westcott et al. showed that the mutational signatures of LADC differ according to the causative chemical: genome, exome, and transcriptome sequencing of genetic- and chemical-induced *KRAS*-driven murine LADC revealed that the chemical carcinogens urethane and *N*-nitroso-*N*-methylurea (MNU) caused humanlike SNV and distinct *KRAS* mutations (Q61R for urethane and G12C for MNU) [54].

4.1.2.4 Signatures of Tobacco Smoke

Alexandrov et al. defined mutational signatures in the trinucleotide context (i.e., the bases immediately 5′ and 3′ to each mutated base) and correlated these with clinical exposure data across more than 20 cancer types and 10,000 patients, identifying the smoking signature 4 (C>A transversion) [34, 55]. Lung tumors of smokers and nonsmokers do not only display distinct mutational signatures and gene expression profiles [34, 55], but also different inflammatory signatures [56]. In comparison with never-smokers, the tumor microenvironment of smokers includes fewer resting mast cells and CD4+ memory T cells, both linked with favorable survival [56]. Furthermore, tobacco smoking induces pro-inflammatory changes in the tumor microenvironment of squamous cell lung carcinomas, as determined by interferon-c signaling, cytosolic activity, and immune infiltration [57]. These data are in line with clinical studies that show that smokers with LADC have a higher response to immune checkpoint inhibitors [58]. Moreover, lung tumors of smokers and nonsmokers exhibit distinct DNA methylation profiles [59, 60].

4.2 The Tumor Microenvironment

4.2.1 The Role of the Microenvironment in Tumor Formation and Progression

In addition to the molecular heterogeneity of tumor cells, there is also cellular heterogeneity of the tumor microenvironment with which tumor cells interact [61, 62]. While tumor initiation is mediated by mutations in oncogenic driver genes, tumor progression is rather affected by interactions between cancer cells and their microenvironment. Oncogenic changes of tumor cells establish complex inflammatory signaling networks through suppression of homeostatic chemokines and de novo production of cytokines, chemokines, and their receptors by both cancer and stromal cells [63–66]. This complex network results in the migration and infiltration of various cellular populations, including tumor-associated macrophages (TAMs), mast cells, lymphocytes, and other cells to the stoma in response to chemokine gradients created by stromal and malignant cells of a tumor, which results in the establishment of an inflammatory microenvironment [67].

4.2.1.1 Tumor-Associated Macrophages (TAMs)

TAMs are the most abundant inflammatory cell type in tumors, represent a crucial component of the tumor microenvironment, and have a key role in cancer progression as indicated by several studies which describe a slower tumor growth after the depletion of macrophages, as well as by the association of TAM with poor disease outcome [68, 69]. The expression of growth factors such as colony stimulating factor (CSF)-1 and chemokines in cancers results in the recruitment of circulating monocytes which differentiate to macrophages. In addition to their physiological roles in immune response, phagocytosis, antigen-presentation, and pathogen killing, macrophages are implicated in tumor promotion via immunoediting [64, 70], although there is also evi-

dence of their antitumor functions, dependent on the cytokine microenvironment of the tumor [70]. Macrophages enable angiogenesis through secretion of proangiogenic mediators like vascular endothelial growth factor (VEGF) and angiopoietins (ANG)-1 and ANG-2 and mediate invasion and metastasis by producing growth factors and matrix metalloproteases (MMP). In order for TAM to acquire protumorigenic functions, they polarize from a pro-inflammatory (M1) to an "alternatively activated" anti-inflammatory (M2) phenotype.

4.2.1.2 T Lymphocytes

T cell populations infiltrate tumors and play key roles in the establishment of an inflammatory microenvironment which favors cancer progression. CD8 memory T cells are antigen-presenting cells with tumor suppressor activity and are related with good prognosis in human tumors [71]. The interplay between CD8 and CD4 T cells is important for tumor immunity. CD4 T helper 1 (Th1) cells enable recruitment and proliferation of CD8 T cells through an interferon (IFN)-γ- and IL-2-dependent mechanism [72]. CD4 cells' presence in the tumor microenvironment has also been linked with good prognosis [71]. Th2 CD4 cells have ambiguous roles in tumor progression, as Fridman et al. reported that they promote tumor growth [71], although other studies link them with favorable outcome in breast cancer patients [160, 161]. T regulatory cells (Treg) function as immune suppressors, which, through the secretion of IL-10 and transforming growth factor (TGF)-β, prevent the clearance of cancer cells by the immune system [73, 74].

4.2.1.3 B Lymphocytes

B lymphocytes are recruited to tumor sites in response to T helper cell-secreted C-X-C-motif chemokine ligand (CXCL) 13 [75]. Tumor-infiltrating B cells activate nuclear factor (NF)-κB canonical and noncanonical pathways through the secretion of lymphotoxin, mediating tumor growth and cell proliferation, as well as angiogenesis [76–78]. Furthermore, B cells promote metastasis by inducing increased expression of IL-8 [79].

4.2.1.4 Cancer-Associated Fibroblasts (CAFs)

CAFs are an important cell population within the tumor microenvironment that promotes cancer progression and invasion [80, 81]. As a component of the stroma, fibroblasts are responsible for the production of collagens and fibronectin and the subsequent synthesis of the extracellular matrix (ECM) [82] and the basement membrane [83]. During carcinogenesis, normal stromal fibroblasts undergo several changes including their morphological characteristics, their expression of cell surface markers [81], and their metabolism via the reverse Warburg effect [84]. The causes for transformation of fibroblasts to CAF are unknown, but mutations appear to occur in these cells, too, such as inactivation of *TP53* and *PTEN* [85] and loss of heterozygosity (LOH) [86]. Furthermore, CAF production can be induced by epithelial-to-mesenchymal transition (EMT) and endothelial-to-mesenchymal transition (EndMT) [81]. CAFs have been associated with enhanced tumor growth [87, 88], cell migration and invasion [89], and a pro-inflammatory microenvironment that facilitates metastasis [90–92].

4.2.1.5 The ECM of the Tumor Microenvironment

The ECM is a complex network of macromolecules with different physical and biochemical properties, and its deregulation is one of the hallmarks of cancer [93]. The deposition of different collagens is increased during tumor formation and progression [94]. Furthermore, breast cancer ECM appears to be stiffer than normal breast ECM, mediating tumor cell invasion and progression via a lysyl oxidase (LOX)-dependent mechanism [95]. ECM changes potentiate the deregulation of cellular behavior and enable malignant transformation [96]. Moreover, tumor ECM has a key role in angiogenesis, as many ECM compounds interact with VEGF regulating the formation of new vascular branchings [97]. Tumor cells, TAM, and CAF secrete MMP that remodel the ECM of tumors [61] and mediate angiogenesis [96]. ECM can also mediate the differentiation and maturation of immune cells and

the promotion of an inflammatory tumor microenvironment [96].

4.3 Impact of Tobacco Smoke on the Tumor Microenvironment

4.3.1 Acute Effects of Continued Smoking

4.3.1.1 Angiogenesis

Exposure to tobacco smoke has been linked to the formation of new vessels (neoangiogenesis) [98], with nicotine being the most well-studied compound responsible for this [99]. Angiogenic dysplasia lesions were more frequent in the bronchi of smokers compared with nonsmokers and were related to higher risk for lung cancer [100]. Furthermore, exposure to environmental tobacco smoke induced tumor growth and enhanced vessel density in a murine model of lung cancer and stimulated circulating endothelial cell precursors [101], in accord with data that demonstrate that tobacco smoke exposure of murine lung tissues increases angiogenesis and circulating leukocytes [102]. When Lewis lung cancer cells were injected in mice, systemic nicotine administration enhanced tumor growth by increasing capillary density [103]. The mechanism of tobacco smoke-mediated angiogenesis includes stimulation of endothelial nicotinergic acetylcholine receptors (nAchR) of the α7 homodimeric type by nicotine with subsequent interactions between nAchR and angiogenic growth factor receptors [104].

4.3.1.2 Tobacco-Triggered EMT

During carcinogenesis, polarized epithelial cells undergo EMT and acquire a mesenchymal phenotype. EMT has been linked with molecular, biochemical, and morphological cellular changes that lead to detachment from the basolateral membrane, loss of cell adhesion, cytoskeletal reorganization, changes in the interaction with the ECM, and angiogenesis. Cells that undergo EMT acquire higher migration capacity and invasion potential, both required for conversion of benign cells to invasive cancer cells [105]. Furthermore, EMT can give birth to CAF in the tumor microenvironment that, in turn, contribute to cancer progression [81]. Tobacco smoke has been linked with EMT: MCF7 breast cancer cells acquired mesenchymal phenotypes upon long-term aqueous tobacco smoke exposure in vitro, which enhanced their potential for growth, migration, and invasion, as well as their metastatic potential in vivo [106]. Endobronchial biopsies of COPD patients revealed that smokers had a hyperfragmented basement membrane with increased expression of MMP9, the fibroblast protein S100A4, and the mesenchymal marker vimentin compared to nonsmokers [107]. Tobacco smoke induces the expression of mesenchymal markers α-smooth muscle actin (α-SMA), vimentin, and type I collagen in human bronchial epithelial cells (HBEC) derived from nonsmokers [108]. These data together indicate that tobacco smoke contains a variety of active compounds that trigger EMT via different signaling pathways.

ROS and EMT

Milara et al. reported that tobacco smoke-induced EMT is mediated by ROS [108]. Increased ROS production results in NF-κB activation [109], as well as Rac1-mediated MMP3 expression [110]. The subsequent Rac1/MMP3-mediated binding of NF-κB subunits p65 and cRel to the Snail promoter, a key transcription factor for EMT [111], which inhibits the expression of epithelial junction proteins while inducing the expression of cytoskeleton proteins [112]. Another mechanism which underlies the potential of ROS to induce EMT includes activation of tumor necrosis factor (TNF) converting enzyme (TACE) [113] which subsequently activates epidermal growth factor receptor (EGFR) signaling via the Ras/Raf/MAPK, PI3K/Akt, and Src pathways, thereby enhancing cell proliferation and migration [114]. Src signaling, a key for EMT, is directly activated by ROS family members peroxynitrite and H_2O_2 resulting in increased expression of mesenchymal proteins, cytoskeletal reorganization, and disruption of cell matrix adhesion [115]. Along other lines, tobacco

smoke-induced ROS decreased Na,K-ATPase activity and NaK-α1 levels, resulting in disruption of tight junctions, alterations in cell polarity, and early EMT [116]. In conclusion, ROS mediate EMT by increasing cellular invasion potential into the ECM, by mediating ECM remodeling, by decreasing cellular adhesion, and by increasing cell motility (Fig. 4.1) [117].

Nicotine in EMT

The role of nicotine in inducing tumor growth and metastasis has been described in mouse models of LADC in vivo [118]. Nicotine mediates EMT through nAchR-dependent and nAchR-independent mechanisms [119]. nAchR-independent nicotine-induced EMT primarily rests on activation of TGFβ signaling [108, 120–123], which results in disassembly of epithelial tight junctions, cytoskeletal changes, downregulation of E-cadherin, and nuclear translocation of β-Catenin. Wnt signaling is also activated by nicotine and promotes EMT [124]. Moreover, Wnt enhances expression of Snail, a key to EMT [125]. nAchR-independent nicotine-induced EMT is also mediated by periostin, which is upregulated by nicotine, subsequently increasing Snail expression, cell proliferation, and invasion [119, 126]. Nicotine also mediates EMT via nAchR binding with subsequent recruitment of β-arrestin and Src and activation of MAPK [119, 127, 128]. In addition, nicotine increases mucin MUC4 production in pancreatic cancer through

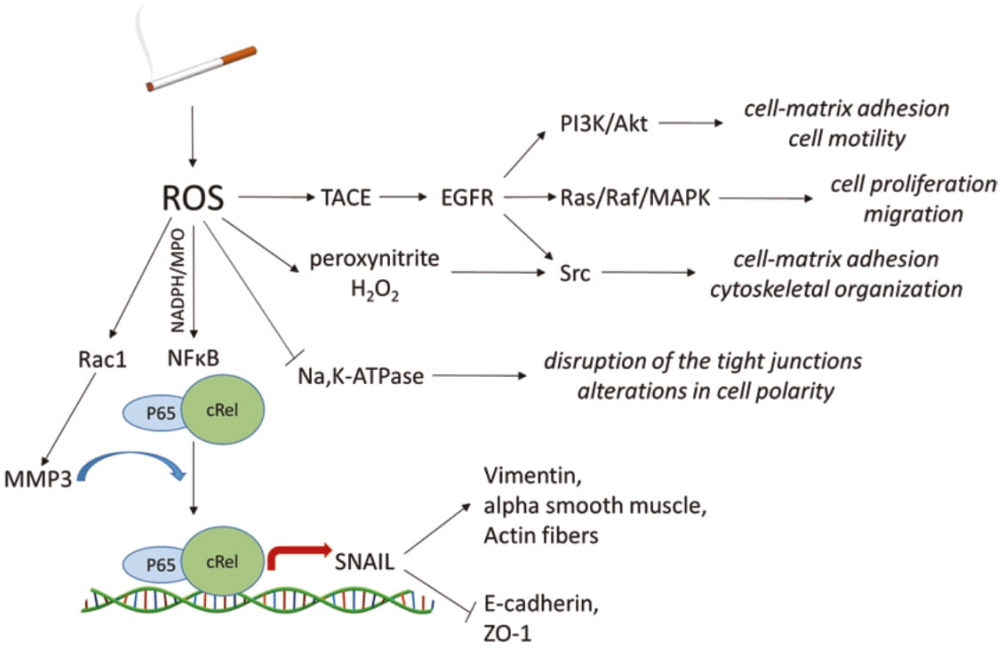

Fig. 4.1 ROS mediate tobacco smoke-induced EMT. The molecular mechanisms implicated in the induction of EMT driven by ROS include the activation of NF-κB signaling pathway, which in combination with the Rac1-mediated MMP3 expression regulates the transcriptional activation of Snail, resulting in the inhibition of the expression of epithelial junction proteins and the induction of the expression of cytoskeleton proteins. The cascade of TACE activation, EGFR signaling, Ras/Raf/MAPK, PI3K/Akt, and Src pathways regulate cell-matrix adhesion and enhance cell motility. ROS- mediated inhibition of Na,K-ATPase activity further contributes in EMT

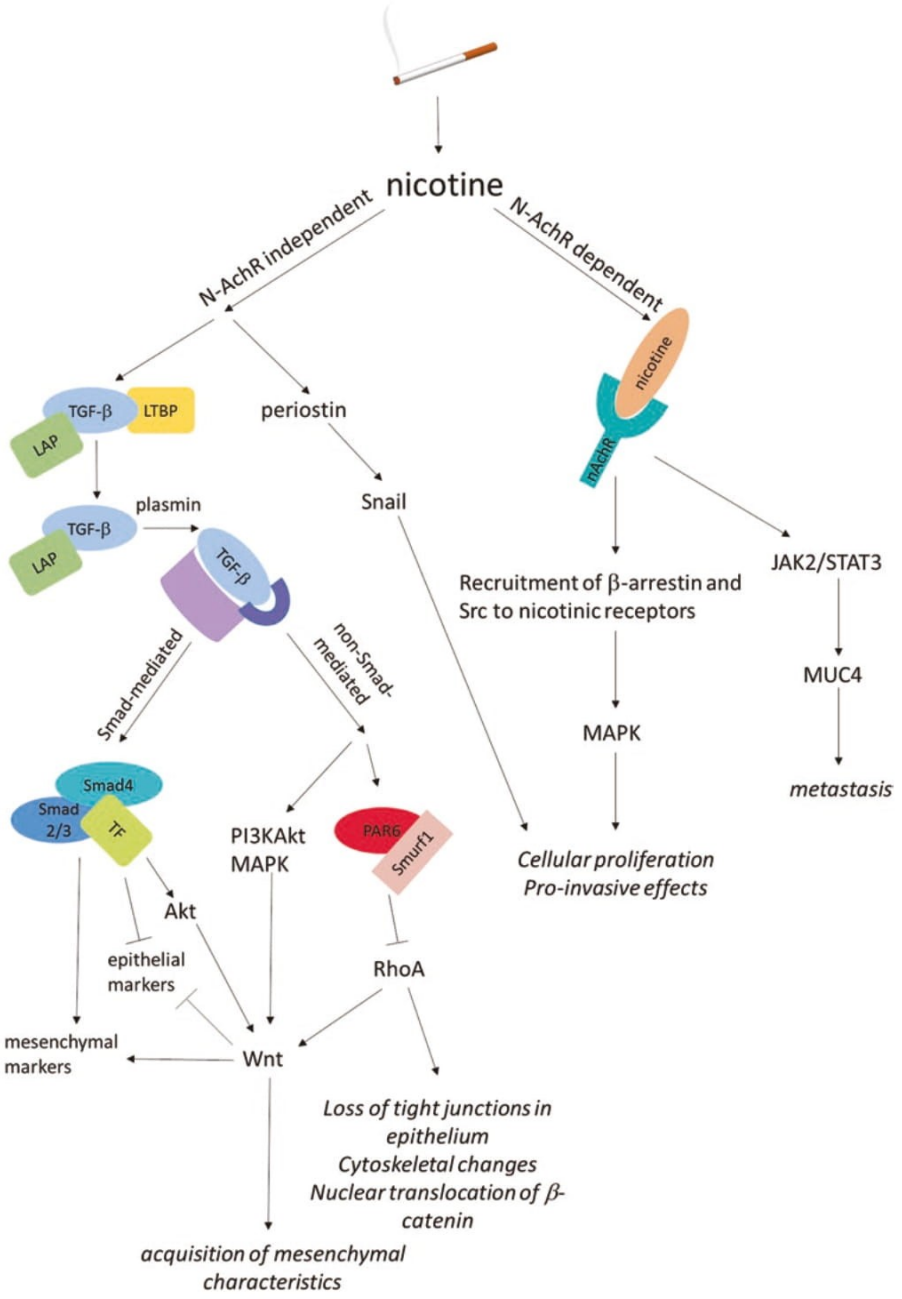

Fig. 4.2 Nicotine mediates tobacco smoke-induced EMT. The nA-chR-independent molecular mechanisms of nicotine-mediated EMT include TGFβ signaling, Wnt signaling and periostin-mediated Snail activation. The nAchR-dependent mechanisms include the recruit-ment of β-arrestin and Src to nicotinic receptors, the activation of MAPK cascade as well as the activation of activation of α7nAchR/JAK2/STAT3 signaling. The subsequent alterations in epithelial tight junctions, cytoskeletal changes, enhancement of cell motility and invasion enhance EMT

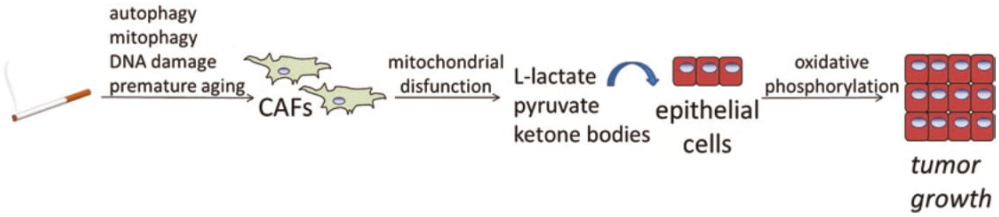

Fig. 4.3 Tobacco smoke-induces metabolic alterations through two-compartment tumor metabolism. Autophagy, mitophagy, DNA damage and premature aging convert immortalized human stromal fibroblasts in CAFs which undergo myofibroblast differentiation and mitochondrial dysfunction, resulting in secretion of high-energy mitochondrial fuels. The epithelial cancer cells use these metabolites enhancing tumor growth

activation of α7nAchR/JAK2/STAT3 signaling, thereby inducing metastasis (Fig. 4.2) [129].

PAH in EMT

PAH are organic compounds which consist of two or more fused aromatic rings. BαP, a compound of tobacco smoke that belongs to the PAH family, is connected with increased expression of EMT-related genes such as fibronectin, TWIST, and TGF-β2 [130]. Furthermore, PAH mediate activation of arylhydrocarbon receptors (AhR), which subsequently activate the transcription factor Slug, thereby enhancing EMT [131]. AhR-induced c-Jun N-terminal kinase (JNK) activation results in cytoskeletal remodeling and increased cellular migration [132].

4.3.1.3 Tobacco-Induced Metabolic Alterations

Tobacco smoke metabolically mediates cancer progression via autophagy and premature aging in the tumor microenvironment [133]. Tobacco smoke induces autophagy, mitophagy, DNA damage, and premature aging of immortalized human stromal fibroblasts, resulting in the production of CAF that mediate tumor growth [80, 133, 134]. CAFs undergo myofibroblast differentiation and mitochondrial dysfunction, resulting in secretion of high-energy mitochondrial fuels, such as L-lactate, pyruvate, and ketone bodies. These metabolites are subsequently used by epithelial cancer cells, thereby enhancing ATP generation via oxidative phosphorylation and promotion of tumor growth. This energy shuttling has been coined two-compartment tumor metabolism [134]. Tobacco smoke can also induce the reverse Warburg effect [84], by accelerating aging in the host microenvironment, which through a paracrine mechanism leads to cancer promotion (Fig. 4.3).

4.3.1.4 Tobacco Smoke-Induced Acute Inflammation of the Tumor Microenvironment

Acute effects of tobacco smoke have been studied in both in vitro and in vivo systems. In all models, neutrophils were found to be recruited immediately after acute smoke exposure, followed by alveolar macrophages. Eosinophils also increase in response to acute smoke exposure. Fibroblasts are implicated in the respiratory inflammatory signature induced by acute smoke exposure, through their inhibition and subsequent abnormalities in the repair mechanisms of the lung [135]. Except for the regulation of the recruitment of immune cells, tobacco smoke acute effects on inflammatory processes are also mediated via regulation of expression of various inflammatory mediators, such as neutrophil elastase, leukotrienes, and IL-6 [135].

4.3.2 Perpetual Impact of Past Smoke Exposure

4.3.2.1 Tobacco Smoke-Induced Chronic Inflammation

Chronic inflammation is the result of the failure of inflammatory cells to eliminate pathogens and

it involves both the adaptive and innate immune systems. The lungs are continuously exposed to environmental agents that can cause injury and have been strongly linked to chronic obstructive pulmonary disease (COPD) and lung cancer [136–138]. Tobacco smoke contains many components with immunomodulatory function, such as nicotine, ROS, nitrogen oxide, acrolein, carbon monoxide, and toxins [139, 140]. These components induce inflammatory mediator release (IL-8 and TNF-α) and chemokine secretion by airway epithelial cells [141, 142], through induction of epithelial intracellular cascades, such as Ras [143], MAPK, NF-κB, STAT, AP/1, and ERK [144–146]. These result in regulation of the inflammatory cell cycle, but also altered regulation of cell death [146], culminating tobacco smoke-induced airway inflammation. Another mechanism that has been suggested to mediate tobacco smoke-induced inflammation of the airways involves thymic stromal lymphopoietin (TSLP) secreted by both epithelial [147] and airway smooth muscle cells [148], which induces dendritic cell activation resulting in Th2 polarization [149] and subsequent allergic airway inflammation. Except for the induction of pro-inflammatory responses, tobacco smoke also diminishes the responsiveness to infections, with both mechanisms synergistically leading to chronic inflammation. Tobacco smoke downregulates the expression of the endogenous secreted antimicrobial peptide human beta defensin-2 compromising immune responses [150]. Furthermore, tobacco smoke suppresses the phagocytic function of alveolar macrophages [151], as well as the functions of circulating NK cells by downregulating IFN-γ and TNF-α in smokers [152]. Moreover, tobacco smoke induces mucus hypersecretion, resulting in diminished clearance of infections [153]. In conclusion, tobacco smoke triggers airway inflammation and impairs defense against infections and pathogens, all together leading to chronic inflammation (Fig. 4.4).

4.3.2.2 Epigenetic Changes

Smokers and nonsmokers show distinct profiles of DNA methylation [59, 60]. In vitro studies demonstrated that exposure of respiratory epithelial cells to tobacco smoke induces epigenetic changes [154]. Vaz et al. exposed HBEC cells to tobacco smoke for 10–15 months and observed changes in colony formation potential, EMT properties, MEK, RAS, EGFR, and WNT signaling and malignant phenotype after induction of $KRAS^{V12}$ mutations. However, whole exome sequencing did not reveal any driver mutations underlying the effects of tobacco smoke exposure. Changes in the DNA methylation pattern of the cells exposed to tobacco smoke were observed in genes which are frequently methylated in lung adenocarcinoma and squamous cell carcinoma, such as SFRP2, SFRP5 and WIF1, implicated in WNT signaling; MSX1, mediating the p53 function; and BMP3, WIF1 and GATA4, important for the RAS/MAPK signaling cascade. [155]. The mechanism underlying the effects of tobacco smoke on DNA methylation pattern might include AhR, which is a transcription factor mediating downstream histone modification related to risk of cancer [156, 157]. Thus tobacco smoke causes epigenetic changes, driven by mutations such as single $KRAS^{V12}$ mutation, which synergistically lead to oncogenic transformation of respiratory epithelial cells [158].

4.4 Future Trends and Directions

The pattern of accumulation of mutations inflicted by tobacco smoke during oncogenesis, the cell types of origin of lung adenocarcinoma, and the molecular mechanisms implicated during the progress of the disease have not been completely determined [35, 54, 159]. Understanding the cellular and molecular base of different causative factor-induced LADC through physiologically relevant mouse models of environmentally induced LADC, high-throughput sequencing, and carefully phenotyped and molecularly characterized human cohorts could lead to the discovery of new therapeutic targets, contribute to personalized medicine, and help for integration of exposure/molecular data into mechanistic risk prediction models.

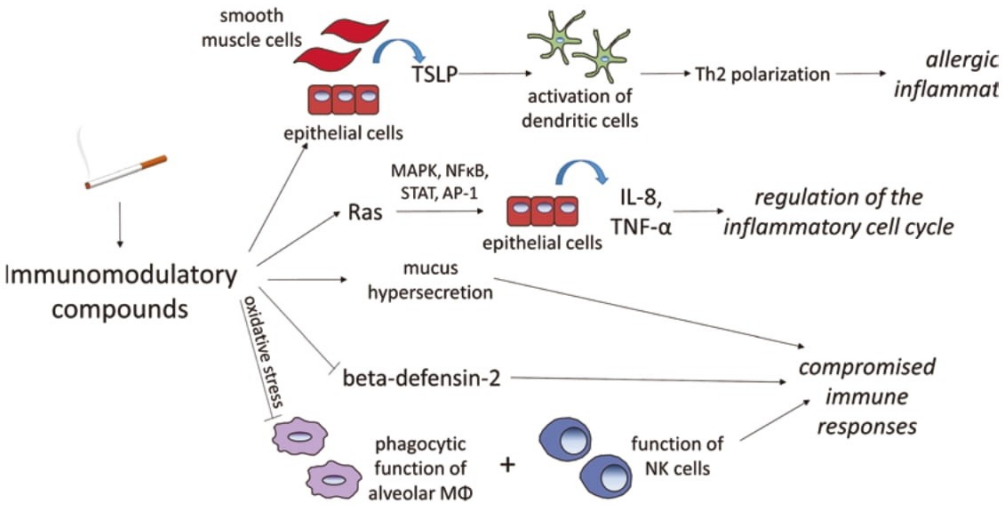

Fig. 4.4 Tobacco smoke favors chronic inflammation. The immunomodulatory compounds of tobacco smoke induce the secretion of TSLP from the epithelial and airway smooth muscle cells, with the subsequent activation of dendritic cells and Th2 polarization, re-sulting in allergic inflammation. Ras, MAPK, NF-κB, STAT, AP/1, and ERK cascades mediate the secretion of IL-8, TNF-α and chem-okines by airway epithelial cells, regulating the inflammatory cell cycle. The reduction of responsiveness to infections is mediated by the inhibition of beta defensin-2 and the suppression of the functions of both alveolar MΦ, and NK cells

References

1. Itier V, Bertrand D (2001) Neuronal nicotinic receptors: from protein structure to function. FEBS Lett 504:118–125
2. Benowitz NL, Hukkanen J, Jacob P (2009) Nicotine chemistry, metabolism, kinetics and biomarkers. Handb Exp Pharmacol 192:29–60
3. Deutsch-Wenzel RP, Brune H, Grimmer G, Dettbarn G, Misfeld J (1983) Experimental studies in rat lungs on the carcinogenicity and dose-response relationships of eight frequently occurring environmental polycyclic aromatic hydrocarbons. J Natl Cancer Inst 71:539–544
4. Stanton MF, Miller E, Wrench C, Blackwell R (1972) Experimental induction of epidermoid carcinoma in the lungs of rats by cigarette smoke condensate. J Natl Cancer Inst 49:867–877
5. Hecht SS (1999) Tobacco smoke carcinogens and lung cancer. J Natl Cancer Inst 91:1194–1210
6. Alexandrov K, Rojas M, Geneste O, Castegnaro M, Camus AM, Petruzzelli S, Giuntini C, Bartsch H (1992) An improved fluorometric assay for dosimetry of benzo(a)pyrene diol-epoxide-DNA adducts in smokers' lung: comparisons with total bulky adducts and aryl hydrocarbon hydroxylase activity. Cancer Res 52:6248–6253
7. Rojas M, Camus AM, Alexandrov K, Husgafvel-Pursiainen K, Anttila S, Vainio H, Bartsch H (1992) Stereoselective metabolism of (−)-benzo[a] pyrene-7,8-diol by human lung microsomes and peripheral blood lymphocytes: effect of smoking. Carcinogenesis 13:929–933
8. Nebert DW, Dalton TP, Okey AB, Gonzalez FJ (2004) Role of aryl hydrocarbon receptor-mediated induction of the CYP1 enzymes in environmental toxicity and cancer. J Biol Chem 279:23847–23850
9. Matter B, Wang G, Jones R, Tretyakova N (2004) Formation of diastereomeric benzo[a]pyrene diol epoxide-guanine adducts in p53 gene-derived DNA sequences. Chem Res Toxicol 17:731–741
10. Magee PN, Barnes JM (1956) The production of malignant primary hepatic tumours in the rat by feeding dimethylnitrosamine. Br J Cancer 10:114–122
11. Boyland E, Roe FJ, Gorrod JW (1964) Induction of pulmonary tumours in mice by mitrosonornicotine, a possible constituent of tobacco smoke. Nature 202:1126
12. Hecht SS, Chen CB, Ornaf RM, Jacobs E, Adams JD, Hoffmann D (1978) Reaction of nicotine and sodium nitrite: formation of nitrosamines and fragmentation of the pyrrolidine ring. J Org Chem 43:72–76
13. Hecht SS (1998) Biochemistry, biology, and carcinogenicity of tobacco-specific N-nitrosamines. Chem Res Toxicol 11:559–603
14. Huff JE, Melnick RL, Solleveld HA, Haseman JK, Powers M, Miller RA (1985) Multiple organ carcinogenicity of 1,3-butadiene in B6C3F1 mice after 60 weeks of inhalation exposure. Science 227:548–549

15. Fiore-Donati L, Chieco-Bianchi L, De Benedictis G, Maiorano G (1961) Leukaemogenesis by urethan in new-born Swiss mice. Nature 190:278–279
16. Guyer MF, Claus PE (1947) Tumor of the lung in rats following injections of urethane (ethylcarbamate). Cancer Res 7:342–345
17. Law LW, Precerutti A (1963) Inhibition by urethan (ethyl carbamate) of virus induction of leukaemia in C3H mice. Nature 200:692–693
18. Salmon AG, Zeise L, Painter P, Landy D (1991) Consistent estimates of urethane carcinogenic potency using pharmacokinetic and time-dependent models. In: Garrick BJ, Gekler WC (eds) The analysis, communication, and perception of risk. Boston, MA, Springer, pp 469–484
19. Lilis I, Ntaliarda G, Papaleonidopoulos V, Giotopoulou GA, Oplopoiou M, Marazioti A, Spella M, Marwitz S, Goldmann T, Bravou V, Giopanou I, Stathopoulos GT (2019) Interleukin-1β provided by KIT-competent mast cells is required for KRAS-mutant lung adenocarcinoma. Oncoimmunology 8:1593802
20. Stathopoulos GT, Sherrill TP, Cheng D-S, Scoggins RM, Han W, Polosukhin VV, Connelly L, Yull FE, Fingleton B, Blackwell TS (2007) Epithelial NF-kappaB activation promotes urethane-induced lung carcinogenesis. Proc Natl Acad Sci U S A 104:18514–18519
21. Vreka M, Lilis I, Papageorgopoulou M, Giotopoulou GA, Lianou M, Giopanou I, Kanellakis NI, Spella M, Agalioti T, Armenis V et al (2018) IκB kinase α is required for development and progression of KRAS-mutant lung adenocarcinoma. Cancer Res 78:2939–2951
22. Godwin WS, Subha VR, Feroz KM (2010) ^{210}Po radiation dose due to cigarette smoking. Curr Sci 98:681–686
23. Sakoda A, Fukao K, Kawabe A, Kataoka T, Hanamoto K, Yamaoka K (2012) Radioactivity of 210Pb in Japanese cigarettes and radiation dose from smoking inhalation. Radiat Prot Dosim 150:109–113
24. Mussalo-Rauhamaa H, Jaakkola T (1985) Plutonium-239, 240Pu and 210Po contents of tobacco and cigarette smoke. Health Phys 49:296–301
25. Zagà V, Lygidakis C, Chaouachi K, Gattavecchia E (2011) Polonium and lung cancer. J Oncol 2011:860103
26. Prasad S, Gupta SC, Tyagi AK (2017) Reactive oxygen species (ROS) and cancer: role of antioxidative nutraceuticals. Cancer Lett 387:95–105
27. Valavanidis A, Vlachogianni T, Fiotakis K (2009) Tobacco smoke: involvement of reactive oxygen species and stable free radicals in mechanisms of oxidative damage, carcinogenesis and synergistic effects with other respirable particles. Int J Environ Res Public Health 6:445–462
28. Federal Food, Drug, and Cosmetic Act—Definitions; Section 900. https://www.fda.gov/tobacco-products/rules-regulations-and-guidance/section-900-federal-food-drug-and-cosmetic-act-definitions. Content current as of: 21 June 2018; Accessed on 25 June 2019
29. Keithly L, Ferris Wayne G, Cullen DM, Connolly GN (2005) Industry research on the use and effects of levulinic acid: a case study in cigarette additives. Nicotine Tob Res 7:761–771
30. Alpert HR, Agaku IT, Connolly GN (2016) A study of pyrazines in cigarettes and how additives might be used to enhance tobacco addiction. Tob Control 25:444–450
31. Paumgartten FJR, Gomes-Carneiro MR, de Oliveira ACAX (2017) The impact of tobacco additives on cigarette smoke toxicity: a critical appraisal of tobacco industry studies. Cad Saude Publica 33(Suppl 3):e00132415
32. IARC Working Group on the Evaluation of Carcinogenic Risks to Humans (2004) Tobacco smoke and involuntary smoking. IARC Monogr Eval Carcinog Risks Hum 83:1–1438
33. Penning TM (2011) Chemical carcinogenesis. Springer Science & Business Media, New York
34. Alexandrov LB, Ju YS, Haase K, Loo PV, Martincorena I, Nik-Zainal S, Totoki Y, Fujimoto A, Nakagawa H, Shibata T et al (2016) Mutational signatures associated with tobacco smoking in human cancer. Science 354:618–622
35. Cancer Genome Atlas Research Network (2014) Comprehensive molecular profiling of lung adenocarcinoma. Nature 511:543–550
36. Siegel RL, Miller KD, Jemal A (2018) Cancer statistics, 2018. CA Cancer J Clin 68:7–30
37. Ramalingam SS, Owonikoko TK, Khuri FR (2011) Lung cancer: new biological insights and recent therapeutic advances. CA Cancer J Clin 61:91–112
38. Travis WD, Brambilla E, Nicholson AG, Yatabe Y, Austin JHM, Beasley MB, Chirieac LR, Dacic S, Duhig E, Flieder DB et al (2015) The 2015 World Health Organization classification of lung tumors: impact of genetic, clinical and radiologic advances since the 2004 classification. J Thorac Oncol 10:1243–1260
39. Alberg AJ, Brock MV, Ford JG, Samet JM, Spivack SD (2013) Epidemiology of lung cancer: diagnosis and management of lung cancer, 3rd ed: American College of Chest Physicians evidence-based clinical practice guidelines. Chest 143:e1S–e29S
40. Behjati S, Gundem G, Wedge DC, Roberts ND, Tarpey PS, Cooke SL, Van Loo P, Alexandrov LB, Ramakrishna M, Davies H et al (2016) Mutational signatures of ionizing radiation in second malignancies. Nat Commun 7:12605
41. Furukawa K, Preston DL, Lönn S, Funamoto S, Yonehara S, Matsuo T, Egawa H, Tokuoka S, Ozasa K, Kasagi F et al (2010) Radiation and smoking effects on lung cancer incidence among atomic bomb survivors. Radiat Res 174:72–82
42. Preston DL, Ron E, Tokuoka S, Funamoto S, Nishi N, Soda M, Mabuchi K, Kodama K (2007) Solid

cancer incidence in atomic bomb survivors: 1958–1998. Radiat Res 168:1–64
43. Thun M, Peto R, Boreham J, Lopez AD (2012) Stages of the cigarette epidemic on entering its second century. Tob Control 21:96–101
44. Sun S, Schiller JH, Gazdar AF (2007) Lung cancer in never smokers—a different disease. Nat Rev Cancer 7:778–790
45. Wakelee HA, Chang ET, Gomez SL, Keegan TH, Feskanich D, Clarke CA, Holmberg L, Yong LC, Kolonel LN, Gould MK et al (2007) Lung cancer incidence in never smokers. J Clin Oncol 25:472–478
46. Campbell JD, Alexandrov A, Kim J, Wala J, Berger AH, Pedamallu CS, Shukla SA, Guo G, Brooks AN, Murray BA et al (2016) Distinct patterns of somatic genome alterations in lung adenocarcinomas and squamous cell carcinomas. Nat Genet 48:607–616
47. George J, Lim JS, Jang SJ, Cun Y, Ozretić L, Kong G, Leenders F, Lu X, Fernández-Cuesta L, Bosco G et al (2015) Comprehensive genomic profiles of small cell lung cancer. Nature 524:47–53
48. Devarakonda S, Morgensztern D, Govindan R (2015) Genomic alterations in lung adenocarcinoma. Lancet Oncol 16:e342–e351
49. Kanellakis NI, Giannou AD, Pepe MA, Agalioti T, Zazara DE, Giopanou I, Psallidas I, Spella M, Marazioti A, Arendt KAM et al (2019) Tobacco chemical-induced mouse lung adenocarcinoma cell lines pin the prolactin orthologue proliferin as a lung tumour promoter. Carcinogenesis. pii: bgz047. https://doi.org/10.1093/carcin/bgz047. [Epub ahead of print]
50. Xue J, Yang S, Seng S (2014) Mechanisms of cancer induction by tobacco-specific NNK and NNN. Cancers 6:1138–1156
51. Murphy SE, Isaac IS, Ding X, McIntee EJ (2000) Specificity of cytochrome P450 2A3-catalyzed alpha-hydroxylation of N′-nitrosonornicotine enantiomers. Drug Metab Dispos 28:1263–1266
52. Wong HL, Murphy SE, Hecht SS (2005) Cytochrome P450 2A-catalyzed metabolic activation of structurally similar carcinogenic nitrosamines: N′-nitrosonornicotine enantiomers, N-nitrosopiperidine, and N-nitrosopyrrolidine. Chem Res Toxicol 18:61–69
53. Yuan J-M, Knezevich AD, Wang R, Gao Y-T, Hecht SS, Stepanov I (2011) Urinary levels of the tobacco-specific carcinogen N′-nitrosonornicotine and its glucuronide are strongly associated with esophageal cancer risk in smokers. Carcinogenesis 32:1366–1371
54. Westcott PMK, Halliwill KD, To MD, Rashid M, Rust AG, Keane TM, Delrosario R, Jen K-Y, Gurley KE, Kemp CJ et al (2015) The mutational landscapes of genetic and chemical models of Kras-driven lung cancer. Nature 517:489–492
55. Alexandrov LB, Nik-Zainal S, Wedge DC, Aparicio SAJR, Behjati S, Biankin AV, Bignell GR, Bolli N, Borg A, Børresen-Dale A-L et al (2013) Signatures of mutational processes in human cancer. Nature 500:415–421
56. Li X, Li J, Wu P, Zhou L, Lu B, Ying K, Chen E, Lu Y, Liu P (2018) Smoker and non-smoker lung adenocarcinoma is characterized by distinct tumor immune microenvironments. Oncoimmunology 7:e1494677
57. Desrichard A, Kuo F, Chowell D, Lee K-W, Riaz N, Wong RJ, Chan TA, Morris LGT (2018) Tobacco smoking-associated alterations in the immune microenvironment of squamous cell carcinomas. J Natl Cancer Inst 110:1386–1392
58. Rizvi NA, Hellmann MD, Snyder A, Kvistborg P, Makarov V, Havel JJ, Lee W, Yuan J, Wong P, Ho TS et al (2015) Cancer immunology. Mutational landscape determines sensitivity to PD-1 blockade in non-small cell lung cancer. Science 348:124–128
59. Belinsky SA (2004) Gene-promoter hypermethylation as a biomarker in lung cancer. Nat Rev Cancer 4:707
60. Gao X, Zhang Y, Breitling LP, Brenner H (2016) Tobacco smoking and methylation of genes related to lung cancer development. Oncotarget 7:59017–59028
61. Balkwill FR, Capasso M, Hagemann T (2012) The tumor microenvironment at a glance. J Cell Sci 125:5591
62. Chen Z, Fillmore CM, Hammerman PS, Kim CF, Wong K-K (2014) Non-small-cell lung cancers: a heterogeneous set of diseases. Nat Rev Cancer 14:535–546
63. Allavena P, Germano G, Marchesi F, Mantovani A (2011) Chemokines in cancer related inflammation. Exp Cell Res 317:664–673
64. Balkwill F (2004) Cancer and the chemokine network. Nat Rev Cancer 4:540–550
65. Balkwill FR (2012) The chemokine system and cancer. J Pathol 226:148–157
66. Mantovani A, Allavena P, Sica A, Balkwill F (2008) Cancer-related inflammation. Nature 454:436–444
67. Bronte V, Cingarlini S, Marigo I, De Santo C, Gallina G, Dolcetti L, Ugel S, Peranzoni E, Mandruzzato S, Zanovello P (2006) Leukocyte infiltration in cancer creates an unfavorable environment for antitumor immune responses: a novel target for therapeutic intervention. Immunol Investig 35:327–357
68. Sharma SK, Chintala NK, Vadrevu SK, Patel J, Karbowniczek M, Markiewski MM (2015) Pulmonary alveolar macrophages contribute to the premetastatic niche by suppressing antitumor T cell responses in the lungs. J Immunol (Baltimore, MD) 1950(194):5529–5538
69. Zaynagetdinov R, Sherrill TP, Polosukhin VV, Han W, Ausborn JA, McLoed AG, McMahon FB, Gleaves LA, Degryse AL, Stathopoulos GT et al (2011) A critical role for macrophages in promotion of urethane-induced lung carcinogenesis. J Immunol (Baltimore, MD) 1950(187):5703–5711

70. Pollard JW (2004) Tumour-educated macrophages promote tumour progression and metastasis. Nat Rev Cancer 4:71–78
71. Fridman WH, Pagès F, Sautès-Fridman C, Galon J (2012) The immune contexture in human tumours: impact on clinical outcome. Nat Rev Cancer 12:298
72. Ostroumov D, Fekete-Drimusz N, Saborowski M, Kühnel F, Woller N (2018) CD4 and CD8 T lymphocyte interplay in controlling tumor growth. Cell Mol Life Sci (CMLS) 75:689–713
73. Campbell DJ, Koch MA (2011) Treg cells: patrolling a dangerous neighborhood. Nat Med 17:929
74. Zaynagetdinov R, Stathopoulos GT, Sherrill TP, Cheng DS, McLoed AG, Ausborn JA, Polosukhin VV, Connelly L, Zhou W, Fingleton B et al (2012) Epithelial nuclear factor-κB signaling promotes lung carcinogenesis via recruitment of regulatory T lymphocytes. Oncogene 31:3164–3176
75. Bindea G, Mlecnik B, Tosolini M, Kirilovsky A, Waldner M, Obenauf AC, Angell H, Fredriksen T, Lafontaine L, Berger A et al (2013) Spatiotemporal dynamics of intratumoral immune cells reveal the immune landscape in human cancer. Immunity 39:782–795
76. Ammirante M, Luo J-L, Grivennikov S, Nedospasov S, Karin M (2010) B-cell-derived lymphotoxin promotes castration-resistant prostate cancer. Nature 464:302–305
77. Luo J-L, Tan W, Ricono JM, Korchynskyi O, Zhang M, Gonias SL, Cheresh DA, Karin M (2007) Nuclear cytokine-activated IKKalpha controls prostate cancer metastasis by repressing Maspin. Nature 446:690–694
78. Woo JR, Liss MA, Muldong MT, Palazzi K, Strasner A, Ammirante M, Varki N, Shabaik A, Howell S, Kane CJ et al (2014) Tumor infiltrating B-cells are increased in prostate cancer tissue. J Transl Med 12:30
79. Lund FE (2008) Cytokine-producing B lymphocytes-key regulators of immunity. Curr Opin Immunol 20:332–338
80. Capparelli C, Chiavarina B, Whitaker-Menezes D, Pestell TG, Pestell RG, Hulit J, Andò S, Howell A, Martinez-Outschoorn UE, Sotgia F et al (2012) CDK inhibitors (p16/p19/p21) induce senescence and autophagy in cancer-associated fibroblasts, "fueling" tumor growth via paracrine interactions, without an increase in neo-angiogenesis. Cell Cycle 11:3599–3610
81. Xing F, Saidou J, Watabe K (2010) Cancer associated fibroblasts (CAFs) in tumor microenvironment. Front Biosci (Landmark Ed) 15:166–179
82. Benedict WF, Jones PA, Laug WE, Igel HJ, Freeman AE (1975) Characterisation of human cells transformed in vitro by urethane. Nature 256:322–324
83. Chang HY, Chi J-T, Dudoit S, Bondre C, van de Rijn M, Botstein D, Brown PO (2002) Diversity, topographic differentiation, and positional memory in human fibroblasts. Proc Natl Acad Sci U S A 99:12877–12882
84. Pavlides S, Whitaker-Menezes D, Castello-Cros R, Flomenberg N, Witkiewicz AK, Frank PG, Casimiro MC, Wang C, Fortina P, Addya S et al (2009) The reverse Warburg effect: aerobic glycolysis in cancer associated fibroblasts and the tumor stroma. Cell Cycle 8:3984–4001
85. Kurose K, Gilley K, Matsumoto S, Watson PH, Zhou X-P, Eng C (2002) Frequent somatic mutations in PTEN and TP53 are mutually exclusive in the stroma of breast carcinomas. Nat Genet 32:355–357
86. Fukino K, Shen L, Patocs A, Mutter GL, Eng C (2007) Genomic instability within tumor stroma and clinicopathological characteristics of sporadic primary invasive breast carcinoma. JAMA 297:2103–2111
87. Koukourakis MI, Giatromanolaki A, Harris AL, Sivridis E (2006) Comparison of metabolic pathways between cancer cells and stromal cells in colorectal carcinomas: a metabolic survival role for tumor-associated stroma. Cancer Res 66:632–637
88. Kuperwasser C, Chavarria T, Wu M, Magrane G, Gray JW, Carey L, Richardson A, Weinberg RA (2004) Reconstruction of functionally normal and malignant human breast tissues in mice. Proc Natl Acad Sci U S A 101:4966–4971
89. Powell DW, Mifflin RC, Valentich JD, Crowe SE, Saada JI, West AB (1999) Myofibroblasts. I. Paracrine cells important in health and disease. Am J Physiol 277:C1–C9
90. Baggiolini M (1998) Chemokines and leukocyte traffic. Nature 392:565–568
91. Mueller L, Goumas FA, Affeldt M, Sandtner S, Gehling UM, Brilloff S, Walter J, Karnatz N, Lamszus K, Rogiers X et al (2007) Stromal fibroblasts in colorectal liver metastases originate from resident fibroblasts and generate an inflammatory microenvironment. Am J Pathol 171:1608–1618
92. Nakagawa H, Liyanarachchi S, Davuluri RV, Auer H, Martin EW, de la Chapelle A, Frankel WL (2004) Role of cancer-associated stromal fibroblasts in metastatic colon cancer to the liver and their expression profiles. Oncogene 23:7366–7377
93. Hanahan D, Weinberg RA (2000) The hallmarks of cancer. Cell 100:57–70
94. Zhu GG, Risteli L, Mäkinen M, Risteli J, Kauppila A, Stenbäck F (1995) Immunohistochemical study of type I collagen and type I pN-collagen in benign and malignant ovarian neoplasms. Cancer 75:1010–1017
95. Levental KR, Yu H, Kass L, Lakins JN, Egeblad M, Erler JT, Fong SFT, Csiszar K, Giaccia A, Weninger W et al (2009) Matrix crosslinking forces tumor progression by enhancing integrin signaling. Cell 139:891–906
96. Lu P, Weaver VM, Werb Z (2012) The extracellular matrix: a dynamic niche in cancer progression. J Cell Biol 196:395–406

97. Mott JD, Werb Z (2004) Regulation of matrix biology by matrix metalloproteinases. Curr Opin Cell Biol 16:558–564
98. Gazdar AF (2003) Environmental tobacco smoke, carcinogenesis, and angiogenesis: a double whammy? Cancer Cell 4:159–160
99. Heeschen C, Weis M, Cooke JP (2003) Nicotine promotes arteriogenesis. J Am Coll Cardiol 41:489–496
100. Keith RL, Miller YE, Gemmill RM, Drabkin HA, Dempsey EC, Kennedy TC, Prindiville S, Franklin WA (2000) Angiogenic squamous dysplasia in bronchi of individuals at high risk for lung cancer. Clin Cancer Res 6:1616–1625
101. Zhu B, Heeschen C, Sievers RE, Karliner JS, Parmley WW, Glantz SA, Cooke JP (2003) Second hand smoke stimulates tumor angiogenesis and growth. Cancer Cell 4:191–196
102. Rao SP, Sikora L, Hosseinkhani MR, Pinkerton KE, Sriramarao P (2009) Exposure to environmental tobacco smoke induces angiogenesis and leukocyte trafficking in lung microvessels. Exp Lung Res 35:119–135
103. Heeschen C, Jang JJ, Weis M, Pathak A, Kaji S, Hu RS, Tsao PS, Johnson FL, Cooke JP (2001) Nicotine stimulates angiogenesis and promotes tumor growth and atherosclerosis. Nat Med 7:833–839
104. Lee J, Cooke JP (2012) Nicotine and pathological angiogenesis. Life Sci 91:1058–1064
105. Kalluri R, Weinberg RA (2009) The basics of epithelial-mesenchymal transition. J Clin Invest 119:1420–1428
106. Di Cello F, Flowers VL, Li H, Vecchio-Pagán B, Gordon B, Harbom K, Shin J, Beaty R, Wang W, Brayton C et al (2013) Cigarette smoke induces epithelial to mesenchymal transition and increases the metastatic ability of breast cancer cells. Mol Cancer 12:90
107. Sohal SS, Reid D, Soltani A, Ward C, Weston S, Muller HK, Wood-Baker R, Walters EH (2010) Reticular basement membrane fragmentation and potential epithelial mesenchymal transition is exaggerated in the airways of smokers with chronic obstructive pulmonary disease. Respirology (Carlton Victoria) 15:930–938
108. Milara J, Peiró T, Serrano A, Cortijo J (2013) Epithelial to mesenchymal transition is increased in patients with COPD and induced by cigarette smoke. Thorax 68:410–420
109. Milara J, Cortijo J (2012) Tobacco, inflammation, and respiratory tract cancer. Curr Pharm Des 18:3901–3938
110. Radisky DC, Levy DD, Littlepage LE, Liu H, Nelson CM, Fata JE, Leake D, Godden EL, Albertson DG, Nieto MA et al (2005) Rac1b and reactive oxygen species mediate MMP-3-induced EMT and genomic instability. Nature 436:123–127
111. Cichon MA, Radisky DC (2014) ROS-induced epithelial-mesenchymal transition in mammary epithelial cells is mediated by NF-kB-dependent activation of Snail. Oncotarget 5:2827–2838
112. Cano A, Pérez-Moreno MA, Rodrigo I, Locascio A, Blanco MJ, del Barrio MG, Portillo F, Nieto MA (2000) The transcription factor snail controls epithelial-mesenchymal transitions by repressing E-cadherin expression. Nat Cell Biol 2:76–83
113. Zhang Z, Oliver P, Lancaster JR, Schwarzenberger PO, Joshi MS, Cork J, Kolls JK (2001) Reactive oxygen species mediate tumor necrosis factor alpha-converting, enzyme-dependent ectodomain shedding induced by phorbol myristate acetate. FASEB J 15:303–305
114. Borrell-Pagès M, Rojo F, Albanell J, Baselga J, Arribas J (2003) TACE is required for the activation of the EGFR by TGF-α in tumors. EMBO J 22:1114–1124
115. Zhang H, Liu H, Borok Z, Davies KJA, Ursini F, Forman HJ (2012) Cigarette smoke extract stimulates epithelial-mesenchymal transition through Src activation. Free Radic Biol Med 52:1437–1442
116. Huynh TP, Mah V, Sampson VB, Chia D, Fishbein MC, Horvath S, Alavi M, Wu DC, Harper J, Sarafian T et al (2012) Na,K-ATPase is a target of cigarette smoke and reduced expression predicts poor patient outcome of smokers with lung cancer. Am J Physiol Lung Cell Mol Physiol 302:L1150–L1158
117. Mori K, Shibanuma M, Nose K (2004) Invasive potential induced under long-term oxidative stress in mammary epithelial cells. Cancer Res 64:7464–7472
118. Davis R, Rizwani W, Banerjee S, Kovacs M, Haura E, Coppola D, Chellappan S (2009) Nicotine promotes tumor growth and metastasis in mouse models of lung cancer. PLoS One 4:e7524
119. Vu T, Jin L, Datta PK (2016) Effect of cigarette smoking on epithelial to mesenchymal transition (EMT) in lung cancer. J Clin Med 5:44
120. Bhowmick NA, Ghiassi M, Bakin A, Aakre M, Lundquist CA, Engel ME, Arteaga CL, Moses HL (2001) Transforming growth factor-beta1 mediates epithelial to mesenchymal transdifferentiation through a RhoA-dependent mechanism. Mol Biol Cell 12:27–36
121. Lechapt-Zalcman E, Prulière-Escabasse V, Advenier D, Galiacy S, Charrière-Bertrand C, Coste A, Harf A, d'Ortho M-P, Escudier E (2006) Transforming growth factor-beta1 increases airway wound repair via MMP-2 upregulation: a new pathway for epithelial wound repair? Am J Physiol Lung Cell Mol Physiol 290:L1277–L1282
122. Ozdamar B, Bose R, Barrios-Rodiles M, Wang H-R, Zhang Y, Wrana JL (2005) Regulation of the polarity protein Par6 by TGFbeta receptors controls epithelial cell plasticity. Science 307:1603–1609
123. Willis BC, Borok Z (2007) TGF-beta-induced EMT: mechanisms and implications for fibrotic lung disease. Am J Physiol Lung Cell Mol Physiol 293:L525–L534

124. Zou W, Zou Y, Zhao Z, Li B, Ran P (2013) Nicotine-induced epithelial-mesenchymal transition via Wnt/β-catenin signaling in human airway epithelial cells. Am J Physiol Lung Cell Mol Physiol 304:L199–L209
125. Yook JI, Li X-Y, Ota I, Fearon ER, Weiss SJ (2005) Wnt-dependent regulation of the E-cadherin repressor snail. J Biol Chem 280:11740–11748
126. Wu S-Q, Lv Y-E, Lin B-H, Luo L-M, Lv S-L, Bi A-H, Jia Y-S (2013) Silencing of periostin inhibits nicotine-mediated tumor cell growth and epithelial-mesenchymal transition in lung cancer cells. Mol Med Rep 7:875–880
127. Dasgupta P, Rastogi S, Pillai S, Ordonez-Ercan D, Morris M, Haura E, Chellappan S (2006) Nicotine induces cell proliferation by beta-arrestin-mediated activation of Src and Rb-Raf-1 pathways. J Clin Invest 116:2208–2217
128. Dasgupta P, Rizwani W, Pillai S, Kinkade R, Kovacs M, Rastogi S, Banerjee S, Carless M, Kim E, Coppola D et al (2009) Nicotine induces cell proliferation, invasion and epithelial-mesenchymal transition in a variety of human cancer cell lines. Int J Cancer 124:36–45
129. Momi N, Ponnusamy MP, Kaur S, Rachagani S, Kunigal SS, Chellappan S, Ouellette MM, Batra SK (2013) Nicotine/cigarette smoke promotes metastasis of pancreatic cancer through α7nAChR-mediated MUC4 upregulation. Oncogene 32:1384–1395
130. Yoshino I, Kometani T, Shoji F, Osoegawa A, Ohba T, Kouso H, Takenaka T, Yohena T, Maehara Y (2007) Induction of epithelial-mesenchymal transition-related genes by benzo[a]pyrene in lung cancer cells. Cancer 110:369–374
131. Ikuta T, Kawajiri K (2006) Zinc finger transcription factor Slug is a novel target gene of aryl hydrocarbon receptor. Exp Cell Res 312:3585–3594
132. Diry M, Tomkiewicz C, Koehle C, Coumoul X, Bock KW, Barouki R, Transy C (2006) Activation of the dioxin/aryl hydrocarbon receptor (AhR) modulates cell plasticity through a JNK-dependent mechanism. Oncogene 25:5570–5574
133. Salem AF, Al-Zoubi MS, Whitaker-Menezes D, Martinez-Outschoorn UE, Lamb R, Hulit J, Howell A, Gandara R, Sartini M, Galbiati F et al (2013) Cigarette smoke metabolically promotes cancer, via autophagy and premature aging in the host stromal microenvironment. Cell Cycle 12:818–825
134. Salem AF, Whitaker-Menezes D, Lin Z, Martinez-Outschoorn UE, Tanowitz HB, Al-Zoubi MS, Howell A, Pestell RG, Sotgia F, Lisanti MP (2012) Two-compartment tumor metabolism: autophagy in the tumor microenvironment and oxidative mitochondrial metabolism (OXPHOS) in cancer cells. Cell Cycle 11:2545–2556
135. van der Vaart H, Postma DS, Timens W, ten Hacken NHT (2004) Acute effects of cigarette smoke on inflammation and oxidative stress: a review. Thorax 59:713–721
136. Coussens LM, Zitvogel L, Palucka AK (2013) Neutralizing tumor-promoting chronic inflammation: a magic bullet? Science 339:286–291
137. Crusz SM, Balkwill FR (2015) Inflammation and cancer: advances and new agents. Nat Rev Clin Oncol 12:584–596
138. Houghton AM (2013) Mechanistic links between COPD and lung cancer. Nat Rev Cancer 13:233–245
139. De Flora S, Ganchev G, Iltcheva M, La Maestra S, Micale RT, Steele VE, Balansky R (2016) Pharmacological modulation of lung carcinogenesis in smokers: preclinical and clinical evidence. Trends Pharmacol Sci 37:120–142
140. Lee J, Taneja V, Vassallo R (2012) Cigarette smoking and inflammation: cellular and molecular mechanisms. J Dent Res 91:142–149
141. Kode A, Yang S-R, Rahman I (2006) Differential effects of cigarette smoke on oxidative stress and proinflammatory cytokine release in primary human airway epithelial cells and in a variety of transformed alveolar epithelial cells. Respir Res 7:132
142. Pace E, Ferraro M, Siena L, Melis M, Montalbano AM, Johnson M, Bonsignore MR, Bonsignore G, Gjomarkaj M (2008) Cigarette smoke increases Toll-like receptor 4 and modifies lipopolysaccharide-mediated responses in airway epithelial cells. Immunology 124:401–411
143. Reynolds PR, Kasteler SD, Schmitt RE, Hoidal JR (2011) Receptor for advanced glycation end-products signals through Ras during tobacco smoke-induced pulmonary inflammation. Am J Respir Cell Mol Biol 45:411–418
144. Iles KE, Dickinson DA, Wigley AF, Welty NE, Blank V, Forman HJ (2005) HNE increases HO-1 through activation of the ERK pathway in pulmonary epithelial cells. Free Radic Biol Med 39:355–364
145. Kroening PR, Barnes TW, Pease L, Limper A, Kita H, Vassallo R (2008) Cigarette smoke-induced oxidative stress suppresses generation of dendritic cell IL-12 and IL-23 through ERK-dependent pathways. J Immunol (Baltimore, MD) 1950(181):1536–1547
146. Liu X, Togo S, Al-Mugotir M, Kim H, Fang Q, Kobayashi T, Wang X, Mao L, Bitterman P, Rennard S (2008) NF-kappaB mediates the survival of human bronchial epithelial cells exposed to cigarette smoke extract. Respir Res 9:66
147. Nakamura Y, Miyata M, Ohba T, Ando T, Hatsushika K, Suenaga F, Shimokawa N, Ohnuma Y, Katoh R, Ogawa H et al (2008) Cigarette smoke extract induces thymic stromal lymphopoietin expression, leading to T(H)2-type immune responses and airway inflammation. J Allergy Clin Immunol 122:1208–1214
148. Smelter DF, Sathish V, Thompson MA, Pabelick CM, Vassallo R, Prakash YS (2010) Thymic stromal lymphopoietin in cigarette smoke-exposed human airway smooth muscle. J Immunol (Baltimore, MD) 1950(185):3035–3040
149. Liu Y-J, Soumelis V, Watanabe N, Ito T, Wang Y-H, de Waal Malefyt R, Omori M, Zhou B, Ziegler

SF (2007) TSLP: an epithelial cell cytokine that regulates T cell differentiation by conditioning dendritic cell maturation. Annu Rev Immunol 25:193–219
150. Herr C, Beisswenger C, Hess C, Kandler K, Suttorp N, Welte T, Schroeder J-M, Vogelmeier C, R Bals for the CAPNETZ Study Group (2009) Suppression of pulmonary innate host defence in smokers. Thorax 64:144–149
151. Green GM (1968) Cigarette smoke: protection of alveolar macrophages by glutathione and cysteine. Science 162:810–811
152. Mian MF, Lauzon NM, Stämpfli MR, Mossman KL, Ashkar AA (2008) Impairment of human NK cell cytotoxic activity and cytokine release by cigarette smoke. J Leukoc Biol 83:774–784
153. Chung KF (2005) Inflammatory mediators in chronic obstructive pulmonary disease. Curr Drug Targets Inflamm Allergy 4:619–625
154. Liu F, Killian JK, Yang M, Walker RL, Hong JA, Zhang M, Davis S, Zhang Y, Hussain M, Xi S et al (2010) Epigenomic alterations and gene expression profiles in respiratory epithelia exposed to cigarette smoke condensate. Oncogene 29:3650–3664
155. Vaz M, Hwang SY, Kagiampakis I, Phallen J, Patil A, O'Hagan HM, Murphy L, Zahnow CA, Gabrielson E, Velculescu VE et al (2017) Chronic cigarette smoke-induced epigenomic changes precede sensitization of bronchial epithelial cells to single-step transformation by KRAS mutations. Cancer Cell 32:360–376.e6
156. Joshi AD, Mustafa MG, Lichti CF, Elferink CJ (2015) Homocitrullination is a novel histone H1 epigenetic mark dependent on aryl hydrocarbon receptor recruitment of carbamoyl phosphate synthase 1. J Biol Chem 290:27767–27778
157. Schnekenburger M, Peng L, Puga A (2007) HDAC1 bound to the Cyp1a1 promoter blocks histone acetylation associated with Ah receptor-mediated trans-activation. Biochim Biophys Acta 1769:569–578
158. Clark SJ, Molloy PL (2017) Smoke-induced changes to the epigenome provide fertile ground for oncogenic mutation. Cancer Cell 32:278–280
159. Sutherland KD, Song J-Y, Kwon MC, Proost N, Zevenhoven J, Berns A (2014) Multiple cells-of-origin of mutant K-Ras-induced mouse lung adenocarcinoma. Proc Natl Acad Sci U S A 111:4952–4957
160. Zhu, J., Yamane, H., Cote-Sierra, J., Guo, L. & Paul, W. E. (2006) GATA-3 promotes Th2 responses through three different mechanisms: induction of Th2 cytokine production, selective growth of Th2 cells and inhibition of Th1 cell-specific factors. Cell Res. 16, 3–10 .
161. Yoon, N.K., Maresh, E.L., Shen, D., Elshimali, Y., Apple, S., Horvath, S., Mah, V., Bose, S., Chia, D., Chang, H.R., Goodglick, L (2010) Higher levels of GATA3 predict better survival in women with breast cancer. Hum. Pathol. 41, 1794–1801

Acknowledgements

The studies of the present PhD dissertation were conducted in the Molecular Lung Carcinogenesis laboratory of Comprehensive Pneumology Center, Helmholtz Center in Munich, as well as in the Molecular Respiratory Carcinogenesis laboratory of Faculty of Medicine, University of Patras in Greece, under the direct supervision of Prof. Dr. med. Behr and Dr. Stathopoulos. I would like to express my gratitude to both of them for the opportunity and the honor to have their guidance and support throughout the process of building a solid theoretical and experimental background, as well as approaching biological phenomena through a holistic prism. I am additionally grateful to my Target Agreement Committee members Prof. Dr. med. Thomas Gudermann and Prof. Dr. Markus Rehberg for their critical intellectual input, their support and appreciation of all efforts and difficulties during the progress of my doctoral studies.

A big “thank you” to each of my talented and brilliant colleagues, Dr. Andrea Schamberger, Dr. Anne-Sophie Lamort, Dr. Mario Pepe, Dr. Kristina Arendt, Lilith Trassl, Jianlong Jia, Benteng Deng, Asma Bin Snkar, for creating an environment of trust, respect and support. Furthermore, I am truly grateful for working with Dr. Ioannis Lilis, Dr. Magda Spella, Giannoula Ntaliarda, Dr. Ioanna Giopanou, Dr. Antonella Marazioti, Anthi Krontira. Additionally, I thank Ayse Yazigli for making working with her a pleasure, Aydan Sardogan and Ceylan Onursal for bringing laughs and sweets in stressful days and Ashesh Chakraborty for funny moments in the office and for motivating me to “do some science”. A special “thank you” to Ms. Sabine Behrend for being my co-traveler from the very first until the last moment of this journey.

LMU Research Training Group GRK2338 “Targets in Toxicology” (funded by DFG- Deutsche Forschungsgemeinschaft) fulfilled my ambition to widen my scientific horizons, collaborate with world leading experts in an international environment, and contribute scientifically in the field of my interest. Prof. Dr. med. Thomas Gudermann, Dr. Julia Brandt, Dr. Steffi Resenberger, Yves Haufe, Jonas Tigges, Katharina Müller-Dott, Christian Schremmer, Xin Zhang, Erika Gonzales Rodrigues, Michal Mastalerz, Barbara Julia Spix, Paula Vaccarello, Sarah Zeitlmayr, Florian Schelter, it was my great pleasure to be a member of this group.

Last but importantly, I want to express my gratitude to Dr. Stathopoulos for always being driven by the best for all of his students, not only on a scientific, but also on a personal level, to Yves for standing by me, and to my family for unconditionally supporting me in every single step until now and for giving me strength to continue.